

ISSN 0387-6144

*BULLETIN OF THE*  
**RESEARCH LABORATORY FOR NUCLEAR REACTORS**

VOL. 36

2012



**RESEARCH LABORATORY FOR NUCLEAR REACTORS**  
**TOKYO INSTITUTE OF TECHNOLOGY**

BULLETIN OF THE RESEARCH LABORATORY FOR NUCLEAR REACTORS

*BULL. RES. LAB. NUCL. REACTOR, Vol.36, 2012*

**CONTENTS**

<b>Research Staffs</b> .....	1
 <b>I. Celebration of Professor Aritomi's and Professor Shimada's 65th Birthdays</b>	
I.1 ON THE OCCASION OF RETIREMENT Masanori ARITOMI .....	3
I.2 In the Quest for Energy Development -Starting with the development of nuclear fusion and ending with the proposal for power problem solution- Ryuichi SHIMADA .....	10
 <b>II. Research Reports</b>	
<b>A. Energy Engineering</b>	
A.1 Difference in Rotational Temperatures between Neutral Molecules and Molecular Ions of Low-Pressure Microwave N <sub>2</sub> or O <sub>2</sub> Discharge Plasmas Hiroshi AKATSUKA, Atsushi NEZU and Haruaki MATSUURA .....	15
A.2 DSMC Simulation of Arc-Jet Flow with Low Ionization Degree along Open-Field-Line Hiroshi AKATSUKA, Atsushi NEZU and Haruaki MATSUURA .....	16
A.3 Study on High Speed Lithium Jet for Neutron Source of Boron Neutron Capture Therapy (BNCT) Minoru TAKAHASHI, Tooru KOBAYASHI, Mingguang ZHANG, Michael MAK, Jiri STEFANICA, Vaclav DOSTAL, and Wei ZHAO .....	17
A.4 Carbon Recycling Ironmaking System Driven by High Temperature Gas Reactor Yukitaka KATO .....	19
A.5 Numerical Analyses on Joule-Heated Glass Furnace for Disposal of High-Level Radioactive Waste Nobuyoshi TSUZUKI and Hiroshige KIKURA .....	22
A.6 A Very Low Velocity Measurement Using Ultrasonic Velocimetry Hiroshige KIKURA and Yasushi TAKEDA .....	23
A.7 Basic Study of Velocity Profile Measurement by an Air-Coupled Ultrasonic System Hiroshige KIKURA .....	24

A.8	Durability of Mg-Co Mixed Hydroxide on Cyclic Operation for Chemical Heat Storage Junichi RYU and Yukitaka KATO .....	25
A.9	Geometrical Network Approach for An Evaluation of Heat-Transfer Coefficient in Dropwise Condensation Noriyuki WATANABE and Masanori ARITOMI .....	26
<b>B. Mass Transmutation Engineering</b>		
B.1	Systematic Measurement of keV-Neutron Capture Cross Sections and Capture Gamma-Ray Spectra of Pd Isotopes Masayuki IGASHIRA, Kazushi TERADA and Tatsuya KATABUCHI .....	27
B.2	Neutron-Irradiation-Induced Crystalline Defects in $\beta$ -Si <sub>3</sub> N <sub>4</sub> and Recovery by Thermal Annealing Toyohiko YANO, Tomoyuki YAMAGAMI and Katsumi YOSHIDA .....	29
B.3	A Study on Advanced Reprocessing System Based on Use of Cyclic Urea Derivatives with Highly Selective Precipitation Ability to U(VI) Tomoya SUZUKI, Takeshi KAWASAKI, Koichiro TAKAO, Masayuki HARADA, Masanobu NOGAMI, and Yasuhisa IKEDA .....	33
B.4	Electrochemical and Spectroelectrochemical Studies on [UO <sub>2</sub> Cl <sub>4</sub> ] <sup>2-</sup> in 1-Ethyl-3-methylimidazolium Based Ionic Liquids Toshinari OGURA, Koichiro TAKAO, Kotoe SASAKI, Tsuoyoshi ARAI, Yasuhisa IKEDA .....	34
B.5	Dynamics Studies on Water Confined in Polymer Brushes by Low-Field Pulsed NMR Takehiko TSUKAHARA .....	35
B.6	Liquid-Liquid Extraction of Cadmium(II) Ion with Hydrophobic TPEN Derivatives Yusuke INABA, Atsunori MORI and Kenji TAKESHITA .....	36
B.7	Development of Cesium Recovery Process by Hydrothermal Treatment and Coagulation-Sedimentation Hideharu TAKAHASHI, Kenji TAKESHITA, Chie IGUCHI and Yusuke INABA ...	38
B.8	Calculation of Heavy-Ion Stopping in Foam Targets Coupled with 1D Hydrodynamics Yoshiyuki OGURI .....	40
B.9	Prediction and Observation of Curvature-Driven Potential Effects on Electronic Properties of One-Dimensional Condensed Matters Jun ONOE, Takahiro ITO, Hiroyuki SHIMA, Hideo YOSHIOKA and Shin-ichi KIMURA .....	43
B.10	Local Structural Analysis of Thorium Fluoride in Molten Mono- and Divalent Cationic Fluoride Mixtures for Molten Salt Reactor Concept Haruaki MATSUURA, Atsushi NEZU and Hiroshi AKATSUKA .....	46

B.11	Fluoride Addition Effect on the Electrochemistry and Local Structure of Neodymium Cation in Molten Chlorides Haruaki MATSUURA, Atsushi NEZU and Hiroshi AKATSUKA .....	47
B.12	Local Structural Analysis of Neodymium Cation in Molten Various Chlorides for Pyrochemical Reprocessing of Nuclear Fuel Haruaki MATSUURA, Atsushi NEZU and Hiroshi AKATSUKA .....	48
B.13	Formation of Carbon Interphase on SiC Fibers in SiC Fiber-Reinforced SiC Matrix Composites by Electrophoretic Deposition Katsumi YOSHIDA and Toyohiko YANO .....	49
B.14	Resourceability on Nuclear Fuel Cycle Masaki OZAWA .....	52
B.15	Transmutation Study on Fission Product Palladium for Denaturing Isotopic Composition Toshio YOSHIOKA, Masaki OZAWA and Masaki SAITO .....	54
B.16	Experimental Study on Diffusion of Metal in Lead-Bismuth Eutectic in Thin Tube Minoru TAKAHASHI, Shunichi NUMATA, Eriko IRISAWA-YAMAKI and Weidong WU .....	56

### **C. System and Safety Engineering**

C.1	Progress in Innovative Nuclear Reactor Study and Nuclear Safety Study Toru OBARA .....	59
C.2	Development of Methodology for Plutonium Categorization (IV) - Effect of Compression on Rossi-alpha- Yoshiki KIMURA <sup>*1</sup> and Masaki SAITO .....	60
C.3	Effects of Inner Axial Blanket and Minor Actinides on Extension of Core Life-time of Large-scale FBR Erina HAMASE <sup>*1</sup> and Masaki SAITO .....	62
C.4	Positional Stabilization of Torus Plasma with Simple Helical Coils Shunji TSUJI-IIO and Hiroaki TSUTSUI .....	64
C.5	Test Particle Simulation for High Frequency Glow Discharge in Magnetic Field Hiroaki TSUTSUI and Shunji TSUJI-IIO .....	65
C.6	Evaluation of Fukushima Dai-ichi Nuclear Power Plant Accident Kazumi KITAYAMA, Takao ISHIZUKA, Nobuyoshi TSUZUKI, Hiroshige KIKURA and Masanori ARITOMI .....	66
C.7	Current Issues and Future Scope of Japan's Nuclear Regulatory Agency Tetsuo SAWADA .....	67

**III. Co-operative Researches**

III.1 Co-operative Researches within Tokyo Institute of Technology ..... 73

III.2 Co-operative Researches with outside of Tokyo Institute of Technology ..... 73

III.3 Themes Supported by Grants-in-Aid for Scientific Research of  
the Ministry of Education, Culture, Sports, Science and Technology ..... 76

**IV. List of Publications** ..... 77

**Research staffs of  
RESEARCH LABORATORY FOR NUCLEAR REACTORS,  
TOKYO INSTITUTE OF TECHNOLOGY**

**Director**

Masanori ARITOMI      Distinguished Professor

**Energy Engineering Division**

Masayuki IGASHIRA      Professor  
Satoshi CHIBA      Professor  
Masanori ARITOMI      Distinguished Professor  
Hiroshi AKATSUKA      Associate Professor  
Minoru TAKAHASHI      Associate Professor  
Yukitaka KATO      Associate Professor  
Tetsuo SAWADA      Assistant Professor  
Junichi RYU      Assistant Professor  
Kotaro KONDO      Assistant Professor

**System and Safety Engineering Division**

Ryuichi SHIMADA      Distinguished Professor  
Masaki SAITO      Professor  
Yasuhisa IKEDA      Professor  
Shunji IIO      Associate Professor  
Hiroshige KIKURA      Associate Professor  
Toru OBARA      Associate Professor  
Hiroaki TSUTSUI      Assistant Professor  
Etsuko KOIZUMI      Assistant Professor  
Yoshitalia Meiliza      Assistant Professor

**Mass Transmutation Engineering Division**

Toyohiko YANO      Professor  
Kenji TAKESHITA      Professor  
Yoshiyuki OGURI      Professor  
Jun ONOE      Associate Professor  
Yoshihisa MATSUMOTO      Associate Professor  
Noriyosu HAYASHIZAKI      Associate Professor  
Takehiko TSUKAHARA      Associate Professor  
Masao NOMURA      Assistant Professor  
Haruaki MATSUURA      Assistant Professor  
Masayuki HARADA      Assistant Professor  
Katsumi YOSHIDA      Assistant Professor  
Tatsuya KATABUCHI      Assistant Professor  
Jun NISHIYAMA      Assistant Professor

**International Nuclear Research Cooperation Center**

Masaki OZAWA      Professor

**Common Staffs**

Noriyuki WATANABE      Assistant Professor  
Koichiro TAKAO      Assistant Professor  
Tadashi YOSHIDA      Visiting Professor  
Fumiaki KAWAKAMI      Visiting Professor  
Mishra Kaushala Prasad      Visiting Professor  
Takatoshi TAKEMOTO      Visiting Associate Professor  
Eiichi ASANO      Visiting Associate Professor

**Technical Staffs**

Masamitsu IMAI      Senior Technical Specialist  
Mitsuo MATSUZAKI      Senior Technical Specialist  
Hitoshi FUKUDA      Senior Technical Specialist  
Ken-ichi TOSAKA      Senior Technical Specialist  
Atsushi NEZU      Senior Technical Specialist

## I.1 ON THE OCCASION OF RETIREMENT

**Masanori ARITOMI**  
Director and Distinguished Professor  
Research Laboratory for Nuclear Reactors  
Tokyo Institute of Technology

I was employed in this Laboratory at the beginning of April in 1975 and will retire at the end of March this year in 2013. My major research activities during 38 years are put down in this paper.

### 1. Thermo-Hydraulic Instabilities in Parallel-Channel Boiling System

#### 1.1 Density Wave Instability<sup>[1]-[5]</sup>

The density wave instability occurring in forced-convection up-flow passing through a parallel channels were studied theoretically and experimentally, using water as test fluid. Two analytical models were proposed to analyze density wave instability. One was a non-linear analytical model (PARALLEL) solved for the time elapsed and was applicable to systems with more than three channels with the same flow conditions or different flow conditions between channels. The other was a linear complex analytical model (PALCOMP) solved on a complex plane and is applicable to two channel system with or without different flow conditions.

The limit of the stable flow in such a parallel channel system (the stable boundary), and the nature of inlet flow oscillation in the unstable region were experimentally investigated under various conditions of inlet velocity, heat flux, inlet liquid temperature, cross section of channel and entrance throttling.

The parallel channel boiling system possessed a characteristic oscillation that is quite independent of the magnitude and duration of the initial disturbance. The stable boundary is influenced by the characteristic frequency of the system as well as by the exit quality when this is low. Upon raising the exit quality and reducing the characteristic frequency, the system increases its instability. Entrance throttling effectively contributes to stabilization of the system. In respect of the amplitude of flow oscillation, a widely applicable quantitative result could not be obtained, but it was indicated that the amplitude ratio tended to augment with increasing departure from the stable boundary into the unstable region. The period of frequency of the flow oscillation was sensitively dependent on the time required by the fluid to pass through the preheating region.

Close agreement was obtained between calculations and experiments in respect of the stable boundary and the period of the flow oscillation in the unstable region. The model was further applied to three and four parallel channels, the results of which indicate that the flow instability behavior in such multiple channels were quite similar to that observed on the two-channel system, in

such aspects as the stable boundary, as well as the period and the development of flow oscillations in the unstable region.

The system, where the thermo-hydraulic flow conditions in two channels were different from each other, was studied theoretically and experimentally, in order to make clear the effects of the different conditions on the flow instabilities. The different conditions between parallel channels were made artificially by changing the entrance throttling, the heater length and the heat flux. Close agreement between the experimental results and analytical ones was obtained in regard to the stable boundary and the period of the flow oscillation in the unstable region. The reliability of the analytical models and the generality of the experimental results were confirmed.

Consequently, the instability in the system where the own characteristic frequencies were approximately equal in two channels almost agree with the one obtained under the uniform condition equivalent to the average operating condition in two channels, such as the different entrance throttling and the different heater length. On the other hand, the system, where the characteristic frequencies differ from two channels, becomes more stable with increasing the difference of flow condition, such as the different heat fluxes.

The steam generator (SG) of liquid metal cooled fast breeder reactor (LMFBR) is composed of multiple tubes with the different flow conditions from each other. Most of the computer codes developed to evaluate the flow stability analyzed a representative tube on the basis of the assumption of the constant pressure drop between the feed water header and the steam one as single channel. Since the method selecting the representative channel had never been investigated, three cases about the representative channels were studied analytically. The exact solutions about the stable boundary for three and four channels with the different heat flux and/or entrance throttling were analyzed by PALLALEL code. The first approximate case, which selects the average operating conditions as the one of the representative channel, evaluates more stable side. The second approximate case, which selects the most unstable channel as the representative channel, evaluates the stable boundary on the conservative side. The third approximate case, which selects the most unstable pair of channels as two representative channels, evaluates exactly the stable boundary.

## 1.2 Other Thermo-Hydraulic Instabilities

To clarify the mechanism of the limit cycle oscillation observed in 1 MW SG for LMFBR without the thermal insulated downcomer of Power Reactor and Nuclear Fuel Development Corp, the effect of boiling in downcomer on the flow instability was studied experimentally using twin U-type parallel boiling channels. The slug excursion instability, which did not belong to Bouré's classification of two phase flow instabilities, was observed. The slug excursion instability is affected with the magnitude and nature of disturbance and with the history of flow conditions, which is the most different feature from the density wave instability. It was considered from the results that the limit cycle oscillation observed in the 1 MW SG was slug excursion instability.<sup>[4]</sup>

Thermo-hydraulic instability was investigated experimentally in a boiling two-phase flow system, composed of a vertical N-shaped boiling channel and an adiabatic bypass between an inlet plenum and an outlet one, using Freon 113 as a test fluid. Instability caused by the blockage of flow by vapor, which could not be found in Bouré's classification of two-phase flow instabilities, was observed. The flow maps in each section, static characteristics, stable flow limits and characteristics of this instability were studied under various conditions to clarify the mechanism. The inlet velocity decreases when a vapor slug combining in the inverted U-shaped bend obstructs the flow. The vapor slug flowing into the downcomer increases the void fraction therein, resulting in increased gravitation loss. Consequently, flow instability is brought about. There are two types of instabilities. One is the perfect blockage type where the inlet velocity becomes zero in the heated channel and is kept intact. The other is oscillation type where the inlet velocity decreases to a certain value and oscillates around it. The boundary, where either of the two types occurred, is determined by the relation between the increases in the gravitational loss of boiling channel and in the frictional loss of the bypass flow rate. For the oscillation type instability, the period of flow oscillation depends only on vapor flow rate and decreases with its increase. On the other hand, the amplitude ratio decreases as both the vapor flow rate and the inlet velocity, before flow excursion increases.<sup>[6]</sup>

## 2. Thermo-Hydraulics during Start-Up in Natural Circulation Boiling Water Reactors<sup>[7]-[10]</sup>

Many concepts, in which passive and simplified functions were actively adapted, were proposed for the next generation LWRs, and the natural circulation BWR was one such proposal. Advantages and disadvantages of the natural circulation BWR were considered as compared with current BWRs. From the results, thermo-hydraulic instabilities, which may appear during start-up, greatly influence the concept feasibility, so that they were investigated experimentally under conditions simulating normal and abnormal start-up processes. It was clarified that three kinds of thermo-hydraulic instabilities may occur during its start-up according to its procedure and reactor configuration, which were (1) geysering induced

by condensation, (2) natural circulation instability caused by hydrostatic head fluctuation in the steam separator and/or divided chimney and (3) density wave oscillation. Driving mechanisms of the geysering and the natural circulation instability, which had never understood enough, were inferred from the results. The difference of thermo-hydraulic behavior during start-up process between thermal natural circulation boiler and the Dodewarad reactor (natural circulation BWR) was considered.

The driving mechanisms of geysering were investigated in parallel boiling channel under both natural and forced circulation conditions. The mechanism of geysering occurring in parallel boiling channels under forced circulation conditions is identical to that under natural circulation conditions. For geysering to occur, both the formation of a large bubble covering the whole flow cross section and sub cooled condition in the outlet plenum are necessary. As long as these conditions are satisfied and the condensing rate of a large bubble is superior to the whole circulation rate, flow reversal occurs, and then geysering is induced. Therefore, superheated liquid is not necessary for geysering to occur in parallel boiling channels. As velocity increases, the flow is stabilized as for geysering since it becomes difficult to satisfy the above conditions simultaneously. As subcooling increases, subcooled boiling is enhanced, and the mixing in fluid becomes more active at the same equilibrium quality because of the higher heat flux, so that the formation of a large bubble becomes difficult. Consequently, the upper velocity limitation of the geysering occurrence becomes lower with an increase in inlet subcooling. Bubbles are not easily coalesced in the heated section under subcooled conditions but are readily coalesced in non-heated section of parallel boiling channels. Consequently geysering becomes more unstable with an increase in non-heated length.

The driving mechanisms of in-phase natural circulation oscillation were investigated in parallel boiling channels under natural circulation conditions. It is induced by hydrostatic head fluctuation in a long vertical non-heated channel due to alternate flow of vapor and liquid while the vapor generation rate is insufficient and liquid phase was nearly saturated. The period of natural circulation oscillation is much longer than that of density wave instability and can be well correlated with the circulation rate. The amplitude of pressure drop oscillation in a non-heated vertical channel in the downstream to the heated section was well correlated with the amplitude of kinetic energy for the natural circulation rate. This fact proves that the in-phase natural circulation oscillation is induced by hydrostatic head fluctuation in the non-heated vertical riser.

In terms of the flow oscillation mode, the thermal hydraulic instabilities in vertical multi-combined channels under natural circulation conditions have been experimentally investigated. The multi-combined channels consist of two parts; a non-heated single channel section installed downstream and a heated parallel channels

section installed upstream. The flow oscillation modes at the parallel channels section could be roughly classified into three different types according to the length ratio of each channel. The in-phase flow oscillation (such as natural circulation oscillation) was frequently induced when the single channel was longer than the parallel channels. On the other hand, the out-of-phase flow oscillations (such as geysering and density wave oscillation) were dominantly induced when the parallel channels were longer than the single channel. Especially in case that length of the single section was almost equal to that of the parallel section, the intermediate-phase flow oscillation was induced. The intermediate-phase flow oscillation was basically the out-of-phase flow oscillation due to the pressure fluctuation in the parallel channels, but the range of the flow oscillation periodically increased or decreased in a certain width due to the hydrostatic head fluctuation in the single channel.

### 3. Gas Leakage Rate from Transportation Cask of Radioactive Materials<sup>[11]-[13]</sup>

A sealing function is essential for transportation casks of radioactive materials in order to prevent radioactive materials from being released into the environment. In the safety analysis report, the release rate of radioactive materials into the environment was evaluated by using the method specified in ANSI N14.5. However, there were still problems of the evaluation method, so that leakage rate from very narrow tubes and orifices were investigated experimentally using helium gas to obtain fundamental data for choked flow, non-choked free expansion flow and laminar flow with gas expansion. An evaluation method of leakage rate of  $10^{-4}$  to  $0.5\text{cm}^3/\text{s}$  was developed. A simplified evaluation method was proposed for the leakage rate of  $10^{-4}$  to  $10^{-2}\text{cm}^3/\text{s}$  related closely to the sealing performance of the cask. The points, to which attention should be paid for using correlations specified ANSI N14.5, were discussed.

Gas leakage rates from a very narrow orifice and a capillary tube simulating a leak path were investigated experimentally using helium, argon, nitrogen and air as working fluids in order to understand hydrodynamics of choked flow, non-choked free expansion flow and laminar flow in a very narrow leak path. The contraction coefficient of choked flow from very narrow orifices was obtained. An evaluation model of gas leakage rate from capillary tubes was proposed, in which the acceleration loss in the entrance region, friction loss in laminar flow with gas expansion effect and exit loss for choked flow or non-choked free expansion flow were modeled. As for gas leakage rate of  $10^{-4}$  to  $10^{-2}\text{cm}^3/\text{s}$ , the proposed simplified evaluation method was verified for various gases.

The leak path of scratch on the O-ring surface cannot be regarded as a circular tube, but it can be evaluated by approximate evaluation method by a circular tube proposed in ANSI N14.5, provided that  $D^4/a$  is used for the characteristics of the leak path:  $D$  means leak path diameter and  $a$  does its length. Provided that no defect is detected on the O-ring surface by visual inspection, the

gas leakage from the O-ring surface with an elastomeric O-ring is less than  $10^{-4}\text{cm}^3/\text{s}$  which is two figures less than the criteria specified in its safety analysis report. When leak path diameter is evaluated, it is appropriate to use the width of O-ring groove as the leak path length for elastomer O-ring. The simplified evaluation method can be applied to multi-leak paths as long as their characteristic value  $D^4/a$  defined as the summation of each leak path is applied. Moreover, the gas leakage rate from multi-leak path under operation condition with different from testing ones can also be evaluated using the characteristic value  $D^4/a$ .

## 4. Flow Characteristics of Bubbly Flow

### 4.1 Measurements of Bubbly Flow Using Ultrasonic Velocity Profile Monitor<sup>[14]-[18]</sup>

The measurement system, combining an ultrasonic velocity profile monitor with a video data processing unit, was developed to clarify its multi-dimensional flow characteristics and to offer a data base to validate numerical codes for multi-dimensional two-phase flow. The system can measure simultaneously velocity profile in both gas and liquid phases and void fraction profile for bubbly flow in a channel, an average bubble diameter and void fraction. The developed measurement system was applied to measure flow characteristics of a bubbly countercurrent flow in a vertical rectangular channel to verify the capability, where bubbles flow upward and water downward.

The measurement system was applied to fully developed bubbly countercurrent flows in a vertical rectangular channel. Both bubble and water velocity profiles and void fraction profiles were investigated statistically. Turbulence intensity profiles in a continuous liquid phase was defined as a standard deviation of velocity fluctuation, and the two-phase multiplier profile of turbulence intensity in the channel was clarified as a ratio of the standard deviation of flow fluctuation in a bubbly countercurrent flow to that in water single phase flow. Water downward velocities become higher with leaving the wall but bubble rising velocities decrease because of higher water velocities. The relative velocities between both phases are scarcely varied in the channel. Void fraction profiles are almost constant except for those near wall. The turbulence intensity is greater than that in liquid single phase flows and increased with going toward the center of the channel from the wall. The distribution parameter and drift velocity used in the drift flux model for bubbly countercurrent flow were calculated from the obtained velocity profiles of both phases and void fraction profile. The distribution parameter is 1.0 and the drift velocity is the same value as proposed for bubbly upflows by Zuber and Findlay.

The developed measurement system was applied to fully developed bubbly cocurrent flows in a vertical rectangular channel. Both bubble and water velocity profiles and void fraction profiles were investigated statistically. In both concurrent and countercurrent flows, the relative velocities are almost constant at every point in

the channel because the bubble rise velocity is induced by the balance of the buoyancy and the interfacial drag force. The void fraction profiles of bubbly cocurrent flows are different from those of bubbly countercurrent flows. Void fraction profiles of bubbly concurrent flows decrease near the center of channel at low void fraction (the saddle-type distribution), but they show the maximum value in the center at high void fraction (the mountain-type distribution). The two-phase multiplier profiles of turbulence intensity were examined and the results were compared with those in bubbly countercurrent flows. Under conditions where the saddle-type void fraction profile appears in bubbly cocurrent flows, the turbulence intensity near the wall is lower than that in water single phase flows. On the other hand, under conditions where the mountain-type void fraction profile appears in bubbly cocurrent flows, turbulence intensity in the channel is larger than that in water single phase flows. Concerning the drift flux model, the distribution parameter and drift velocity were obtained directly from both bubble and water velocity profiles and void fraction profiles, and their results were compared with those in bubbly countercurrent flows. The distribution parameter is 1.0 in both bubbly concurrent and countercurrent flows, and the drift velocities are almost the same value as proposed Zuber and Findlay.

The flow structure around a bubble was studied experimentally in air-water countercurrent bubbly flow whose void fraction was smaller than 7%. The bubble Reynolds number was ranged between 700 and 1000. Most bubbles had an ellipsoidal shape and rose up with wobbling motions. The experimental results plotted in the form of non-dimensional velocity profiles show that the velocity field around a bubble has a structure similar to the turbulent boundary layer on a solid wall. On the other hand, an earlier analytical study by Moore used an assumption of a spherical bubble rising in liquid irrotationally, and the solution was derived that the flow around a bubble being composed of a thin boundary layer and its outer main stream in potential flow. Moore's theoretical analysis can be applied only to bubbly Reynolds number from 10 to 50-200. In this range the boundary layer around a bubble is considered to be laminar. When a bubble is influenced by the wake of the leading bubbles, the flow is highly agitated by the vortex shed from the rear part of the leading bubbles. As a result, the flow transition from laminar to turbulence can take place under the condition of low bubble Reynolds number. As the value becomes much larger than 1000, the velocity profile in the boundary layer surrounding a bubble shows a good agreement with the one for turbulent boundary layer. When a bubble rises up in liquid without the influence of the leading bubbles, the flow in boundary layer remains until bubble Reynolds number becomes larger than 1000.

The experiments were carried out for air-water bubbly flows in a 20mm × 100mm vertical channel having a void fraction smaller than 3%. Two ultrasonic transducers were installed on the outer surface of the test channel with a

contact angle of 45° off the vertical axis, one facing upward and the other facing downward. By applying statistical methods to the two directional velocity profiles, Reynolds stress profiles were calculated. Furthermore, to clarify the wake effect induced by the leading bubbles, the velocity profiles are divided into two types of data. The first one is for all of the liquid data and the other is the data which does not include the wake effect. For  $Re_1 \leq 1,593$ , it was observed that the bubbles suppressed the liquid turbulence. Furthermore, comparing with the Reynolds stress profiles in bubbly flows, it was found that Reynolds stress profiles varied with the amount of bubbles present in the flow and the effect of wake causes turbulence in the liquid.

#### 4.2 Measurements of Bubbly Flows Using Wire-Mesh Tomography<sup>[19]-[22]</sup>

A wire-mesh sensor, which is based on local conductivity measurement, was applied to studies on the characteristics of bubbly flow in a rectangular channel (20mm × 100mm). Special design of the sensor allowed the measurement of the local instantaneous true gas velocity besides the measurement of the local instantaneous void fraction. Data processing method for an electrode-mesh sensor was proposed. A cluster-algorithm was proposed for the evaluation of bubble size distribution and volume flow reconstruction. The validity of this algorithm for spatial field reconstruction was benchmarked by theoretical considerations as well as comparison of the calculated with alternatively measured data. Good agreement was stated. The achieved information was used to obtain plots showing the bubble/slug velocity (up to the second statistical momentum) depending on the spherical-equivalent bubble diameter. This information was measured inside a transient bubble flow with void fraction of up to 20%. Occurring phenomena are explained by presented Fourier spectra of the cross-sectional averaged void fraction and the gas volume flow. The qualitative disturbance of the flow by the electrode wires was considered.

The applied sensor scan the local void fraction distribution in two parallel planes, separated 1.5mm in flow direction, with a resolution of 6.1mm × 2.2mm and an overall sampling rate of 1200 Hz (all 256 points). Extensive data processing method was developed that offers the possibility to evaluate the local instantaneous void fraction, bubble rising velocity and bubble volume as well as their time and cross-sectional averaged values. These averages were used to conclude on the local distribution of the superficial gas velocity. The proposed algorithms were applied to bubble flow. Accuracy in the prediction of void fraction was found within 5% by comparison with video data processing unit supplied data. The reconstructed volume flow showed uncertainties in the order to up to 10% for true gas velocities lower 300mm/s and up to 30% above. The approximate shapes of bubbles have been reconstructed. The gas volume flow through the sensor evaluated was compared with

measurements by a laminar flow meter.

To investigate the accuracy of wire mesh tomography (WMT) for measurement of gas liquid flows, the experimental study focused on its intrusive feature has been carried out. The WMT principle is based on the dependency upon electrical conductivity on the local void fraction. The applied wire mesh sensor consisted of two measuring planes. Each plane had  $8 \times 32$  crossing points with spatial resolution of  $2.22\text{mm} \times 3.03\text{mm}$  and wire diameter of  $0.125\text{mm}$ . The measurements were compared with the results obtained by an image data processing unit. For bubbly flows, the low gas intensity zone (the saddle-type void fraction distribution) is characterized by the deceleration, while the high gas intensity zone (the mountain-type distribution) is characterized by the deformation. The disturbance level on both bubble motion and deformation is reduced for bubbly-slug transition. Although the sensor caused large bubble deceleration (40-50%) at low gas intensity, it is supposed to be reduced for high gas intensity. The sensor did not affect the upstream flow within the spatial resolution ( $2\delta$ ) and gas velocity is recovered after  $4-8\delta$  downstream from the sensor.

The developing characteristics of upward air-water flow were studied for non-symmetric initial condition in a vertical tube of  $50\text{mm}$  diameter. Wire mesh sensor was utilized to obtain the local characteristics of gas phase such as void fraction, gas velocity and bubble size. To generate the non-symmetric initial flow condition, air was supplied from a single injection hole and mixed into the liquid flow inside the pipe through a narrow -ring shaped exit. In this case, large bubble could be generated at the inlet. In this experiment, the characteristics of bubble formation at the inlet and flow evolution along the channel were emphasized. The results showed the capability of the measurement technique to analyze the non-symmetric distribution of the gas phase. The effects of superficial gas and liquid velocity on the bubble distributions and on the local void fraction spreading at the inlet were clarified. The flow evolution dominated by bubble coalescence and break up is discussed in term of the development of Sauter mean diameter over the cross-section of the pipe. The results also showed inconsistency with uniform flow conditions at low gas flux. Hence, the effect of phase distribution spreading was proposed. The development of rising gas velocity in term of mean bubble size during coalescence and break up was revealed.

##### 5. Decontamination of Contaminated Water with Flocculating and Settling Technology<sup>[23]-[25]</sup>

My group had revealed from a chemical analysis of the turbid water in cutting asphalt pavement surface that its water contains not only high in suspended solids but also high in hydrogen-ion concentration (pH) level and in the volume of normal-hexane extracts, and that the carcinogenic polycyclic aromatic hydrocarbon (PAH) is contained in it. Therefore, the treatment technology to prevent the turbid water from being discharged into sewages was initially developed. The flocculants to make

flocculate and set suspended solids and to make them liquid-solid separating were developed. As the result, the flocculating and settling technology was established through these processes, which can control pH, shift substances of normal-hexane extracts and PAH from the turbid water to the aggregation and sedimentation.<sup>[26]</sup>

The development of a stationary purification system of the turbid water was initiated in order to make expansion of the processing capacity. At the time when almost of all the construction of the system was completed, Fukushima Dai-ichi Nuclear Power Plant (NPP) accidents occurred. For the purpose of supplying agricultural water, a stationary purification system of the turbid water had been improved to purify contaminated water. Two kinds of flocculants had been developed on the basis of preliminary tests: One compounds iron ferrocyanide and the other does not. With use of this system and flocculants, a demonstration test was conducted to apply the decontamination technology on contaminated water in two swimming pools in an elementary school located at Motomiya City, Fukushima Prefecture. It was proved from the results that both the developed purification system and flocculants were established as the practicable decontamination technology of the contaminated water: The treatment rate was  $10\text{m}^3/\text{h}$  and the elimination factor of radioactive materials was higher than 99%.

It was clarified from the results that ionized cesium (Cs) rarely exists in the stagnant water in pools, ponds, lakes and so on at the time when nine months passed since Fukushima Dai-ichi nuclear power plant accidents. It is necessary to use the flocculants compounding iron ferrocyanide in the case where ionized Cs exists in water. From the above-mentioned results, the following problems were pointed out: One problem was cyanide dissolution in the purified water and the other one was the dissolution from the dehydration sludge.

For the purpose of decontaminating residential buildings, roads, rubble, and so on, the high-pressure water washing decontamination system was developed, which were composed of a recovery system for contaminated washing water and mobile purification system of liquid-solid settling technology by flocculants. The high-pressure washing technology applied in this demonstration test can be used for both high- and ultrahigh-pressure washing decontamination and water surface chipping, by changing pumps and attachments. These systems were applied to decontaminate pools, concrete floor and side ditch around the pool in an elementary school located at Motomiya City, Fukushima Prefecture as a demonstration test. Additionally, to compare decontamination effects, the tests, to chip and decontaminate surfaces of outer concrete and asphalt pavement had been conducted. From the results, high-pressure water jet decontamination systems have been practically proven.

The high-performance mobile purification units of contaminated water which was capable for carrying with trucks were developed, and the demonstration test was performed in Minami-soma City, Fukushima Prefecture to

purify the contaminated water in a pond and generated by the high-pressure water washing in a Public Hall. It was made clear from the test results that the dehydration sludge separated by liquid-solid settling of the contaminated water of around 1,000Bq/l became a high radionuclide concentration of about 185,000Bq/kg.

## Reference

- [1] Masanori ARITOMI, Shigebumi AOKI and Akira INOUE: Instability in Parallel Channel of Forced-Convection Boiling Upflow System, (I) Mathematical Model; *Journal of Nuclear Science and Technology*, Vol.14, No.1 (1977) pp.22-30.
- [2] Masanori ARITOMI, Shigebumi AOKI and Akira INOUE, Instability in Parallel Channel of Forced-Convection Boiling Upflow System, (II) Experimental Results, *Journal of Nuclear Science and Technology*, Vol.14, No.2 (1977) pp.88-96.
- [3] Masanori ARITOMI, Shigebumi AOKI and Akira INOUE, Instability in Parallel Channel of Forced-Convection Boiling Upflow System, (III) System with Different Flow Conditions between Two Channels, *Journal of Nuclear Science and Technology*, Vol.16, No.5 (1979) pp.343-355.
- [4] Masanori ARITOMI, Shigebumi AOKI and Akira INOUE, Instability in Parallel Channel of Forced-Convection Boiling Upflow System, (IV) Instabilities in Multi-Channel System and with Boiling Downcomer, *Journal of Nuclear Science and Technology*, Vol.18, No.5 (1981) pp.329-340.
- [5] Masanori ARITOMI, Shigebumi AOKI and Akira INOUE, Instability in Parallel Channel of Forced-Convection Boiling Upflow System, (V) Consideration of Density Wave Instability, *Journal of Nuclear Science and Technology*, Vol.20, No.4 (1983) pp.286-301.
- [6] Masanori ARITOMI, Akira INOUE and Hiroshi ISHIDA, Thermo-hydraulic Instability due to a Blockage of Flow by Vapor in a Boiling Two-phase Flow System (Experimental Results Concerning the Mechanism), *JSME International Journal*, Vol.30, No.260 (1987) pp.296-302.
- [7] Masanori ARITOMI, Jing Hsien CHIANG, Tohru NAKAHASHI, Masumi WATARU and Michitsugu MORI, Fundamental Study on Thermo-Hydraulics during Start-Up in Natural Circulation Boiling Water Reactors, (I) Thermo-Hydraulic Instabilities, *Journal of Nuclear Science and Technology*, Vol.29, No.7 (1992) pp.631-641.
- [8] Masanori ARITOMI, Jing Hsien CHIANG and Michitsugu MORI, Fundamental studies on Safety-Related Thermo-Hydraulics of Natural Circulation Boiling Parallel Channel Flow Systems under Startup Conditions (Mechanism of Geysering in Parallel Channels), *Nuclear Safety*, Vol.33, No.2 (1992) 170-182.
- [9] Jing Hsien CHIANG, Masanori ARITOMI and Michitsugu MORI, Fundamental Study on Thermo-Hydraulics during Start-Up in Natural Circulation Boiling Water Reactors, (II) Natural Circulation Oscillation Induced by Hydrostatic Head Fluctuation, *Journal of Nuclear Science and Technology*, Vol.30, No.3 (1993) pp.203-211.
- [10] Noriyuki WATANABE, Masanori ARITOMI and Hiroshige KIKURA, Thermal Hydraulic Flow Oscillation Characteristics in Multifurcated Channels under Natural Circulation and Low-Pressure Conditions, *Journal of Nuclear Science and Technology*, Vol.45, No. 2 (2008) pp.160-170.
- [11] Masanori ARITOMI, Ninghau Li, Tsuyoshi Noura, Michio YOKOZEKI, Ryouji ASANO and Nagao NIYOMURA, Evaluation Method of Gas Leakage Rate from Transportation Casks of Radioactive Materials, *Journal of Nuclear Science and Technology*, Vol.30, No.10 (1993) pp.991-1000.
- [12] Masanori ARITOMI, Ninghau LI, Ryouji ASANO and Hiroyuki ASANO, Evaluation Method of Gas Leakage Rate from Transportation Casks of Radioactive Materials, (II) Effect of Kinds of Gases on Leakage Rate, *Journal of Nuclear Science and Technology*, Vol.31, No.4 (1994) pp.264-273.
- [13] Masanori Aritomi, Ryouji Asano, Ninghau Li and Tsunemichi Kawa, Evaluation Method of Gas Leakage Rate from Transportation Casks of Radioactive Materials (Gas Leakage Rates from Scratches on O-ring Surface), *Nuclear of Science Journal*, Vol.32, No.1 (1995) pp.1-9.
- [14] Masanori ARITOMI, Shirong ZHOU, Makoto NAKAJIMA, Yasushi TAKEDA, Michitsugu MORI and Yuzuru YOSHIOKA, Measurement System of Bubbly Flow Using Ultrasonic Velocity Profile Monitor and Video Data Processing Unit, *Journal Nuclear of Science and Technology*, Vol.33, No.12 (1996) pp.915-923.
- [15] Masanori ARITOMI, Shirong ZHOU, Makoto NAKAJIMA, Yasushi TAKEDA and Michitsugu MORI, Measurement System of Bubbly Flow Using Ultrasonic Velocity Profile Monitor and Video Data Processing Unit, (II) Flow Characteristics of Bubbly Countercurrent Flow, *Journal of Nuclear Science and Technology*, Vol.34, No.8 (1997) pp.783-791.
- [16] Shirong ZHOU, Yumiko SUZUKI, Masanori ARITOMI, Mitsuo MATSUZAKI, Yasushi TAKEDA and Michitsugu MORI, Measurement System of Bubbly Flow Using Ultrasonic Velocity Profile Monitor and Video Data Processing Unit, (III) Comparison of Flow Characteristics between Bubbly Concurrent and Countercurrent Flows, *Journal of Nuclear Science and Technology*, Vol.35, No.5 (1998) pp.335-343.
- [17] Yumiko Suzuki, Masamichi Nakahawa, Masanori Aritomi, Hideki Murakawa, Hiroshige Kikura and Michitsugu Mori, Microstructure of the Flow Field around a Bubble in Counter-current Bubbly Flow, *Experimental Thermal and Fluid Science* Vol.26 Nos.2-4 (2002) 221-227.
- [18] Hideki MURAKAWA, Hiroshige KIKURA and Masanori ARITOMI, Measurement of Liquid Turbulent Structure in Bubbly Flow at Low Void Fraction Using Ultrasonic Doppler Method, *Journal of Nuclear Science and Technology*, Vol.40, No.9 (2003) pp.644-654.
- [19] S. Richter, M. Aritomi, H. -M. Prasser and R. Hampel, Approach towards spatial phase reconstruction in transient bubbly flow using a wire-mesh sensor, *International Journal of Heat and Mass Transfer*, Vol.45 (2002) pp.1063-1075.
- [20] Steffen RICHTER and Masanori ARITOMI, A New Electrode-mesh Tomograph for Advanced Studies on Bubbly Flow Characteristics, *JSME International Journal, Series B*, Vol.45, No.2 (2002) pp.565-576.
- [21] Weerin WANGJIRANIRAN, Yuichi MOTEGI, Steffen RICHTER, Hiroshige KIKURA, Masanori ARITOMI and Kazuhiko YAMAMOTO, Intrusive Effect of Wire Mesh Tomography on Gas-liquid Flow Measurement, *Journal of Nuclear Science and Technology*, Vol.40, No.11 (2003) pp.932-940.

- [22] W. Wangjiraniran, M. Aritomi, H. Kikura, Y. Motegi and H. –M. Prasser, A study of non-symmetric air water flow using wire mesh sensor, *Experimental Thermal and Fluid Science* Vol.**29** (2005) pp.315-322.
- [23] Masanori Aritomi, Toshihiro Adachi, Shigeki Hosobuchi and Noriyuki Watanabe, Decontamination technology of contaminated water with flocculating and settling technology, *Journal of Power and Energy Systems*, Vol.**6**, No.3 (2012) 412-422.
- [24] Masanori Aritomi, Akihiro Tagawa, Toshihiro Adachi, Shigeki Hosobuchi, Noriyuki Watanabe and Yasuhiro Fujita, *Journal of Nuclear Science and Technology*, Vol.**50**, No.1 (2013) to be published.
- [25] Masanori Aritomi, Akihiro Tagawa, Toshihiro Adachi, Shigeki Hosobuchi, Noriyuki Watanabe and Junko Takanashi, *Journal of Nuclear Science and Technology*, Vol.**50** (2013) to be published.
- [26] J. Takanashi, S. Hosobuchi and M. Aritomi, Study on water treatment system for cutting asphalt road (1st Report, Development of water treatment system for cutting asphalt road), *Trans. JSME, Series B*, Vol.**75**, No.760, (2009) pp.2504-2510. (in Japanese)

## I.2 In the Quest for Energy Development -Starting with the development of nuclear fusion and ending with the proposal for power problem solution-

Ryuichi SHIMADA

### 1. Preface

I am greatly honored for the opportunity to review my research for 25 years in this article. My career summary and my presented papers are listed at the end of this article. Here, I describe the summary of my research investigations.

### 2. Development of the fusion test facility, JT-60 (from 1975 to 1988)

The Breakeven Plasma Test Facility (later named JT-60) shown in Fig.1 was a national project at the time when Japan was enjoying its rapid economic growth. The project took 10 years to develop, and the JT-60 facility was constructed at a total production cost of 200 billion. Out of this total cost, the power supply unit, where I was mainly involved with, costs 33 billion. Thereafter, the operation and experiments, which spanned 25 years, cost 400 billion. Thus, the total cost of this national project went as much as 600 billion. As the first step in nuclear fusion development, the JT-60 project achieved a critical plasma condition, thereby gaining prominent recognition from all over the world. The technical success of the JT-60 project was followed by the International Thermonuclear Experimental Reactor project. The operation of the JT-60 facility lasted for 25 years and was completed without causing any serious accident. In 2010, the JT-60 project was awarded the “One step on Electro-Technology—Looking Back to the Future—” from the Institute of Electrical Engineers of Japan. This award delighted me the most.

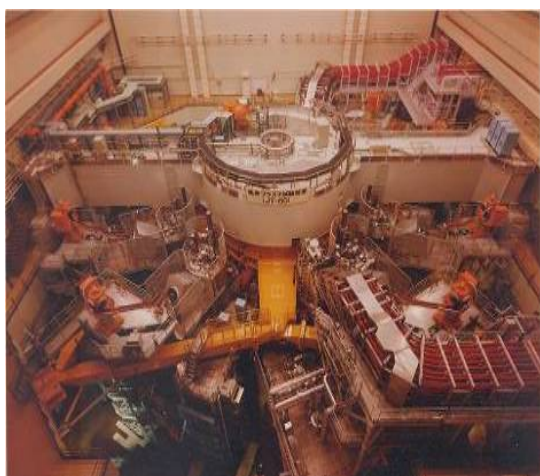


Fig. 1 Breakeven Plasma Test Facility (JT-60)

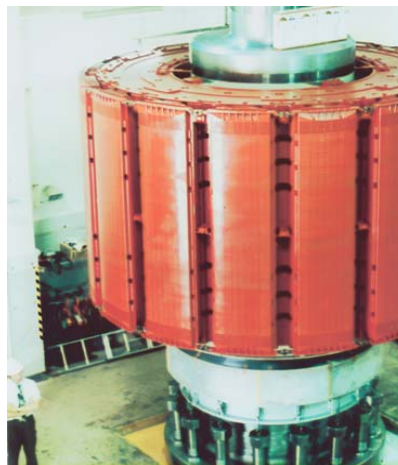


Fig. 2 Construction site of the flywheel generator

Figure 2 shows the construction site of the world's largest JT-60 flywheel generator. The person at the lower part of the figure is the author. This generator was the basis of the Flywheel Frequency Stabilizer Rotary Energy Storage (ROTRES), constructed by the Okinawa Electric Power Company, Inc. in 1995. At present, this power storage technology is the most important development item. ROTRES receives attention because it is effective in stabilizing the power fluctuation of the wind-power generation system.

### 3. Development of the power storage technologies

The most expected result among the energy technologies is the power storage technology, although its realization is quite difficult. The flywheel generator shown in Fig. 2, which was developed for nuclear fusion, is the largest in the world, and its charge/discharge energy can reach as much as 4 GJ. The power-saving effect of the flywheel generator was demonstrated to be two times the construction cost. The flywheel generator has become indispensable in stabilizing the power systems for renewable energy, projected to achieve widespread use in the future. This prediction is based on its operation records achieved in Okinawa for more than 10 years.

I developed a force-free coil, which was once the dream of electromagnet engineers, with knowledge learned from my participation in the research on the equilibrium and stability control of tokamak plasma. The coil thus developed is the force-balanced coil used in the superconducting magnetic energy storage (SMES) system.

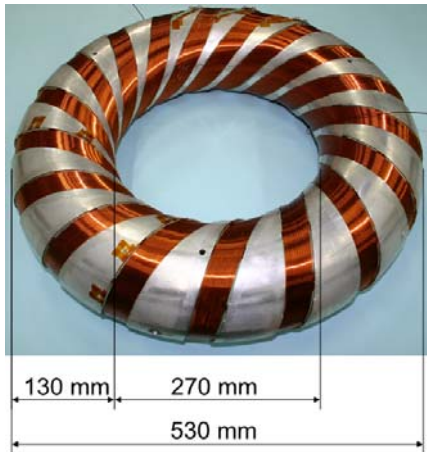


Fig. 3 6.3T superconducting coil

When a coil that simulates the current trajectory in a tokamak plasma is formed by a superconductive electric wire, the coil current does not induce an electromagnetic force on the coil frame. This coil can eliminate the need for bedrock to support large SMESs, which may cause technical problems. Accordingly, the support structure is downsized to reduce the weight to be cooled and heat penetration, thereby producing a low-cost, high-performance superconductive coil. The theory was actually tested by students who conducted an experiment with a hand-rolled coil, using a few thousand liters of liquid helium. Finally, they succeeded in generating a strong magnetic field of as much as 6.3 T (shown in Fig. 3). Thus, the correctness of the theory was verified. Because the size of the test equipment is 1/10 of the actual unit, we can estimate that the possible power storage amounts to 60 MWh if 4,000 coils are set up. This amount of stored power can sufficiently supply the total 24-h power consumption in a section of an area in Tokyo, such as the Odaiba district.



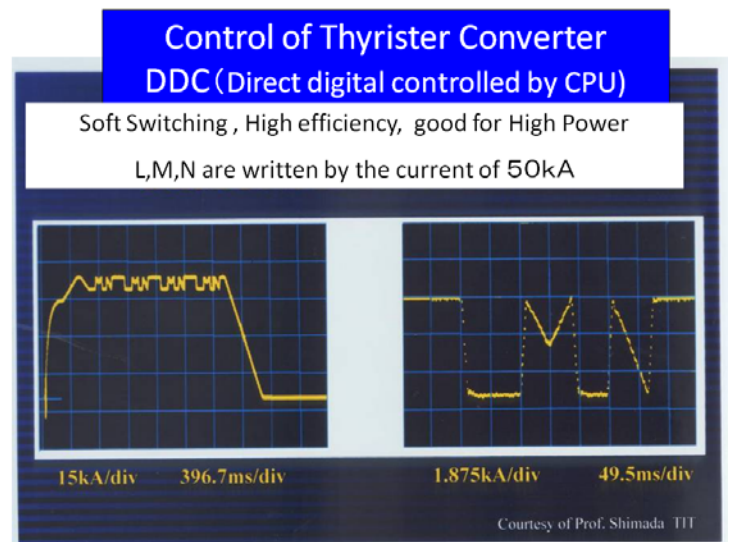
Fig. 4 Fabrication of the superconductive coil by the students



Fig. 5 Illustration of the SMES located in the Odaiba district in Tokyo

4. Development of the power conversion technologies

The fusion test facility JT-60 excited the huge electromagnetic coil using a thyristor converter with a maximum power of 100 MW and controlled the plasma using the generated magnetic fields. The thyristor power conversion was performed using the coil current digitally controlled by a microcomputer. Its control accuracy is well known to be of such a high degree that the alphabetical characters “L,” “M,” and “N” could be written by the current waveforms.



This current control technology is based on the current-type power conversion. The concept underlying this technology was developed by the author, who transferred to the Tokyo Institute of Technology. My colleagues and I employed this concept to develop the Magnetic Energy Recovery Switch (MERS) and, subsequently, a series power control conversion, which leads to its evolution as an ideal current switch.

MERS accumulates magnetic energy in the switch without disposing energy and releases it into the load, allowing the switch to be flipped to ON/OFF without losing energy. In addition, it can inject a voltage into the reactance. It can be widely applied from large-scale fields (such as in electric power transmission, where it allows increase in the electric energy carried by transmission lines by lowering the reactance, and in wind-power generators, where it allows efficient conversion of the wind power to electric power) to small-scale areas (such as light modulation for fluorescent/mercury lamps).

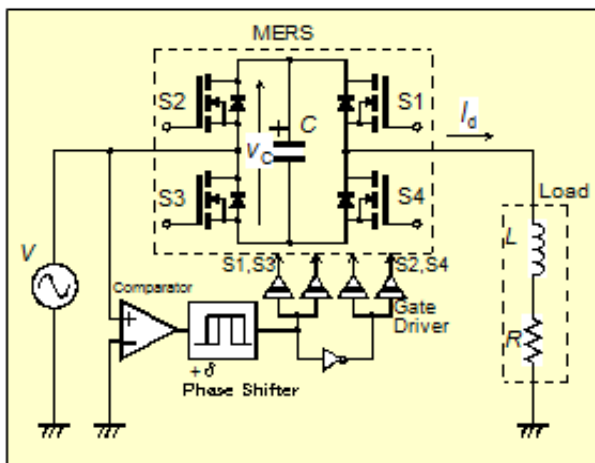
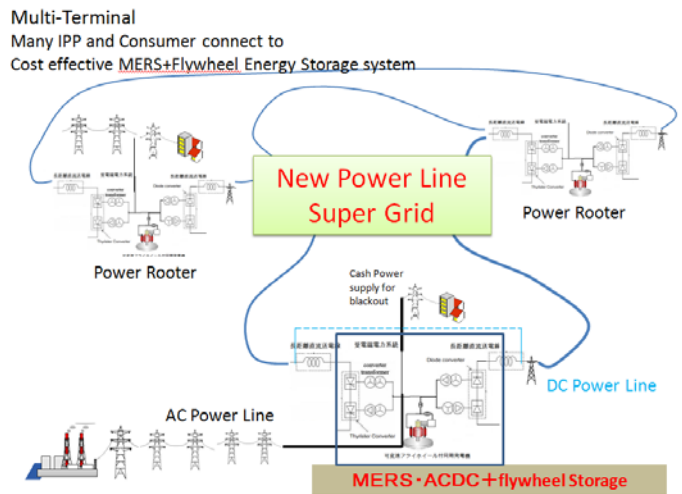


Fig. 6 AC control switch, MERS

The JT-60 thyristor converter is a prototype of the high-voltage direct current (HVDC) electric power transmission system. It is developed into a new main line for power transmission, which can be distributed throughout Japan. This concept is a 21<sup>st</sup> century-specific proposal to resolve the 50/60-Hz frequency-assignment problem of Japan's power system, to provide uninterrupted power supply, and to deal with the output-power fluctuation of renewable energy.

**5. Global electric network (GELNET)**

GELNET is an HVDC multi-terminal voltage source grid composed of a set of dispersively arranged SMESs. It is the main artery of the energy transmission that traverses the Japanese islands, that is, a new main line of supergrid transmission network that runs through Japan. Further, this network will be linked to the networks of the countries in other continents using submarine cables, thereby evolving into a GELNET.



The power plan needed for post-quake reconstruction is not to unify the frequencies of the AC power in Japan (50/60 Hz) but to realize a Japan-island-traversing supergrid transmission network ahead of the other countries in the world. This supergrid transmission network is based on the concept that a large wide-area electric power interchange should comprise DC interconnection and short-distance local networks composed of 50/60-Hz AC transmission lines.

GELNET is the goal of this concept. GELNET fulfills the ideal that “humans can live happily and peacefully anywhere on Earth if they can use 100 W of electricity,” which is the aim of the Tokyo Technology Solution Research Institute organized by the Tokyo Institute of Technology. Figure 7 is obtained by superposing the images of the Earth at night, taken from the outer space. This figure shows that the peaceful regions are bright, although they are obscure.

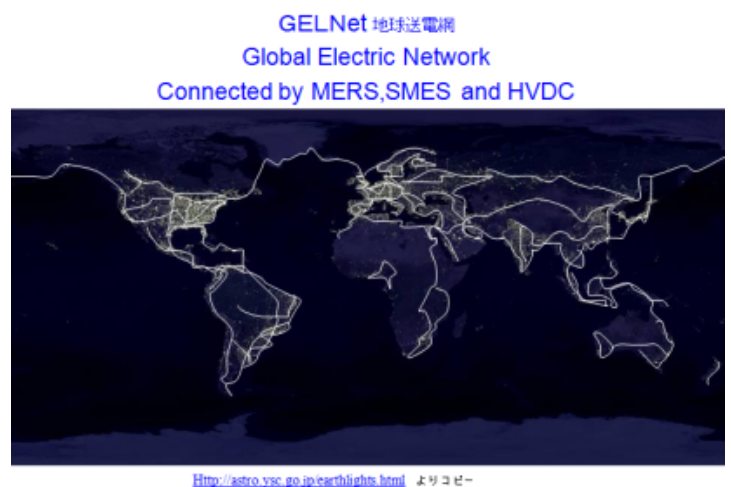


Fig. 7 Earth view at night and GELNET

A supergrid plan has already been proposed in Europe, as well as in Africa and in North and South America. In Asia, however, it has not yet been proposed. Hence, Japan prepares the supergrid plans for Asia.

Because Japanese lived in a stable-electricity environment, most of them might consider that the electric stability they experienced is a world standard. When I went to India, I experienced a peculiar situation where the electric power supply i.e., a 240-V-specific wall outlet, supplied 180 V during the day and 300 V at night. At midnight, I observed a bright electric lamp that lit darkly under normal conditions. Further, when the voltage dropped, fluorescent and mercury lamps did not light satisfactorily. Because a 2-h power outage occurs daily, expensive apartments and offices have engine generators ready. Currently, the living condition would be much better if stable electricity is always available. The practical problems of electricity and energy supply and the solution scheme for these problems in Asia are summarized as follows:

- Even in these days in the 21<sup>st</sup> century, billions of Asians still do not benefit from electricity.
- Because not enough petroleum energy is available in Asia, new energy resources such as renewable energy must be explored.
- Although bio, wind power, ocean, and solar energies cannot supply enough power densities and are dispersed, these energy resources offer such advantages as providing employment when used in under-populated areas.
- AC power is suitable for local-area transmission, and DC power is appropriate for long-range transmission.
- GELNET can level out the power demand and price.
- Addressing the ecological concern, energy saving, effective energy utilization, and energy generation should be carried out.

Considering the current energy problems in the world and the global warming countermeasures, Japan could contribute considerably using energy saving, superconductivity, and power electronic technologies. The most particularly important item is to consider the actions that could contribute in efficiency.

## 6. Conclusion

In retrospect, all my research fields involved problems associated with energy development. In particular, regarding problems concerning magnetic energy, my research started with the magnetically confined plasma for the development of nuclear fusion, continued with the reactance problems for power transmission line, and finally extended to the proposal for the near-future electric power system.

I was truly happy that I was able to conduct such a wide range of research field and discuss the near-future electric power system, even today, while clinging to my ideals. It was the free research environment provided by

the university that allowed me to conduct a various research activities. In conclusion, I would like to express my gratitude again to all the concerned persons who have helped me materialize my dreams.

## Brief of my career summary and presented papers.

Ryuichi Shimada was born in 1948 in Tochigi, Japan. He received the B.E.E and M.S.E.E degrees from Tokyo Institute of Technology, Tokyo, JAPAN in 1970 and 1972, respectively, and the Doctor degree of Engineering in electrical engineering from Tokyo Institute of Technology, Tokyo, Japan in 1975.

From 1975 to 1988, he was a researcher of Nuclear Fusion development and especially, an Electrical Engineer in the Japan Atomic Energy Research Institute, Tokaimura, Ibaraki, Japan. He developed the world largest Tokamak type Fusion Experimental machine, JT-60. He was a group leader of the power supplies development of JT-60. In 1986, He was a responsible director of JT-60 Operation and Experiment. In 1988, he became an associate professor of Department of Electrical Electronics Engineering at Tokyo Institute of Technology, Tokyo, Japan. In 1990, He became a professor and joined the Research Lab. For Nuclear Reactors, Tokyo Institute of Technology, where he is presently a professor of System and Safety Engineering division of Laboratory. From 2005, he is now professor of the Integrated Research Institute, Solutions Research Division, Earth Solutions Research Group, Tokyo Institute of Technology.

Prof. Shimada has received the 1985 Outstanding Achievement Award from IEE of Japan, the 1976 and 2000 Outstanding Paper Award from IEE of Japan. Recently, he has received the 2003 Excellent Published Book Award from IEE of Japan.

## Main presented papers

- Jan Arild Wiik, Fransisco Danang Wijaya and Ryuichi Shimada: Characteristics of the Magnetic Energy Recovery Switch (MERS) as a Series FACTS Controller; *IEEE Trans. on Power Delivery*, vol. **24**, no. 2, pp. 828-836, April 2009.
- S. Nomura, K. Kasuya, N. Tanaka, K. Tsuboi, H. Tsutsui, S. Tsuji-Iio, R. Shimada: Experimental Results of a 7-T Force-Balanced Helical Coil for Large-Scale SMES; *IEEE Transactions on Applied Superconductivity*, vol. **18**, no. 2, pp. 701-704, June 2008.
- Jan. A. Wiik, Arkadiusz Kulka, Takanori Isobe, Kazuhiro Usuki, Marta Molinas, Taku Takaku, Tore Undeland and Ryuichi Shimada: Loss and Rating Considerations of a Wind Energy Conversion System with Reactive Compensation by Magnetic Energy Recovery Switch (MERS); *EPE Journal*, vol. **18**, no. 3, pp. 25-30, September 2008.

- S. Nomura, K. Kasuya, N. Tanaka, H. Tsutsui, S. Tsuji-Iio, R. Shimada: Development of a One Tenth Sized Model Coil for 100-MJ Class SMES Using Force-Balanced Coil Concept; *IEEE Transactions on Applied Superconductivity*, vol. **17**, no. 2, pp. 1998-2001, June 2007.
- Taku Takaku, Takanori Isobe, Jun Narushima, Hiroaki Tsutsui, Ryuichi Shimada: Power Factor Correction Using Magnetic Energy Recovery Current Switches; *Electrical Engineering in Japan (English translation of Denki Gakkai Ronbunshi)*, vol. **160**, no. 3, pp. 56-62, August 2007.
- S. Nomura, H. Tsutsui, N. Watanabe, C. Suzuki, S. Kajita, Y. Ohata, T. Takaku, E. Koizumi, S. Tsuji-Iio, and R. Shimada,: Demonstration of the Stress-Minimized Force-Balanced Coil Concept for SMES; *IEEE Transactions on Applied Superconductivity*, vol. **13**, no.2, pp. 1852-1855, June 2003.
- S. Nomura, K. Yamagata, D. Ajiki, N. Watanabe, H. Ajikawa, S. Tsuji-Iio, R. Shimada, M. Kyouto, and Y. Sato: Construction of 320-kJ Superconducting Force-Balanced Coil; *IEEE Transactions on Applied Superconductivity*, vol. **10**, no.1, pp. 820-823, March 2000.
- Ryuichi Shimada et al.: JT-60 Power Supplies; *Fusion Engineering & Design*, 5, 1987.
- Ryuichi Shimada et al.: A 215MVA Flywheel Motor-Generator with 4GJ Discharge Energy for JT-60 Toroidal Field Coil power supply System; *IEEE Trans. Energy Conversion* Vol. **EC-2** pp. 2 1987.

## A.1 Difference in Rotational Temperatures between Neutral Molecules and Molecular Ions of Low-Pressure Microwave N<sub>2</sub> or O<sub>2</sub> Discharge Plasmas

Hiroshi AKATSUKA, Atsushi NEZU and Haruaki MATSUURA

For a microwave discharge nitrogen plasma with its discharge pressure about 1 Torr, we found that the rotational temperature  $T_r$  of the first negative system (1NS) of N<sub>2</sub><sup>+</sup> B <sup>2</sup>Σ<sub>u</sub><sup>+</sup> state is about 50 % times higher than that of the second positive system (2PS) of N<sub>2</sub> C <sup>3</sup>Π<sub>u</sub> state, as shown in Fig. 1 by OES measurement. For 2PS, we found  $0.07 \leq T_r [\text{eV}] \leq 0.15$ , which is considered to be reasonable as an approximate value to the gas translational temperature [1]. On the other hand, the rotational temperature of 1NS is higher than that of 2PS, found to be about 0.13 – 0.34 eV. It is considered that this is partly because most of the excited molecular ions are generated by the electron impact from the ground state of ion, not of neutral molecule, where the electron temperature ranges from 2 to 4 eV and the electron density from  $1 \times 10^{11}$  to  $1 \times 10^{12}$  cm<sup>-3</sup>. Therefore, under the present discharge conditions, the rotational temperature could have a component that is originated from the ions N<sub>2</sub><sup>+</sup>. It indicates that the rotational temperature of 1NS has some information on ion temperature if the rotational motion of ions is equilibrated with their translational motion.

Meanwhile, Fig. 2 shows that the rotational temperature of 1NS of O<sub>2</sub><sup>+</sup> b <sup>4</sup>Σ<sub>g</sub><sup>-</sup> state is almost the same as that of atmospheric absorption band (A-band) of O<sub>2</sub> b <sup>1</sup>Σ<sub>g</sub><sup>+</sup> state [2]. The electron temperature and density are almost the same with those of the nitrogen plasma. Consequently, we consider that O<sub>2</sub><sup>+</sup> b <sup>4</sup>Σ<sub>g</sub><sup>-</sup> state is mostly produced from the electron impact from the ground state (X state) of O<sub>2</sub><sup>+</sup> ion. However, the rotational temperature is almost the same with that of neutral O<sub>2</sub> b <sup>1</sup>Σ<sub>g</sub><sup>+</sup> state, which is quite different from N<sub>2</sub> plasma. Now we consider that the rotational temperature of the ground state of O<sub>2</sub><sup>+</sup> ion, that is, O<sub>2</sub><sup>+</sup> X <sup>2</sup>Σ<sub>g</sub><sup>+</sup> state should be much higher than that of the O<sub>2</sub><sup>+</sup> b <sup>4</sup>Σ<sub>g</sub><sup>-</sup> state due to the difference in the intermolecular distance  $R$ , where that of the b state  $R_b = 1.2797$  Å is much larger than

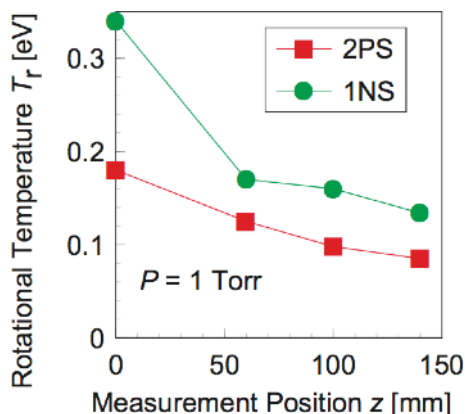


Fig. 1. Rotational temperature of 2PS band of N<sub>2</sub> and that of 1NS band of N<sub>2</sub><sup>+</sup> of N<sub>2</sub> plasma depicted in Ref. [1].

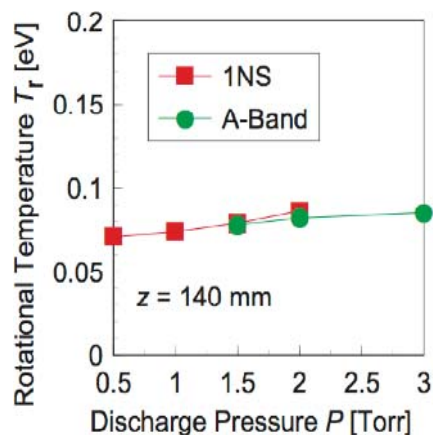


Fig. 2. Rotational temperature of A-band of O<sub>2</sub> and that of 1NS of O<sub>2</sub><sup>+</sup> of O<sub>2</sub> plasma in Ref. [2].

that of the ground state,  $R_X = 1.1171$  Å. The angular momentum of both X and b states are almost conserved before and after the electron impact excitation due to a small mass of an electron. Therefore, the rotational temperature of the X state  $T_r(X)$  of O<sub>2</sub><sup>+</sup> ion should be estimated as  $T_r(X) \sim T_r(b) \times (R_b/R_X)^2 = 1.32 \times T_r(b)$ . This value, in some sense, gives a similar result with that of nitrogen plasma, where the intermolecular distance of both B and X states of N<sub>2</sub><sup>+</sup> ion is almost the same. Consequently, it is considered that the ground-state molecular ion has higher rotational temperature than neutral molecule, both for nitrogen and oxygen discharge plasmas under the present discharge conditions. We should further study the reason why molecular ions have higher rotational temperature than neutral molecules.

### References

- [1] T. Sakamoto, H. Matsuura, and H. Akatsuka: J. Appl. Phys., **101**, 023307 (2007).
- [2] T. Sakamoto, K. Naoi, H. Matsuura, and H. Akatsuka: Jpn. J. Appl. Phys., **45**, 243 (2006).

## A.2 DSMC Simulation of Arc-Jet Flow with Low Ionization Degree along Open-Field-Line

Hiroshi AKATSUKA, Atsushi NEZU and Haruaki MATSUURA

We have been studying fluid dynamic characteristics of arc-jet helium plasma flowing along open-field-line experimentally [1]. However, it is still difficult for us to understand the rigorous physics of acceleration/deceleration of ions in the plasma flow as well as variation in space potential. We should carry out numerical simulation by modeling the plasma flow to understand the plasma flow entirely. The objective of the present study is to understand the plasma flow at the open-magnetic field by numerical simulation.

The plasma has low ionization degree, which indicates that we must solve the flow of neutral particles simultaneously. We must also treat the ion flow as a rarefied dynamic flow since the Knudsen number of the ion flow  $Kn$  is larger than about 0.15. Consequently, we applied the Direct Simulation Monte Carlo (DSMC) method to solve the Boltzmann equation stochastically. We solve the problem as an axi-symmetric problem, where particle movement is treated as 3-D while the collision as 2-D. To overcome the statistical fluctuation of ions as minor species, we applied weighting factor method and solved the neutral particles simultaneously [2]. Although we should solve electrons simultaneously, we supposed that the electron density, velocity and temperature are the same with those of ions, respectively, for simple analysis. We also assumed that the space potential was already given as the values observed experimentally [1]. We applied maximum collision number method to simulate collisions, where we considered elastic and charge-transfer collisions between an ion and a neutral particle, and elastic collisions between neutral particles [3].

Figure 1(a) – 1(c) show dependence of number density, Mach number and temperature of both ions and neutral particles, respectively, calculated for the on-axis  $r = 0$ . It was found that the larger ionization degree results in the larger maximum Mach number in the vicinity of diverging magnetic field, and that it causes the further extension of the acceleration domain. It was also found that the lower ionization degree makes the maximum ion temperature higher. We found that the numerical results of Mach number and temperature qualitatively agree with our previous experimental results, where the best agreement was for the assumption of ionization degree  $10^{-2}$ .

### References

- [1] K. Yoshida, T. Shibata, A. Nezu, H. Matsuura and H. Akatsuka, *J. Plasma Fusion Res. Series*, **8**, 923 – 927 (2009).
- [2] T. Ichiki, T. Sakamoto, H. Matsuura and H. Akatsuka, *J. Plasma Fusion Res. Series*, **8**, 768 – 772 (2009).
- [3] H. Akatsuka, A. N. Ezoubtchenko and M. Suzuki, *J. Phys. D: Appl. Phys.*, **33**, 948 – 959 (2000).

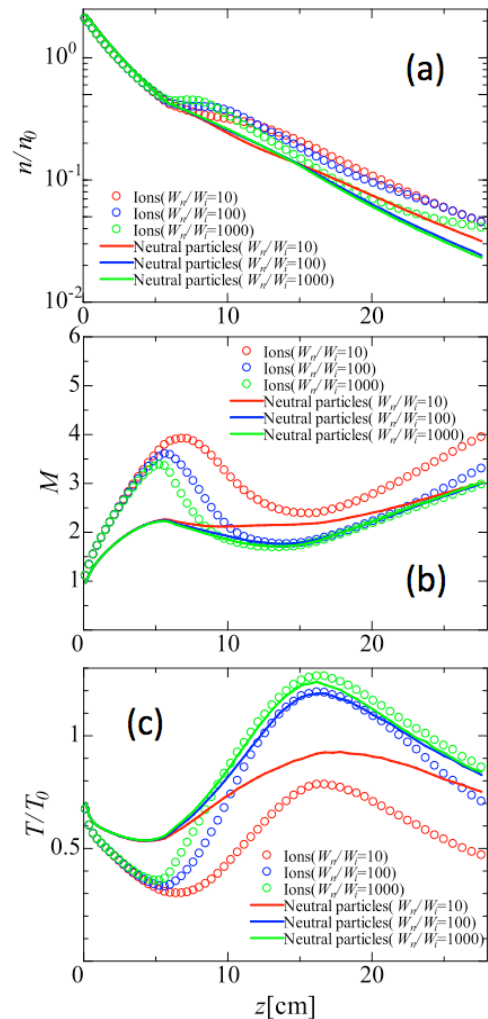


Fig. 1. Numerical results calculated for on-axis ( $r = 0$ ) condition; (a) number density, (b) Mach number and (c) temperature. Weighting factor is the reciprocal ionization degree, which were set to be 10, 100 and 1000.

### A.3 Study on High Speed Lithium Jet for Neutron Source of Boron Neutron Capture Therapy (BNCT)

Minoru TAKAHASHI, Tooru KOBAYASHI, Mingguang ZHANG, Michael MAK, Jiri STEFANICA, Vaclav DOSTAL, and Wei ZHAO

#### 1. Introduction

The medical systems of the boron neutron capture therapy (BNCT) adjacent to hospitals can be realized if more compact neutron source than research nuclear reactors are developed by using a lithium target and a proton beam accelerator. However, a solid lithium target has the disadvantages that it is damaged by the proton beam quickly and high power density cannot be cooled well. A flowing liquid lithium target can solve both of the problems. Thus, a thin sheet jet and a thin film flow on a concave wall are chosen as the candidates of the liquid lithium target. In the present study, a lithium hydrodynamic experiment was conducted to observe the stability of the candidates of the liquid lithium target.

#### 2. Experimental Apparatus and Procedure

Fig. 1 shows a schematic drawing of the test section. It is a vertical cylindrical vessel made of stainless steel. Lithium enters the test section from the top flange and flows down through the bottom outlet.

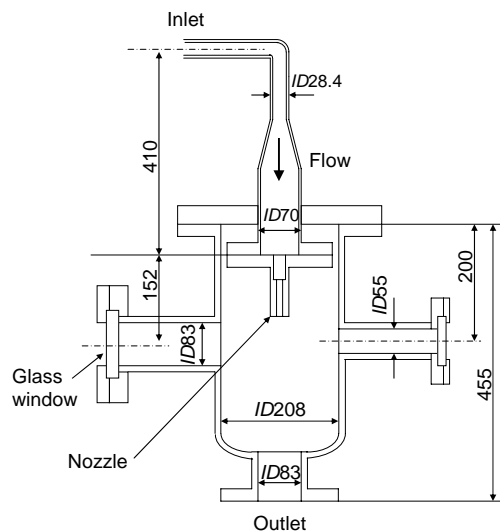
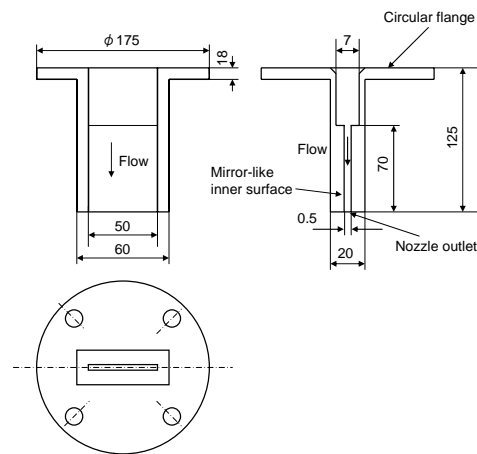


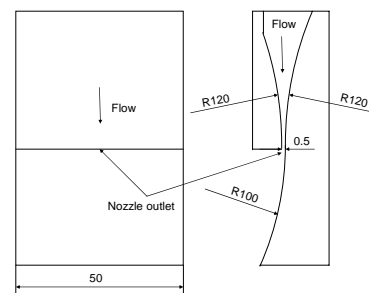
Fig. 1 Test section

Fig. 2 shows the two types of test nozzles prepared for the lithium experiment. The straight nozzle (Fig. 2(a)) was used to form a sheet jet with a thickness of 0.5 mm and a width of 50 mm. The nozzle length is 70 mm, which corresponds to  $70D_e$ , where  $D_e$  is the hydraulic diameter. The fully developed flow at the outlet contains no disturbances caused by a flow in the upstream of the nozzle. Therefore, a long nozzle is chosen to damp the disturbances

at the nozzle inlet. The drawback of the long nozzle is that a friction pressure loss is very high. The curved nozzle (Fig. 2(b)) is prepared to form a stable sheet jet and a film flow on a concave wall with lower friction loss than the straight nozzle. The gap size is 0.5 mm and the width is 50 mm. It is expected that the collision of the sheet jet on the concave wall may stabilize the film flow as well as the increase of the saturation temperature.



(a) Straight nozzle



(b) Curved nozzle  
(c)

Fig. 2 Test nozzles

The experimental conditions are summarized in Table 1. The conditions were chosen in the range of practical lithium target conditions. The flows in the nozzles are turbulent according to Reynolds number. Weber numbers based on the hydraulic diameter  $D_e$  are much higher than unity, which means that the inertia force of turbulent velocity fluctuation overcomes the surface tension force of the wave with a scale of  $D_e$ . This suggests the possibility of droplet splashing from the surfaces of the jet and the film flow due to turbulent dynamic pressure fluctuation.

Table 1 Experimental conditions

Temperature (°C)	250 - 305
Ar gas pressure (MPa)	Saturation pressure, 0.11 - 0.16
Average velocity, $V$ (m/s)	5 - 29
Reynolds number, $Re$	$5.1 \times 10^3 - 3.3 \times 10^4$
Weber number, $We$	$3.2 \times 10^1 - 1.1 \times 10^3$

### 3. Experimental Result

#### 3.1. Behaviors of sheet jets discharged from straight nozzle

Fig. 3 shows the stationary surfaces of lithium sheet jets at the Ar gas pressure a little higher than the atmospheric pressure and under the vacuum condition, i. e. at the saturation pressure of lithium. If the surfaces of the jets are smooth, the illuminated stroboscope light reflects from the surfaces to the specific direction without coming to a front camera. Therefore, the smooth surfaces are observed as dark areas. On the other hand, wavy surfaces, the edge of the sheets and droplets that splash from the surfaces are observed as dark and bright lights. Therefore, the observed dark areas indicate the smooth surfaces of the sheet jets. The sheet surface was wavy at the velocity of 19.8 m/s, but the continuous jet area was large enough for the beam target. The surface was wavy and disturbed at 17.4 m/s in Fig. 3(b). However, the continuous jet area was large enough for the beam target at 17.4 m/s. From the comparison of Fig. 3(a) with Fig. 3(b), the influence of pressure on the sheet jet behavior was not appreciable.

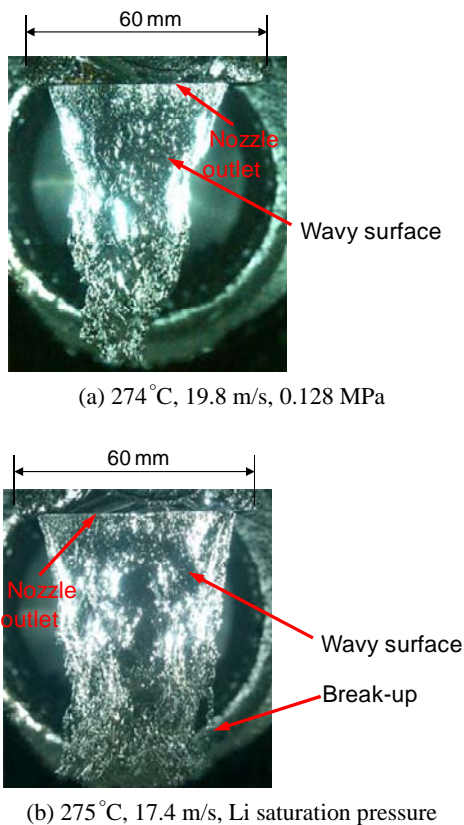


Fig. 3 Observation of lithium sheet jets

#### 3.2. Behaviors of film flow on concaved wall discharged from curved nozzle

Fig. 4 shows the stationary surfaces of the lithium film flows on concaved wall at pressures a little higher than the atmospheric pressure and at the saturation pressure of lithium. A film flow was wavy at 10.0 m/s at 0.112 MPa. At the saturation pressure of lithium, a splitting film flow was observed since the solid particles blocked the outlet of the nozzle partially.

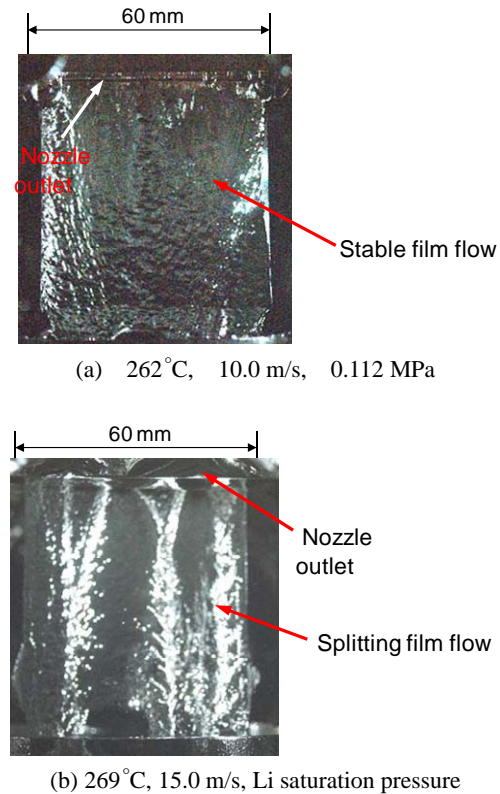


Fig. 4 Observation of lithium film flow on the concave wall

### 4. Conclusion

A lithium hydrodynamic experiment was conducted to observe the stability of the candidates of the liquid lithium target. The stability of the sheet jet and the film flow was confirmed at the velocities up to a certain conditions. The effect of pressure on the stability was not appreciable in the present range of pressure conditions.

### Acknowledgment

The present study was supported by the Grant-in-Aid for Scientific Research, Kiban-kenkyu A, No.20240054 (2008-2010) (MEXT).

### Reference

M. Takahashi, T. Kobayashi, M. Zhang, M. Mak, J. Stefanica, V. Dostal, W. Zhao, "Study on High Speed Lithium Jet for Neutron Source of Boron Neutron Capture Therapy (BNCT)," The 19th Int. Conf. on Nucl. Eng. (ICONE19), Oct.24-25,2011, Osaka, Japan, ICONE19 -43192.

## A.4 Carbon Recycling Ironmaking System Driven by High Temperature Gas Reactor

Yukitaka KATO

### 1. INTRODUCTION

Energy supply security is important matter for industrial and economical developments of a society. Steep change and instability of the market prices of primary energy sources is causing economic confusion in any ages. This study discusses for establishment of energy supply security from the stand point of carbon recycle use. Carbon is the most important energy media for manufacturing industry and social life of human being. Carbon supply security is an essential condition for a sustainable society. In Japan, the supply of fossil fuels of primary energy almost depends on import. Enthalpy of import fuel is 82% ( $18.9 \times 10^{18}$  J) of all of using primary energy in Japan [1]. 7% of fossil fuel is consumed for ironmaking process. The Kyoto protocol came into effect in 2005. Japan has undertaken obligation to follow the protocol, and is required drastic reduction of carbon dioxide ( $\text{CO}_2$ ) emission. However,  $\text{CO}_2$  reduction connects with restriction of usage of carbon resources and causes depression of activity of manufacturing and service industries. Co-establishment of carbon supply security and reduction of  $\text{CO}_2$  emission is an important subject for a development of a modern society.

A new energy system in which carbon is reused cyclically was discussed. A carbon recycle system has already existed in nature as a natural carbon neutral system. A concept of an Active Carbon Recycling Energy System, ACRES, was proposed against natural carbon recycling energy system [2].  $\text{CO}_2$  is regenerated artificially in hydrocarbons consuming a primary energy source with no- $\text{CO}_2$  emission, and re-used cyclically in ACRES. ACRES recycles carbon, and transform energy without  $\text{CO}_2$  emission. Carbon recycling ironmaking system can be established by ACRES concept. The feasibility of carbon recycling ironmaking system driven by high-temperature gas reactor system was discussed thermodynamically in this study.

### 2 STRUCTURE OF ACRES

The structure of ACRES shown in Fig. 1 consists of three elemental processes of carbon material usage,  $\text{CO}_2$  recovery and separation, and carbon material regeneration. In the usage process, carbon materials can be used as both a heat source and a material.  $\text{CO}_2$  generated from carbon material consumption is recovered by physical and chemical sorptions. Recovered  $\text{CO}_2$  in a sorption material is separated thermally from the sorption material by a heat input. This process produces highly concentrated  $\text{CO}_2$ . Recovered  $\text{CO}_2$  is regenerated into carbon material in the

regeneration process. The regeneration process is endothermic and requires an energy input.

If the carbon recycling system can be established thermally and kinetically, it is expected that the system is diffused easily into conventional industries.

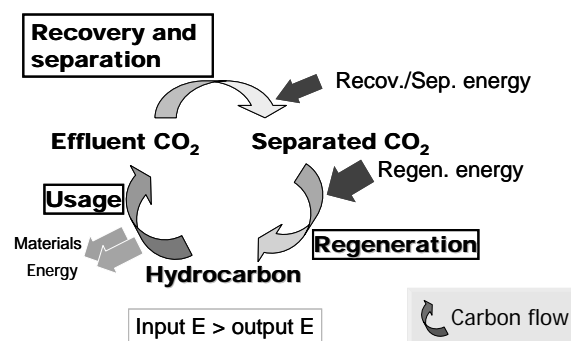


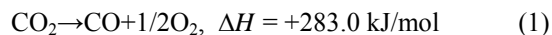
Fig. 1 Structure of the concept of ACRES

#### 2.1 ACRES with CO

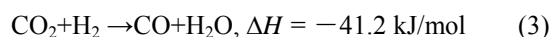
Carbon monoxide (CO) and pure carbon (C) have higher energy density than  $\text{H}_2$ , and other hydrocarbons. CO is in gas phase, easily transformable and popular energy material for ironmaking process. Then, ACRES using CO is expected as a practical process.

CO usage, recovery and separation processes are able to be covered by conventional industrial technologies. Development of efficient CO regeneration process is the most important for the establishment of ACRES.

CO is regenerative from  $\text{CO}_2$  by electrolysis (Eq. (1)) using a solid oxide fuel cell [3].



A two-step reaction of hydrogen production by water electrolysis and hydrogen reduction of  $\text{CO}_2$  with the hydrogen (Eqs. (2) and (3)) is also a practical process for CO regeneration.



Introduction of  $\text{H}_2$  from other  $\text{H}_2$  production processes is also practical choice. Enthalpy balance of ACRES for CO is shown in Fig. 2. Required enthalpies per one molecule of CO for the processes of usage and regeneration are depicted in low heating value (LHV). Regeneration process is assumed to be used hydrogen for

CO regeneration by the two-step reaction in Eqs. (2) and (3).

Production of H<sub>2</sub> of 1 mol needs an enthalpy of 242 kJ/mol-CO. Reduction of CO<sub>2</sub> into CO with H<sub>2</sub> is endothermic reaction required heat input of 41 kJ/mol-CO. Because CO has higher energy density than H<sub>2</sub>, CO is one of the most useful energy media in chemical processes.

Both CO<sub>2</sub> electrolysis and H<sub>2</sub> reduction have possibility for the regeneration. Because H<sub>2</sub> reduction process is relatively more conventional than CO<sub>2</sub> electrolysis, H<sub>2</sub> reduction of CO<sub>2</sub> is discussed mainly in this study.

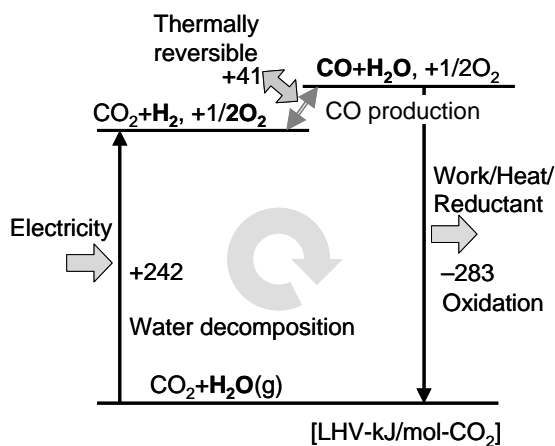


Fig. 2 Enthalpy balance of ACRES with CO

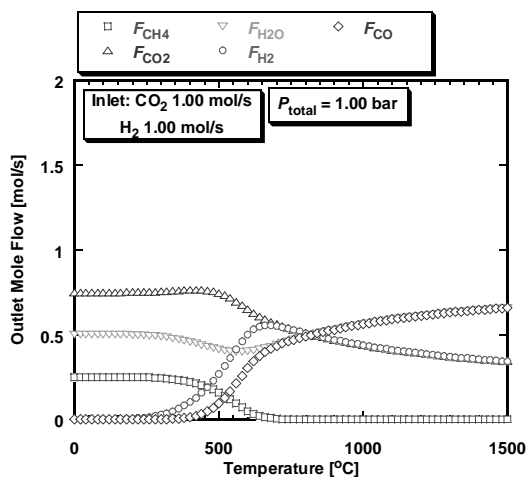


Fig. 3 Chemical reaction equilibrium for H<sub>2</sub> reduction of CO<sub>2</sub> by an ideal equilibrium reactor

## 2.2 Chemical Equilibrium for H<sub>2</sub> Reduction of CO<sub>2</sub>

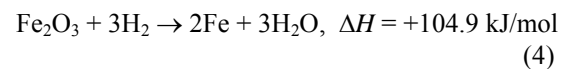
A chemical reaction equilibrium for H<sub>2</sub> reduction of CO<sub>2</sub> in Eq. (3) was calculated by a process simulator of Aspen Plus ver. 2006.5 as shown in Fig. 3. It was assumed in the evaluation that the reaction proceeded in an ideal

equilibrium reactor under a total pressure of 1.00 bar, inlet flows of CO<sub>2</sub> and H<sub>2</sub> were set as 1 mol/s each and the reaction produced CO, H<sub>2</sub>O, O<sub>2</sub>, CH<sub>4</sub>. Fig. 4 shows relationship between reaction temperature and outlet mole flows of products from the reactor. CO was dominant products at over 800°C. It means that CO regeneration in Fig. 3 needs heat input over 800°C. Surplus heats at high-temperatures around 800°C generated from high-temperature processes can be utilized in the reaction. Energy saving of the high-temperature processes is achievable by endothermic CO regeneration in ACRES. Because formation enthalpy of CO is higher than one of H<sub>2</sub> as shown in Eqs. (1) and (2), the ACRES for CO can recover all of enthalpy of H<sub>2</sub>. CO is popular media for conventional ironmaking process. Then, it was expected that CO is one of the most appropriate candidates for a regenerative media in ACRES.

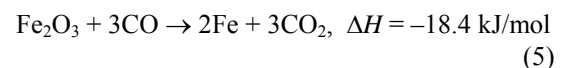
## 3. CARBON RECYCLING IRONMAKING SYSTEM BASED ON ACRES

Application of ACRES to an ironmaking process is proposed in Fig. 3. The system is a carbon recycling ironmaking system. It is assumed that the primary energy for CO regeneration is supplied from a high temperature process as works in electricity, heat and H<sub>2</sub>. High temperature gas cooled type nuclear reactor (HTGR) which demonstrated heat output at 950°C[4] is a candidate of the primary energy source. Regenerated CO is used for the reduction of iron oxide into pure iron. CO<sub>2</sub> generated from the reduction is regenerated into CO again by the CO<sub>2</sub> reduction process. Oxygen as the by-products of CO can be a useful material for other oxidation processes.

Iron(III) oxide (hematite), Fe<sub>2</sub>O<sub>3</sub>, is employed as a raw material for the process in the following discussion. An ironmaking process using hydrogen is discussed in a previous work [5]. Fe<sub>2</sub>O<sub>3</sub> reduction by hydrogen is an endothermic reaction and requires an external heat input.



In contrast, Fe<sub>2</sub>O<sub>3</sub> reduction by CO is an exothermic reaction and proceeds with self-heating.



CO reduction is advantageous for the ironmaking process in comparison with hydrogen reduction. The reaction is usual in conventional iron making. Direct reduction processes for Fe<sub>2</sub>O<sub>3</sub> in which CO and H<sub>2</sub> gasses are used directly for the reduction, have been discussed [6]. ACRES ironmaking process is fundamentally a zero CO<sub>2</sub> emission process. This process could be a possible way to reduce CO<sub>2</sub> emission.

ACRES is an energy transformation system with energy consumption. The direct supply of a primary energy in an energy-demanding process without ACRES has the highest efficiency with the smallest energy loss. When a carbon material recycled in ACRES is useful for energy demanding process compared with primary energies of heat or electricity, the ACRES is expected to have a practical value. In conventional ironmaking process, CO has a higher affinity to processes than electricity and heat of primary energies. ACRES has the potential applicability in the process.

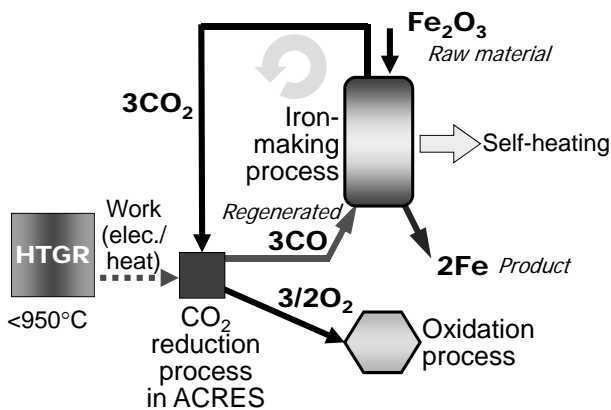


Fig. 4 ACRES for ironmaking system

### 3.1 Scale of ACRES for Ironmaking System

Scale of ACRES for ironmaking process using a conventional blast furnace was evaluated. Evaluation result is shown in Table 1. HTGR combined with a helium gas-turbine power generator which had capacity of thermal output of 600 MW-thermal was employed for supply of primary energy sources for process [7]. CO regeneration process consists of water electrolysis for  $\text{H}_2$  production and thermally  $\text{H}_2$  reduction of  $\text{CO}_2$ . Although it was better to use electricity for the electrolysis and high-temperature heat for the reduction, it was assumed that both reaction energies were supplied by electricity generated from the gas-turbine generator. From a previous research for conventional blast furnace in Japan [8], it was assumed that carbon amount emitted as off gas from a blast furnace is around 400 kg-C/ton-pig-iron and mole ratio between CO and  $\text{CO}_2$  in the off gas is around 1:1.  $\text{CO}_2$  of 16.7 kmol/ton-pig-iron is emitted from a blast furnace. It was concluded that one unit of HTGR was capable to regenerate CO for pig-iron production of 57.2 kg-pig-iron/s. Conventional blast furnace produces pig iron at around 100 kg-pig iron/s. Then around two units of HTGR are required for a conventional blast furnace.

### Conclusions

For an establishment of a practical ACRES, selection of recycling carbon material medium and primary energy source for the system drive were important. CO was the most suitable for a recycle medium in ACRES, because CO had higher energy density and affinity to conventional ironmaking process in comparison with  $\text{H}_2$ . HTGR was a candidate of primary energy source of ACRES. ACRES with CO driven by output from HTGR was one of the most applicable combinations for carbon recycling ironmaking system. Hydrogen reduction of  $\text{CO}_2$  was practical way for CO regeneration. Mixture of  $\text{CO}_2$  and CO which was emitted as off-gas from blast furnace was capable to be used directly for the  $\text{CO}_2$  reduction. The reduction could eliminate  $\text{CO}_2$  separation process from the mixture, and was expected to have higher economic efficiency than other CO regeneration process. One or two plants of HTGR are corresponding with one unit of conventional blast furnace. Experimental demonstration of ACRES process would be required for further discussion.

Table 1 Scale of ACRES for pig iron production

Thermal output of HTGR [MW-thermal]	600
He temperature at inlet of He gas-turbine [ $^{\circ}\text{C}$ ]	850
Reference gas-turbine power efficiency [%]	45.0
Electric output from gas-turbine [MW-electricity]	270
Carbon from off gas [kg-C/ton-pig-iron]	400
Mole ratio between CO: $\text{CO}_2$ in off gas	1 : 1
$\text{CO}_2$ in off gas [mol/ton-pig-iron]	$16.7 \times 10^3$
Enthalpy for $\text{CO}_2$ regeneration into CO [kJ/mol]	283
Pig iron production rate per a HTGR [ton-pig-iron/s]	$57.2 \times 10^{-3}$

### References

- [1] Minister of Economy, Trade and Industry (METI), Figure No. 201-1-3, METI, Tokyo, Japan (2006).
- [2] Kato, Y. *ISIJ-Int.*, 50(1) (2010), P. 181-185.
- [3] Kusama, H. et al., *Catalysis Today*, 28 (1996), P. 261-266
- [4] Fujikawa, S. et al., *J. Nucl. Sci. Technol.*, 41(2004), P. 1245-1254.
- [5] T. Murayama, S. Ishimatsu and K. Sawamura: *Tetsu-to-Hagane*, 63(1977), P. 1090-1977.
- [6] Bonalde, A.; Henriquez, A.; Manrique, M., *ISIJ-Int.*, 45 (2005), P. 1255-1260.
- [7] Kunitomi, K. et al., *Transact. Atomic Energy Soc. Japan*, 1 (2002), P. 352-360.
- [8] Ujisawa, Y. et al., *ISIJ-Int.*, 45(10) (2005), P. 1379-1385.

## A.5 Numerical Analyses on Joule-Heated Glass Furnace for Disposal of High-Level Radioactive Waste

Nobuyoshi TSUZUKI and Hiroshige KIKURA

Nuclear power plants or other facilities of nuclear fuel cycle produce high-level radioactive wastes. The High-level radioactive waste is reprocessed into waste liquid, and the waste liquid is mixed into molten glass in a Joule-heated glass furnace to make vitrified waste. In the glass furnace, glass (and radioactive waste) is heated by electrical current, Joule-heated, where three kinds of field – flow field, electrical field and magnetic field – arise and interfere one another. Thus, very complicated flow behavior is produced in the Joule-heated glass furnace.

The shape of glass furnace is simulated by a cubic cavity in these calculations to simplify the various problems in glass furnace. Dimensions of the model are calculated from the public data of TVF [1], the test-type vitrification furnace. The cavity consists of two electrode plates on facing sides and constant temperature wall on the top working as a heat sink (Figure 1). Other planes are considered as adiabatic.

In order to solve the couple analysis including the three field (flow, electrical and magnetic fields), GSMAC-FEM [2] is utilized because edge finite element method (edge-FEM) can examine coupled analyses with magnetic field. Magnetic permeability of molten glass is difficult to measure due to its high temperature ( $\approx 1200^\circ\text{C}$ ) and mixed radioactive waste including platinum group metal particles. Thus, relative magnetic permeability of working fluid to vacuum ( $\mu_r$ ) in this study is varied from 1.0 to 2.0.

The simulation calculations show the flow behavior in this cubic cavity as follows. Joule heating induces volumetric upflow due to buoyancy. Top surface of constant temperature generates downflows by separation of cooled boundary fluid. Downflows occurred everywhere of the top surface, and unsteady flow behavior is maintained steadily, like experimental with less magnetic permeability fluid executed in the last year. We named this unstable state as ‘chaotic steady state.’ And simulation calculations can show magnitude change of averaged forces (buoyancy, diffusion force, Lorentz force and convection force) in the beginning of Joule heating. These results are shown in Figure 2. In the case of low magnetic permeability ( $\mu_r = 1.0$ , (a)), the rises of diffusion force and convection force are slow. On the other hand, in the case of high magnetic permeability ( $\mu_r = 2.0$ , (b)), the rises of these forces are fast. From the velocity distribution results, higher magnetic permeability induces earlier and faster volumetric upflow. Early upflow makes steady flow pattern, in which upflow in the center and downflow near the wall, and it makes the beginning time of chaotic downflow from somewhere of the top surface later. However, magnitudes of all forces after enough time passed (more than 1 hour) become almost same in both cases.

Numerical analyses suggest that magnetic field effects on the flow behavior in the beginning of Joule heating. High magnetic permeability leads early and fast chaotic downflows which occur from somewhere of the top surface. However, named ‘chaotic steady state’ will appear after 1-2 hours, and averaged magnitude of each forces becomes almost same in the case  $\mu_r$  is 1-2. Consequently, it is concluded that the effect of magnetic permeability will become negligible after several hours passed in this system.

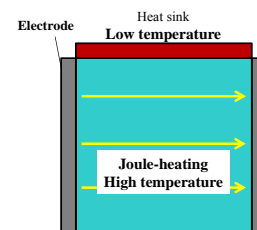


Figure 1 Schematic diagram of the cubic cavity model.

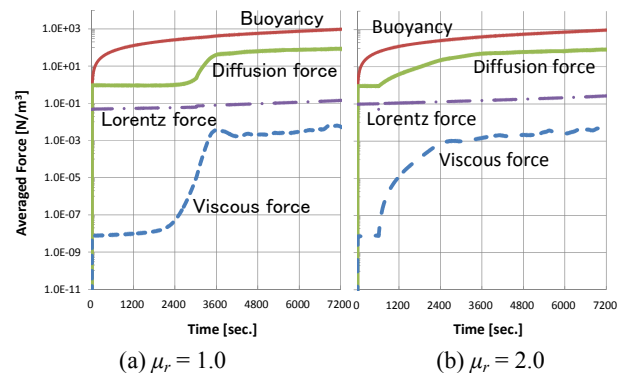


Figure 2 Time dependencies of volume averaged values of forces.

### References

- [1] JAEA, Thermal hydraulic analysis using experimental data of TVF cold test, JNC TN8410 98-008 (1998) [in Japanese].
- [2] T. Tanahashi: GSMAC-FEM, IPC (1991) [in Japanese].
- [3] N. Tsuzuki, H. Kikura, H. Kawai, T. Kawaguchi, A. Inagaki, E. Ochi, Simulation calculation of unsteady flow in cubic cavity under Joule-heating condition, *Proc. The 48th National Heat Transfer Symposium*, Okayama, (2011-6), pp. 727 – 728 [in Japanese].
- [4] N. Tsuzuki, H. Kikura, Y. Saito, H. Kawai, G. Hashimoto, A. Inagaki, E. Ochi, Numerical analysis for flow behavior of molten glass under Joule-heating, *Proc. the Symposium of Visualization Society of Japan 2011 Toyama*, Toyama, B108 (2011-9) [in Japanese].
- [5] N. Tsuzuki, H. Kikura, Y. Saito, H. Kawai, G. Hashimoto, A. Inagaki, E. Ochi, Flow behavior change under Joule-heating condition with magnetic permeability of the fluid, *Proc. Thermal Engineering Conference 2011*, Shizuoka, D211 (2011-10) [in Japanese].

## A.6 A Very Low Velocity Measurement Using Ultrasonic Velocimetry

Hiroshige KIKURA and Yasushi TAKEDA

Isolation of High Level Radioactive Wastes (HLWs) from biosphere and its disposition in a deep geological repository is an urgent problem and vitrification technique of HLW has to be improved in the industrial scale. This vitrification melter is operated with internal Joule-heat generation, and the temperature of glass exceeds 1000°C. For understanding a thermal hydraulics behavior of the vitrification melter, experimental technique has to be invented. Several velocity measurement techniques such as PIV/PTV, LDA had been developed. However, because of high temperature and opaqueness, these techniques cannot to be applied for glass melts. To overcome these difficulties, we focused ourselves on UVP technique[4]. Realization of such a technique has difficulties in two fold; high temperature and very low velocity. We already demonstrated ultrasonic measurement technique inside glass melts employing buffer-rod [5]. In this paper, we present a system developed to measure an extremely low velocity flow.

FFT-based Doppler method is a conventional method to obtain flow velocity profile. The Doppler-shift frequency  $f_{Di}$  and flow direction are determined by their peak value. Therefore, flow velocity  $V_i$  is calculated as Eq. (1).

$$V_i = \frac{f_{Di}}{2f_0} c \quad (1)$$

where  $f_0$  is center frequency of transmitted signal, and  $c$  is sound speed in the fluid. Because a spectrum is calculated at discrete points, velocity values have limitations as follows:

$$V_{max} = \frac{f_{PRF}}{4f_0} c \quad (2) \quad V_{step} = \frac{f_{PRF}}{N_j f_0} c \quad (3)$$

where  $f_{PRF}$  is a pulse repetition frequency, and  $N_j$  is a number of pulse emissions. Practically, the peak of the spectra is calculated from three point Gaussian curve fitting to improve the velocity resolution. Nevertheless, this  $V_{step}$  could be equal to the lower velocity limitation. Since this technique does not require high speed ADC, it has been widely used. However, there is a trade-off relationship between temporal and velocity resolutions depending on  $N_j$ .

In order to measure very low velocity with high accuracy, we developed new data processing method, named as 'Phase Difference method.' From conjugate complex product of two successive functions, phase difference  $\Delta\theta$  is obtained. Therefore, flow velocity  $V_{ij}$  is calculated as Eq. (4).

$$V_{ij} = \frac{f_{PRF}}{4\pi f_0} c \cdot \Delta\theta_{ij} \quad (4)$$

Since this technique can calculate velocity from two echoes, the temporal resolution of this method can be expressed as Eq. (5).

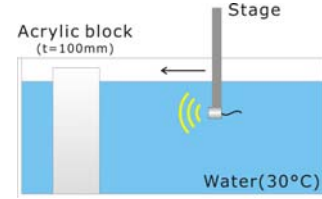


Fig. 1 Schematic diagram of experimental apparatus

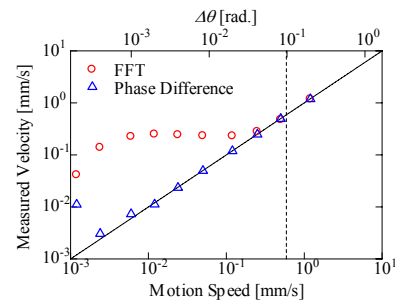


Fig. 2 Measured velocity versus motion speed for FFT method and phase difference method ( $f_{PRF} = 100$  Hz)

$$V_{ij} = \frac{f_{PRF}}{4\pi f_0} c \cdot \Delta\theta_{ij} \quad (5)$$

As for  $V_{max}$ , it is equal to Eq. (2) because the range of  $\Delta\theta$  remains between  $-\pi$  and  $\pi$ .

**Figure 1** shows a schematic illustration of verifying experimental setup. A transducer is immersed in a water of 30°C and fixed on the stage. The stage moves toward and backward the wall at a constant speed. Motion speeds can be controlled by PC from 0.0012 to 5 mm/s. The measured velocities are depicted in **Fig. 2**. With FFT-based method, measured values don't agree with real value especially when the motion speed is slower than  $10^{-1}$  mm/s, however, measured values with Phase Difference method agree well till the motion speed is as slow as around  $10^{-3}$  mm/s.

### References

- [1] T. Ihara and H. Kikura : Ultrasound Characteristics in High-temperature Fluid, *JSME Fluids Engineering Conference 2010, Yonezawa, Japan* (2010-10), pp.527, [in Japanese].
- [2] T. Ihara, H. Kikura, Y. Takeda, E. Ochi and A. Inagaki : Ultrasound Characteristics in High-Temperature Fluid, *The 8th ASME-JSME Thermal Engineering Joint Conference, Hawaii, USA* (2011-3), CD-ROM Paper No. AJTEC2011-44243.
- [3] T. Ihara, K. Tanaka, H. Kikura, Y. Takeda, E. Ochi and A. Inagaki, The Study of Velocimetry in High Temperature Flow, *The 19th International Conference on Nuclear Engineering (ICONE19)*, Paper No. ICONE19-43617 (2011-5).
- [4] T. Ihara, H. Kikura and H. Murakawa, The Basic Study of Phased Ultrasonic Array Velocimetry, *IEICE Technical Report, Ultrasonics*, 111, 29-34 (2011-4) [in Japanese].
- [5] T. Ihara, H. Kikura and Y. Takeda, The Basic Study of Ultrasound Characteristics and Velocimetry in Molten Glass, *Trans. JSME, Series B*, 78, 485-489 (2012-3) [in Japanese].

## A.7 Basic Study of Velocity Profile Measurement by an Air-Coupled Ultrasonic System

Hiroshige KIKURA

In nuclear power plants, flow measurement systems in high temperature surroundings are needed to monitor plants. However, ultrasonic measurement cannot be applied to high - temperature fluid. Piezo-electric devices in ultrasonic transducers lose piezoelectric property over Curie temperature. Thus, ultrasonic waves have some limitations in high-temperature flow measurement. However, air is good insulator and those high temperature can be prevented by air layer. Therefore, we focused on air-coupled ultrasonic waves.

Measuring configuration for air-coupled ultrasonic flow measurement is depicted in **Figure 1**. Upstream transducer emits ultrasonic waves. asound propagates in air and passes into cylindrical pipe, then ultrasonic waves convert into guided waves which propagate along the surface of pipes and longitudinal waves which propagate in fluid flowing along pipes. Several kinds of ultrasonic waves are received by a receiving transducer. When time difference method is applied for ultrasonic flowmeters, longitudinal waves are used to measure and guided waves are regarded as noises in this system. It is necessary to isolate received signals of longitudinal waves from those of guided waves. The signals of longitudinal waves are specified experimentally by obstructing. Longitudinal waves cannot exist when obstacles exist in the center of pipe, however, the longitudinal wave can be observed when there is no obstacles.

The principle of air-coupled ultrasonic flow meter is as follows. Two transducers are necessary for this air-coupled ultrasonic system like shown in Figure 1. At first, upstream transducer emits ultrasonic wave and downstream transducer receives them. Next, downstream transducer emits waves and upstream transducer receives them. There is propagation time difference between two signals due to working fluid velocity though the waves traveled for the same distance. There is relationship between the propagation time difference and the fluid flow rate as,

$$V = \frac{C_w^2}{2D \tan \phi} \Delta t$$

where  $V$  is average flow velocity,  $C_w$  is sound speed in the fluid,  $D$  is diameter of the pipe,  $\phi$  is angle between direction of ultrasound and crosssection plane of pipe, and  $\Delta t$  is propagation time difference.

Development of hardware, i. e. transducers for air-coupled measuring and external amplifier, and software to distinguish longitudinal wave from noisy echo signal realised air-coupled flow measuring. Figure 2 shows the results of flow velocity using developed air-coupled ultrasonic system for vertical pipe flow. Horizontal axis shows flowrate measured by existing clamp-on ultrasonic

flowmeter, and vertical axis shows flowrate measured by air-coupled ultrasonic flow measuring. Error bars shows deviations of measured velocities. The solid line is drawn by the least-squares method. The R2 value of this fitting is 0.9398. The slope of this line is 0.98. Though there is some errors, agreement between real flow rate and measured value by air-coupled flow system is confirmed by this test experimental result.

Evaluation for an air-coupled ultrasonic flowmeter was executed and the result suggests the availability of the method. In order to improve the accuracy of flowrate measurement with air-coupled ultrasonic system, application of Pulse Doppler Method will be examined.

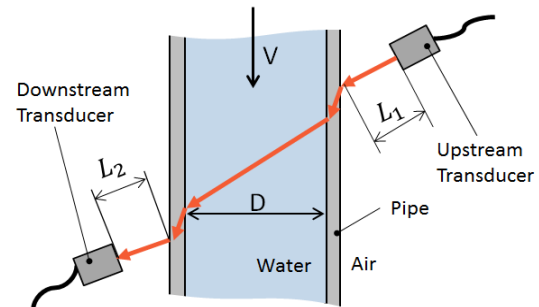


**Figure 1** Measurement configuration for air-coupled ultrasonic system.

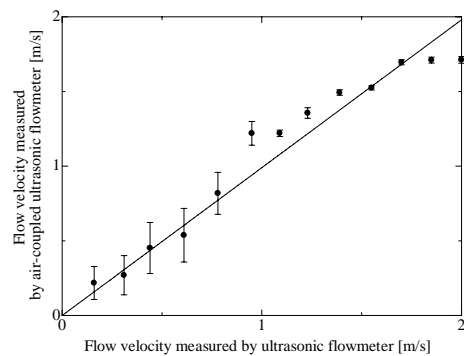


**Figure 2** Measured flow velocity for a vertical pipe.

### References

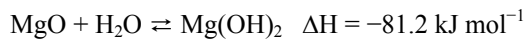
- [1] K. Tsukada, T. Ihara and H. Kikura, Study for non-contacting flowmeter using air-coupled ultrasonic system, *Proc. 5th Presentation session for students' research by AESJ Kanto-Koetsu Office*, p. 12 (2012-3). [in Japanese]
- [2] K. Tsukada, T. Ihara and H. Kikura, Basic Study on Velocimetry using air-coupled ultrasonic measurement technique, *Proc. 2011 JSEM Annual Conference on Experimental Mechanics*, **A213** pp. 216-221 (2011-8).[in Japanese]
- [3] K Tanaka, H Kikura, Basic study of air propagation ultrasonic velocity profile method, *IEICE Technical Report*, **110**, p. 107-112 (2011-1).[in Japanese]

## A.8 Durability of Mg-Co Mixed Hydroxide on Cyclic Operation for Chemical Heat Storage

Junichi RYU and Yukitaka KATO

### Introduction

The heat storage technologies of waste heat from industrial processes and co-generation systems will contribute to “Energy Saving”. Especially, chemical heat storage technology is very interesting in view of their heat storage capacity. In recent years, the technologies of chemical heat pump and chemical heat storage are widely studied for the reduction of energy consumption and CO<sub>2</sub> emission. Chemical heat pump system with the reaction between magnesium oxide (MgO) and water vapor has been reported by our group. [1]



In this system, thermal energy above 350°C is required for practical heat storage operation. Recently, chemically modified magnesium hydroxide – metal salt added magnesium hydroxide, and magnesium containing mixed hydroxide – were proposed as new type material for chemical heat storage by our group. These materials can store thermal energy around 280 °C. [2-5] The heat storage density of these materials are higher than authentic magnesium hydroxide under 280°C of heat storage condition. In this work, durability of Mg-Co mixed hydroxide on cyclic operation for chemical heat storage was studied by TG method.

### Experimental

Mg-Co mixed hydroxides (Mg<sub>x</sub>Co<sub>1-x</sub>(OH)<sub>2</sub>) were prepared by co-precipitation method. The reaction between sample and water vapour was tested by thermogravimetric method. Dehydration operation was carried out at 300°C under Ar flow, and hydration operation was carried out at 110°C with 57.8 kPa of water vapour (Ar balance). The molar fraction of hydroxide in the sample and reaction conversion were calculated from the weight change of sample.

### Results

The reaction conversion for hydration ( $\Delta X_1$ ) and dehydration ( $\Delta X_d$ ) of Mg-Co mixed hydroxides are shown in Figure 1. The reactivity for each reaction of samples with composition  $x$  between 0.70 and 0.98 were higher than other samples.

The change of hydration conversion with cyclic operation for Mg-Co mixed hydroxides are shown in Figure 2. The hydration conversion of samples with composition  $x$  between 0.75 and 0.98 were higher stability for hydration (40% ~ 60%) with 16 cycles operation. Especially, the sample with  $x = 0.95$  (Mg<sub>0.95</sub>Co<sub>0.05</sub>(OH)<sub>2</sub>)

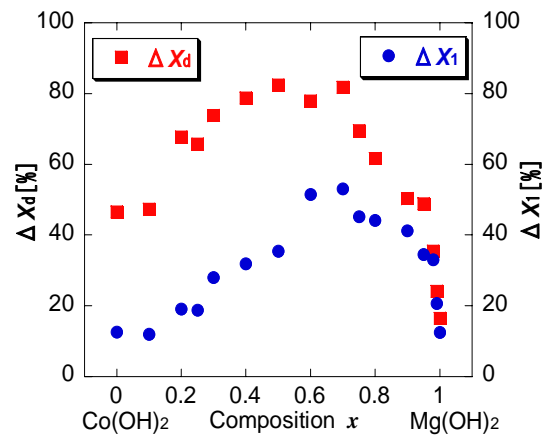


Figure 1 Reaction conversion for dehydration and hydration of Mg-Co mixed hydroxides.

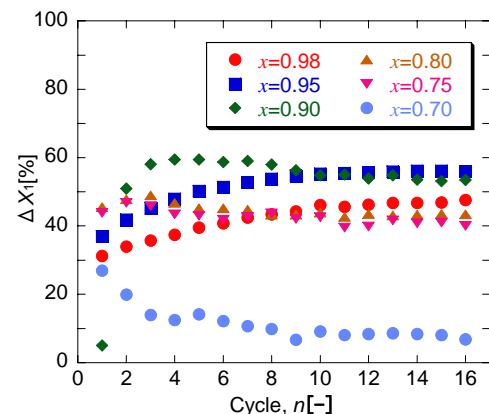


Figure 2 The change of hydration conversion with cyclic operation for Mg-Co mixed hydroxides.

show the highest stability, and the average heat output capacity of this sample was 730 kJ/kg.

The degradation mechanism with cyclic operations and the effect of metal salt addition should be studied further.

### References

- [1] Y. Kato et al., *Appl. Therm. Eng.*, **16**, 852 (1996).
- [2] J. Ryu et al., *J. Chem. Eng. Jpn.*, **40**, 1281 (2007).
- [3] J. Ryu et al., *Chem. Lett.*, **37**, 1140 (2008).
- [4] H. Ishitobi et al., *Appl. Therm. Eng.*, available online.
- [5] H. Ishitobi et al., *J. Chem. Eng. Jpn.*, **45**, 58 (2012).

## A.9 Geometrical Network Approach for An Evaluation of Heat-Transfer Coefficient in Dropwise Condensation

Noriyuki WATANABE and Masanori ARITOMI

Condensation is roughly divided into two categories of dropwise condensation and filmwise condensation. It is well known in general that the heat-transfer coefficient of dropwise condensation is about 15~20 times higher than that of a film wise condensation. Many studies on dropwise condensation have been conducted in order to utilize the condensation technology in various industrial plants<sup>[1]</sup>. So called “high-performance heat-transfer tubes for a condensation” are designed so that condensate films are actively removed from the surface to promote dropwise condensation. Most of the surfaces are mechanically and chemically processed in micrometer or nanometer scales. Thus, when the shape and chemical composition of surface become more complicated, the temperature distribution on the surface tends to be non-uniform. Previously, a heat-transfer coefficient on the surface was almost evaluated by extrapolating from the local gradient of temperature in the surface. However, it is difficult to apply above approach under such a complicated surface. Therefore, it is required to establish a direct method for evaluating the heat-transfer coefficient on the surface. This paper proposes a direct method for evaluating the dropwise condensation heat-transfer coefficient by the image of dropwise condensation on the surface. In this method, stochastic and geometrical network theory was applied.

To establish the direct method for evaluating the dropwise heat-transfer coefficient, the following theoretical equation for dropwise condensation heat-transfer coefficient, which was proposed by Hatamiya and Tanaka (1986), was referred,

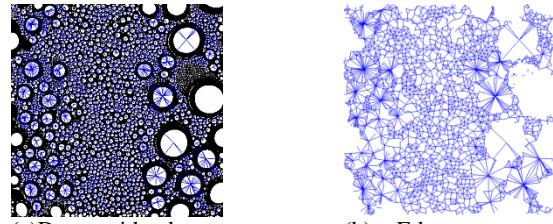
$$h = \int_{r_{\min}}^{r_{\max}} 2\pi r^2 \frac{h_{fg}}{\Delta T_{sub} v_l} \dot{r}_e(r) N(r) dr \quad (1)$$

where  $\dot{r}_e(r)$ ,  $N(r)$  are growth rate of drops and density of drop-size distribution, respectively. It is clear that the theoretical equation did not consider the configuration of neighboring drops because the equation is a function of drop radius. In even the drops that having same radii, the neighboring drop distributions are commonly different. Hence, the above equation is not appropriate for evaluating the dropwise condensation heat-transfer coefficient.

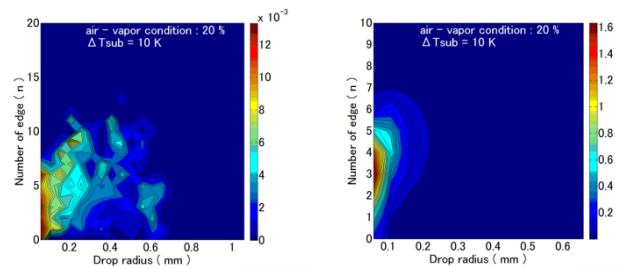
In order to solve such a problem, we introduced a concept of stochastic and geometrical network theory to equation (1). Firstly, each drop was connected to neighboring drops with “edge” (see Fig. 1). Secondary, the growth rate of drops and the density of drop-size distribution were redefined as functions of the radius and the number of edge,  $\dot{r}_e(r, E)$ ,  $N(r, E)$ , respectively (see Fig. 2). Finally, we redefined the dropwise condensation heat-transfer coefficient as follow:

$$h = \int_{E_{\min}}^{E_{\max}} \int_{r_{\min}}^{r_{\max}} 2\pi r^2 \frac{h_{fg}}{\Delta T_{sub} v_l} \dot{r}_e(r, E) N(r, E) dr dE \quad (2)$$

It is expected that the evaluation by equation (2) is more precise than that by equation (1) because the equation (1) consider the configuration of neighboring drops. The dropwise condensation heat-transfer coefficient evaluated by equation (2) is shown in Fig. 3. The heat-transfer coefficient evaluated by extrapolating from the local gradient of temperature in the surface is also shown in the figure. It is clear from the figure that the heat-transfer coefficient evaluated by equation (2) was underestimated compared with that by the local gradient of temperature. It is considered that the discrepancy was caused by the fact that equation (2) did not consider the geometrical exclusion effect between drops. Therefore, it is required that equation (2) considering the geometrical exclusion effect would be developed for an excellent evaluation of the heat-transfer coefficient.



(a) Drops with edge structure (b) Edge structure  
Fig. 1 Representative image of dropwise condensation



(a) growth rate of drops:  $\dot{r}_e(r, E)$  (b) drop-size distribution:  $N(r, E)$   
Fig. 2 Representative features of dropwise condensation factors

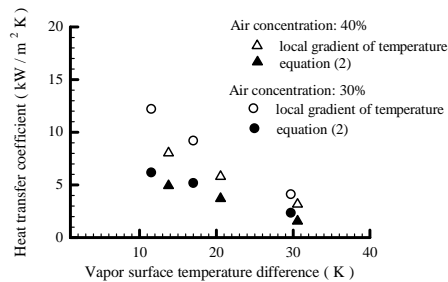


Fig. 3 Comparison of evaluated heat-transfer coefficients

### Reference

[1] Masahiro Kawakubo, Masanori Aritomi, Hiroshige Kikura and Toshihiro Komeno, *J. Nucl. Sci. and technol.* **46**(4), 339-345(2009).

## B.1 Systematic Measurement of keV-Neutron Capture Cross Sections and Capture Gamma-Ray Spectra of Pd Isotopes

Masayuki IGASHIRA, Kazushi TERADA and Tatsuya KATABUCHI

### 1. Introduction

Nuclear waste includes long-lived fission products (LLFPs). Currently, the deep geological disposal of nuclear waste is the national policy in Japan. However, it needs the long-term management that prevents the public from suffering radiological hazard due to LLFPs. Thus, the nuclear transmutation of LLFPs into stable or short-lived nuclides is an attractive option to decrease the hazard.

The neutron capture cross sections of LLFPs are important physical quantities for the research and development of nuclear transmutation systems, because the performance of system using neutron capture reaction depends on these quantities directly.

The nuclide  $^{107}\text{Pd}$  is one of the most important LLFPs. However, there is only one experimental data of its neutron capture cross section at the thermal neutron energy.

On the other hand, keV-neutron capture cross sections of stable Pd isotopes are also important for design of  $^{107}\text{Pd}$  transmutation system because stable Pd isotopes are inherently contained in  $^{107}\text{Pd}$  batch in reprocessing unless isotope separation is performed.

Our research group started a project of systematic measurement of the keV-neutron capture cross sections and capture gamma-ray spectra of  $^{107}\text{Pd}$  and stable Pd isotopes in 2010. We finished the measurement of  $^{106}\text{Pd}$  at incident neutron energies below 100 keV in 2011. We present the experimental results in this report.

### 2. Experiments

The detail of experimental procedure has been given in Ref. [1]. Only brief description is given here.

The capture cross section and capture gamma-ray spectrum of  $^{106}\text{Pd}$  and  $^{108}\text{Pd}$  were measured at incident neutron energies below 100 keV, using the 3 MV Pelletron accelerator of the Research Laboratory for Nuclear Reactors at the Tokyo Institute of Technology. An experimental arrangement is shown in Fig.1.

Pulsed neutrons were produced by the  $^7\text{Li}(p,n)^7\text{Be}$  reaction with a pulsed proton beam (1.5 ns width, 4 MHz repetition rate) from the accelerator. The incident neutron spectrum on a capture sample was measured by a Time of Flight (TOF) technique with a  $^6\text{Li}$ -glass scintillation detector (5 mm diam.  $\times$  5 mm thick).

The  $^{106}\text{Pd}$  sample was highly isotopically enriched metal (98.4% enrichment), and the net weights was 0.88 g. A gold sample was used as a standard sample of capture cross section. The distance between the neutron source and the sample was 12 cm.

Capture gamma rays emitted from the sample were detected with a large anti-Compton NaI(Tl) spectrometer by means of a TOF method. The main NaI(Tl) detector of the spectrometer had a diameter of 15.2 cm and a length of 30.5 cm, and was centered in an annular NaI(Tl) detector (33.0 cm OD  $\times$  35.6 cm length) for Compton suppression. The detectors were shielded with a combination of various materials: borated paraffin, borated polyethylene, Cd,  $^6\text{LiH}$  and potassium free lead [2]. Capture gamma rays were observed at an angle of  $125^\circ$  with respect to the proton beam direction. The pulse height (PH) and TOF of signals from the spectrometer were sequentially recorded in a list-mode data format and then, were analyzed offline.

The runs for the  $^{106}\text{Pd}$ ,  $^{197}\text{Au}$  and blank were repeated cyclically, thereby for changes in experimental conditions such as the incident neutron spectrum averaging out.

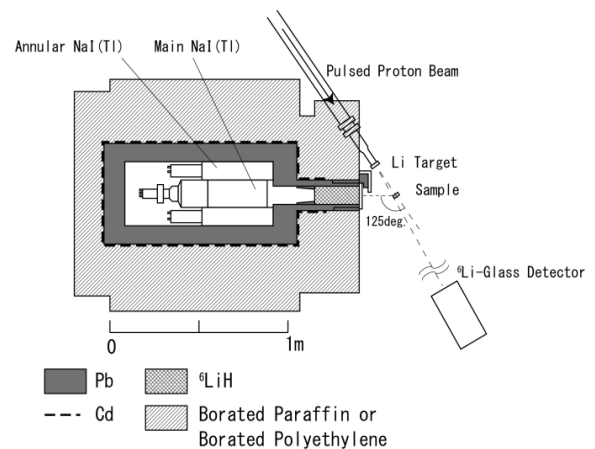


Fig.1 Experimental setup for capture cross section measurement.

### 3. Data Processing

In order to obtain the capture yields of the  $^{106}\text{Pd}$  and  $^{197}\text{Au}$  samples, a pulse-height weighting technique was applied to the net capture gamma-ray PH spectra. The evaluated data of the  $^{197}\text{Au}$  capture cross section from ENDF/B-VII.0 was used as standard cross section.

Corrections for the neutron self-shielding and multiple-scattering in the sample were made by a Monte-Carlo method [3]. Moreover, other corrections were made for the gamma-ray scattering and absorption in the sample.

The capture gamma-ray spectra were derived by unfolding the net capture gamma-ray PH spectra with the response matrix of the gamma-ray spectrometer. Unfolding process was done by using a computer code, FERDOR.

#### 4. Experimental Results

The derived capture cross section of  $^{106}\text{Pd}$  is shown in Figs. 2. The evaluated data of JENDL-4 and ENDF/B-VII.1 are shown for comparison. The evaluated cross section data shown in Fig. 2 are averaged over the same energy bins as the present data.

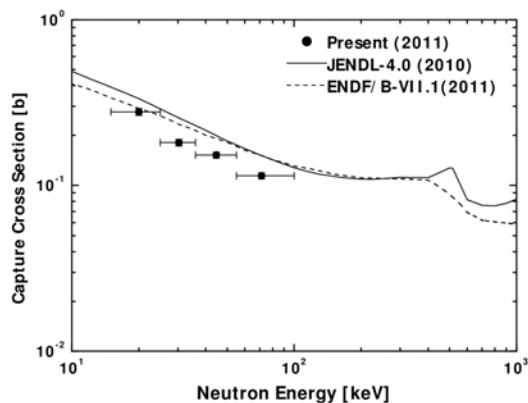


Fig. 2 Neutron capture cross section of  $^{106}\text{Pd}$ .

In the evaluations of both JENDL-4 and ENDF-B/VII, the capture cross section of  $^{106}\text{Pd}$  was calculated from statistical model. These evaluations overestimate the capture cross section by about 15% from the present results.

The measured capture  $\gamma$ -ray spectrum of  $^{106}\text{Pd}$  is shown in Figs. 3. The primary transitions from the capture state to low-lying states were clearly observed.

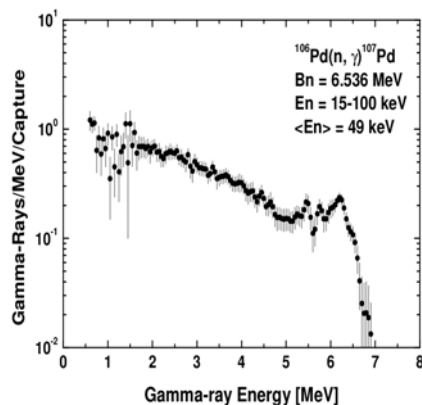


Fig. 3 Neutron capture gamma ray spectrum of  $^{106}\text{Pd}$ .

#### 5. Conclusions

We have measured the neutron capture cross section and capture gamma-ray spectrum of  $^{106}\text{Pd}$  at incident neutron energies below 100 keV to provide nuclear data relevant to the study on the transmutation of  $^{107}\text{Pd}$  and to obtain important physical quantities such as gamma-ray strength function and nuclear level density, which are useful for the theoretical calculation of capture cross section.

#### References

- [1] S. Mizuno *et al.*, *J. Nucl. Sci. Technol.*, **36**, 493 (1999).
- [2] M. Igashira, H. Kitazawa and N. Yamamuro, *Nucl. Instrum. Methods*, **A245**, 432 (1986).
- [3] K. Senoo *et al.*, *Nucl. Instrum. Methods*, **A339**, 556 (1994).

## B.2 Neutron-Irradiation-Induced Crystalline Defects in $\beta$ - $\text{Si}_3\text{N}_4$ and Recovery by Thermal Annealing

Toyohiko YANO, Tomoyuki YAMAGAMI and Katsumi YOSHIDA

A hot-pressed  $\text{Si}_3\text{N}_4$  ceramics was neutron-irradiated in the JOYO fast reactor. Based on high-resolution electron microscope observation, several kinds of tiny interstitial dislocation loops on the  $\{10\bar{1}0\}$  (denoted as A-loops) or  $\{11\bar{2}0\}$  (denoted as B-loops) planes were identified. Area density and average size of each planar defect was greater after irradiation to higher doses at higher temperatures. The density of A-loops was higher than that of B-loops, regardless of irradiation conditions. After annealing, size distribution of the A-loops was not changed up to 1350°C in the case of the specimen irradiated at the lowest temperature ( $0.5 \times 10^{26}$  n/m<sup>2</sup> at 377°C). On the other hand, the number of dislocations with diameter smaller than 4 nm decreased at over 900°C and the loop size distribution shifted larger size after annealing at temperatures higher than 1350°C in the case of higher irradiation temperature specimen ( $0.4 \times 10^{26}$  n/m<sup>2</sup> at 542°C) [1].

### 1. Introduction

$\text{Si}_3\text{N}_4$  is amazing structural ceramics which can be used at high-temperatures. Excellent strength with high fracture toughness and relatively higher thermal conductivity are confirmed. Therefore,  $\text{Si}_3\text{N}_4$  was nominated as a candidate material for first wall, r. f. window or high heat-flux components of fusion reactors.

High energy neutron irradiation induces several types of crystalline defects into ceramics, and these defects modify materials' properties. It is reported that  $\text{Si}_3\text{N}_4$  and SiAlON ceramics retain, more than many oxide ceramics, flexural strength and thermal diffusivity after irradiation up to  $1.0 \times 10^{24}$  n/m<sup>2</sup> at 150°C. Small swelling and relatively large drop of thermal diffusivity after irradiation up to  $2.8 \times 10^{25}$  n/m<sup>2</sup> ( $E > 0.1$  MeV) at 742°C were reported. We reported that the dimensional stability of  $\text{Si}_3\text{N}_4$  after concurrent neutron irradiation up to the order of  $10^{26}$  n/m<sup>2</sup> was superior to that of SiC, and higher thermal diffusivity was kept relatively as same as that of SiC [2-5]. After the high dose neutron irradiation, dislocation loops were densely formed mostly parallel to the [0001] axis. The structural configurations of the two types of them were identified [6, 7]. Each configuration could be created by rearrangement of  $\text{SiN}_4$  tetrahedra. In the Type-I dislocation, one  $\text{SiN}_4$  tetrahedral layer was inserted into  $\{10\bar{1}0\}$  planes (A-loops), and in the Type-II structure it was inserted into  $\{11\bar{2}0\}$  planes (B-loops). Type-I or Type-II dislocations are forbidden to intersect other dislocations, but they can connect to different type dislocations.

In this study, the size distribution and change in size of these planar defects after post-irradiation annealing are reported to understand their thermal stability and associated physical property changes of  $\text{Si}_3\text{N}_4$ .

### 2. Experimental Procedures

$\text{Si}_3\text{N}_4$  ceramics was obtained by the hot-pressing with full density ( $3.33\text{g/cm}^3$ ). The  $\text{Si}_3\text{N}_4$  phase was dominantly  $\beta$  type. The dimensions of the specimens were  $1.2 \times 1.2 \times 15.5$  mm<sup>3</sup> for swelling measurement. Neutron irradiation was performed in the JOYO experimental fast reactor. Four sets of specimens were irradiated in the following conditions. T51:  $2.8 \times 10^{26}$  n/m<sup>2</sup> ( $E > 0.1$  MeV), 520°C, T57:  $3.7 \times 10^{26}$  n/m<sup>2</sup>, 727°C; T71:  $0.5 \times 10^{26}$  n/m<sup>2</sup>, 377°C and T73:  $0.4 \times 10^{26}$  n/m<sup>2</sup>, 542°C. A part of the irradiated specimens was sliced and thinned by Ar ion milling for TEM observation. All high-resolution electron microscopy (HREM) micrographs were taken along the [0001] axis. Based on HREM observation, size of each planar defect, mainly loops, was measured and size distribution was obtained. After annealing under vacuum, the change in size distribution was again observed. From magnified images, clear dislocations as same as reported previously [6, 7] or portions with irregular atomic arrangement at least more than a few  $a$ -axis's length along a plane with strain contrast were identified as planar crystalline defects.

### 3. Results and Discussion

From electron micrographs of the as-irradiated specimens, three different microstructures were observed. In the T71 specimen, no clear loop formation was identified, but small strain contrasts were densely observed throughout grains. In the T73 specimen tiny loop-like contrasts with distorted strain contrast were observed here and there. On the contrary, length of defect was extended in the T51 and T57 specimens. Figure 1 shows typical HREM images from these specimens. Dislocation loops were frequently observed as differently contrasted portions compared to the normal hexagonal atomic configuration in the T51, T57 specimens (c, d, g) and smaller number in the T73 specimen (b). Defects were looked-like line defects lying along the  $\langle 11\bar{2}0 \rangle$  or  $\langle 10\bar{1}0 \rangle$  directions if it was looked along the [0001] axis. These were mostly A-loops or B-loops. In the T71 specimen, there were small areas where atomic arrangement did not clearly indicate the formation of loops (i. e. presence of an extra layer) but contrast

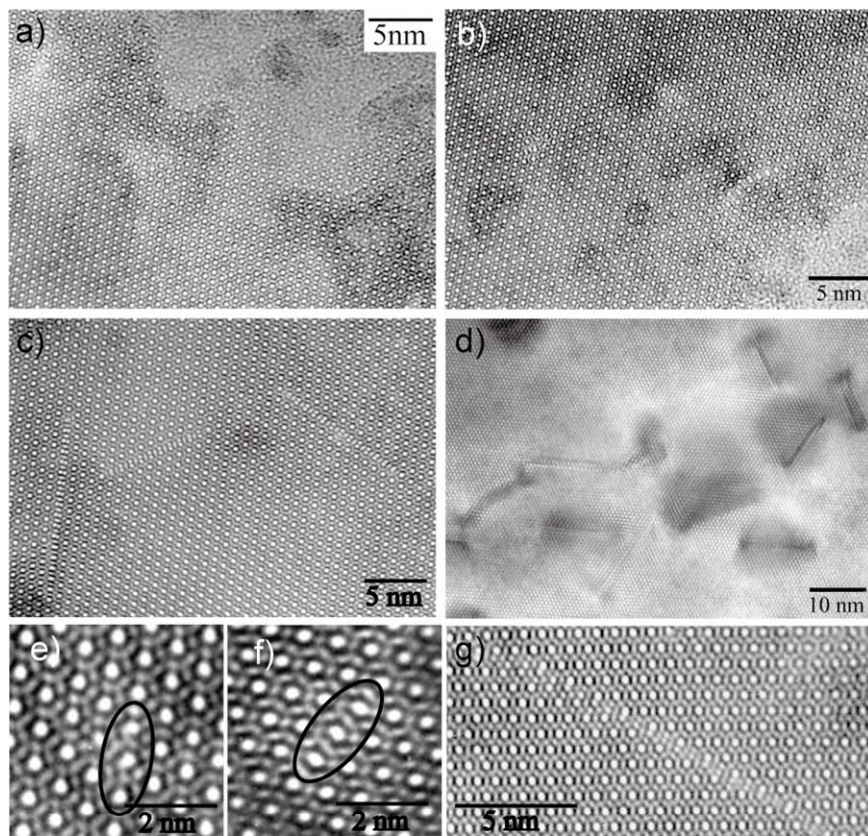


Fig. 1. High-resolution electron micrographs of as-irradiated specimens. (a) T71( $0.5 \times 10^{26}$  n/m<sup>2</sup>, 377°C), (b) T73( $0.4 \times 10^{26}$  n/m<sup>2</sup>, 542°C), (c) T51( $2.8 \times 10^{26}$  n/m<sup>2</sup>, 520°C), (d) T57( $3.7 \times 10^{26}$  n/m<sup>2</sup>, 727°C), (e) T71, (f) T71, (g) T51.

Table 1. Total diameter of planar defects per unit area and average defects diameter.

	Habit plane	T71	T73	T51	T57
Total diameter of planar defects per unit area ( $\mu\text{m}^{-1}$ )	{10 $\bar{1}$ 0}	8.2	8.5	23.0	22.0
	{11 $\bar{2}$ 0}	0.51	0.65	3.3	2.0
Average planar defect diameter (nm)	{10 $\bar{1}$ 0}	3.7	3.8	8.2	10.4
	{11 $\bar{2}$ 0}	4.0	4.5	6.5	8.6

was different from perfect crystal and showed strain contrast, as indicated with circles in (e) and (f).

It was observed that both total amount of defect, mainly loops, and average diameter of defects were higher in the T51 and T57 ( $3\text{--}4 \times 10^{26}$  n/m<sup>2</sup>) specimens than those of the T71 and T73 specimens ( $4\text{--}5 \times 10^{25}$  n/m<sup>2</sup>). Comparison of total amount of defects by habit planes, amount of A-loops was much larger than B-loops in spite of various irradiation conditions.

Figure 2 indicates size distribution of A-loops of the as-irradiated specimens. It was clear that most of the defects formed in the T71 and T73 specimens were smaller size (less than 4 nm) defects. It is considered that the size of defects around a few nm corresponded to a few unit cell length of the *a*-axis of  $\beta\text{-Si}_3\text{N}_4$  (0.76 nm), therefore these size should be the boundary size to form a loop. The number of the defect in the range less than 4 nm

included such a defect shown in Fig. 1(e, f). The density of defects with 4–8 nm in size in the T73 specimen was slightly higher than that of the T71 specimen. Otherwise, in the T51 and T57 specimens, size distribution of loops was broad and extended to larger size up to 20 nm. The average loop size of the T57 specimen was larger than that of the T51 specimen.

From microstructure observation of the T71 specimen annealed at higher temperature than 900°C, the strain contrast of defects was not obviously observed. In the T73 specimen, the clear dislocations were observable. After annealing at 1350°C, extended defects were observed.

Figures 3 and 4 indicate size distribution of A-loops of the T71 and T73 specimens after annealing, respectively. In the T71 specimen, distribution of the

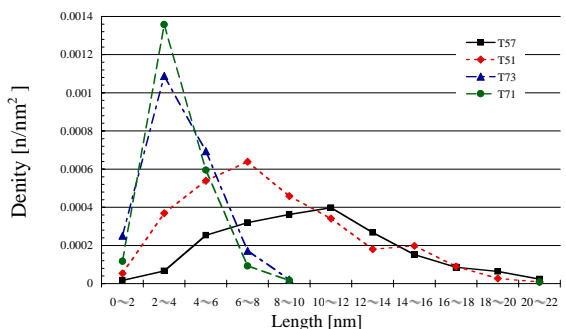


Fig. 2. Size distribution of A-loops of the as-irradiated specimens.

defect size did not change due to the annealing. On the contrary, distribution of defect size in the T73 specimen was modified gradually. Up to 900°C, the frequency of loops with 2~6 diameter increased, and then at 1350°C or higher annealing temperature most frequent size of loops was sifted to be 4~6 nm. From statistical analysis, total length of the defects per unit area in the T71 specimen increased slightly but the average size did not change due to annealing up to 1350°C for A-loops. Total length of the defects per unit area increased three times but the average size did not change due to annealing up to 1350°C for B-loops. Original amount of the latter defect was very small. Consequently, sum of the area of dislocation loops per unit area was estimated to increase ~25% after annealing at 1350°C. In the case of the T73 specimen, the same tendencies were observed for defects on the both habit planes.

Neutron irradiation response of  $\beta$ - $\text{Si}_3\text{N}_4$  is categorized into two groups. One is the case of lower dose at relatively lower irradiation temperature such as the T71 specimen, and in this case interstitial dislocation loops recognizable by HREM are not formed in the crystal during irradiation. The other group is that irradiated at higher dose at relatively higher temperature, such as the T51 and T57 specimens. The T73 specimen is close to the former case. Previously we considered that in the case of former irradiation conditions, there was no interstitial loop, and the specimen contains mostly point defects. In this case, recovery of length or thermal diffusivity can be explained by the annihilation of points defects. In the present study, it was clarified that even in the T71 specimen (and the T73 specimen), we can recognize the presence of small clusters less than a few nanometer. The area density of the defects was very low. These defects are stable (size and density) up to higher temperature than 1350°C, and total area of loops slightly increases due to annealing. Therefore, large part of defects should be existed as point defects, and small part are formed into clusters with diameter of a few nanometer. Once these clusters are formed, they are stable up to high temperature. Then, recovery of length and thermal diffusivity are

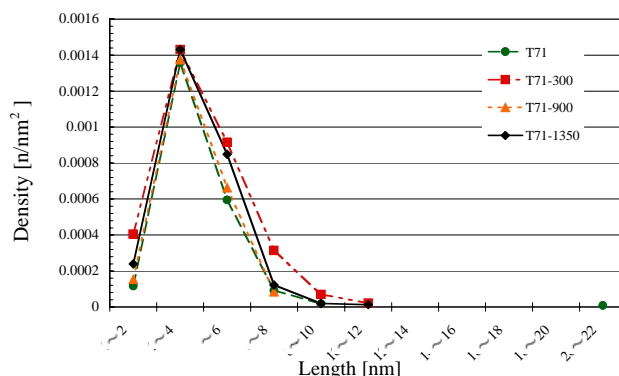


Fig. 3. Size distribution of A-loops of the T71 specimen after annealing at 300, 900 and 1350°C.

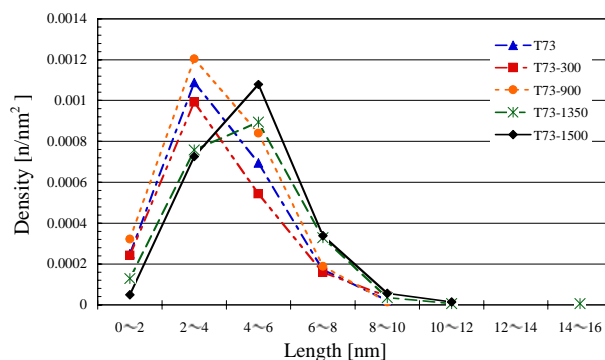


Fig. 4. Size distribution of A-loops of the T73 specimen after annealing at 300, 900, 1350°C for 1 h and step-heated up to 1500°C.

observed clearly by annihilation of points defects. Since average size of these very small defects did not changed by annealing up to 1350°C, the sink strength of these defects for interstitials may be weak. In the case of T73 specimen, most frequent size of defects shifted to slightly larger size after annealing over 900°C. It can be explained by the decrease of smaller defects by absorbing vacancies, resulting in higher relative concentration of larger defects.

In the case of relatively higher dose at higher temperature irradiation conditions, A-loops and B-loops are clearly and densely observed. Comparing the T51 and T57 specimens, average length of both loops in the T57 specimen was slightly greater than that of the T51 specimen. It was explained that the irradiation temperature of the T57 specimen was markedly higher than the case of the T51 specimen, and then the loops could be enlarged easier during irradiation. But once extended loops are formed, there are six equivalent planes (each two are same orientation) in the crystal due to crystal symmetry in both planes, they cannot cross each other. Therefore, growth of loops next to existing loops may be restricted [8]. As a result, point defects may be over saturated in the crystal and then recombine soon. Therefore, the defect density showed saturation-like feature. Another specimen

irradiated under resemble condition with the T51 or T57 specimens indicated that the size and density of dislocations were not significantly modified by the annealing up to 1500°C. Then, the interstitial dislocations are very stable with low sink strength. Therefore, it is the reason for small irradiation swelling and difficulty of recovery in macroscopic length or thermal diffusivity of  $\beta$ -Si<sub>3</sub>N<sub>4</sub>, once the stable interstitial loops are formed.

#### 4. Conclusions

Size distribution and density of the planar defects induced into the  $\beta$ -Si<sub>3</sub>N<sub>4</sub> by the neutron irradiation and changes by post-irradiation thermal annealing were evaluated. Lower fluence and lower temperature irradiation, very small (less than 4 nm) nuclei of planar defects were observed. These defects did not extend by the heat treatment, and were relatively stable up to high temperature, whereas part of smallest defects were annihilated after annealing more than 900°C. Density and average size of A- and B-loops increased by the higher dose irradiation in the order of 10<sup>26</sup> n/m<sup>2</sup>. These loops were also very stable up to high temperature without significant growth. Number density of A-loops was much higher than that of B-loops regardless of irradiation conditions.

#### References

- [1] T. Yano, T. Yamagami, K. Yoshida and M. Akiyoshi, *J. Nucl. Mater.*, **417** (2011) 972-975
- [2] T. Yano, M. Akiyoshi, K. Ichikawa, Y. Tachi and T. Iseki, *J. Nucl. Mater.*, **289** (2001) 102-109.
- [3] M. Akiyoshi, K. Ichikawa, T. Donomae and T. Yano, *J. Nucl. Mater.*, **307-311** (2002) 1305-1309.
- [4] M. Akiyoshi, N. Akasaka, Y. Tachi and T. Yano, *J. Ceram. Soc. Japan*, **112**[5] (2004) S1490-1494.
- [5] M. Akiyoshi, T. Takagi, T. Yano, N. Akasaka and Y. Tachi, *Fusion Eng. Design*, **81** (2006) 321-325.
- [6] M. Akiyoshi, T. Yano, M. Jenkins, *Phlos. Mag.* **A81** (2001) 683-697.
- [7] M. Akiyoshi, T. Yano, M. Jenkins, *Philos. Mag. Lett.* **81** (2001) 251-258.
- [8] M. Akiyoshi, N. Akasaka, Y. Tachi and T. Yano, *J. Nucl. Mater.*, **329-333** (2004) 1466-1470.

### B.3 A Study on Advanced Reprocessing System Based on Use of Cyclic Urea Derivatives with Highly Selective Precipitation Ability to U(VI)

Tomoya SUZUKI, Takeshi KAWASAKI, Koichiro TAKAO, Masayuki HARADA, Masanobu NOGAMI, and Yasuhisa IKEDA

We have developed an advanced reprocessing system for spent FBR fuels based on two precipitation processes [1-5]. In this system, first only U(VI) species are precipitated using a pyrrolidone derivative with low hydrophobicity and donicity, and secondly residual U(VI) and Pu(IV, VI) are precipitated simultaneously using a pyrrolidone derivatives (NRP) with higher precipitation ability. From the studies on precipitation ability of NRP to U(VI), Pu(IV), and Pu(VI) species in HNO<sub>3</sub>, we selected *N-n*-butyl-2-pyrrolidone (NBP) and *N*-neopentyl-2-pyrrolidone (NNpP) as the precipitants for the first and second precipitation processes, respectively. Furthermore, it was found that these precipitants have high stability under irradiation and heating, that a part of the precipitant component in the precipitates is evaporated and recovered at 150 ~ 170 °C, and that the carbon residue of UO<sub>2</sub> pellets prepared by the incineration of the precipitates of U(VI)-NBP or -NNpP is *ca.* 100 ppm. From these results, it was expected that our proposed system is basically feasible. However, U(VI) species were found to be coprecipitated with a part of Pu(IV) in the first precipitation process. This is as one of problems to be solved,

Hence, we have tried to find out new precipitants which can precipitate more selectively U(VI) in the first precipitation process. As a result, *N,N'*-dimethyl-propyleneurea, DMPU, Fig. 1) as a precipitant was selected, because DMPU has lower hydrophobicity and stronger donicity than NBP [6].

In the present study, we have investigated the precipitation ability of DMPU to U(VI) and U(IV), and also the selectivity to U(VI) from the viewpoints of log*P* (measure of hydrophobicity) of L and solubility and m.p. (melting point) of UO<sub>2</sub>(NO<sub>3</sub>)<sub>2</sub>(L)<sub>2</sub> (L = DMPU or NRP) to 3.0 M HNO<sub>3</sub> solution to find the factors for controlling selectivity of precipitants.

The complexes were synthesized by adding two equiv. of L to ethanol solution dissolved UO<sub>2</sub>(NO<sub>3</sub>)<sub>2</sub>·6H<sub>2</sub>O (0.40 M). These complexes were used to measure solubility and M.P. Precipitation ratio (P.R.) of DMPU to U(IV) were determined by using HNO<sub>3</sub> solutions containing only U(IV) (0.15 M). The U(IV) solution was prepared electrochemically from 3.0 M HNO<sub>3</sub> solution dissolving appropriate amount of UO<sub>2</sub>(NO<sub>3</sub>)<sub>2</sub>·6H<sub>2</sub>O. The P.R. values of DMPU to U(IV) were also determined by using HNO<sub>3</sub> solutions containing U(VI) (1.5 M) and U(IV) (0.15 M), where the amount of precipitant being able to precipitate U(VI) in a yield of 70 % was added.

It is found that the hydrophobic NRP with longer *n*-alkyl chain has lower solubility. On the other hand, the solubility of 2-pyrrolidone (NHP) with higher M.P. is lower than that of *N*-methyl-2-pyrrolidone (NMP). This result indicates that the NHP-U(VI) precipitates have

strong interaction each other. The DMPU complex has also strong interaction, because of its high M.P. (211°C). However, the hydrophobicity of DMPU is lower than that of NProP. Hence, it is suggested that precipitation ability of DMPU to U(VI) is similar to that of *N*-cyclohexyl-2-pyrrolidone (NCP).

In order to compare precipitation ability of DMPU to Pu(IV) with that of NProP, *N*-butyl-2-pyrrolidone (NBP) and NCP, we carried out precipitation experiments by using U(IV). Precipitates of U(IV) with DMPU and NProP were not observed. In case of NBP and NCP, viscous NRP phase contained U(IV) was formed. For NCP with higher hydrophobicity, the P.R. value of U(IV) was higher. Therefore, it is suggested that DMPU with lower hydrophobicity is hard to precipitate U(IV).

In U(VI) and U(IV) co-existence system, selectivity of DMPU to U(VI) compared with NBP and NCP was also examined. Figure 2 shows plots of P.R. values of U(IV) against stirring time. As seen from Fig. 2, the P.R. value of U(IV) with DMPU is smaller than those with NBP and NCP. In case of NBP, the P.R. value decreases with stirring.

From these results, it is expected that DMPU is useful precipitant for the first precipitation process.

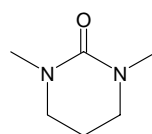


Fig. 1. Chemical formula of DMPU.

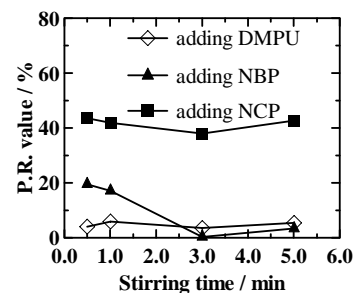


Fig. 2. Plots of P.R. values of U(IV) against stirring time for the precipitation reactions with DMPU, NBP, and NCP in the U(VI)-U(IV) coexistence systems.

#### References

- [1] N. Koshino, N. Asanuma, M. Harada, Y. Morita, T. Chikazawa, T. Kikuchi, Y. Ikeda, *Prog. Nucl. Energy*, **47**, 406 (2005).
- [2] K. Yamazaki, T. Chikazawa, Y. Tamaki, T. Kikuchi, M. Hanzawa, Y. Morita, Y. Ikeda, *Prog. Nucl. Energy*, **47**, 414 (2005).
- [3] Y. Morita, Y. Kawata, H. Mineo, N. Koshino, N. Asanuma, Y. Ikeda, K. Yamazaki, T. Chikazawa, T. Tamaki, T. Kikuchi, *J. Nucl. Sci. Technol.*, **44**, 354 (2007).
- [4] K. Takao, K. Noda, Y. Morita, K. Nishimura, and Y. Ikeda, *Crystal Growth & Design*, **8**, 2364 (2008).
- [5] Y. Morita, K. Takao, S.-Y. Kim, Y. Kawata, M. Harada, M. Nogami, K. Nishimura, and Y. Ikeda, *J. Nucl. Sci. Technol.*, **46**, 1129 (2009).
- [6] T. Suzuki, T. Kawasaki, and Y. Ikeda, *Acta Cryst.*, **E67**, m18 (2011).

## B.4 Electrochemical and Spectroelectrochemical Studies on $[\text{UO}_2\text{Cl}_4]^{2-}$ in 1-Ethyl-3-methylimidazolium Based Ionic Liquids

Toshinari OGURA, Koichiro TAKAO, Kotoe SASAKI, Tsuyoshi ARAI, Yasuhisa IKEDA

Room temperature ionic liquids (ILs) are expected to be useful media for recovering uranium from spent nuclear fuels and solid wastes contaminated with uranium[1], *e.g.*, as media for extraction and electrolytic deposition. Hence, the extraction behavior of uranyl species from aqueous to IL phase, the electrochemical behavior of uranyl species in ILs, and so on have been studied[2-9].

In the present study, we have examined the electrochemical behavior of uranyl(VI) species,  $(\text{EMI})_2\text{UO}_2\text{Cl}_4$ , in the mixture of EMICl and EMIBF<sub>4</sub> (EMI = 1-ethyl-3-methylimidazolium) to obtain the basic data for evaluating application of ILs to pyro-reprocessing process. We used the mixture of EMICl and EMIBF<sub>4</sub> as the reaction media, because this mixture is liquid at room temperature.

The UV-visible absorption spectrum of the EMICl and EMIBF<sub>4</sub> mixture dissolved  $[\text{EMI}]_2[\text{UO}_2\text{Cl}_4]$  ( $5.48 \times 10^{-2}$  M) was found to be consistent with those of  $[\text{UO}_2\text{Cl}_4]^{2-}$  in 1-butyl-3-methylimidazolium bis(trifluoromethylsulfonyl) imide and *N*-butyl-*N*-methylpyrrolidinium bis(trifluoromethylsulfonyl)imid at room temperature ( $[\text{UO}_2^{2+}]/[\text{Cl}^-] = 1/5$ ). This indicates that the uranyl species in the EMICl and EMIBF<sub>4</sub> mixture exist as  $[\text{UO}_2\text{Cl}_4]^{2-}$ .

Figure 1 shows the cyclic voltammograms of the EMICl and EMIBF<sub>4</sub> mixture dissolved  $[\text{EMI}]_2[\text{UO}_2\text{Cl}_4]$  ( $6.06 \times 10^{-2}$  M). As seen from Fig. 2, one redox couple is observed around -1.0 V vs. Fc/Fc<sup>+</sup>. Furthermore, it was found that the values of  $(E_{\text{pc}} + E_{\text{pa}})/2$  ( $E_{\text{pc}}$  and  $E_{\text{pa}}$  are peak potentials for cathodic and anodic peaks, respectively) are constant (-0.989 V vs. Fc/Fc<sup>+</sup>) regardless of the scan rates, and that a plot of  $i_{\text{pc}}$  (the peak currents of cathodic peaks) against  $v^{1/2}$  gives a linear relationship with slope of 8.21. Furthermore, we estimated the standard rate constant ( $k^0$ ) based on the kinetic parameter ( $\psi$ ) proposed by Nicholson. The  $k^0$  value was estimated as  $(2.7\sim 2.8) \times 10^{-4}$  cm/s in the range of scan rates from 50 to 300 mV/s. The estimated value is in the range of the  $k^0$  value ( $(4.0 \sim 9.9) \times 10^{-3} > k^0 > (2.7 \sim 6.6) \times 10^{-7}$ ) for the quasi-reversible reaction on the basis of the reversibility factor ( $A$ ) of Matsuda and Ayabe. These results suggest that the electrochemical reaction of  $[\text{UO}_2\text{Cl}_4]^{2-}$  proceeds quasi-reversibly.

In order to examine the reduction product, we carried out spectroelectrochemical studies using optically transparent thin layer electrode (OTTLE) cell in the range from 0 to -1.306 V. The result is shown in Fig. 2. The isosbestic point is found to be observed around 350 nm. In addition, from the Nernstian plot, the electron stoichiometry ( $n$ -value) and the formal potential were evaluated as 0.99 and -0.99 V, respectively. These results indicate that  $[\text{U}^{\text{VI}}\text{O}_2\text{Cl}_4]^{2-}$  is reduced to  $[\text{U}^{\text{V}}\text{O}_2\text{Cl}_4]^-$  in the mixture of EMICl and EMIBF<sub>4</sub>, and the resulting  $[\text{U}^{\text{V}}\text{O}_2\text{Cl}_4]^-$  species are relatively stable.

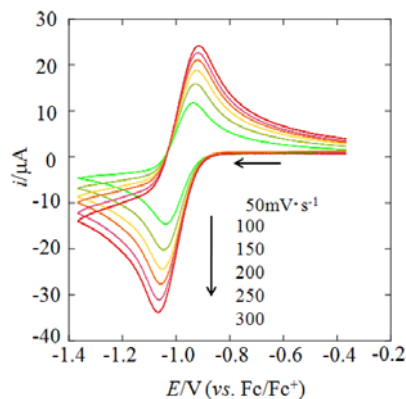


Fig. 1. Cyclic voltammograms of the solutions prepared by dissolving  $[\text{EMI}]_2[\text{UO}_2\text{Cl}_4]$  into the mixture of EMICl and EMIBF<sub>4</sub>.  $[\text{UO}_2^{2+}] = 6.06 \times 10^{-2}$  M, Scan rates ( $v$ ) = 50~300 mV/s, Temp. = 25 °C.

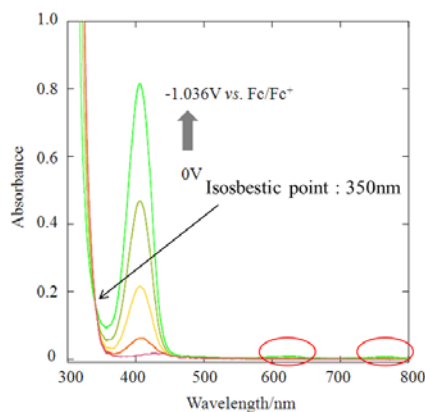


Fig. 2. UV-visible absorption spectra measured at the applied potential from 0.0 to -1.036 V vs. Fc/Fc<sup>+</sup> for the mixture of EMICl and EMIBF<sub>4</sub> dissolving  $[\text{EMI}]_2[\text{UO}_2\text{Cl}_4]$  ( $5.48 \times 10^{-2}$  M). Optical path length = 0.021 cm.

### References

- [1] V.A. Cocalia, K.E. Gutowski, and R.D. Rogers, *Coord. Chem. Rev.*, **250**, 755 (2006).
- [2] M. Deetlefs, C.L. Hussey, T.J. Mohammed, K.R. Seddon, J.-A. Berg, and J.A. X0ra, *Dalton Trans.*, 2334 (2006).
- [3] K. Binnemans, *Chem. Rev.*, **107**, 2592 (2007).
- [4] P. Giridhar, K.A. Venkatesan, S. Subramanian, T.G. Srinivasan, P.R.V. Rao, *J. Alloys Compd.* **448**, 104 (2008).
- [5] C.J. Rao, K.A. Venkatesan, K. Nagarajan, and T.G. Srinivasan, *Radiochim. Acta*, **96**, 1 (2008).
- [6] Y. Ikeda, K. Hiroe, N. Asanuma, and A. Shirai, *J. Nucl. Sci. Technol.*, **46**, 158 (2009).
- [7] Y. Ohashi, N. Asanuma, M. Harada, Y. Wada, T. Matsubara, and Y. Ikeda, *J. Nucl. Sci. Technol.*, **46**, 771 (2009).
- [8] C. Gaillarf, A. Chaumont, I. Billard, C. Hennig, A. Ouadi, S. Georg, and G. Wipff, *Inorg. Chem.*, **49**, 6484 (2010).
- [9] T.J. Bell and Y. Ikeda, *Dalton Trans.*, **40**, 10125 (2011).

## B.5 Dynamics Studies on Water Confined in Polymer Brushes by Low-Field Pulsed NMR

Takehiko TSUKAHARA

Studies on water molecules inside biological nanospaces such as smart polymers and membranes has gained importance for controlling the biomedical and analytical functions of biomolecules on the surface. However, limited information at molecular level is available about the interactions between water molecules and polymers on the surface. Nuclear Magnetic Resonance (NMR), which is sensitive to the variation of slow molecular motion, should be helpful in determining the dynamical properties of water in nanoconfinement environments [1-3]. Thus, in this study, we examine temperature-dependence of the magnetic relaxation times ( $T_1$ ,  $T_2$ ) of water in the fabricated poly(N-isopropylacrylamide) (PNIPAAm) brushes using low-field pulsed NMR, and evaluate the correlation between hydration states and phase transition phenomena of PNIPAAm brushes.

PNIPAAm brushes were prepared through surface-initiated atom transfer radical polymerization (ATRP) using porous silica beads (pore size: 5~30 nm, particle size 5  $\mu\text{m}$ ). ATRP initiators were immobilized onto porous silica beads by silane coupling reaction. NIPAAm were polymerized to graft onto the initiator-immobilized surfaces using  $\text{CuCl}/\text{CuCl}_2/\text{Me}_6\text{TREN}$  (Fig. 1). The PNIPAAm brush beads were immersed in water, and the  $T_1$  and  $T_2$  values of water were measured respectively by inversion recovery and CPMS pulse sequences at various temperatures. For obtaining supporting information of the surface properties, contact angles and differential scanning calorimetry (DSC) of PNIPAAm brushes were measured.

The results of the  $T_1$  and  $T_2$  values of water in PNIPAAm brushes are shown in Fig. 2. The  $T_1$  and  $T_2$  values for 5~12 nm pore silica beads were discontinuously changed at 25~30°C, which is similar to phase transition temperature by contact angle and DSC results. These changes in relaxation time of water suggest that the mobility of water around PNIPAAm brush is decreased by holding into aggregated polymer chains above its phase transition temperature. The  $1/T_2 - 1/T_1$  value, which relates with a degree of proton transfer, of water in PNIPAAm brush beads was higher than that in bare silica beads above the phase transition temperature, but similar values at lower temperature regions. The restricted water due to aggregation of dehydrated PNIPAAm chains will form well-ordered hydrogen bonding networks in confined small spaces, resulting in high proton transfer rate.

In 30 nm pore of PNIPAAm brush beads, the relaxation times were linearly changed with increasing temperature. In contrast, a decrease of  $T_1$  value was observed in 5 nm porous beads with increasing temperature. This fact indicates that water mobility in 5 nm pore was restricted by dehydration of PNIPAAm brushes.

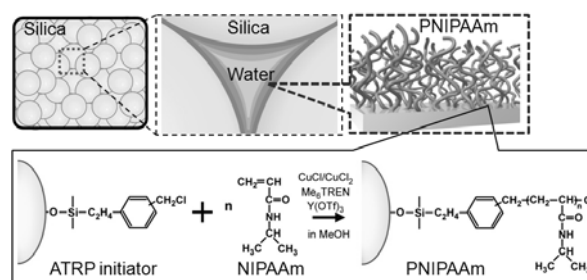


Fig. 1 The radical polymerization procedures on porous silica beads for making PNIPAAm brush.

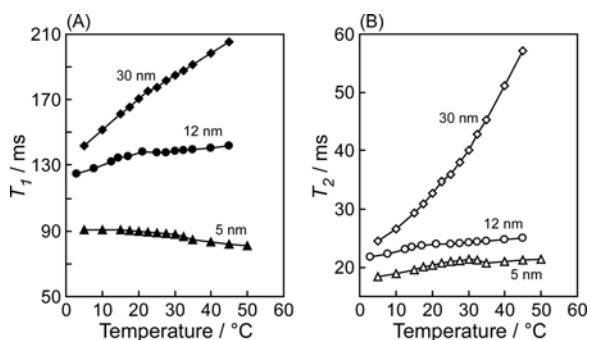


Fig. 2 Temperature- and beads size-dependence of (A)  $T_1$  and (B)  $T_2$  of water in PNIPAAm using low-field pulsed NMR.

### References

- [1] T. Tsukahara, et al., *Angew. Chem. Int. Ed.*, **46**, 1180 (2007),
- [2] T. Tsukahara, et al., *J. Phys. Chem. B*, **113**, 10808 (2009).
- [3] T. Tsukahara, et al., *Chem. Soc. Rev.*, **39**, 1000 (2010).

## B.6 Liquid-Liquid Extraction of Cadmium(II) Ion with Hydrophobic TPEN Derivatives

Yusuke INABA, Atsunori MORI and Kenji TAKESHITA

TPEN, *N,N,N',N'*-(tetrakis-2-pyridylmethyl)ethylenediamine, is recognized as a hexadentate ligand with six nitrogen donors and has been shown to chelate a variety of soft metal ions such as Hg, Cd, Au and Pd. It was also shown to be effective for chelation of *f*-block metals and separation of minor actinides from high level radioactive waste (HLW) has been an attractive issue.<sup>1-5</sup> Thereby TPEN derivatives have been employed as an extracting agent for variety of metal ions in organic solvents. We envisaged that modification of the structure of TPEN would enhance hydrophobicity and tolerance to the contact of acidic aqueous layer during the extraction. Herein, we report syntheses of novel TPEN derivatives bearing hydrophobic alkyl substituents and studies on the extraction behaviors of cadmium ion with the synthesized extracting agents.

### Results and discussion

The synthetic pathway of novel TPEN derivatives bearing alkyl side chains (**PyC5** and **PyC(C4)<sub>2</sub>**) and the structure of **PyOC4** are summarized in Scheme 1.

With these TPEN derivatives extraction studies were carried out using cadmium(II) ion. A nitric acid solutions of Cd(NO<sub>3</sub>)<sub>2</sub> (1 mM) were subjected to the extractions with the above chloroform solutions of **PyOC4**, **PyC5** and **PyC(C4)<sub>2</sub>** (1 mM). The experiments were carried out under various pH values of Cd(II) solutions. The %extraction value of Cd was estimated by measuring the concentration of the aqueous phase after extraction by ICP-AES analyses. Figure 1 shows the results of the extraction.

Hydrophobic TPEN derivatives **PyC5** and **PyC(C4)<sub>2</sub>** bearing alkyl chains on the pyridine rings were found to extract the Cd(II) ion highly efficiently over the acidic pH ranges of 0-2. The effect would be due to the improved hydrophobicity by the introduction of long-chained substituent on the pyridine ring. The electron-donating characteristics of alkyl group would also enhance the chelating ability of pyridine nitrogen.

### Conclusions

In summary, we synthesized novel TPEN derivatives bearing alkyl side-chains involving the chain length and the branched structures. These derivatives could extract Cd(II) ion highly efficiently over the acidic pH ranges, which would be applied for the separation of minor actinides from high level radioactive wastes (HLW).

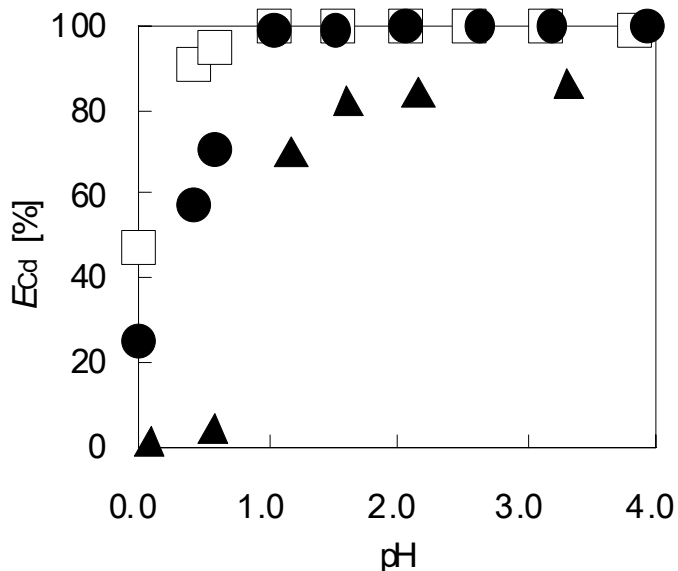
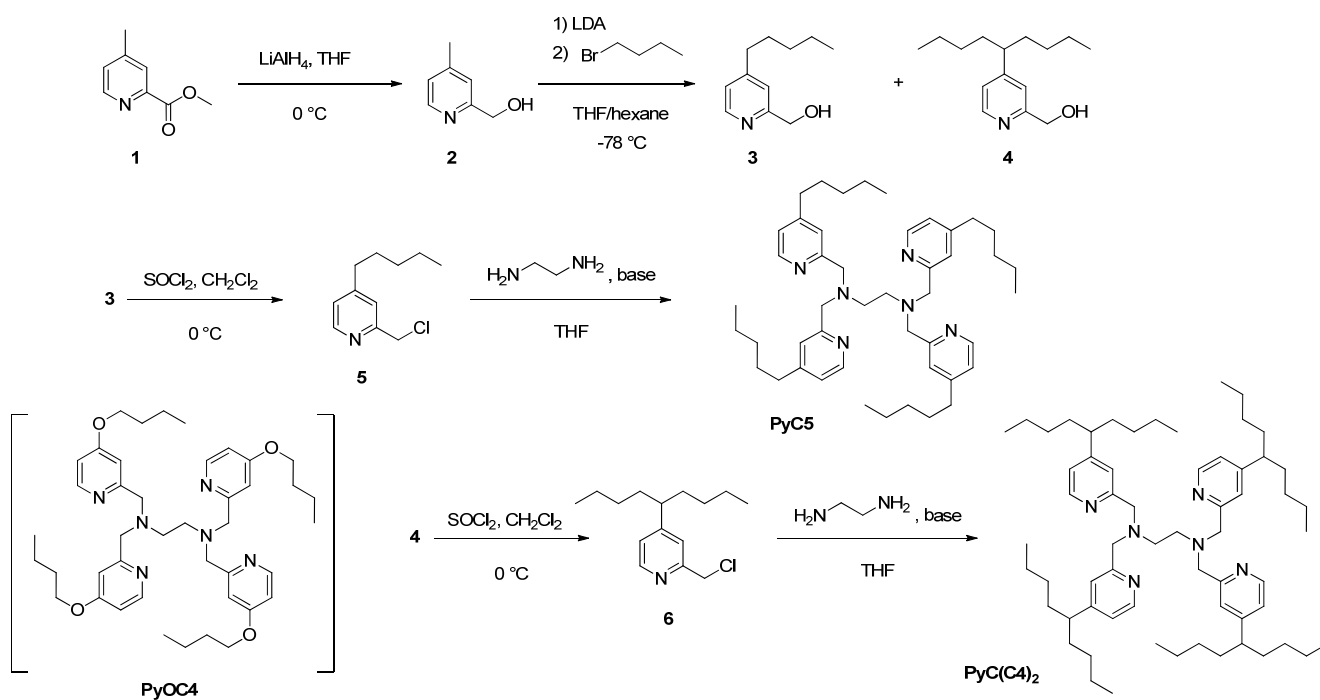


Figure 1. Dependence of pH on %extraction of Cd<sup>2+</sup> with PyOC4 (▲), PyC5 (●) and PyC(C4)<sub>2</sub> (□).

### References and notes.

1. Watanabe, M., Mirvaliev, R., Tachimori, S., Takeshita, K., Nakano, Y., Morikawa, K., Mori, R. Separation of americium(III) from lanthanide by encapsulating hexadentate-ligand. *Chem. Lett.* **31**, 1230-1231 (2002).
2. Mirvaliev, R., Watanabe, M., Matsumura, T., Tachimori, S., Takeshita, K. Selective separation of Am(III) from Ln(III) with a novel synergistic extraction system, *N,N,N',N'*-tetrakis(2-methylpyridyl)ethylenediamine (TPEN) and carboxylic acid in 1-octanol. *J. Nucl. Sci. Technol.* **41**, 1122-1124 (2004).
3. Ogata, T., Takeshita, K.; Fugate, G. A.; Mori, A. Extraction of soft metals from acidic media with nitrogen-donor ligand TPEN and its analogs. *Sep. Sci. Technol.* **43**, 2630-2640 (2008).
4. Takeshita, K., Watanabe, K., Nakano, Y., Watanabe, M. Solvent extraction separation of Cd(II) and Zn(II) with the organophosphorus extractant D2EHPA and the aqueous nitrogen-donor ligand TPEN. *Hydrometallurgy* **70**, 63-71 (2003).
5. Takeshita, K., Watanabe, K., Nakano, Y., Watanabe, M. Extraction of Cd(II) and Zn(II) with dialkylthiophosphinic acid and hexadentate nitrogen-donor ligand. *Chem. Lett.* **32**, 96-97 (2003).



Scheme 1. Syntheses of TPEN derivatives.

## B.7 Development of Cesium Recovery Process by Hydrothermal Treatment and Coagulation-Sedimentation

Hideharu TAKAHASHI, Kenji TAKESHITA, Chie IGUCHI and Yusuke INABA

### 1. Introduction

The radioactive substances were released by the accident at Fukushima Daiichi nuclear power plant, and the environment surrounding the nuclear reactor site was polluted extensively. To clean up the polluted environment, we are developing the cesium recovery process which combined the hydrothermal treatment using subcritical water and the coagulation-sedimentation [1-8]. In this report, especially, we discuss the applicability of the cesium recovery process to decontaminate polluted soils and plants.

### 2. Methodology

The cesium recovery process consists of four steps (see Fig.1), ①Collecting contaminants and pre-treatment, ②Stripping cesium from contaminants to liquid phase (hydrothermal / blasting treatment and washing), ③Separation of cesium from liquid phase as a sediment (coagulation-sedimentation and sediment recovery), ④Final disposal of cesium enriched adsorbent (calcination, solidification and disposal).

Under high temperature (about 200~300°C) and high pressure (about 2 ~ 9MPa, in our experiment), water (subcritical water) can decompose and solubilize organic substances to liquid phase by only water, because the ionic product of the water changes to high. Therefore, we tried to apply the subcritical water on cesium recovery process for stripping cesium from organic substances in polluted soils and plants to liquid phase (i.e. hydrothermal treatment).

Additionally, we are developing a blasting treatment that the physical structure of an inorganic substance in polluted soils and plants might be destroyed by performing rapid decrease of pressure, and cesium in it might be stripped to liquid phase.

In the coagulation-sedimentation, the cesium in the liquid phase is selectively adsorbed by ferric ferrocyanide, and its sediment recovery is carried out by a coagulant.

### 3. Results and discussion

In the case of the polluted agricultural soil (55,000Bq/kg) containing radioactive cesium at Nagadoro area in Iitate-mura, the hydrothermal treatment and the blasting treatment (200 °C, about 2 MPa, Solid-liquid weight ratio 0.75 ~ 3.0) were conducted. As the result, distribution ratio of cesium to the liquid phase became about 85%. This test showed that the hydrothermal treatment and the blasting treatment are effective to decontaminate polluted soils.

Furthermore, as for the stripped cesium in liquid phase

by only hydrothermal treatment (260 °C, about 5.1 MPa, and solid-liquid weight ratio 3.0), when the coagulation-sedimentation was carried out, the almost whole quantity of cesium, about 99.8%, was collected.

In the case of the polluted plants, we used imitated polluted plant leaf containing non-radioactive cesium. In this experiment, the leaves of broadleaf tree (Genus *Prunus*) are immersed in aqueous solution of non-radioactive cesium chloride for 24 hours, and then, washed by water, and dried. To the imitated polluted plants, the hydrothermal treatment (260 °C, about 5.1 MPa, and solid-liquid weight ratio 2.0) was conducted. As a result, distribution ratio of cesium to the liquid phase became about 86.9%. This test showed that the hydrothermal treatment is effective for decontaminating polluted plant. Furthermore, by washing the solid phase with distilled water after hydrothermal treatment, the distribution ratio of cesium to the liquid phase is improved, up to about 96.6%.

Moreover, the coagulation-sedimentation was carried out to its liquid phase. The almost whole quantity of cesium, about 99.7%, was collected, as same as the soil experimental result.

### 4. Summary

Although the experiment of actual polluted plants containing radioactive cesium needs to be conducted, both experimental results (soil and plant) lead to the conclusion that the cesium recovery process combining the hydrothermal treatment using subcritical water and the coagulation-sedimentation can be effective for decontamination of both.

### Acknowledgements

We thank Prof. Masanori Aritomi, Prof. Yasuhisa Ikeda (Tokyo Institute of Technology) and Prof. Tatsuya Suzuki (Nagaoka University of Technology) for developing of coagulation-sedimentation techniques. We also appreciate the cooperation in research and development of Toagosei Co., Ltd., Dainichiseika Color & Chemicals Mfg.Co., Ltd., CDM Consulting Co., Ltd., Radioactive Waste Management and Nuclear Facility Decommissioning Technology Center (RANDEC) and NPO. Saiseisha. In addition, in this report, the contents related to decontamination of agricultural soil are a part of research results achieved in our empirical study supported by the Ministry of Agriculture, Forestry and Fisheries (MAFF) of Japan in fiscal 2011.

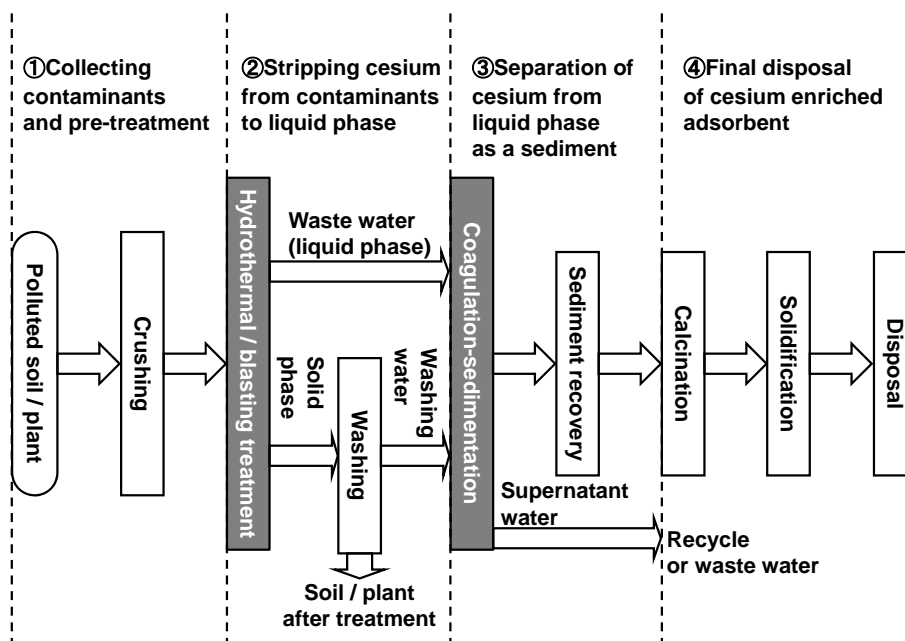


Fig.1 Cesium Recovery Process by Hydrothermal Treatment and Coagulation-Sedimentation

## References

- [1] K. Takeshita, Y. Ikeda, T. Suzuki, T. Ogata and M. Aritomi: Restoration of Environmental Pollution by Fukushima NPP Accident (Invited Lecture); *The 43rd Autumn Meeting of the Society of Chemical Engineers*, Nagoya, Japan, T208 (2011). [in Japanese]
- [2] K. Takeshita: Restoration of Water, Soil and Sewage Sludge contaminated by Fukushima Nuclear Accident (Plenary Lecture); *PROCESSES IN ISOTOPES AND MOLECULES (PIM2011)*, Cluj-Napoca, Romania, PL-12 (2011).
- [3] K. Takeshita, Chemistry Today, *Kagaku-Dojin Publishing Company, Inc.*, **490**, 43-47 (2012). [in Japanese]
- [4] K. Takeshita and T. Ogata: Application of Ion Exchange Technique to Decontamination of Polluted Water Generated by Fukushima Nuclear Disaster; *Journal of Ion Exchange*, **23**(1), 1-5 (2012). [in Japanese]
- [5] K. Kanazawa, K. Yoshikawa, K. Takeshita, T. Ogata and K. Kaku: Cs removal from fallen leaves using hydrothermal treatment; *The 5th Student Members Kanto Branch Meeting of the Atomic Energy Society of Japan*, Fujisawa, Japan, A13, 13 (2012). [in Japanese]
- [6] T. Fukuda, T. Ogata and K. Takeshita: Removal of cesium by coagulation-sedimentation method using ferric ferrocyanide; *The 5th Student Members Kanto Branch Meeting of the Atomic Energy Society of Japan*, Fujisawa, Japan, A14, 14 (2012). [in Japanese]
- [7] K. Takeshita, H. Takahashi, K. Mogami and A. Ishido: Recovery of Cesium from Polluted Soil by Hydrothermal Decomposition – Coagulation Settling Combined Process; *The 77th Annual Meeting of the Society of Chemical Engineers*, Tokyo, Japan, Q118, 663 (2012). [in Japanese]
- [8] T. Fukuda, T. Ogata and T. Kenji: Adsorption separation of cesium using ferrocyanide; *The 77th Annual Meeting of the Society of Chemical Engineers*, Tokyo, Japan, Q121, 666 (2012). [in Japanese]

## B.8 Calculation of Heavy-Ion Stopping in Foam Targets Coupled with 1D Hydrodynamics

Yoshiyuki OGURI

### 1. Introduction

In relation to ion-driven inertial fusion research, it has been experimentally verified that stopping power of heavy ions is enhanced when the target is highly ionized. Similar effects are observed not only for ionization but also for other changes of electronic state in the target[1].

Low density foams are widely used as targets for inertial fusion experiments. By using foams, target density and size can be independently controlled in accordance with the purpose of the experiment. From a microscopic point of view, a foam is a complex heterogeneous mixture of solid and vacuum (or gas). Such a microstructure changes with hydrodynamic motion including atomic excitations and ionizations during heating. Thus, the change of the projectile stopping power in foams during heating can be very complex. However, in designing beam parameters of ion-driven warm dense matter (WDM) experiments with low-density foam targets, the foams are usually regarded as homogeneous media, and the mass stopping power is assumed to be equal to that of homogeneous room-temperature materials. For more detailed design of the experimental setup, the initial inhomogeneous porous structure of the foam target should be taken into account[2].

In this paper we present results of numerical study on the heavy-ion stopping in foam targets with subcell-scale hydro motions induced by the energy deposition of incident ions themselves. Calculation of the projectile energy loss taking into account the target temperature- and density dependence is briefly introduced. The results on the energy loss profile are compared with those for the homogeneous equivalent target in consideration of the density- and temperature distribution during irradiation.

### 2. Method of calculation

To simulate a porous foam target, we employed a simple 1D periodic multilayer model consisting of thin solid slabs and gaps between them. This model is illustrated in Fig. 1. The averaged pore diameter and cell-wall thickness of the foam were represented by the gap width between the slabs and the slab thickness, respectively. Residual gases in the pores were simulated by dilute ( $\rho = 10^{-3}\rho_{\text{solid}}$ ) vapor of the wall material. Note that the present method has a limitation that the multidimensional mixing due to hydrodynamic instability cannot be treated, and therefore homogenization is underestimated.

In this work, we must take into account changes of stopping cross section due to changes in size, excitation,

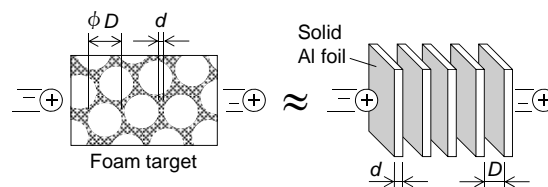


Fig. 1: 1D multilayer structure simulating a foam target.

and ionization of the target atoms during the heating and expansion. To assess the target condition, we used the phase space density distribution of electrons in the target atoms evaluated by a finite-temperature Thomas-Fermi model with given atomic radii corresponding to given densities. A simple binary encounter model was employed to calculate the total electronic stopping cross section  $S_e$  by integrating the energy transfer from the projectile to each target electron[3]. The projectile charge was evaluated using a simple Thomas-Fermi scaling. The total cross section  $S$  was obtained as  $S = S_e + S_n$ , where  $S_n$  denotes the nuclear stopping cross section.

We used a combination of  $^{11}\text{Na}$  projectiles and subrange  $^{13}\text{Al}$  foam targets with  $\rho = 0.05\rho_{\text{solid}}$  for the analysis. The incident projectile energy was adjusted so that the Bragg peak could be at the center of the target[1]. For this adjustment, as has been done in previous studies, the stopping power data for room-temperature solid-density Al was used. The hydrodynamic motion of the multilayer target was calculated with a 1D computer code MULTI. We assumed that the targets are irradiated by a pulsed beam with a temporal flux profile

$$\phi(t) = \phi_0 \sin\left(\frac{\pi t}{\tau}\right)$$

during  $0 < t < \tau$ . The pulse duration  $\tau$  and the peak flux  $\phi_0$  are 2 ns and  $4 \text{ GW/mm}^2$ , respectively. It follows that the total energy deposition  $\phi_0 \tau/2$  is  $4 \text{ J/mm}^2$ .

### 3. Results and discussion

#### 1) Temperature- and density-dependent ion stopping

Figure 2(a) shows the stopping cross section calculated for solid density targets as a function of the projectile energy for different temperatures. Even if the target is heated up to  $kT = 10 \text{ eV}$ , we see practically no change of the Bragg curve. In this figure, data from the SRIM code for solid-density room-temperature Al target are plotted for comparison. The shape of the calculated curves

including the Bragg peak agrees well with that of the SRIM data.

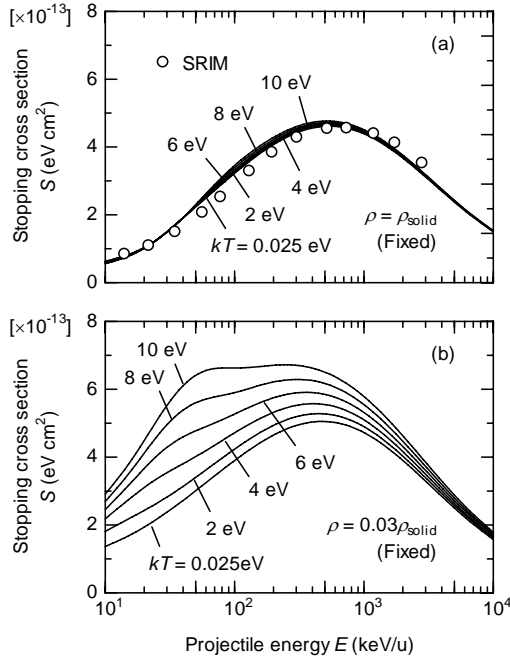


Fig. 2: Stopping cross section as a function of the projectile energy for different target temperatures and densities.

Figure 2(b) shows the results for  $\rho = 0.03\rho_{\text{solid}}$  targets. The stopping cross section increases with the target temperature, especially at low projectile energies. Also the Bragg-peak position shifts slightly toward the low energy. This result is explained by the increase of the low velocity portion of the bound electrons due to excitation. At higher temperatures, a small bump appears in the low velocity region corresponding to the thermal speed of electrons. This bump is attributed to the enhanced stopping by free electrons which has been observed in highly ionized plasma targets. The data of stopping cross sections calculated for  $0.025 \text{ eV} \leq kT \leq 10 \text{ eV}$  and  $10^{-4}\rho_{\text{solid}} \leq \rho \leq 10\rho_{\text{solid}}$  were embedded in the hydrodynamics code.

## 2) Target mass thickness

From the curve for  $kT = 0.025 \text{ eV}$  in Fig. 2(a), by ignoring the temperature- and density dependence of the stopping cross section, we determined an appropriate combination of target mass thickness and incident projectile energy to achieve an energy deposition profile with a given required homogeneity. We assumed that the limit of acceptable inhomogeneity is  $\pm 2.5\%$ . In this case the incident energy  $E_{\text{in}}$  and the exit energy  $E_{\text{out}}$  are automatically determined to be  $1.01 \text{ MeV/u}$  and  $0.29 \text{ MeV/u}$ , respectively. The corresponding energy deposition in the target is  $\Delta E \equiv E_{\text{in}} - E_{\text{out}} = 16.5 \text{ MeV}$ ,

which is 71% of the incident projectile energy. By integrating  $1/S$  from  $E_{\text{in}}$  to  $E_{\text{out}}$ , the target areal thickness was determined to be  $3.72 \times 10^{19} \text{ cm}^{-2}$ , which corresponds to  $123 \mu\text{m}$  for the  $\rho = 0.05\rho_{\text{solid}}$  Al target.

## 3) Target hydrodynamics and the projectile stopping

Figure 3(a) and (b) show streak images of the density- and the temperature profiles for the foam target with 7 layers. The wall thickness  $d$  and the gap between adjacent walls  $D$  are  $0.9 \mu\text{m}$  and  $20 \mu\text{m}$ , respectively. The results for a homogeneous target with the same macroscopic density are shown in Fig. 3(c) and (d) for comparison. The macroscopic hydrodynamic response of the foam is very similar to that of the homogeneous target. However, the

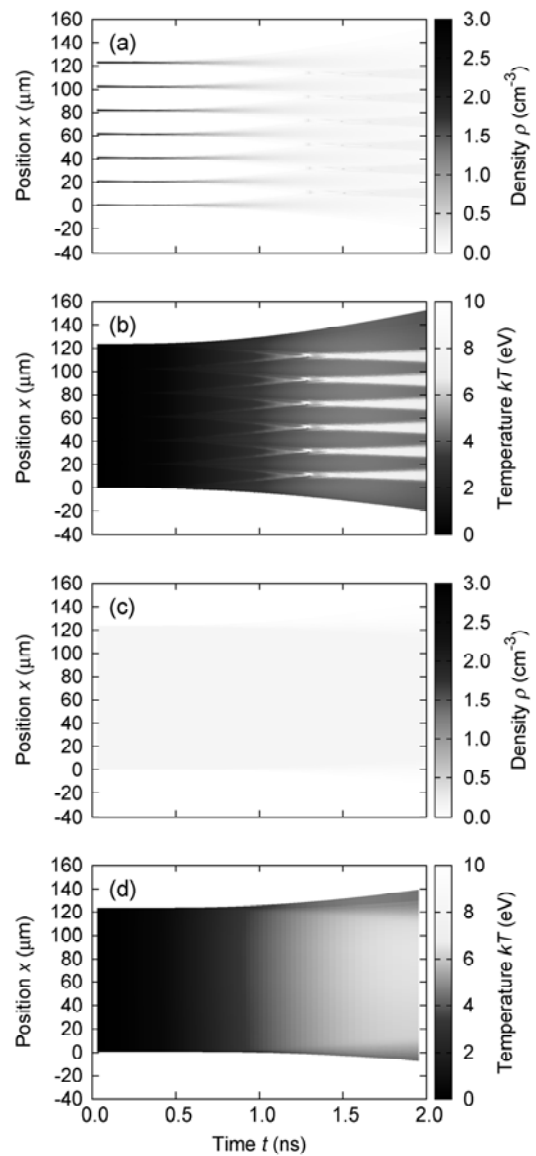


Fig. 3: Streak images of the density- and temperature profiles for the multi-layer ((a), (b)) and homogeneous ((c), (d)) targets.

expansion of the foam target looks slightly faster, owing to higher pressure gradient at the both end regions. For the foam target, the expansion speed of each slab exceeds 10 km/s, and the gaps are filled with the blow-off materials within the pulse duration. However, one sees that the layered structure is not yet homogenized even at the end of heating. Also we recognize small hot spots appear at  $t \approx 1.3$  ns in Fig. 3(b).

Figure 4 shows the temporal evolution of the depth profiles of projectile energy and specific power deposition. Also the result for homogeneous target is inserted for comparison. Before the gaps are filled with the jet from the foils ( $t = 0.5$  ns), we see a stepwise decrease of the projectile energy. At the end of the irradiation ( $t = 2.0$  ns), the profile is rather smooth, but still shows a periodic behavior owing to the hot dense regions. We clearly see that the averaged specific power deposition increases by a factor of few % during the heating. At the end of the pulse duration, the homogeneity of the specific power deposition is rather high, and the profile is almost same as that for homogeneous target except for both end regions.

Similar analyses were performed for other pore sizes. When changing the pore (gap) size, we adjusted the number and the thickness of the slabs so that the gross density and the total thickness of the target could be constant. Figure 5 shows the total projectile energy loss  $\Delta E$  in the target as a function of time for different pore sizes. The result for homogeneous equivalent is shown for comparison. At  $t = 0$ , the energy loss for every nonzero pore size is equal, since it is determined by the stopping due only to the solid phase. From Fig. 2, one sees that the

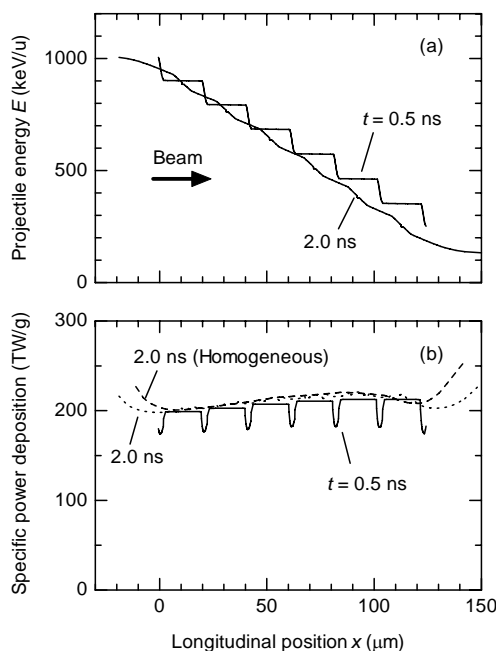


Fig. 4: Depth profiles of (a) the projectile energy and (b) specific power deposition. In (b), the data for homogeneous equivalent target is inserted for comparison.

mass stopping power decreases with increasing the target density, if the temperature is fixed. During the whole irradiation, as shown in Fig. 3(a), there always remain small high-density segments in the foam target. Accordingly, even at the end of the pulse duration, the energy loss is still slightly lower than that for homogeneous target. Nevertheless we have verified that the total energy loss can be recovered by using small pore sizes.

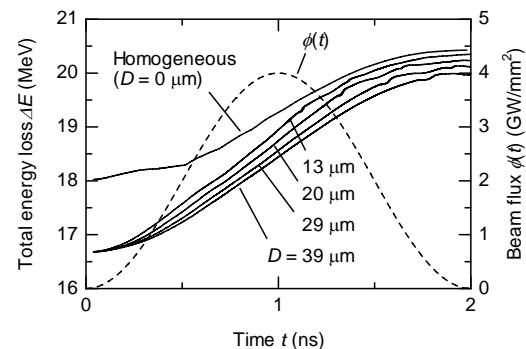


Fig. 5: Total energy loss as a function of time for different pore sizes  $D$ . The dashed line is the beam flux waveform. For  $D = 13, 20, 29$  and  $39$   $\mu\text{m}$ , the wall thicknesses are  $d = 0.61, 0.86, 1.2$  and  $1.5$   $\mu\text{m}$ , respectively.

#### 4. Conclusions

From the 1D calculation above, we found that the initial inhomogeneity of the target is not completely smeared out even after the gap (pore) is filled with the blow-off materials. As a result, the projectile energy loss and energy deposition profile were not exactly same as that expected for homogeneous target, even at the end of the beam-pulse duration of 2 ns. This result implies those the parameters of WDM samples prepared from foam targets might be not completely well-defined. However, this problem may be overcome if a sufficiently fine-grained ( $D \ll 10$   $\mu\text{m}$ ) foam is employed.

#### References

- [1] Y. Oguri and J. Hasegawa, *2011 Annual Meeting of the Atomic Energy Society of Japan N27* (2011) p. 679.
- [2] Y. Oguri and J. Hasegawa, *Meeting Abstract of the Physical Society of Japan* **64** [2], Part 2, 25aZB-2 (2009) p. 49.
- [3] Y. Oguri and J. Hasegawa, *The Papers of Technical Meeting on Pulsed Power Technology, IEE Japan*, **PPT-07-48-55** (2007) pp. 29-33.

## B.9 Prediction and Observation of Curvature-Driven Potential Effects on Electronic Properties of One-Dimensional Condensed Matters

Jun ONOE, Takahiro ITO, Hiroyuki SHIMA, Hideo YOSHIOKA and Shin-ichi KIMURA

### ABSTRACT

Whether or not Riemannian space affects the electronic properties of condensed matters on a much smaller scale is of great interest. Although Riemannian geometry has been applied to quantum mechanics since the 1950s, nobody has yet answered this question, because the electronic properties of materials with Riemannian geometry have not been examined experimentally. We report here the prediction and observation of curvature-driven potential effects on the electronic properties of one-dimensional metallic condensed matters such as Tomonaga-Luttinger liquids.

### INTRODUCTION

In 1916, Einstein first applied Riemannian geometry to explain the distortion of time-space by a gravitational field [1], by introducing the metric tensor used in Riemannian geometry. Four years later, his prediction was confirmed by the observation of a gravitational lens [2].

It is of great interest to know whether or not the Riemannian (curved) space affects the electronic properties of condensates at a much smaller scale than that of the universe. More than a half-century ago, an issue called “operator ordering ambiguity” was reported after attempts to handle quantum mechanics in Riemannian space [3]. Thereafter, to resolve this issue, the confining potential approach was developed [4, 5] and used extensively to predict the influence of a curvature-driven scalar potential on the electronic states [6–12] and electron-transport properties [13–15] of many different curved quantum systems with complex geometrical shapes [6–15]. Although there have been many such theoretical predictions, we have, however, not obtained any evidence for the above question yet, because nobody has yet successfully synthesized materials that enable the examination of electronic properties in Riemannian space. We report here the prediction and observation of Riemannian curvature potential effects on electronic states such as the Tomonaga-Luttinger liquid (TLL) behavior.

### THEORETICAL PREDICTION

Recently, we theoretically demonstrated that the TLL exponent  $\alpha$  monotonically increases with increasing periodic deformation degree ( $\delta r$  in FIG. 1) of a 1D metallic cylinder, and clarified that the increase in  $\alpha$  is caused by the scalar potential driven by Riemannian geometrical curvatures [16].

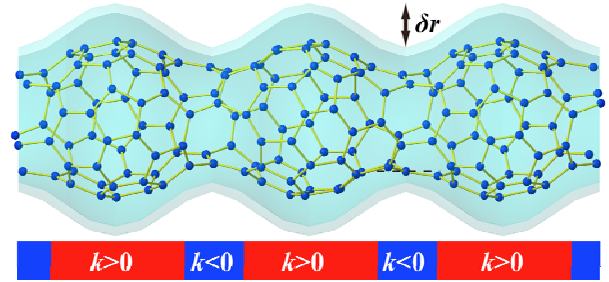


FIG. 1. Schematic illustration of a one-dimensional metallic  $C_{60}$  polymer with an uneven peanut-shaped structure similar to the cross-linked structure of the P08  $C_{120}$  stable isomer predicted using the general Stone-Wales rearrangement. The  $\delta r$  denotes the degree of uneven deformation.

We will briefly describe the theoretical treatment used to estimate the TLL exponent  $\alpha$  of a 1D tube deformed from straight to an uneven peanut-shaped tube.

The TLL exponent  $\alpha$  determines the power-law singularity of the single-particle density-of-states  $D(\omega, T)$  near  $E_F$ , which is given as

$$D(\omega, T = 0) \propto |\hbar\omega - E_F|^\alpha \quad \text{and} \quad D(\omega = 0, T) \propto T^\alpha \quad (1)$$

Since  $\alpha$  is a function of the Fermi velocity  $v_F = \left( \frac{d\omega}{dk} \right)_{E_F}$  and the Fourier component of the Coulomb interaction  $V(q)$ , its evaluation requires the determination of the energy dispersion curves  $\omega = \omega(k)$  and the electrons' eigenmodes  $\psi$  close to the  $E_F$ .

The difference in the  $\alpha$  value between metallic SWCNTs and the 1D uneven peanut-shaped  $C_{60}$  polymer can be attributed to the presence of a non-vanishing geometrical curvature that strongly affects both  $\omega(k)$  and  $\psi$  in the following systems. When a geometrically curved surface  $S$  is embedded in the 3D space, a point  $\mathbf{R}$  in the vicinity of  $S$  can be written as

$$\mathbf{R} = \mathbf{r}(u_1, u_2) + u_3 \mathbf{n}(u_1, u_2) \quad (2)$$

Here,  $\mathbf{r}$  resides on  $S$  and  $\mathbf{n}$  is normal to  $S$ . The curvilinear coordinates  $(u_1, u_2)$  span  $S$ , and  $u_3$  measures the distance from  $S$ . The motion of electrons confined to  $S$  can be expressed using the Hamiltonian in terms of  $(u_1, u_2)$ :

$$H = -\frac{\hbar^2}{2m^*} \left[ \frac{1}{\sqrt{g}} \partial_i \left( \sqrt{g} g^{ij} \partial_j \right) + (h^2 - k) \right], \quad [i, j = 1, 2] \quad (3)$$

Here,  $g = \det(g^{ij})$ ,  $g^{ij} = g_{ij}^{-1}$ ,  $g_{ij} = (\partial_i \mathbf{R}) \cdot (\partial_j \mathbf{R})$ ,  $m^*$  is the effective mass of the electrons, and  $h = h(g_{ij})$  and  $k = k(g_{ij})$  respectively denote the mean curvature and the Gaussian curvature, which are functions of  $g_{ij}$  and describe the curved geometry of  $S$ . Einstein's convention was used in eq. (3). The first term in the Hamiltonian is proportional to the Laplacian on  $S$ , representing the effect of geometrical curvature on the kinetic energy of electrons. The second term ( $h^2 - k$ ) is called an effective potential arising from the geometrical curvature of  $S$ , which causes the increase in  $\alpha$  observed in the present work. The details [including the derivation of eq. (1) from eq. (3)] of this theoretical part were described in ref. 16.

## OBSERVATION

We previously examined the formation of new nanocarbon allotropes by 3-keV electron-beam (EB) irradiation of  $C_{60}$  films at room temperature under ultrahigh vacuum (UHV) conditions, and found that a 1D  $C_{60}$  polymer with an uneven peanut-shaped cross-linked structure (see Fig. 1) roughly close to that of the P08  $C_{120}$  stable isomer [17-25] obtained from the general Stone-Wales (GWS) rearrangement [26]. The 1D uneven peanut-shaped polymer has both positive and negative Gaussian curvatures ( $k > 0$  and  $k < 0$ ) [27], which differ from conventional nanocarbons: i) graphenes ( $k = 0$ ), ii) fullerenes ( $k > 0$ ), iii) nanotubes ( $k = 0$  at body,  $k > 0$  at the spherical edge), and iv) hypothetical Mackay crystals ( $k < 0$ ). To the best of our knowledge, the 1D uneven peanut-shaped  $C_{60}$  polymer is the only condensates with a negative Gaussian curvature whose physical properties can be examined experimentally. Although there have been reports of nanocarbons with negative Gaussian curvatures [28-31], these were merely observed by transmission electron microscopy, and no properties derived from their negative curvatures were demonstrated.

The *in situ* photoemission spectroscopy (PES) system used for the present study of the valence electronic structure of a 1D metallic peanut-shaped  $C_{60}$  polymer consisted of three UHV chambers. A UHV chamber (base pressure:  $1 \times 10^{-7}$  Pa) equipped with a Knudsen-cell and an EB gun was connected to a UHV load-lock preparation chamber (base pressure:  $2 \times 10^{-7}$  Pa) via a gate valve. After a  $C_{60}$  film (20–30 nm thick) was formed on a copper (Cu) substrate by sublimation of  $C_{60}$  powder (99.98% pure) in the Knudsen-cell at 673 K for 3 min after residual organic solvents included in the powder were removed at 473 K, the pristine  $C_{60}$  film was transferred to a UHV analysis chamber (base pressure:  $1 \times 10^{-8}$  Pa) and the *in situ* PES of pristine  $C_{60}$  and 1D uneven peanut-shaped

polymer films were measured with an energy resolution of 12 meV, using the monochromatic He II $\alpha$  emission line (40.806 eV), to examine the  $\pi$ -electron behavior near  $E_F$  for the outermost layers of the 1D polymer film. Details of experimental conditions were described elsewhere [32].

We observed the behavior of the TLL exponent  $\alpha$  in Riemannian space by examining the power-law dependence of the PES spectral functions with respect to both binding energy ( $\omega$ ) and temperature ( $T$ ). Figure 2 shows the PES spectra in the vicinity of  $E_F$  in the temperature range of 30–350 K. As the temperature decreased from 350 to 30 K, the spectral function  $D(\omega, T = 0)$  exhibited a power-law dependence on the binding energy  $\omega$  near  $E_F$  [ $D(\omega, T = 0) \propto |\hbar\omega - E_F|^\alpha$ ] as was observed for metallic single-wall carbon nanotubes (SWCNTs) exhibiting TLL states [33].

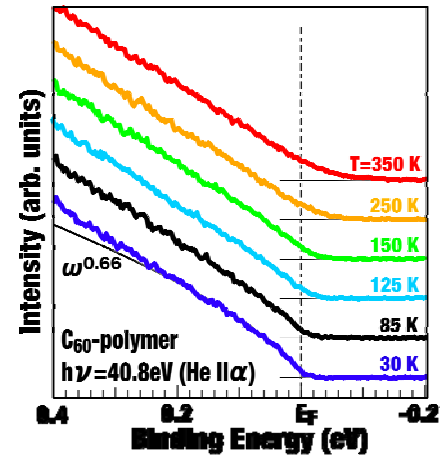


Fig. 2. Temperature dependence of the photoemission spectra of a 1D uneven peanut-shaped  $C_{60}$  polymer in the vicinity of the Fermi level ( $E_F$ ).

By fitting the PES spectra with a power-law function of the binding energy [ $D(\omega, T = 0) \propto |\hbar\omega - E_F|^\alpha$ ] in an energy range of 18–70 meV, we obtained an exponent  $\alpha$  of 0.66, as shown in Fig. 3(a). Since the TLL  $\alpha$  value depends on the choice of an energy range set for fitting, we examined various energy range sets within 18–100 meV (a fitting accuracy of  $\pm 0.02$ ), and obtained  $\alpha$  to be  $0.65 \pm 0.08$ . In a similar manner, Fig. 3(b) plots the temperature dependence of the ratio of the photoemission intensity at  $E_F$  to the intensity at 0.5 eV in binding energy on a log-log scale, and demonstrates a power-law dependence on temperature [ $D(\omega = 0, T) \propto T^\alpha$ ] in the range of 30–350 K, in which the exponent  $\alpha$  was obtained to be  $0.59 \pm 0.04$ . Judging from the results of Fig. 3, the TLL  $\alpha$  for the 1D uneven peanut-shaped  $C_{60}$  polymer can be concluded to be ca. 0.6, which is significantly larger than that of ca. 0.5

(0.43–0.54) for metallic SWCNTs [34–36]. In our theoretical prediction [16], when the radial modulation degree ( $\delta r$ ) of the uneven structure increased from 0 nm (a straight tube) to 0.16 nm (an uneven peanut-shaped tube), the TLL exponent  $\alpha$  increased from 0.5 to 0.6 (see Fig. 4). As shown in Fig. 1, the  $\delta r$  can be estimated to be ca. 0.14 nm, which is in good agreement with the predicted value [32].

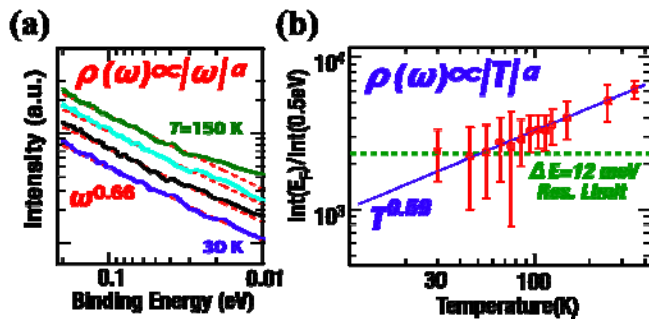


Fig. 3. The power law dependence of the PES spectral function shown in Fig. 2 on the binding energy (a) and temperature (b).

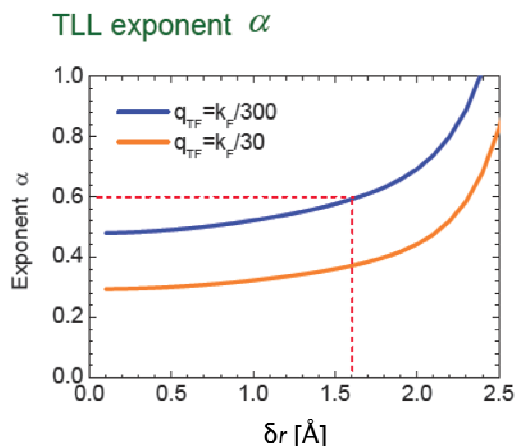


Fig. 4. Plot of TLL exponent  $\alpha$  as a function of the radial modulation degree  $\delta r$ .

## SUMMARY

The results of Fig. 3 show an increase in the TLL  $\alpha$ , representing the first observation of the Riemannian geometrical effects, which have been well known to occur in the universe on a very large scale, on the electronic properties of condensed matter at a nanometer scale.

## ACKNOWLEDGMENT

The present work was partially supported by the Joint Studies Program of the Institute for Molecular Science (IMS), and was financially supported by a Grant-in-Aid for Scientific Research on Innovative Areas (No.21200032) from the Ministry of Education, Culture, Sports, and Technology (MEXT).

## REFERENCES

- [1] A. EINSTEIN, *Ann. Phys.* **49**, 769 (1916).
- [2] F.W. DYSON et al., *Philos. Trans. Royal Soc. London* **220A**, 291 (1920).
- [3] B.S. DEWITT, *Phys. Rev.* **85**, 653 (1952).
- [4] H. JENSEN and H. KOPPE, *Annal. Phys.* **63**, 586 (1971).
- [5] R.C.T. DA COSTA, *Phys. Rev. A* **23**, 1982 (1981).
- [6] G. CANTELE et al., *Phys. Rev. B* **61**, 13730 (2000).
- [7] H. AOKI et al., *Phys. Rev. B* **65**, 035102 (2001).
- [8] M. ENCINOSA and L. MOTT, *Phys. Rev. A* **68**, 014102 (2003).
- [9] N. FUJITA and O. TERASAKI, *Phys. Rev. B* **72**, 085459 (2005).
- [10] M. KOSHINO and H. AOKI, *Phys. Rev. B* **71**, 073405 (2005).
- [11] J. GRAVESEN and M. WILLATZEN, *Phys. Rev. A* **72**, 032108 (2005).
- [12] B. JENSEN, *Phys. Rev. A* **80**, 022101 (2009).
- [13] A.V. CHAPLIK and R.H. BLICK, *New J. Phys.* **6**, 33 (2004).
- [14] A. MARCHI et al., *Phys. Rev. B* **72**, 035403 (2005).
- [15] G. CUOGHI et al., *Phys. Rev. B* **79**, 073410 (2009).
- [16] H. SHIMA, H. YOSHIOKA and J. ONOE, *Phys. Rev. B* **79**, 201401 (R) (2009).
- [17] J. ONOE et al., *Appl. Phys. Lett.* **82**, 595 (2003).
- [18] J. ONOE et al., *Appl. Phys. Lett.* **85**, 2741 (2004).
- [19] J. ONOE et al., *Phys. Rev. B* **75**, 233410 (2007).
- [20] J. ONOE et al., *J. Phys. Conf. Ser.* **61**, 899 (2007).
- [21] Y. TODA, S. RYUZAKI and J. ONOE, *Appl. Phys. Lett.* **92**, 094102 (2008).
- [22] J. ONOE et al., *Appl. Phys. Lett.* **97**, 241911 (2010).
- [23] A. TAKASHIMA, J. ONOE and T. NISHII, *J. Appl. Phys.* **108**, 033514 (2010).
- [24] J. ONOE et al., *J. Phys.: Condens. Matter* **24**, 175405 (2012).
- [25] After a  $C_{60}$  film (a few layers) formed on a gold (111) surface was irradiated with electron-beam for 1 min uniformly, we measured *in situ* STM of the sample, and observed the 1D bright lines (indicating a higher local density-of-states than in the other area) which strongly supports the formation of the 1D conducting  $C_{60}$  polymers.
- [26] H. UENO et al., *Fullerene Sci. Technol.* **6**, 319 (1998).
- [27] The Gaussian curvature ( $k$ ) at a given point on a general curved surface is defined to be the product of the maximum ( $\kappa_{\max}$ ) and minimum ( $\kappa_{\min}$ ) curvatures obtained among a myriad of curved lines generated when a myriad of normal surfaces cross the given point on the curved surface.
- [28] D.E. LUZZI and B.W. SMITH, *Carbon* **38**, 1751 (2000).
- [29] M. TERRONES et al., *Phys. Rev. Lett.* **89**, 075505 (2002).
- [30] A.G. NASIBULIN et al., *Nature Nanotech.* **2**, 156 (2007).
- [31] M. KOSHINO et al., *Nature Chem.* **2**, 117 (2010).
- [32] J. ONOE et al., *EPL (Europhys. Lett.)* **98**, 27001 (2012).
- [33] H. ISHII et al., *Nature* **426**, 540 (2003).
- [34] R. LARCIPRETE et al., *Phys. Rev. B* **71**, 115435 (2005).
- [35] R. EGGER and A.O. GOGOLIN, *Eur. Phys. J. B* **3**, 281 (1998).
- [36] H. YOSHIOKA, *Physica E* **18**, 212 (2003).

## B.10 Local Structural Analysis of Thorium Fluoride in Molten Mono- and Divalent Cationic Fluoride Mixtures for Molten Salt Reactor Concept

Haruaki MATSUURA, Atsushi NEZU and Hiroshi AKATSUKA

Molten salt reactor (MSR) is one of the concepts of promising reactor type in the 4<sup>th</sup> generation. Actually, at the Oak Ridge National Laboratory (ORNL) in 1960s, the molten salt reactor experiment (MSRE) had been successively performed for a few years. However, the project at the ORNL had been quitted until the proposal of the idea of a molten salt breeder reactor, which has been introduced two innovative ideas after the MSRE, that is, introduction of a second coolant loop and an online fuel cleaning process in the first coolant/fuel loop. To make realization of the concept, potential study about each process in the salt cleaning may be already done, but it is still lacking of the behaviour of related actinide materials in real system. Of course, recent rapid innovation of using numerical simulation would be possible to reproduce some of the properties, but it is still very important to accumulate the physico-chemical data containing related actinide materials. In this study, ThF<sub>4</sub>-LiF-CaF<sub>2</sub> [1] and ThF<sub>4</sub>-LiF-MgF<sub>2</sub> mixtures are focused for the structural investigation by EXAFS.

ThF<sub>4</sub> was synthesized from ThO<sub>2</sub> under fluorine gas (40 ml/min) at 650 °C for 4 h. Mixtures made by ThF<sub>4</sub>, LiF and CaF<sub>2</sub> or MgF<sub>2</sub> were melted once in a glassy carbon crucible at 1073 K in a quartz chamber filled with an argon atmosphere in high purity. Then, they were mixed with boron nitride powder, and pressed into pellets in 7 mm diameter and 1 mm thickness. The mixing weight ratio of ThF<sub>4</sub> to BN was ca. 1: 2.5. To prevent chemical reaction of sample and contamination of Th compound to outside during heating process in EXAFS measurements, these pellets were installed in a double barrier cell. The 1<sup>st</sup> barrier is made with pyrolytic boron nitride and the 2<sup>nd</sup> barrier is made with boron nitride (HIP) [2]. The electric furnace was filled with He gas at ca. 30 kPa. The Th L<sub>III</sub>-edge EXAFS spectra have been collected with fixed time scan method by the X-ray from a double Si (111) crystals monochromator in transmission mode at BL27B/PF/KEK, Japan. EXAFS data were analysed by using the WinXAS ver.3.1 and the 3<sup>rd</sup> and 4<sup>th</sup> cumulants were introduced for the curve fitting analyses of EXAFS data at molten phase due to their large anharmonic effect in the spectra.

The BF<sub>2</sub> (B = Ca, Mg) concentration dependence of local structural parameters derived from EXAFS of the constant concentration of  $x_{\text{ThF}_4} = 0.25$  are shown in Fig. 1[3]. Although inter-ionic distance seems to be independent from the both concentration of CaF<sub>2</sub> and MgF<sub>2</sub>, coordination number, Debye-Waller factor and C<sub>3</sub> cumulant parameter of MgF<sub>2</sub> mixture are larger than those of CaF<sub>2</sub> in general, and increasing rates depending on the concentration of MgF<sub>2</sub> are

also larger than those of CaF<sub>2</sub>. These facts imply that MgF<sub>2</sub> makes much un-stabilized local environment around Th<sup>4+</sup> than CaF<sub>2</sub> does. The similar tendency is also confirmed at the TbF<sub>3</sub>-LiF-BF<sub>2</sub> (M=Ca, Mg) mixtures. This is caused by the difference between the coulombic interaction of Mg<sup>2+</sup>-F and Ca<sup>2+</sup>-F. Ionic radius of Mg<sup>2+</sup> is smaller than that of Ca<sup>2+</sup>, thus Mg<sup>2+</sup> can easily approach to the coordinated F<sup>-</sup> around Th<sup>4+</sup>. Therefore, Mg<sup>2+</sup> makes un-stabilised local structure around Th<sup>4+</sup> more strongly than Ca<sup>2+</sup> does.

This study was done by a collaboration research with Prof. N. Sato, Tohoku University and Dr. C. Bessada, CEMHTI, CNRS, France.

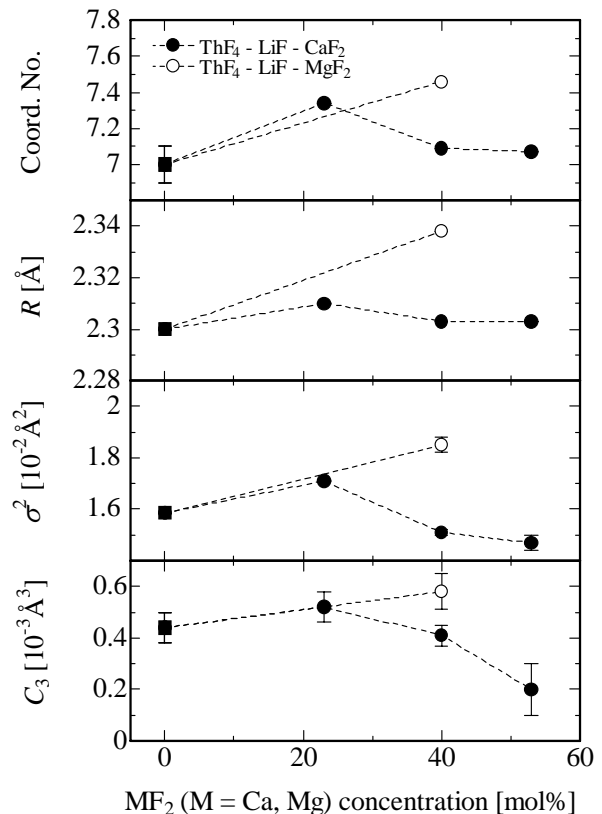


Fig. 1 Structural parameters obtained by EXAFS of molten 0.25ThF<sub>4</sub> - (0.75-x)LiF - x CaF<sub>2</sub> or MgF<sub>2</sub> mixtures (0<x<1), from the top, coordination number, inter-ionic distance, Debye-Waller factor and C<sub>3</sub> cumulant.

### References

- [1] M. Numakura, et al, Prog. Nucl. Ener. 53, (2011) 994.
- [2] C. Bessada, et al, Nucl. Sci. NEA/NSC/DOC 15 (2009) 117.
- [3] M. Numakura, Doctor Thesis, Tokyo Institute of Technology (2011).

## B.11 Fluoride Addition Effect on the Electrochemistry and Local Structure of Neodymium Cation in Molten Chlorides

Haruaki MATSUURA, Atsushi NEZU and Hiroshi AKATSUKA

Neodymium magnet has the strongest magnetism among the magnets currently industrialized, thus it has been used as motors in hybrid cars, electric vehicles, wind farms and medical instruments which are required with strong magnetism. However, over 97 % of the first resource of rare earths including neodymium is now produced in China. If the demand of the electric vehicles and wind farms rapidly increases in the world, it leads to special concern about the lacking of rare earth resource. Therefore, we have focused on nickel misch metal hydride batteries as a secondary resource of rare earths, and investigated applicability of molten salt electrolysis to extract neodymium from them [1]. To find out the much efficient electrochemical condition for the separation of neodymium, the electrochemical behaviour of neodymium in molten LiCl – KCl and LiCl – CaCl<sub>2</sub> eutectic coexisting various amount of LiF has been examined. To elucidate the relationship between the variation of electro-reduction potential and local structure around neodymium cation depending on fluoride concentration in molten chloride, EXAFS experiments of neodymium cation in molten LiCl – KCl – LiF and LiCl – CaCl<sub>2</sub> – LiF have been also carried out.

Cyclic voltammograms and differential pulsed voltammograms have been measured in an argon circulated glove box by using the electrodes as follows: working electrodes: tungsten or nickel electrode, counter electrode: glassy carbon, and reference electrode: Ag in LiCl-KCl eutectic + AgCl (1mol%), respectively. Molten LiCl-KCl or LiCl-CaCl<sub>2</sub> eutectic and quartz was chosen as an electrolyte and a container, respectively. To observe the fluoride addition effect, various amount of LiF was added to be the relative concentration upto 10 times to the concentration of rare earths. EXAFS spectra of Nd L<sub>III</sub>-edge (6.209 keV) were collected with a fixed time scan method by using Si (111) double crystal monochromator in transmission mode at BL7C/PF/KEK. Mixtures of NdCl<sub>3</sub> ( $x = 5\text{mol}\%$ ) in eutectic LiCl – KCl or LiCl – CaCl<sub>2</sub> with LiF in the amount of various times to the concentration of NdCl<sub>3</sub> (0 to 10), were melted once in a glassy carbon crucible at 873 K in a glove box filled with an argon atmosphere in high purity. Then, they were mixed with boron nitride powder, and pressed into pellets. To prevent from the chemical reaction during heating process in EXAFS measurements, these pellets were installed in a cell made with pyrolytic boron nitride and the electric furnace was filled with He gas under 30 kPa. EXAFS data were analysed by using the WinXAS ver.3.1.

The structural functions of molten NdCl<sub>3</sub> – LiCl – KCl – LiF (0 and 6 times of concentration of Nd) and NdCl<sub>3</sub> – LiCl – CaCl<sub>2</sub> – LiF (0, 6 and 10 times of concentration of

Nd) at 873 K are shown in Fig. 1. In both systems, with increasing fluoride concentration, interionic distance between Nd<sup>3+</sup> and anion decreases, that is corresponding to the fact that chloride anions in the 1<sup>st</sup> coordinated sphere around Nd<sup>3+</sup> are exchanged by fluoride anions. The most striking feature derived from these figures is the local structure of Nd<sup>3+</sup> is more affected by fluoride addition in LiCl – KCl eutectic than in LiCl – CaCl<sub>2</sub> eutectic. This is due to the difference of coulombic interaction, i.e., Ca<sup>2+</sup> much strongly coordinates F<sup>-</sup> than K<sup>+</sup> does, thus it prevents fluoride coordination around Nd<sup>3+</sup> in the first coordination sphere. It has been found that the tendency of the negative variation of electro-deposition potential depending on fluoride concentration in LiCl-KCl melt [2] appears much slower than that in LiCl-CaCl<sub>2</sub>, thus profound discussion on the relationship between electrochemical behaviour and local structure can be expected.

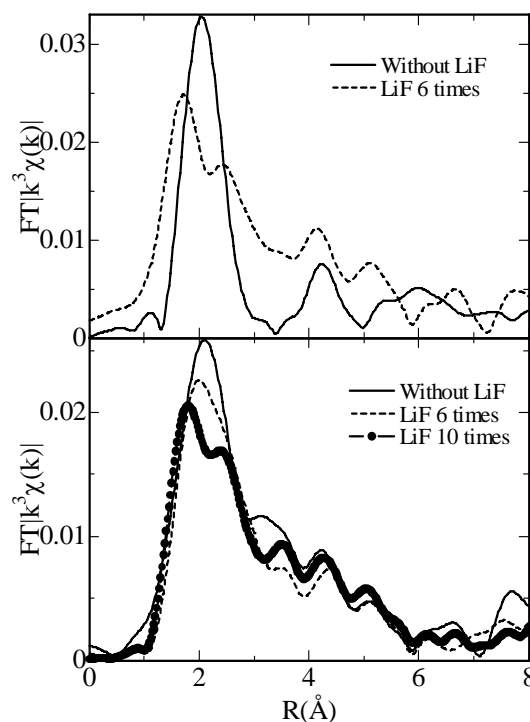


Fig. 1 The structural functions of molten (a) NdCl<sub>3</sub> – LiCl – KCl – LiF (0 and 6 times of concentration of Nd) and (b) NdCl<sub>3</sub> – LiCl – CaCl<sub>2</sub> – LiF (0, 6 and 10 times of concentration of Nd) at 873 K.

\*This study is funded by the Shinsei Foundation.

### References

- [1] H. Matsuura et al, J. Phys. Chem. Solids, 66 (2005) 439.
- [2] Y. Shimohara et al Proc. of 9<sup>th</sup> International Symposium on Molten Salts Chemistry & Technology 2011.

## B.12 Local Structural Analysis of Neodymium Cation in Molten Various Chlorides for Pyrochemical Reprocessing of Nuclear Fuel

Haruaki MATSUURA, Atsushi NEZU and Hiroshi AKATSUKA

It is very essential to grasp the chemical behaviour of fuel elements and fission products in each step of processes in order to make realization of pyrochemical reprocessing of nuclear fuel using chloride melts. Neodymium is one of the fission products as well as the rare earth element having divalent cation through the electrochemical reaction [1]. It seems to be existing the simple relationship between the structural model and electrochemical properties of molten salts, however, even the variation of redox potential depending on various electrolytes has not been well explained scientifically. To obtain the information on the local structure of neodymium cation in various molten electrolytes, the systematic characterization using extended X-ray absorption fine structure (EXAFS) has been carried out.

Since the concentration of neodymium in electrolytes is 1 to 5 molar %, the EXAFS measurements have been carried out using high energy X-ray generated at one of the undulator beamlines, i.e. BL11XU, SPring-8, Japan. The samples of mixture melts have been molten in a quartz vessel kept in an argon circulated glove box and sealed in the quartz cells in a funnel or a rectangular shape (X-ray path: 1.5 mm or 10 mm, respectively) under vacuum condition. EXAFS spectra of neodymium K- Edge (43.571 keV) of these samples heated at 923 K by an electric furnace [2] on the beamline have been obtained by a quick scan in transmission mode. The data analyses have been done using WinXAS 3.1 [3] and FEFF 8.01[4] and the curve fitting analyses introduced the 3<sup>rd</sup> and 4<sup>th</sup> cumulants have been performed since anharmonic oscillation effect cannot be ignored on the spectra at high temperature.

By utilization of X-ray from the undulator beamline, even such as highly diluted solution coexisting with the highly X-ray absorbing element, i.e. NdCl<sub>3</sub>-BaCl<sub>2</sub>-LiCl (1:10:89), could be measured within 5 minutes to obtain decent quality of spectrum. It is epoch making that the similar concentration of the electrolytes will be able to be evaluated by EXAFS. Various structural parameters obtained by assuming 6-coordinated structure for the mixtures of 1 mol % of neodymium in 10 mol % of LiCl exchanged with KCl, CsCl, CaCl<sub>2</sub>, and BaCl<sub>2</sub> are shown in Fig. 1. With reference to the inter-ionic distance between Nd<sup>3+</sup> and Cl<sup>-</sup> in molten pure LiCl, those with K and Ca do not so much varied but that with Cs gets shorten and that with Ba gets expanded. These tendencies are partly following to the structural information obtained for rare earth trichlorides in various alkali cationic chlorides [5,6]. Although the structural information obtained by EXAFS is limited to the 1<sup>st</sup> coordination sphere around neodymium cation, it is found that even in such diluted solution of

neodymium, the local structure has been influenced by the cation existing in the 2<sup>nd</sup> coordination sphere from neodymium. The tendency observed in the melts containing Ba<sup>2+</sup> which has larger cationic size would be one of the useful informations to explain the anomalous tendencies observed in UV-Vis spectroscopy and electrochemical behaviour [7,8]

This study was done by a collaboration research with Prof. A. Uehara, T. Fujii and H. Yamana, Kyoto University. The authors thank to Drs. Y. Okamoto, H. Shiwaku, T. Yaita, JAEA for valuable discussions.

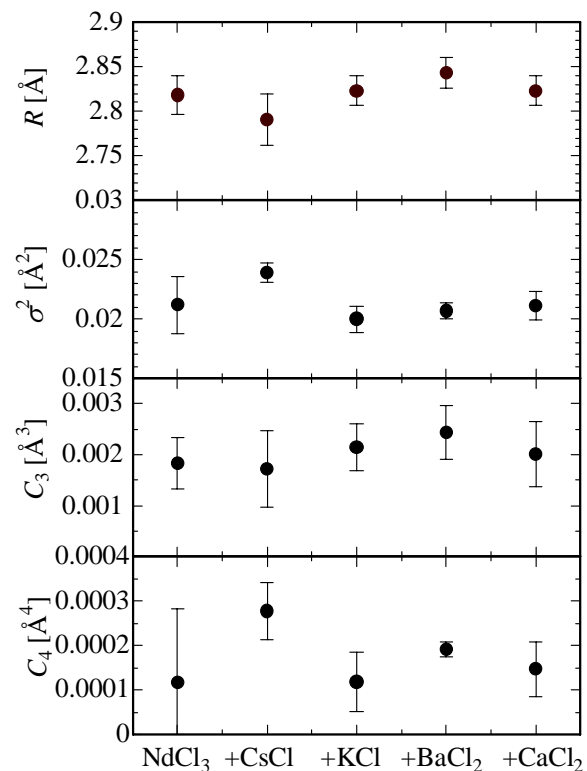


Fig. 1 structure parameters obtained by curve fitting analysis for neodymium in various melts.

### References

- [1] H. Yamana *et al.*, J. Alloys Compd., 408-412 (2006) 66.
- [2] H. Matsuura *et al.*, J. Alloys Compd., 408-412 (2006) 80.
- [3] T. Ressler, J. Synchrotr. Rad., 5 (1998) 118.
- [4] A. L. Ankudinov *et al.*, Phys. Rev. B. 58 (1998) 7565.
- [5] Y. Okamoto *et al.*, J. Synchrotr. Rad., 8 (2001) 1191.
- [6] Y. Okamoto *et al.*, J. Phys. Chem. A, 114 (2010) 4664.
- [7] K. Fukasawa *et al.*, J. Nucl. Mater., 414 (2011) 265.
- [8] K. Fukasawa *et al.*, J. Alloys Compd., 509 (2011) 5112.

## B.13 Formation of Carbon Interphase on SiC Fibers in SiC Fiber-Reinforced SiC Matrix Composites by Electrophoretic Deposition

Katsumi YOSHIDA and Toyohiko YANO

### Introduction

Continuous silicon carbide fiber-reinforced silicon carbide (SiC<sub>f</sub>/SiC) composites, which show a non-brittle fracture behavior and higher fracture energy, are expected to be used as components for gas turbine, spacecrafts and fusion nuclear reactors. In the future fusion power reactor, the reactor concepts based on the use of SiC<sub>f</sub>/SiC composite have been designed by JAEA, ARIES-team and CEA (TAURO). Formation of boron nitride or carbon interphase on the fibers and optimization of the interface between fiber and matrix are one of the most important factors to enhance the mechanical properties of SiC<sub>f</sub>/SiC composites. The optimum interface in a fiber-reinforced ceramic matrix composite plays an important role for promotion of fiber pullout, i.e., sliding and delamination occurs along the interface, and for the inhibition of reaction between fiber and the matrix [1, 2]. Chemical vapor deposition (CVD) is currently used for carbon or boron nitride coating on SiC fibers. We paid attention to electrophoretic deposition (EPD) method to form the carbon interphase on the SiC fiber as the new coating process [3, 4]. In order to obtain the optimum carbon coating on SiC fibers, flaky carbon particles are considered to be effective. In this study, commercial colloidal graphite suspension containing flaky graphite particles was used for the formation of carbon interphase, and carbon interphase was formed on SiC fibers in the cloth by EPD. SiC<sub>f</sub>/SiC composites were fabricated by sheet stacking method and hot-pressing, and their mechanical properties were investigated. For comparison, carbon interphase on SiC fibers in fiber cloth was also formed by dip-coating or vacuum infiltration using the same colloidal graphite suspension, and the effectiveness of carbon interphase on SiC fiber in SiC<sub>f</sub>/SiC composites was investigated.

### Experimental Procedures

Two dimensionally plain-woven polycrystalline Tyranno SA (SiC fiber, Ube Industries, Ltd., Japan) cloth was cut into the size of 35 mm x 50 mm. The suspension of graphite particles for EPD was prepared using a commercial colloidal graphite aqueous solution (Hitasol, Hitachi Powdered Metals, Co., Ltd., Japan). The concentration of the colloidal graphite suspension was adjusted to 0.10 wt%. Small amount of *n*-butylamine was added to the suspension to adjust the pH of the solution to 10. The SiC fiber cloth and the graphite plate with the size of 35 mm x 50 mm were settled at a distance of 10 mm in the colloidal graphite suspension as the anode and the cathode, respectively. Graphite particles were coated on SiC fibers in the cloth by EPD using the colloidal graphite suspension under an applied voltage of 3 V for 10 min, and

then dried at 100°C. For comparison, carbon interphase was also formed on SiC fibers in the cloth by dip-coating or vacuum infiltration using 0.10 wt% of colloidal graphite suspension. Dip-coating was performed by simple dipping of the fiber cloth into the colloidal graphite suspension. In the case of vacuum infiltration, the colloidal graphite suspension was infiltrated in fiber bundles under vacuum using rotary pump for 30 min. After dip-coating or vacuum infiltration, the cloths were dried at 100°C. The carbon interphases of SiC fiber formed by these processes were observed by a field emission scanning electron microscope (FE-SEM).

Beta-SiC powder containing sintering additives consisted of  $\alpha$ -Al<sub>2</sub>O<sub>3</sub> (14 wt%), Y<sub>2</sub>O<sub>3</sub> (4 wt%) and CaCO<sub>3</sub> (2 wt%) were dispersed in water of which pH was adjusted to 10 using *n*-butylamine, and a 10 wt% SiC suspension was prepared. The carbon-coated fiber cloths by each process was dipped into the SiC suspension, and SiC matrix with sintering additives were infiltrated by EPD under an applied voltage of 5 V for 20 min, and the cloth was dried at 100°C. After drying, the fiber cloth was cut into the size of 35 mm x 35 mm.

Two-dimensional SiC<sub>f</sub>/SiC composites were fabricated by sheet stacking method followed by hot-pressing [5, 6]. The SiC sheet was prepared by tape casting using a laboratory-scale tape casting equipment. Details of the composition, organics in the green sheet were described elsewhere [5]. The thickness of the SiC green sheet was about 40-50  $\mu$ m, and the sheet was cut into the size of 35 mm x 35 mm. The fiber cloths coated with carbon and infiltrated with SiC matrix, and the SiC green sheets were stacked alternately. The stacked body was heat-treated at 300°C for 24 h in air under a uniaxial pressure of 20 kPa in order to remove organics from the green sheets in the stacked body. The compact was hot-pressed at 1700°C for 1 h in argon flow under a uniaxial pressure of 40 MPa. Specimens were cut into rectangular bars (3 mm<sup>w</sup> x 2 mm<sup>h</sup> x 35 mm<sup>l</sup>). Bulk density and open porosity of specimens was measured by Archimedes' method. Three-point bending strength was measured at room temperature with a span of 30 mm and a crosshead of 0.1 mm/min. Fracture surface of the composites was observed by FE-SEM.

### Results and Discussion

SEM micrographs of carbon interphases on SiC fibers by EPD, dip-coating and vacuum infiltration are exhibited in Fig. 1. For comparison, SEM micrographs of as-received SiC fibers are also shown in Fig. 1. As-received Tyranno SA fiber is polycrystalline, and consists of fine  $\beta$ -SiC particles. In the case of EPD, the surface of SiC fibers was wholly coated with flaky graphite particles. On the other

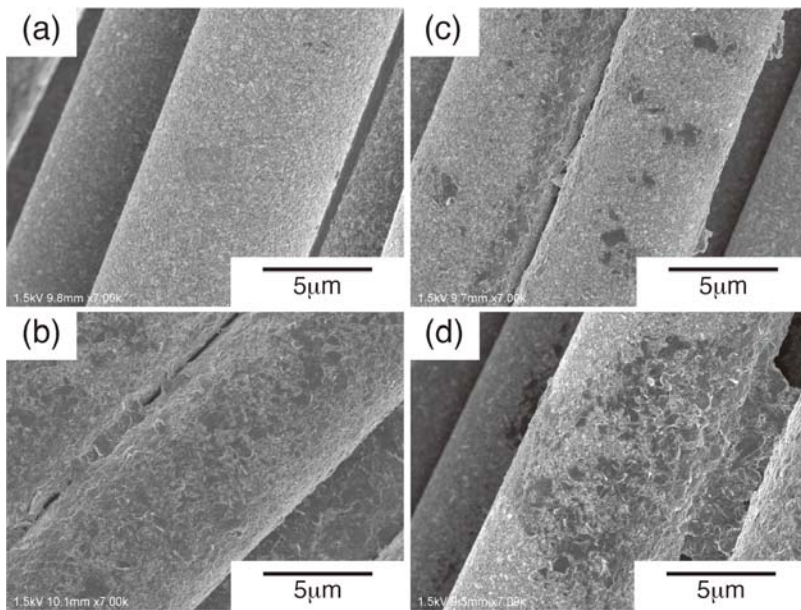


Fig. 1 SEM micrographs of (a) as-received SiC fibers and carbon-coated SiC fibers by (b) EPD, (c) dip-coating and (d) vacuum infiltration.

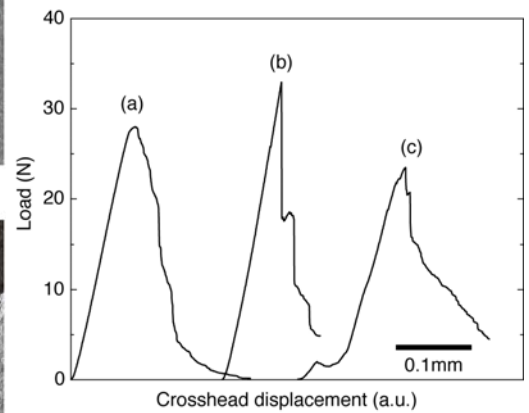


Fig.2 Typical load-displacement curves of SiC<sub>f</sub>/SiC composites in bending test at room temperature. (a) EPD, (b) dip-coating and (c) vacuum infiltration.

hand, graphite particles partially existed on SiC fibers after dip-coating or vacuum infiltration, and homogeneous carbon interphase did not form on SiC fibers. From these results, relatively homogeneous carbon interphase on SiC fibers in the cloth was achieved by EPD using colloidal graphite suspension.

The fiber volume fraction of the SiC<sub>f</sub>/SiC composites was 48-54 %, and these values depended on the thickness of SiC sheet between each SiC fiber cloth. Bulk density and open porosity of the composites were 2.8-2.9 g/cm<sup>3</sup> and 8-9 %, respectively.

Bending strength of the SiC<sub>f</sub>/SiC composites were 90-120 MPa, and the composite reinforced with the carbon-coated fiber cloths by vacuum infiltration showed lower bending strength than the composites reinforced with the carbon-coated fiber cloths by EPD and dip-coating. Figure 2 shows the typical load-crosshead displacement curves of the composites in bending test at room temperature. The composite reinforced with the carbon-coated fiber cloths by EPD and vacuum infiltration showed the similar load-crosshead displacement curves, and the load gradually decreased with an increase in the crosshead displacement after reaching the maximum load. In the case of the composite reinforced with carbon-coated fiber cloths by dip-coating, the load almost linearly increased to the maximum load with increasing the crosshead displacement, and then the load dropped suddenly. From the observation of the fracture surface of SiC<sub>f</sub>/SiC composites after bending test by SEM, the composite using the carbon-coated SiC fiber cloth by EPD exhibited large amount of fiber pullout. On the other hand, the fracture surface of the composite using the carbon-coated SiC fiber cloth by dip-coating was almost flat with small amount of very short fiber pullout. In the

case of the composite using the carbon-coated SiC fiber cloth by vacuum infiltration, it seemed that delamination between each fiber cloth occurred rather than fiber pullout. From the results of load-displacement curves, fracture surface observation and appearance of carbon interphase on SiC fibers, the effect of carbon interphase on SiC fibers by each process on fracture behavior of the composite was discussed as follows;

Dip-coating provided non-uniform carbon interphase on SiC fibers in the cloth, i.e., carbon partially existed on the fibers, and graphite suspension was not infiltrated sufficiently into fiber bundle by simple dipping. In this case, non-uniform carbon coating formed on SiC fibers and carbon existed mainly on the surface of fiber bundle. As a result, optimum interface between fiber and the matrix was not obtained, i.e., carbon interphase on SiC fibers did not act as an interfacial layer effectively, and this interface did not induce fiber pullout. Furthermore, the elastic deformation up to maximum load and the drastic drop of load after reaching the maximum load were also attributed to this interface. In the case of vacuum infiltration, it was easy to infiltrate graphite suspension into fiber bundle. However, vacuum infiltration formed non-uniform carbon interphase on SiC fibers in the bundle, and carbon matrix in fiber cloth was also formed during vacuum infiltration, resulting in the formation of weak interface, i.e., it was easy to occur sliding along matrix/cloth interface. The composite using the carbon-coated fiber cloth by vacuum infiltration showed shear fracture behavior, and delamination between each fiber cloth was observed. This weak interface contributed to the fracture behavior of the composite as shown in Fig. 2(c), and a gentle decrease in the load after reaching the maximum load would correspond to the shear fracture behavior. In the case of

EPD, negatively charged graphite particles were coated well on positively charged SiC fibers as shown in Fig.1(b), and carbon interphase on SiC fibers in the cloth was relatively homogeneous. Furthermore, graphite particles were infiltrated into fiber bundle by electrical force, and relatively homogeneous carbon interphase was also formed on not only SiC fibers at the surface of the bundle but also fibers at the center of the bundle. This homogeneous carbon interphase provided the optimum interface between fiber and the matrix, and promoted fiber pullout during fracture. Matrix components,  $\beta$ -SiC,  $\text{Al}_2\text{O}_3$ ,  $\text{Y}_2\text{O}_3$  and  $\text{CaCO}_3$  particles, were also negatively charged and dispersed under this suspension condition (pH10) in consideration of their iso-electric point, and these matrix components were infiltrated into fiber bundles by electrical force. From these results, it was concluded that EPD using colloidal graphite suspension is effective for the formation of homogeneous carbon interphase on SiC fibers in the cloth, and this fiber cloth is applied for the reinforcement of  $\text{SiC}_f/\text{SiC}$  composites.

### Summary

In this study, carbon interphase was formed on SiC fibers in the cloth by electrophoretic deposition (EPD) method using commercial colloidal graphite suspension, and mechanical properties of  $\text{SiC}_f/\text{SiC}$  composites fabricated by sheet stacking method and hot-pressing were investigated. For comparison, carbon interphase on SiC fibers in the cloth was also formed by dip-coating or vacuum infiltration using the same colloidal graphite suspension, and the effectiveness of carbon interphase on SiC fiber in  $\text{SiC}_f/\text{SiC}$  composites was investigated. Graphite particles partially existed on the SiC fibers after dip-coating or vacuum infiltration, and carbon interphase was non-uniform on SiC fibers. Non-uniform carbon interphase on SiC fiber in the cloth affected the fracture behavior of the composites. In the case of EPD, the surface of SiC fibers was wholly coated with flaky graphite particles. Negatively charged graphite particles were coated well on positively charged SiC fibers, and carbon interphase on SiC fibers in the cloth was relatively homogeneous. Furthermore, graphite particles were infiltrated into fiber bundle by electrical force, and relatively homogeneous carbon interphase was also formed on not only SiC fibers at the surface of the bundle but also fibers at the center of the bundle. This homogeneous carbon interphase provided the optimum interface between fiber and the matrix, and promoted large amount of fiber pullout during fracture.

### References

- [1] T. Yano and K. Yoshida, *Strength, Fracture and Complexity*, **1**, 157-165 (2003).
- [2] K. Yoshida, T. Yano and T. Iseki, *The Technology of Fusion Energy*, **39**, 607-611 (2001).
- [3] K. Yoshida, K. Matsukawa and T. Yano, *J. Nucl. Mater.*, **386-388**, 643-646 (2009).
- [4] K. Yoshida, H. Matsumoto, M. Imai, K. Hashimoto, Y. Toda and T. Yano, *Key Eng. Mater.*, **352**, 77-80(2007).
- [5] K. Yoshida, Budiyanto, M. Imai and T. Yano, *J. Nucl. Mater.*, **258-263**, 1960- 1965(1998).
- [6] K. Yoshida, M. Imai and T. Yano, *Compos. Sci. Technol.*, **61**, 1323-1329 (2001).

## B.14 Resourceability on Nuclear Fuel Cycle

Masaki OZAWA

### Introduction - From wastes to resource, as "Kopernikanische Wendung"

Fission reaction of  $^{235}\text{U}$  will generate more than 40 elements and 400 nuclides in the spent fuel. Among them, 31 elements are categorized as rare metals (NRM; Nuclear Rare Metal), of which some are highly enriched in the spent fuel. Typical yields for such noticeable NRM as Pd, Ru, Rh (light PGM) and La, Nd (light RE) will reach to more than ca. 10kg per metric ton of the reference FBR spent fuel (150GWd/t, cooled 5 years). By a close investigation, individual "exit strategy" can be seen toward their utilization. Namely, **1/** Material/Chemical use; Ru (with stockpile at least 40 years to below BSS level of  $^{106}\text{Ru}$ ), Rh (with long stockpile at least 80 years to below NRPB level of  $^{102}\text{Rh}$ ), Pd (with light shielding or dilution against  $\beta$ ), Mo (without shielding, e.g., source of  $^{99\text{m}}\text{Tc}$ ) and RE (La, Nd, Dy, etc) (without shielding), **2/** Radiochemical use;  $^{137}\text{Cs}$  (e.g.,  $\gamma$  source alternating to  $^{60}\text{Co}$ ),  $^{90}\text{Sr}$ ,  $^{238}\text{Pu}$ , etc, **3/** Additional nuclear fuel;  $^{237}\text{Np}$ ,  $^{241}\text{Am}$  and Cm (as  $^{238,240}\text{Pu}$  by  $\alpha$  decay of  $^{242,244}\text{Cm}$ ) to enhance non-proliferous property of  $^{239}\text{Pu}$ , **4/** Commerce of high expence stable isotope;  $^{99,102,103}\text{Ru}$ ,  $^{103}\text{Rh}$ ,  $^{106}\text{Pd}$  and  $^{107}\text{Ag}$  in the isotope market.

### Advanced ORIENT Cycle, with a multi-functional reprocessing

A concept of Adv.-ORIENT (Advanced Optimization by Recycling Instructive Elements) Cycle strategy[1] was set as shown in Fig.1 under the following directions. **1/** Higher purity on NRM for utilization, but lower DF on actinides permitted for burning in FBR, **2/** Adopt *soft* hydrometallurgical but non-SX separation process with *salt-free* reagents to reduce the secondary rad. wastes, **3/** Deep separation of all actinides into 3-4 groups, e.g., U, Pu/U/Np, Am and Cm, **4/** Allow hydrochloric acid (HCl) in combination with nitric acid ( $\text{HNO}_3$ ) media to sharpen the separability. The most significant policy change is that some fission products shall be no longer wastes but main products, and actinides are just "energy carrier" in the fuel cycle. In the point of back-end risks, a period to reduce the radio-toxicity below the level equivalent to 60 ton of natural uranium is one of the indexes. In Adv.-ORIENT Cycle, by putting the separation factors as 99.9% for all An, 99% for  $^{137}\text{Cs}$  and  $^{90}\text{Sr}$ , 90% for RE, etc, such a period can be dramatically

reduced to around  $1 \times 10^2$  years.

Catalytic electrolytic extraction (CEE), utilizing under potential deposition (UPD) with forming of undissolvable metal solid solution in acidic media, can effectively separate Ru, Tc and Re (Tc simulator) from HLLW with either  $\text{HNO}_3$  or  $\text{HCl}$  media. In the four NRM metal ions mixture solution (corresponded to FBR spent fuel composition), observed deposition yields were typically in the following order; Pd, Rh (>99%) > Re (91%) > Ru (85%) > Tc (69%). During the CEE, Pd or Rh might act as *promoter* at the surface of electrode (i.e.,  $\text{Pd}_{\text{adatom}}$ ) and *mediator* in the bulk solution (i.e., redox ion pair) to accelerate other PGM's deposition. Those co-deposits were, dense and mechanically stable, showing electrochemically high catalytic reactivity on electrolytic hydrogen production. Ru has been confirmed as a dominant element responsible for high reactivity.

Tertiary pyridine resin (TPR), composing a nitrogen atom in six-membered ring, is characterized to simultaneously have two functions as weakly basic anion-exchanger and soft donor ligand. An original idea of combinatory use of conc.HCl and conc. $\text{HNO}_3$  media was based on the facts that recognition of softer ions like  $\text{Am}^{3+}$  and  $\text{Cm}^{3+}$  (5-f elements) was clearer than  $\text{Ln}^{3+}$  (4-f elements) in HCl media, and in  $\text{HNO}_3$  media their distribution depended just on the difference of ionic radius independently either 4-f or 5-f elements. Extractabilities of both  $\text{Am}^{3+}$  and  $\text{Cm}^{3+}$  were improved by enhancing complexation of protonated pyridine with anions due to the dehydration brought by co-existing methanol, and

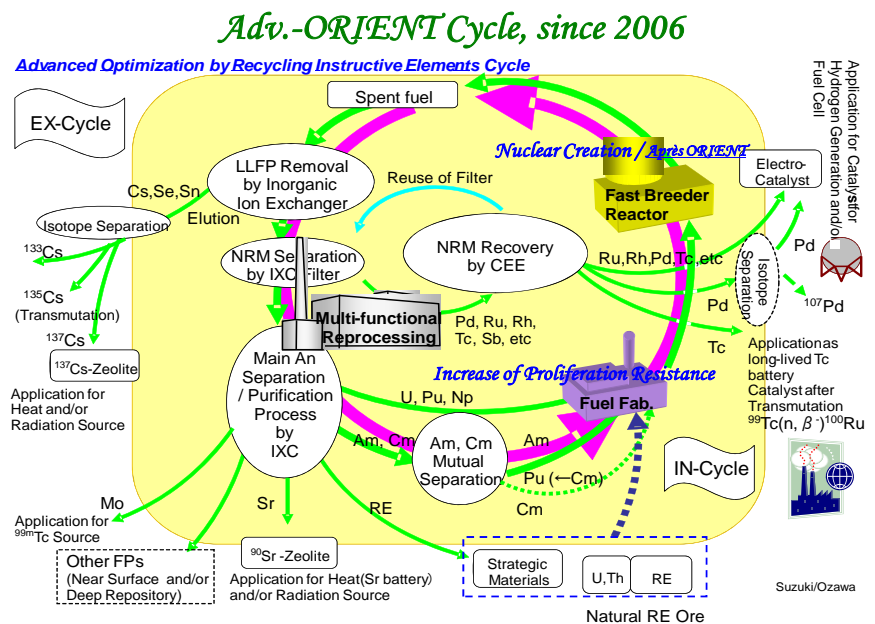
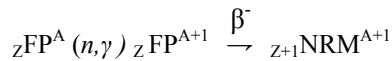


Fig.1 Advanced ORIENT Cycle

thereby increasing  $SF_{Am3+/Cm3+}$ . This scheme was successfully demonstrated using MOX spent fuel irradiated (143.8GWd/t) at the fast experimental reactor “Joyo”.

**Après ORIENT**

*Après ORIENT* will deal with positive transmutation of FPs by  $(n,\gamma)$  reaction to create new elements with highly valuable and strategic and without or less radioactivity as the secondary NRM[2].



Current target FP elements for transmutation / creation are shown in Fig.2.

Based on the calculation with the conditions of even at higher energy (*i.e.*,  $\geq 0.1\text{MeV}$ ) fast neutron spectra with neutron flux ( $\Phi$ ) of  $2.27 \times 10^{15} \text{ n/cm}^2/\text{s}$ , some transmutation possibility (yield) were expected for the systems of Tc to Ru, Ru to Rh/Pd, Ba to La, Pr to Nd, and Eu to Gd/Tb/Dy. Decrease of radiotoxicity will also be expected on the transmutation products of Ru, Pd, Pr and Nd. A softer neutron spectrum should then be considered with expecting higher neutron cross section ( $\sigma$ ). FBR-based calculation study will be made for target FP subassembly with proper neutron moderators. Of course, natural elements as raw material are also in the scope.

**References**

- [1] M.Ozawa, T.Suzuki, S.Koyama, H.Akatsuka, H.Mimura and Y.Fujii, *Progress in Nuclear Energy*, **50** (2008) 476-482, ELSEVIER (2008).
- [2] Masaki Ozawa, 17<sup>th</sup> Symposium on *Separation Science and Technology for Energy Applications*, Gatlinburg, TN, pp38-39(2011).

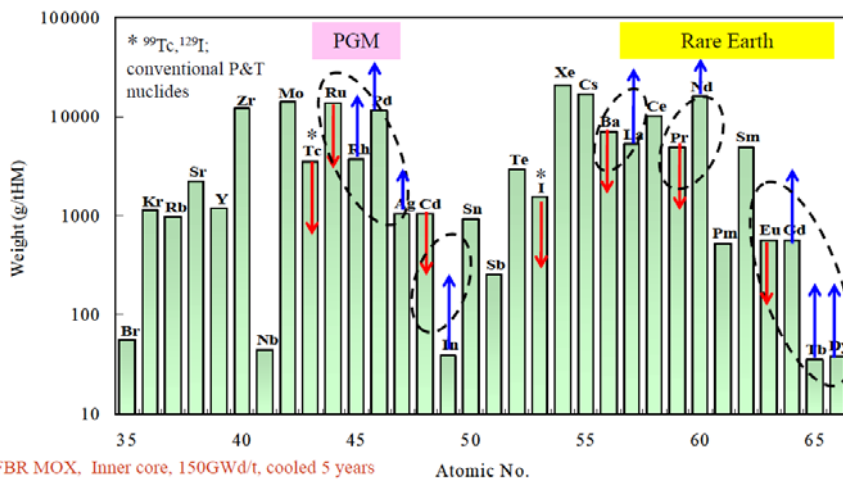


**Fig.2** Target pairs of FP elements for transmutation / creation in *Après ORIENT*

## B.15 Transmutation Study on Fission Product Palladium for Denaturing Isotopic Composition

Toshio YOSHIOKA, Masaki OZAWA and Masaki SAITO

### 1. Introduction

Platinum Group Metals (hereafter PGM) such as Ruthenium (hereafter Ru), Rhodium (hereafter Rh) and Palladium (hereafter Pd) are considered Strategic Elements, because their abundances are low and widely used in the internationally competitive field in Japan such as exhaust gas catalyst of cars [1]. Nowadays, Japan depend almost all of PGM resources on import from abroad. However, this must be issued, because the price change of PGM is highly significant [2]. Therefore, it is necessary to acquire them in our own country. PGM are found in spent fuel of nuclear reactors. As the standards of activities of radionuclide, exemption level (the level of activity or activity concentration to distribute radiation sources which never enter the regulatory control regime, hereafter EL) and clearance level (the level of distributing radiation sources which are released from regulatory control, hereafter CL) are considered [3]. Fig.1 shows the activity change of PGM in spent fuel of LMFBR of 3570MWth. Ru and Rh take long periods to decrease their activities below EL and the activity of Pd never gets below EL.

### 2. Calculation

Pd of PGM is taken as an example for the reason listed above in this study and it is demonstrated whether re-irradiation of separated single element in spent fuel leads to decrease the activity of Pd. Two cases are considered here;

1. Fission product Pd in spent fuel is re-loaded in the reactor and irradiated.
2. Fission product Ru and Rh in spent fuel are re-loaded in the reactor and irradiated.

In the calculations, these elements are positioned in inner core of fast reactor because of expecting high flux. Reactor thermal activity is 3570MWth and irradiation time is 1900day. Pu enrichment in inner core is 18.3wt% and Pu isotopic composition is that of 50GWd/tHM irradiated fuel of presently operating PWR with 5%  $^{235}\text{U}$  fuel followed by 5 years cooling time [5]. The ORIGEN2.2 code was used to provide burnup calculation. In point of one-group cross sections which were needed to calculate, EMOPUUUC.lib was used.

### 3. Results and Discussion

In the first case, the change of isotopic composition of Pd was determined by neutron radiation. Among the isotopes of Pd, the activity of  $^{107}\text{Pd}$  is dominant. Therefore, the efficient neutron capture of  $^{107}\text{Pd}$  leads to decrease the activity of total Pd. In the second case, comparing Pd

created from Ru or Rh with Pd in spent fuel, they must have different activities because of different isotopic composition.

Mass and composition of PGM in spent fuel are shown in Table I, and those of Pd after re-irradiation are shown in Table II. The amount of Ru in spent fuel was much more than the amount of Rh in spent fuel. However, after re-loading of all of them and re-irradiation, the amount of Pd created from Rh was much more than the amount of Pd created from Ru because of high transmutation rate of Pd created from Rh. The activity change of Pd after re-irradiation is shown in Fig.2. The activity of Pd created from re-irradiation Pd was about the same as the activity of Pd in spent fuel. This means that the neutron capture of  $^{107}\text{Pd}$  didn't proceed effectively in this condition. Yet, the activities of Pd created from Ru and Pd created from Rh were much lower than that in spent fuel. The activity of Pd created from Ru was about the same as the  $^{107}\text{Pd}$  EL and the activity of Pd created from Rh was about fifty times lower than the  $^{107}\text{Pd}$  EL.

### 4. Conclusion

It was demonstrated that the transmutation of Pd created from Ru or Rh in spent fuel enabled the activity of Pd to become much lower. In the case of the transmutation product of Pd created from re-irradiation Pd, the activities didn't mostly change in this condition. However, if neutron spectrum changed softly, where the effective cross section of  $^{107}\text{Pd}$  was increased, the activity of Pd effectively became lower. In the Future plan, the change of isotopic composition of re-loaded Pd will be examined for the change of neutron spectrum.

### References

- [1] Y. Fuji et al., *Nuclear eye* 10/2010 (2010)
- [2] G. Adachi et al., *Rare metals handbook* (2011)
- [3] IAEA, *IAEA safety standards series* No. RS-G-1.7(2004)
- [4] T. Ogawa et al., *JAEA Research-2006-042-Incl*, JAEA (2006)
- [5] Y. Meiliza et al., *Journal of Nuclear Science and Technology*, Vol. 45, No. 3, p. 230-237, (2008).

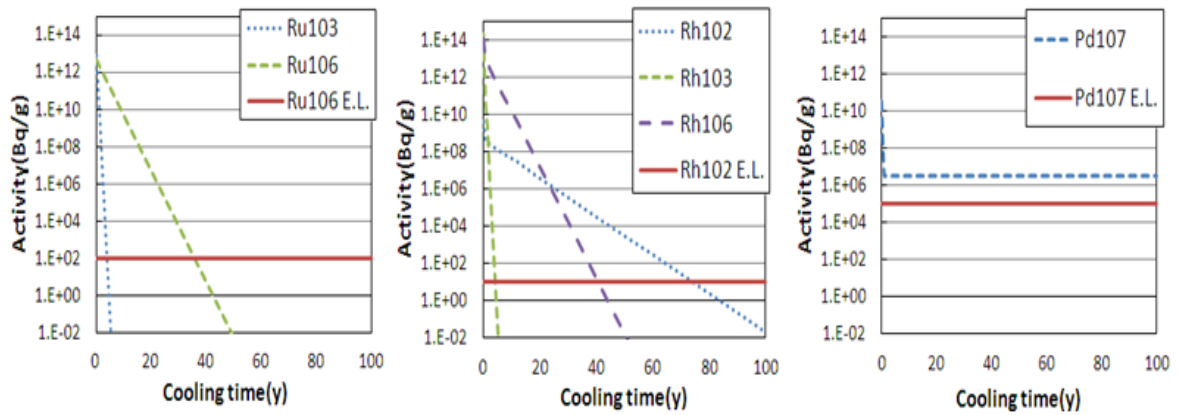


Fig.1. Activities of PGM in spent fuel of fast reactor

Table I. Elements in spent fuel

	Pd		Ru		Rh			
	Mass(g /tHM)	Compo sition(-)	Mass(g/ tHM)	Composit ion(-)	Mass(g /tHM)	Compo sition(-)		
104	4.73E+2	5.46E-2	99	6.51E-2	6.65E-6	102	7.47E-3	2.55E-6
105	2.28E+3	2.63E-1	100	2.70E+2	2.76E-2	103	2.92E+3	1.00E+0
106	2.63E+3	3.04E-1	101	2.90E+3	2.96E-1	103M	9.03E-16	3.09E-19
107	1.55E+3	1.79E-1	102	3.45E+3	3.53E-1	106	1.81E-5	6.17E-9
108	1.35E+3	1.56E-1	103	1.01E-12	1.03E-16			
110	3.86E+3	4.45E-2	104	3.21E+3	3.21E-1			
			106	1.92E+1	1.96E-3			
Total	8.66E+3	1.00E+0	Total	9.79E+3	1.00E+0	Total	2.92E+3	1.00E+0

Table II. Pd after re-irradiation (full loading in spent fuel)

	Pd (Loading Pd)		Pd (Loading Ru)		Pd (Loading Rh)			
	Mass(g /tHM)	Compo sition(-)	Mass(g/ tHM)	Composit ion(-)	Mass(g /tHM)	Compo sition(-)		
104	4.23E+2	4.95E-2	104	3.72E+1	1.59E-1	104	7.89E+2	9.42E-1
105	1.68E+3	1.96E-1	105	1.50E+2	6.43E-1	105	4.31E+1	5.14E-2
106	3.10E+3	3.63E-1	106	4.46E+1	1.91E-1	106	5.05E+0	6.03E-3
107	1.41E+3	1.65E-1	107	1.56E+0	6.68E-3	107	8.43E-2	1.01E-4
108	1.58E+3	1.85E-1	108	1.40E-1	5.97E-4	108	3.97E-3	4.74E-6
110	3.62E+2	4.24E-2	110	4.04E-7	1.73E-9	110	4.31E-9	5.15E-12
Total	8.55E+3	1.00E+0	Total	2.34E+2	1.00E+0	Total	8.37E+2	1.00E+0
			Transmutation rate (%):		Transmutation rate (%):			
			2.39		28.62			

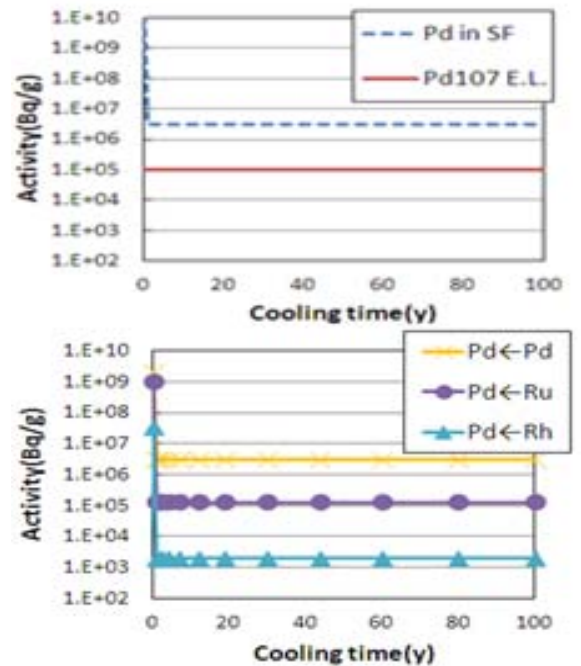


Fig.2. Activity change of Pd in spent fuel and after re-irradiation

## B.16 Experimental Study on Diffusion of Metal in Lead-Bismuth Eutectic in Thin Tube

Minoru TAKAHASHI, Shunichi NUMATA,  
Eriko IRISAWA-YAMAKI and Weidong WU

### 1. Introduction

The diffusion characteristics of dissolved elements from steels in liquid lead-bismuth eutectic (LBE) are important factor for prediction of dissolution rate in the dissolution type of corrosion. The dissolved metallic elements are transported in a LBE circuit and precipitate in low temperature regions due to a solubility limit. Since Ni has the highest solubility in LBE among the elements in steels, preferential dissolution of Ni occurs in the corrosion of austenitic stainless steels. As a result, a phase transfer from a austenitic phase to a ferritic phase takes place. In the present study, the diffusion coefficient of Ni in LBE in the temperature range from 550 to 650°C was determined by means of the capillary method.

### 2. Experiment

#### 2.1. Diffusion experiment

Figure 1 shows the preparation process of a diffusion test tube made of a ceramic crucible containing LBE and Ni powder inside. A ceramic crucible tube made from 40 %SiO<sub>2</sub>-56 %Al<sub>2</sub>O<sub>3</sub> was used as a capillary tube for the diffusion experiment. The inner diameter of the crucible was 2 mm, and the length was 50 mm.

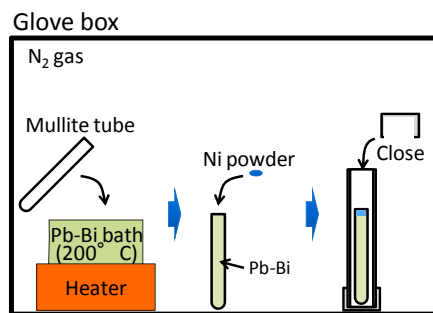


Fig. 1 Preparation of diffusion test tube of a ceramic crucible containing LBE and Ni powder inside

The crucible was filled with liquid LBE and Ni powder was put at the top surface of the liquid LBE. This process was performed in the glove box filled with inert N<sub>2</sub> gas. The crucible was put into a capsule made of a stainless steel tube as shown in Fig. 1. The capsule was closed so that it contained N<sub>2</sub> gas without oxygen. Figure 2 shows a schematic of the capsule and its picture.

Figure 3 shows the capsule in electric furnace and solid LBE rod after heating. The capsule with the crucible containing the Ni and LBE was put into the electric furnace the inside of which was heated up to the test temperature. Then, the temperature close to the sample capsule became

the test temperature in 20 min, and kept constant for 3.5 h. The capsule was kept vertical during the diffusion test duration. After 3.5 h, the capsule was cooled down quickly to the room temperature in air. The solid LBE rod in which Ni diffused was taken out from the crucible, and cut into small pieces as shown in Fig. 3 (b).

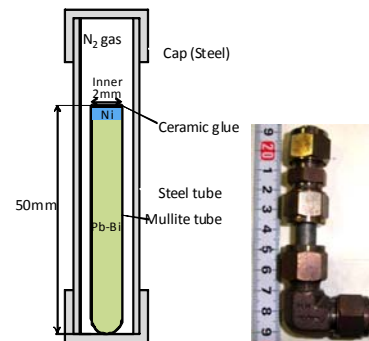
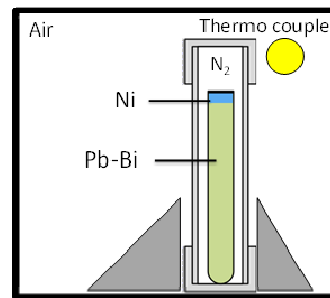


Fig. 2 Schematic of capsule with a ceramic crucible containing LBE and Ni powder inside.

#### Inside of electric furnace



(a) Capsule in electric furnace

#### Pb-Bi sample (after 3.5h)



(b) Solid LBE rod

Fig. 3 Capsule with crucible containing Ni and LBE in electric furnace and solid LBE rod after 3.5 h-heating.

#### 2.2. Measurement of Ni concentration profile in LBE

Axial distribution of Ni concentration in the LBE rod was measured by means of the inductively coupled plasma mass spectroscopy (ICP-MS) method.

The relationship between the Ni concentration in LBE,  $C$ , and the Ni diffusion coefficient in LBE,  $D$ , can be given by

$$(C - C_0)/(C_s - C_0) = 1 - \operatorname{erf}\left[x/(2\sqrt{Dt})\right] \quad (1)$$

where  $t$  is the diffusion time and  $x$  is the distance from the

interface between Ni and LBE,  $C_0$  is the Ni concentration at infinity,  $C_s$  is the Ni concentration in LBE near the interface between the solid Ni and the liquid LBE. Figure 4 shows the theoretical concentration distribution. The value of  $D$  was calculated from the measured axial Ni concentration distribution in LBE using Eq. (1).

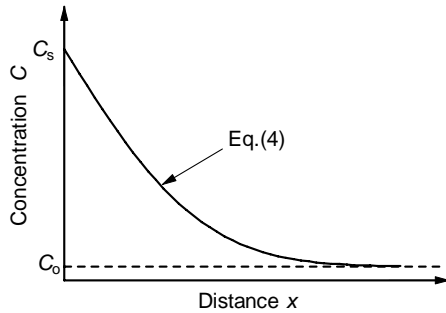


Fig. 4 Theory for concentration distribution.

### 3. Results and Discussion

The measured Ni concentrations in LBE at the temperatures of 650°C are plotted in Fig. 5 in comparison with the theoretical curves of Eq. (1). It is noted that the position at  $x=0$  is not the interface between Ni and LBE in the figure. The curves were drawn so that they are well fitted to the measured data with the assumption that  $C_s$  is equal to the solubility limit of Ni in LBE at each temperature, i. e., 3.2 wt% at 550°C and 4.1 wt% at 650°C.

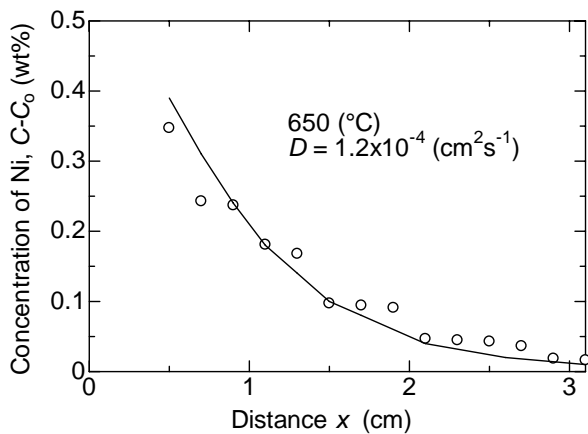


Fig. 5 Measured Ni concentration in LBE with the theoretical curves of Eq. (1) at 650°C.

The diffusion coefficients of Ni at the temperatures of 550°C and 650°C were determined from the fitting of the measured Ni concentration profiles to the theoretical curves, and are shown in Fig. 6. They are compared with the diffusion coefficient of Ag in Pb-44at%Bi expressed by

$$\log D = -7.93 - 0.78 / RT \quad (435^\circ\text{C} < T < 610^\circ\text{C}). \quad (2)$$

and those of Ni in Pb-Bi alloy calculated from Stokes–Einstein equation and Sutherland–Einstein equation:

$$D = kT / N\pi r\eta, \quad (3)$$

where  $k$  is the Boltzmann constant,  $T$  is the temperature,  $r$  is the Ni atomic diameter,  $\eta$  is the viscosity of LBE and  $N$  is 6 for the Stokes–Einstein equation and 4 for the Sutherland–Einstein equation. The viscosity of LBE,  $\eta$  (Pa s), is given by

$$\eta = 4.94 \times 10^{-4} \exp(754/T). \quad (4)$$

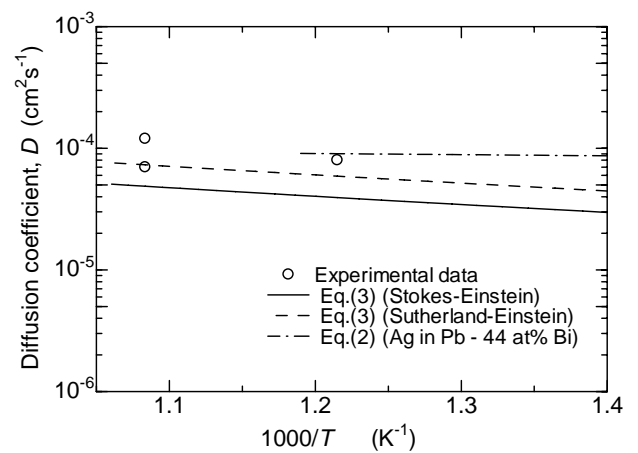


Fig. 6 Measured diffusion coefficients of Ni compared with that of Ag in Pb-45at%Bi and calculated ones of Ni from Stokes–Einstein equation and Sutherland–Einstein equation.

### 4. Conclusion

The diffusion coefficients of Ni in LBE were determined experimentally using capillary method at 650 and 550°C. From the measured axial distribution of diffused Ni concentration in the LBE rod by means of ICP-MS, the diffusion coefficient of Ni in LBE was obtained at the temperatures of 550°C and 650°C.

### Acknowledgment

The authors express their deep acknowledge to Mr. Masao Nomura for his various technical support in ICP-MS measurement.

### Reference

E. Yamaki-Irisawa, S. Numata, M. Takahashi, W. Wu, “Experimental Study on Diffusion of Metals in Lead-Bismuth Eutectic in A Thin Tube,” 19th International Conference of Nuclear Engineering (ICONE19), October 24-25, 2011, Osaka, 2011, ICONE19-43499.

## C.1 Progress in Innovative Nuclear Reactor Study and Nuclear Safety Study

Toru OBARA

Several Studies on innovative nuclear reactors and nuclear safety have been performed. It was intending to give concepts of nuclear reactors for various demands and solutions in nuclear safety.

### 1. Design study of pebble bed reactor with accumulating fuel loading scheme

Neutronic and steady state thermal hydraulic analysis were performed for a reference design of the small simplified pebble bed reactors with accumulating fuel loading scheme and it was shown the reactor concept had excellent burnup characteristics[1,2].

### 2. Study of silicon carbide coating to prevent oxidation of graphite block in high temperature gas cooled reactors

High Temperature Gas Cooled Reactors have excellent passive safety features. One of the important issues in its safety is oxidation of graphite blocks in depressurization accident. The ingress of air will cause the oxidation and it can cause corrosion of graphite blocks. Silicon carbide coating the graphite structures can be effective measure for the issue. But it can cause the absorption of neutrons and change of thermal conductivity. In the study, the effect of the coatings on neutronic characteristics and heat removal performance were analyzed[3].

### 3. Study of particle type burnable poisons for flatterer of excess reactivity in long life high temperature gas cooled reactors

In long life prismatic high temperature gas cooled reactors, the use of burnable poisons to compensate excess reactivity is needed. In the study, particle type burnable poisons were tested to minimize excess reactivity change during the operation. Monte Carlo calculations with burnup calculations were performed for various design of particles[4].

### 4. Study of design concept of small district heating reactor for Mongolia

Nuclear reactor concept based on high gas temperature cooled reactor technology was studied for district heating in Mongolia. A useful concept with passive safety feature after the shutdown was shown[5].

### 5. Design study of small reactor for semiconductor production

A small reactor for NTD Si was proposed in the study. In the study, conventional PWR fuel assemblies were used as fuel. It is intended to irradiate 12 inches silicon ingots. For the uniform doping of such large silicon ingots,

graphite reflectors with graphite spacers between the ingots were employed. It was shown the reactor can achieve high production rate of silicon semiconductors[6].

### 6. Fundamental study for laser oscillation simulation in Nuclear Pumped Laser

In nuclear pumped laser using nuclear reactor, kinetic energy of fission fragments was used for the pumping of laser gas medium. In the study, fundamental analysis was performed for the simulation of laser oscillation by kinetic energy of fission fragments[7].

### 7. Fundamental study of nuclear reactor to oscillate nuclear pumped laser for laser fusion reactor

In the study, nuclear reactor to oscillate nuclear pumped laser, which is used for laser fusion reactor, was studied. Based on the requirement of laser power for laser fusion, fundamental design concept of the reactor was shown[8].

### 8. Preliminary transient analysis in weakly coupled fuel solution tanks

By using the method developed for the kinetic analysis of experimental reactor for nuclear pumped laser oscillation, preliminary analysis were performed in super prompt condition in weakly coupled fuel solution tanks[9,10].

## References

- [1] Dwi Irwanto, Toru Obara, *J. Nucl. Sci. Technol.*, **48**[11], 1385-1395 (2011).
- [2] Dwi Irwanto, Toru Obara, *Trans, Am. Nucl. Soc.*, **105**, 1105-1106 (2011).
- [3] Piyatida Trinuruk, Toru Obara, 2012 AESJ Annual Meeting, D09 (2012).
- [4] Taiki Onoe, Toru Obara, 2012 AESJ Annual Meeting, D08 (2012).
- [5] Odmaa Sambuu, Toru Obara, *Trans, Am. Nucl. Soc.*, **105**, 1160-1161 (2011).
- [6] Byambajav Munkhbat, Toru Obara, *Trans, Am. Nucl. Soc.*, **105**, 1123-1124 (2011).
- [7] Yosuke Isobe, Toru Obara, 2012 AESJ Annual Meeting, D51 (2012).
- [8] Takehito Tomonari, Toru Obara, 2012 AESJ Annual Meeting, D50 (2012).
- [9] Haruka Kikuchi, Toru Obara, *Trans, Am. Nucl. Soc.*, **105**, 535-536 (2011).
- [10] Haruka Kikuchi, Toru Obara, 2011 AESJ Autumn Meeting, N27 (2011).

## C.2 Development of Methodology for Plutonium Categorization (IV) - Effect of Compression on Rossi-alpha-

Yoshiki KIMURA<sup>\*1</sup> and Masaki SAITO

### INTRODUCTION

To evaluate the proliferation resistance of Pu, a function “*Attractiveness (ATTR)*” was proposed as a ratio of the characteristic of potential explosive energy to technical difficulty converting to nuclear explosive devices (NEDs) [1,2,3]. The characteristic of potential explosive energy was defined by rossi-alpha, the ratio of supercriticality to prompt neutron lifetime. The technical difficulty was assumed as functions of specific decay heat (DH, [W/kg]), spontaneous fission neutron rate (SN, [n/g/s]) [1,2,3], and radiation dose rate (RD, [Sv/hr/kg]) was recently introduced as a new factor [4]. The high DH and RD make Pu handling and NED manufacturing technically difficult, and the high SN enhances the probability of pre-detonation. The current function of *ATTR* was proposed as [4]

$$ATTR = \frac{\frac{\alpha_{\infty}}{\alpha_{\infty}^{239}}}{\frac{DH}{DH^{238}} + \frac{SN}{SN^{238}} + \frac{RD}{RD^{238}}} \quad (1).$$

The rossi-alpha and all technical difficulty factors are normalized to their reference values in Pu isotopes.

### EFFECT OF COMPRESSION ON ROSSI-ALPHA

In Eq.(1), the numerator, rossi-alpha in infinite condition ( $\alpha$ -infinity,  $\alpha_{\infty}$ ), characterizes the power excursion of Pu. In actual NEDs, the Pu-cores would be compressed to make them supercritical state.

Figure 1 shows the effect of compression (initial density: 15.8 [g/cc]) on the  $\alpha$ -infinity of Pu isotopes which is the recalculation of the results in earlier study [5]. Supercriticality and prompt neutron lifetime in infinite mass Pu were estimated using MCNP4C(02) code[6] with infinite cell geometry and neutron cross-section library FSXLIB-J33 [7]. The values of  $\alpha$ -infinity at normal density are varied in Pu isotopes and they are changing in proportion to the compression ratio with different rates of increasing. This increasing rate also can be considered as the meaningful feature to characterize the explosive energy.

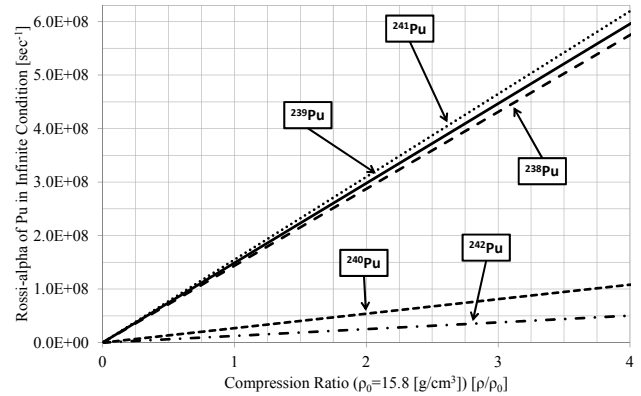


Fig.1 Effect of compression on  $\alpha$ -infinity (recalculating the results in Ref. [5])

In the present paper, the increasing rate of  $\alpha$ -infinity was introduced to the function of *ATTR*. The characteristic of potential explosive energy was defined by the product of  $\alpha$ -infinity and its increasing rate ( $\alpha_{\infty} \times \alpha'_{\infty}$ ). Based on the one-group theory, the  $\alpha$ -infinity is proportional to the compression ratio as:

$$\alpha(\infty, \rho/\rho_0) = \alpha(\infty, 1) \times \frac{\rho}{\rho_0} \quad (2).$$

It can be also confirmed in Fig.1. Therefore, the characteristic of potential explosive energy with consideration of the effect of compression was defined by  $\alpha$ -infinity squared;

$$\alpha(\infty, 1) \times \frac{d}{d(\rho/\rho_0)} \alpha(\infty, \rho/\rho_0) = \alpha^2(\infty, 1) \quad (3).$$

The function of *ATTR* was improved as below,

$$ATTR = \frac{\left( \frac{\alpha_{\infty}}{\alpha_{\infty}^{239}} \right)^n}{\frac{DH}{DH^{238}} + \frac{SN}{SN^{238}} + \frac{RD}{RD^{238}}} \quad (4).$$

In Eq.(4),  $n=1$  characterizes the power excursion of Pu and  $n=2$  includes the effect of compression on rossi-alpha.

### EVALUATION OF PLUTONIUM DENATURING

Figure 2 shows the *ATTR* of Pu normalized by that of  $^{239}\text{Pu}$  as a function of the doping rate of Pu isotopes to pure  $^{239}\text{Pu}$  ( $n=1&2$ ). It also shows the example of Pu categorization [9-12].

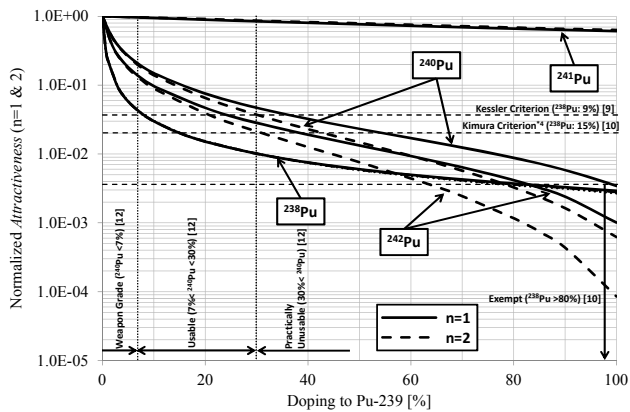


Fig.2 Normalized Attractiveness of denatured Pu ( $n=1$  and 2)

In both cases, *ATTR* of Pu decrease dramatically by even-mass-number Pu isotopes doping, because the technical difficulties converting to NEDs are enhanced. As the number of  $n$  in Eq.(4), *Attractiveness* of Pu decreases more dramatically by  $^{240}\text{Pu}$  and  $^{242}\text{Pu}$  with high doping rate. This is because the  $\alpha$ -infinity of pure  $^{240}\text{Pu}$  and  $^{242}\text{Pu}$  isotope are comparatively lower than that of  $^{239}\text{Pu}$ .

## REFERENCES

1. M. Saito *et al.*, *ANS TRANSACTIONS*, Vol. **96** (2007).
2. M. Saito, *et al.*, *ANS TRANSACTIONS*, Vol. **98** (2008).
3. M. Saito, *Proc. Global09*, Paris, Sep. 6-11, (2009).
4. Y. Kimura, *et al.*, *ANS TRANSACTIONS*, Vol. **103** (2010).
5. M. Saito *et al.*, to be submitted.
6. "MCNP4C," CCC0700, RSICC (2000).
7. JAERI-DATA/CODE 2003-011, JAERI (2003).
8. J.C. Mark, *Science & Global Security*, **4**, 111 (1995).
9. G. Kessler, *Nucl. Sci. Eng.*, **155**, 53-73 (2007).
10. Y. Kimura, *J. Nucl. Sci. Technol.*, Vol.**48**, No.5 (2011).
11. IAEA, INFCIRC/153 (1972).
12. B. Pellaud, *J.Nucl.Mat.Management*,**31**,30 (2002).

\*1 Present Address : Tokai Research and Development Center,  
Japan Atomic Energy Agency

### C.3 Effects of Inner Axial Blanket and Minor Actinides on Extension of Core Life-time of Large-scale FBR

Erina HAMASE\*<sup>1</sup> and Masaki SAITO

#### INTRODUCTION

Minor Actinides (MAs) discharged from the nuclear reactor spent fuel entails a significantly long term radiological issue in geological repository. However, the attractive characteristics of MA as a burnable poison and a fertile material were proposed<sup>1,2</sup>. Based on this proposal, it was reported that if MA was doped into the inner radial blanket arranged at the center of large scale Fast Breeder Reactor (FBR) core, the core life-time could be extended by shifting main fission reaction zone from the active core to the inner radial blanket because <sup>238</sup>Pu transmuted from MA worked as a fissile nuclide<sup>3</sup>. In the present study, the effect of inner axial blanket which is introduced axially at the center of FBR core and doping MA into it on the extension of core life-time is surveyed. Furthermore, the effect of the metal fuel as well as MOX fuel is investigated.

#### METHODOLOGY

For reactivity and burnup calculation, SLAROM<sup>4</sup>, JOINT and CITATION<sup>5</sup> were used with the cross section library, JFS-3-J-3.2R<sup>6</sup>. 70-group effective cross sections were made by homogeneous square cell calculation in the SLAROM, and JOINT converts 70-group effective cross section data format to the CITATION input. Reactivity and burnup calculation were performed with CITATION based on the two-dimensional RZ diffusion theory with nuclide transmutation chain.

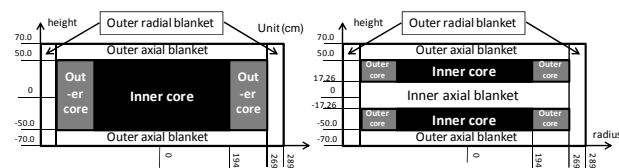


Fig. 1 Core layout of REF-MOX and REF-Metal (left) and CASE A to D (right)

In the present study, 6 cases are analyzed. Based on large-scale sodium-cooling FBR<sup>7</sup>, the case of REF-MOX whose inner and outer core contain MOX fuel of (U-Pu)<sub>2</sub>O<sub>2</sub> with 18.3/20.9wt% Pu enrichment, respectively, and the case of REF-Metal whose inner and outer core contain U-Pu-Zr10% as a metal fuel with 13.1/15.0 wt% Pu enrichment are evaluated. Both of Pu inventories in entire the core, 6,747/7,340 kg (inner/outer core), are set constant and outer radial/axial blankets consist of depleted uranium (DU) oxide and metallic fuel. These

configurations are shown in the left-hand side of Fig. 1. In cases from A to D, the inner axial blanket consisting of DU fuel is arranged at the axial core mid-plane in the right-hand side of Fig. 1 and volume of entire the core is not changed. Since in cases from A to D, Pu inventory in entire the core, 6,747/7,340 kg, is also kept constant, Pu enrichment is increased to 27.8/31.8 wt% in CASE A and B consisting of MOX fuel and 20.1/22.9 wt% in CASE C and D that consist of metallic fuel. Furthermore, in CASE B and D, 40 and 28.5 wt% of MA, equivalent to 9,857 kg heavy metal, is doped into the inner axial blanket.

#### RESULTS AND DISCUSSIONS

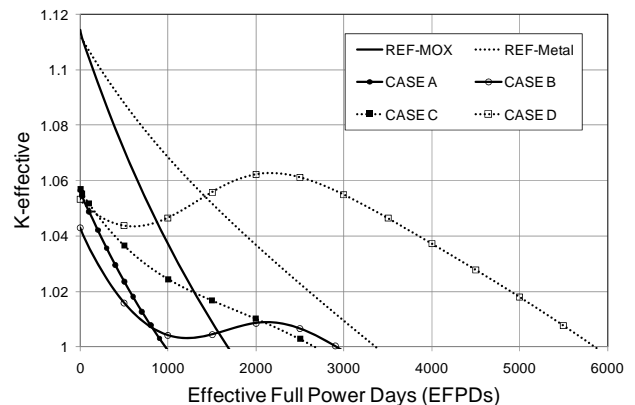


Fig. 2 Effect of inner axial blanket and doping MA on reactivity

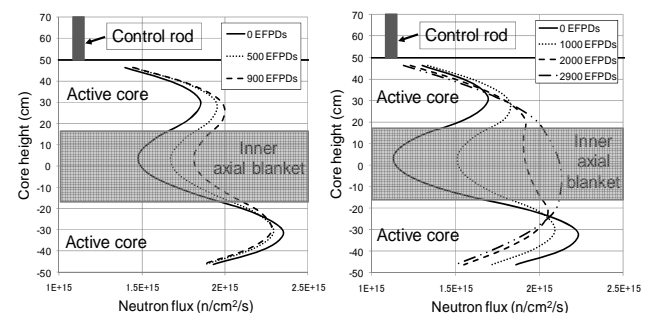


Fig. 3 Neutron flux distribution during irradiation in CASE A (left) and CASE B (right)

Figure 2 shows an illustrative scope of irradiation time-dependent eigenvalue ( $k_{\text{eff}}$ ) for REF-MOX, REF-Metal and CASE A to D. It is found that the initial excess reactivity in CASE A to D is smaller than that in

REF-MOX and REF-Metal because the absorption of  $^{238}\text{U}$  and MA in the inner axial blanket in CASE A to D highly contributes from the beginning of cycle. In CASE A and C, the maximum available Effective Full Power Days (EFPDs) is smaller than REF-MOX and REF-metal. However, it shows that the maximum available EFPDs in CASE B and D are significantly extended keeping the reactivity swing small. In order to investigate the effect of  $^{238}\text{U}$  and MA as a fertile material in the inner axial blanket, the distribution of neutron flux at different reactor operation time in CASE A and B is surveyed as shown in Fig. 3. In CASE A, the neutron flux in the inner axial blanket slightly build and therefore  $^{238}\text{U}$  in the inner axial blanket does not so much affect on the extension of core life-time as the fertile material. On the other hand, in CASE B, it shows that the main fission reaction zone is shifted from the active core to the inner axial blanket. It is because that  $^{238}\text{Pu}$  transmuted from MA in the inner axial blanket plays a role as a fissile nuclide in the same way as the previous study of inner radial blanket<sup>3</sup>. It is found that the inner axial blanket with MA has the possibility of extension of core life-time as well as smaller initial excess reactivity and reactivity swing. It has been also confirmed that the maximum available EFPDs in the metal fuel is increased compared with that in the oxide fuel.

## REFERENCES

1. M. Saito, *Prog. Nucl. Energy*, **40**[3-4], 365-374 (2002).
2. M.Saito, *Int. J. Nucl. Sci. Tec.* **1**[23], 127-138 (2005).
3. E. Hamase *et al.*, *Ann. Nucl. Energy*, **38**[7], 1496-1504 (2011)
4. M. Nakagawa, K. Tsuchihashi, JAERI 1294, Japan Atomic Energy Research Institute, (1984).
5. T. B. Fowler *et al.*, Oak Ridge National Laboratory report, ORNL-TM-2496, Rev2, USA, (1971).
6. G. Chiba *et al.*, *J. Nuc. Sci. Technol.*, **1**[4], 335-340 (2002).
7. M. Naganuma *et al.*, JNC TN9400 2005-051, (2005), [in Japanese].

\*1 Present Address : O-arai Research and Development Center,  
Japan Atomic Energy Agency

## C.4 Positional Stabilization of Torus Plasma with Simple Helical Coils

Shunji TSUJI-IIO and Hiroaki TSUTSUI

Although tokamaks are the most promising magnetic confinement scheme for fusion reactors, it is difficult to avoid disruptions which can cause damages to fusion reactors. At a disruption, large eddy currents are generated in thermal and current quench phases and a feedback system fails to keep the plasma at a desired position. Resulting contact of plasma with first wall will lead to the damages of a reactor by high heat flux and/or induced electromagnetic forces. We are investigating a simple helical coil system which passively stabilizes vertical displacements<sup>1)</sup> and elongates the plasma. It has a potential to avoid an occurrence of VDE (vertical displacement event) which is a problem of vertically elongated tokamaks.

Figure 1 shows the coil configuration schematically. The directions of the current in adjacent coils are opposite with each other. The windings on the top and bottom sides of the plasma produce finite averaged horizontal field  $B_R$ <sup>2)</sup> which stabilizes vertical displacements since it increases toward the coils. While the windings on the outer side of torus produce vertical magnetic field component as plotted in Fig. 2. The finite averaged vertical field pushes the plasma to the inner side of torus and elongates the plasma.

Furthermore, the proposed coils can form closed vacuum magnetic surfaces in combination with poloidal field coils. In the first phase of a disruption when the plasma current does not drop so much, the plasma position is maintained by the averaged  $B_R$  component. In the latter phase, the plasma confinement can be preserved and recovered by heating the plasma up again owing to the closed magnetic surfaces even with small plasma current.

We analyzed magnetic flux surfaces with VMEC with free boundary conditions. Figure 3 shows an example of MHD equilibrium with helical fields. Six helical coils are located around the torus except the inner side of torus as plotted in Fig. 1. The plasma parameters are  $R = 0.3$  m,  $a = 0.08$  m,  $B_T = 0.5$  T,  $I_p = 5.5$  kA. We confirmed that the cross section is elongated, whose averaged ellipticity  $\kappa$  is 1.6. We simulated a disruption as by dropping  $\beta$  and the plasma current and confirmed that the plasma position remains almost unchanged in the major radius direction.

Detailed design of a small tokamak device with simple helical windings is under way to demonstrate VDE suppression experimentally.

### References

- 1) H. Ikezi, K. F. Schwarzenegger: *Phys. Fluids* **22**, 2009 (1979).
- 2) Halold P. Furth, Charles W. Hartman: *Phys. Fluids* **11**, 1110 (1968).

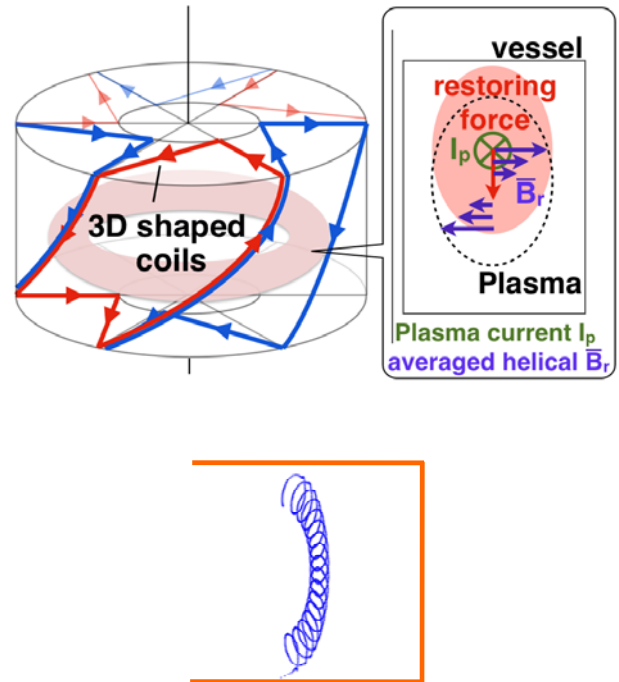


Fig. 2 Poloidal projection plot of the magnetic lines of force with helical fields generated by outer side windings. Straight lines indicate the winding position.

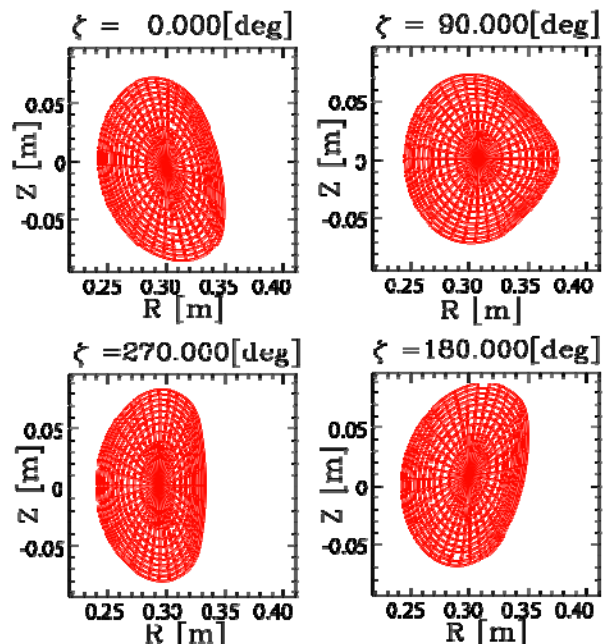


Fig. 3 Example of MHD equilibrium with helical fields computed with VMEC.

## C.5 Test Particle Simulation for High Frequency Glow Discharge in Magnetic Field

Hiroaki TSUTSUI and Shunji TSUJI-IIO

In future fusion devices with superconducting coils, it is required to perform wall conditioning under the influence of strong magnetic fields. High frequency glow discharge cleaning (HF-GDC) is a candidate which has been shown to be available with the presence of magnetic fields, and possibly be applicable to future superconducting devices, such as ITER.

This work reports on numerical studies on the pre-breakdown process of high frequency glow discharge plasma in strong toroidal magnetic field. In this work, the particle-inducing electric fields are assumed to be negligible since the degree of ionization is low at the beginning of the discharge. Thus, the test particle method is used, wherein the particle trajectories are calculated using the guiding center equation and electron-neutral collisions are treated based on Nanbu's method [1].

According to the experiments in EAST, the high frequency glow discharge plasma with toroidal magnetic field becomes more uniform at lower filling pressure [2]. This indicates that the mechanism of plasma uniformity would be clear at the low-pressure limit, wherein the electron mean free path is sufficiently long in comparison with the size of the torus. So, firstly, the collision-less electron trajectories in toroidal magnetic field are calculated to find out the difference between the constant voltage and the pulsed voltage discharges.

For the constant voltage case, the electrons show periodic motion along the magnetic field line. Therefore, their trajectories in phase space are closed as shown in Fig. 1.

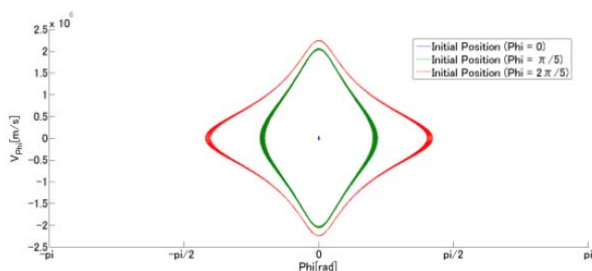


Figure 1 Electron trajectories in phase space (Constant voltage case)

In the pulsed voltage case, all electrons follow the open-straight trajectory during the inactive periods of pulses as shown in Fig. 2. By contrast with the constant voltage case, the energies of some electrons can be high, and the high energy electrons can move freely along the magnetic field line for the pulsed voltage case.

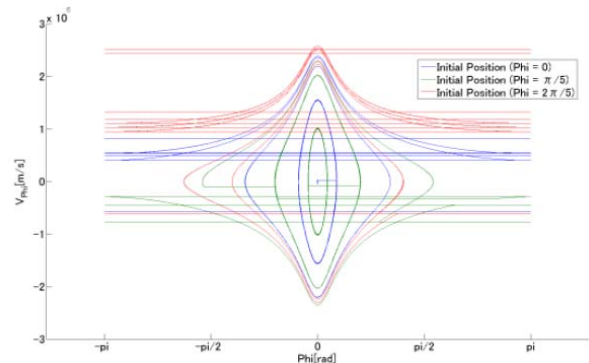


Figure 2 Electron trajectories in phase space (Pulsed voltage case)

Secondly, to understand the impact of the pulsed voltage discharges on ionization process, the test particle simulation has been carried out. For the constant voltage case, it turned out that the multiplication factor became progressively saturated (See Fig. 3). This is because there are only energy losing processes, such as excitation and ionization, in the constant voltage case. In the pulsed voltage case, however, electrons continued to increase during the active periods. As shown in Fig.2, all electrons can move freely during the off periods and therefore some of them can get away from the electrodes. These electrons in turn have larger potential energy at the beginning of the next pulse. Thus, there is a process for obtaining energy in the pulsed discharge case.

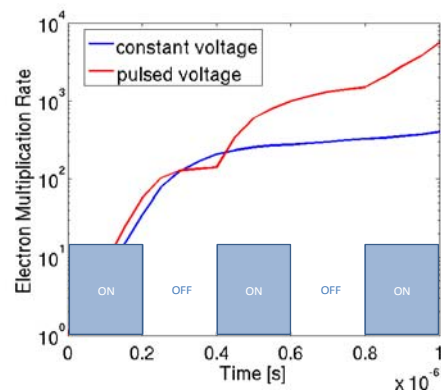


Figure 3 Electron multiplication rate

### References

- [1] K. Nanbu, *Jpn. J. Appl. Phys.*, vol. **33**, pp.4752 - 4753, 1994.
- [2] J. Li et al, Wall conditioning towards the utilization in ITER, *J. Nucl. Mater* (2010)

## C.6 Evaluation of Fukushima Dai-ichi Nuclear Power Plant Accident

Kazumi KITAYAMA, Takao ISHIZUKA, Nobuyoshi TSUZUKI,  
Hiroshige KIKURA and Masanori ARITOMI

A huge earthquake, lately referred as *Higashi-Nihon Dai-Shinsai*, occurred at approximately 100 km east off the coast of Tohoku area at 14:46 on 11<sup>th</sup>, Mar, 2011. The nuclear power plants were damaged especially in Tohoku area by the earthquake and following tsunami, and as a result, severe accidents occurred at 3 units of Fukushima Dai-ichi nuclear power station (1-F) and they released radioactive materials.

The earthquake discharged external power source from 1-F station, and the following tsunami crushed heat sink for removing residual heat. Unit #5-6 of 1-F were not severely troubled because an air-cooled diesel power generator for unit #5-6 could keep working. However, unit #1-#4 lost all electricity and heat sink. Fuel rods of unit #4 were removed from Reactor Pressure Vessel (RPV) for refueling and core cooling for unit #4 was not necessary. Thus, the most important thing for 1-F at that time was coolant injection for cooling the reactor core of unit #1-#3.

Unit #1 of 1-F is a BWR-3 reactor. It has some core cooling facilities, those are Isolation Condenser (IC), High Pressure Coolant Injection system (HPCI), and so on. Tokyo Electric Power Company (TEPCO) decided soon after the earthquake that IC could be applied for regulation of the pressure in RPV, and that HPCI should be applied when the level of coolant water went down. Accordingly, IC was applied four times before tsunami. However, terror for tsunami left IC not working for about 2.5 hours after the first attack of tsunami. Core of unit #1 is supposed to start melting in this non-cooled time, and hydrogen which generated by the reaction between steam and zircalloy in the core exploded at 15:36 12<sup>th</sup>, Mar. The explosion also damaged fire pumps or other apparatus for other units #2-4, and it made harder to inject the coolant water to reactor core of other units.

Unit #2 and #3 (and unit #4 and #5 also) are BWR-4 reactors. A BWR-4 type reactor has Reactor Core Isolation Cooling system (RCIC) instead of IC of BWR-3, and it has HPCI for injection at small or medium sized piping rupture as well as the case of BWR-3. After the earthquake, RCIC was started manually by operators of TEPCO at both units (#2 and #3). RCICs worked to inject cool water to reactor cores for about 20 hours at unit #3, and about 70 hours at unit #2. At unit #3, HPCI automatically followed when RCIC expired and it worked for 14 hours. Thus, RCIC and HPCI worked for 34 hours at unit #3.

However, in the case of unit #2, RCIC worked too long time. Designed working time of RCIC is usually 6-8 hours. 70 hours is extremely over the designed working time, thus, efficiency of RCIC should be decreased before it physically stopped. **Figure 1** shows pressure in RPV of unit #2 after the earthquake. From 20:00 14<sup>th</sup>, Mar., the pressure suddenly rose, thus, RCIC might become non-effective before this. The expired time was assumed around

7:30. Due to no effective core injection and delay of vent from primary containment vessel (PCV), unit #2 might be broken and it released much radioactive materials.

In the case of unit #3, HPCI worked after RCIC expiration. HPCI consumes steam about 10 times larger than that of RCIC. Accordingly, HPCI might spend all steam in short time. Pressure of RPV of unit #3 rapidly fell soon after HPCI started, and it became almost 1 MPa around 19:00, 13<sup>th</sup>, Mar. Thus, HPCI might not fully work after this time. Consequently, coolant water for core of unit #3 might not be injected from this time, and temperature of core of unit #3 might increase due to no injection. In fact, hydrogen explosion occurred at 11:01 on 14<sup>th</sup>, Mar at unit #3.

Severe accidents finally occurred at unit #1-#3 in 1-F mainly due to station black out (SBO) and loss of ultimate heat sink (LUHS). But we think the severe accident could be avoided. PCV vent can reduce not only pressure of PCV but energy in PCV existing as heated steam. Fuel rods were not damaged soon after the SBO and LUHS, thus, radioactive materials doesn't exist in the steam. Hence, early PCV vent before fuel rod damage is very effective to release the residual heat. Naturally, water injection for core cooling with another power and automatic depressurization system (ADS) must be worked with this kind of vent. And rupture disks in ventilation line must be broken for vent, though these rupture disks made difficult to vent in 1-F case in fact. However, this kind of vent doesn't require much reconstruction. The study for utilizing this vent may strengthen the safety of presenting reactors and will help for NPP's re-operation in Japan.

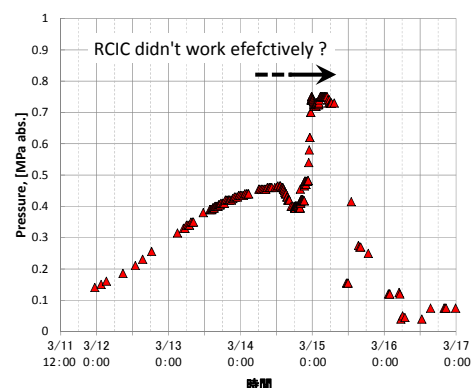


**Figure 1** Pressure in RPV of unit #1, 1-F.

### Reference

- [1] M. Aritomi *et al.*, "What nuclear researchers and engineers can do for public right now," Baifukan (2012-3).

## C.7

## Current Issues and Future Scope of Japan's Nuclear Regulatory Agency

Tetsuo SAWADA

On June 15, 2012, the House of Representatives in Japan passed the Nuclear Regulatory Commission Bill. The Liberal Democratic Party and Komeito reviewed and revised the draft put forth by the ruling Democratic Party of Japan, such that, for instance, the Commission's organizational structure would instead be an "Article 3 Committee," or a government agency with strong independence. Considered an improvement over the original draft, the final bill with all revisions intact appears likely to become law. Beginning with the appointments, the challenges now are how to actually staff and build the organization, and how to enhance genuine competency among the staff. This article discusses the appropriate format of a nuclear regulatory agency with a mission to protect citizens' lives, in order to prevent nuclear disasters like the Fukushima nuclear power plant accident to recur.

### Accidents Always Arise from Unforeseen Circumstances

Just like Three-Mile Island (1979) and Chernobyl (1986), the accident at Fukushima Dai-Ichi Nuclear Power Plant occurred in the wake of unforeseen circumstances, and advanced in the midst of unforeseen circumstances.

In July 1992, a safety relief valve controlling steam within a reactor at Barsebäck Nuclear Power Plant in Sweden opened by mistake. The subsequent blowout of steam caused insulation to strip off, and part of the strainer on the intake side of the emergency reactor-core cooling pump became clogged. Safety inspections at the time set forth neither by the SKI (Swedish Nuclear Power Inspectorate) nor worldwide had foreseen this incident or ensuing development. Here was another "unexpected" incident.

SKI General Director Judith Melin seriously and respectfully acknowledged that safety inspections had not been able to identify the possibility of this incident, and strongly appealed to the Swedish Government for the assessment and evaluation of SKI's inspection capacity by international committee. In order to study the problems concerning SKI safety inspections, the Swedish Government invited opinion leaders within and outside the country to form an assessment committee. The committee noted, "Safety regulatory inspections of SKI are appropriate and high quality. Many procedures, however, are not documented." The deferential acceptance of these points by SKI led to the fresh introduction of a QMS (quality management system).

The respectful reflection on an incident by the head of the regulatory authority, solicitation of global advice with an open stance, and prompt implementation of recommendations made are quite a contrast to Japan. In 2007, the Nuclear and Industrial Safety Agency (NISA) received an IAEA evaluation of just a portion of its

regulatory organization, but the subsequent called-for evaluation across the entire regulatory organization has not been conducted in Japan. The country neglected the "culture of safety" to which Japan itself had contributed ideas to, while doubtful eyes from around the world were cast towards NISA. The consequences were truly dire. The Fukushima Dai-Ichi accident occurred in the midst of this inaction.

The Nuclear Regulatory Agency that was establishment in September 2012 should quickly receive an assessment and evaluation by the IAEA and immediately act on those results. This activity will become the foundation to restoring trust within Japan and internationally.

### 3 Key Points to Regulations

Within a group composed of researchers and experts, I dug deeply for root causes lurking in the backdrop to the Fukushima Dai-Ichi accident, and identified three issues.

- (1) Delay in engagement on new regulatory challenges
- (2) Delay in periodic review of existing safety regulatory policy
- (3) Process lacking where experts and opinion leaders present opposing views for examination.

What should we be doing then? A proposed counter plan is described in the sequence of (1) to (3) next.

(1) Before the Three-Mile Island accident, the U.S. NRC had compiled a general issues program (GIP) that identified problems to be studied in light of safety, and problems where regulatory policy was not established. This program established priority for matters that should be subject to regulation by considering their effectiveness towards safety and requisite costs. The GIP led to formation of a project team composed of NRC technical staff and legal personnel with respect to important safety issues for the study of regulatory policy. The legal personnel participated, since various laws provide the regulatory foundation.

The status of these studies is reported periodically to the U.S. Congress. These efforts are project based, which minimizes the impact of position transfers. Japan should also adopt a format where legal personnel participate from inception like the technical staff. Periodic reporting to the Diet is also necessary in order to ensure these efforts.

(2) The periodic review of existing safety regulations is the key to perennially effective and rational safety regulations. In this context, the NRC implements reviews every five years.

Japan's nuclear energy regulations have accumulated new regulations on top of old regulations remaining in effect, like building a roof atop the roof. Blindly forging ahead with tightened regulations will lead to compliance

fatigue on-site at the power plant, diminish the trust in regulatory policy, and inflict degradation of the culture of safety. Everyone engaged in administering safety regulations for nuclear energy must be seriously aligned here. Periodic reviewing and reassembling into more rational statutes and directives are mandatory, even when existing regulations are scrapped and new regulations are established.

(3) With respect to regulations already in operation, an examination process must be established to address situations when staff members raise opposing views. At the NRC, for instance, anybody with an opposing view must first explain the matter to the head of his or her department in writing, and the relevance of the opposition will be deliberated in a study committee established immediately below the department head. If the holder of the opposing view is not satisfied with the study conclusions, the opposing view may be resubmitted ultimately to an NRC commissioner or the executive director of NRC operations for a re-examination. The results of the examination may be released, if the person with the opposing view so desires.

Safety evaluations for nuclear energy require professional expertise, yet even the professionals do not necessarily agree in their opinions. The regulatory agency, however, must still render an administrative decision. In this type of case, the stability and transparency of regulations improve as discussions and administrative decisions build on each other.

Rooted in an administrative culture spanning more than 1,000 years, the Japanese government system is not well established to capture opposing views. This condition is diametrically opposed to the culture of safety. The regulatory agency must be separated from this administrative culture. In fact, there is a way to accomplish this by creating a strongly independent government agency, called an Article 3 Committee. But the head who governs the regulatory agency with direct influence should not be a minister. Ministers in Japan frequently lack competency, and tend to be replaced frequently over short periods of time as the impact of the political climate takes its toll. Thus, the regulatory agency needs to be isolated and independent of Kasumigaseki (Japanese government departments) and Nagata-cho (Japan's political centre).

The above relates to structural issues of the program itself, but we need people to run the program. No matter how well the program is designed, missteps in its operation will lead to failures. The following recommendation discusses the people factor.

### Competency Available?

The head of a regulatory agency and senior full-time staff assume critical roles in implementing responsive measures, and must thus possess sufficient professionalism to fulfill their duties. Professional expertise is a minimum requirement in handling nuclear safety regulations. Knowledge alone, however, is insufficient. Capabilities are important in terms of human

qualities, such as the ability to guide issues to resolutions and the ability to successfully manage. In short, competency is needed.

Drawing from the practice in Sweden, I believe the following five perspectives should be evaluated with respect to competency.

- (1) Professionalism: Delivering professionalism with respect to nuclear reactor physics, thermohydraulics, safety evaluation methods, etc.
- (2) Personal character: Ethical decision-making, release of creativity, and strong sense of responsibility
- (3) Sociability: Cooperative stance with colleagues, networking ability
- (4) Strategic poise: Capability of judging from overall perspective with long-term outlook
- (5) Operative function: Capability of executing duties by bringing together multiple factors

In fact, these are demanded from all staff members. More senior positions will require a higher level of proficiency. Knowledge associated with nuclear reactor physics, thermohydraulics, and safety evaluation is mandatory. The head of the regulatory agency must have expert knowledge.

The director-general level where heavy responsibilities lie within the regulatory agency will require the following four qualifications.

- (1) Extensive knowledge and experience regarding nuclear reactor safety. Competency as a generalist is required on both the technical side and the organizational communication side.
- (2) Knowledge regarding how the various government institutions function.
- (3) Knowledge of international developments in the field of nuclear reactor safety.
- (4) Excellent track record as manager and leader of scientifically and technologically sophisticated experts.

Of course, a person with all of these abilities is rare. Such director-general candidates, once named to their posts, will be ordered to improve their abilities in guiding issues to resolutions and executing management skills, wherever they lack such abilities.

### Years of Service and Assignment of the Head

The term for the regulatory agency head is also a concern, because a change in top leadership of the agency within short periods is quite harmful and best avoided. The following table shows the terms for the leadership at regulatory agencies in Europe and the U.S.

Table 1. Regulatory Agency Leadership Terms for Major Countries

Country	Top Governance	Term	Number of Members
 U.S. NRC	NRC	5 years	Five appointed to Commission by President, subject to Congressional approval
 France ASN	ASN Board	6 years	Five , of which three are appointed by the President, and one each by the presidents of the National Assembly and Senate.
 Sweden SKI	General Director	7 years, on average	The highest decision-making body is the Council made up of eight , chaired by the SKI General Director.
 Finland STUK	General Director	Lifetime, until 67 years	

The following table provides the years of service of the past agency heads at NISA.

Table 2. Past Heads of NISA and Years of Service

No.	NISA Head	Assumption (Term)
1st	Yoshihiko Sasaki	Jan 2001 (3.5 yr)
2nd	Kazuo Matsunaga	Jun 2004 (1.3 yr)
3rd	Kenkichi Hirose	Sep 2005 (2 yr approx.)
4th	Yasuhisa Komoda	July 200 (2 yr)
5th	Nobuaki Terasaka	July 2009 (2 yr)
6th	Hiroyuki Fukano	Aug 2011-

As the table shows, the NISA Head has alternated approximately every two years, a significant difference in length of service compared to Europe and the U.S.

The NRC Chairman appoints key officials, such as the NRR (Nuclear Reactor Regulation) Director. According to a 2005 survey, the years of service for the four past directors ranged from three to seven years, and all had career experience in the field of nuclear safety for 20 years or more before assuming the position of director. The lesson here is that the leader of Japan's regulatory agency should not be an appointment made simply by the Minister of Environment, or otherwise an appointment exploited for politics.

The senior staff of Japan's nuclear regulatory agency should be appointed with the proper competency and hold the same positions for at least five years. The Executive Director or Council with the authority to appoint the senior staff, therefore, needs to have a term of around five years like the European nations and the U.S. have, and the posts should not be assumed through rotating assignments, based on ceremonial performance evaluations.

### Rely Not on Advisory Boards

What is the appropriate relationship between government nuclear energy agencies and external advisory bodies?

The IAEA asks for the following relationship modes, when a regulatory agency requests opinions from an advisory body or external consultant. These modes are the core to the culture of safety promoted by the IAEA.

"The regulatory agency shall maintain seasoned experts with the ability to evaluate the quality and results of work conducted by external consultants."

"The regulatory agency should not rely on safety evaluation made by external opinion leaders or evaluations made by businesses alone. Thus, the regulatory agency must maintain full-time staff with the capability of examining and evaluating for purposes of regulation, and of evaluating the appropriateness of such evaluations made by external opinion leaders."

"The advice of an advisory body or dedicated technology support group does not release any responsibility associated with decisions made by the regulatory agency."

Up until now, Japan's governmental administration of nuclear regulations has appointed academic experts from university, for example, to the Nuclear Safety Commission and advisory committees. The responses received from these committees supplemented the lack of professionalism at the regulatory agencies, but therein lay a large issue and defect. The resulting structure fostered a monoculture of coziness called the "Nuclear Village."

The bulk of inspection standards employed for safety inspections in Japan has been established by the Nuclear Safety Commission as an advisory body. No other nation has taken this approach, however.

For efficiency and speed in governmental administrative decision-making, for clear identification of responsibilities, and for improved capability of reporting to citizens, the nuclear regulatory agency must increase its numbers of full-time staff who have seasoned professional expertise associated with nuclear energy, and train these

ranks to become professional administrators of nuclear energy.

In Japan, the assignments within the public sector for regulatory administrative personnel have proceeded under a regular succession plan. Such practice is the most harmful for regulation, and exposed its harm in the response by NISA after the Fukushima Dai-Ichi Nuclear Power Plant accident.

At the least, direct hiring into the regulatory agency should take place for candidates desiring regulatory work among those who pass the national civil service examination. That arrangement would provide fundamental retention and improvement to the professionalism associated with regulations. Assignment to the nuclear regulatory agency in opposition to the wishes or intentions of those hired to work at other ministries or agencies must be forbidden.

The immediate securing of specialized knowledge, however, will require the employment of private-sector experts. Such hiring is authorized under the National Civil Service Law, Article 36, where the National Personnel Agency rule establishes an exception to hire private-sector human resources for revitalizing government concerns.

The Law Concerning Exceptions to Hiring and Compensation for Term-Attached Staff for General Positions [trans.] also authorizes hiring for a limited term. Based on these laws, hiring of private-sector human resources would appear to be important. In such cases, however, aggressive appointments of hirees from the private sector to managerial positions based on the principle of competency should take place, with the elimination of any discrimination between those passing the national civil service exam. This step is indispensable in securing human resources and stimulating the organization.

In order to supplement the lack of professional caliber in the past, critical parts of regulations have depended on an advisory program constituted by experts, such as university academics, whose competency was sought. This system aggravated the Fukushima accident, and made the post-accident effects more dire. The advisory mechanism of leaning on each other and structure of coziness are no longer permissible.

### **Disallowing Political Intervention**

Examining the sequence of events after the Fukushima Dai-Ichi accident reveals a frequent change in tone to the announcements made by the Minister in charge. The behavior has been criticized as populism. The nuclear regulatory agency, whether under the government's proposed scheme or the LDP-New Komeito scheme, currently hangs off of the Ministry of Environment. This structure signifies the potential for political intervention or political exploitation, and is quite harmful.

An important subject is selecting the leader for the regulatory agency. Scientists and experts associated with nuclear energy in Japan appear to have no qualifications, since they have managed in practice to neglect any substantive regulations in relation to severe accidents over

the past 30 years. Yet the experts outside the domain of nuclear energy lack the most critically needed competency in terms of expert knowledge of nuclear energy.

Japan stands today as a developing nation in terms of nuclear regulatory affairs. What shall we do? Ideally, among the five advanced nuclear regulatory nations noted above, the best solution would be to select and invite somebody from Sweden or Finland, since these nations have renounced nuclear arms. Moreover, they have taken their own innovative and sincere steps across regulatory administration in general, including severe accidents, since the Three-Mile Island accident. It was further intensified after the Chernobyl. The U.S. would be the next best option, but a difficult one politically and legally. In any event, the people who learn deeply from the insights of these countries should take those jobs at the top and senior levels.

At the same time, many staff, not just the senior staff, should engage actively in exchanges with the regulatory agencies in Europe and the U.S., argue the different views based on the experiences of different nations, and nurture a culture of safety for Japan.

The establishment of a quality management system (QMS) is key for the nuclear regulatory agency to gain tangible results in regulatory administration. The QMS describes the specific implementation of the agency's mission, details the activities for accomplishing the mission, and establishes the policy for securing the training of human resources for the mission. The status of implementation calls for self-evaluation and third-party evaluation, and necessary corrections are made. The IAEA guidelines related to regulatory organizations also call for the regulatory agency to build a QMS.

When NISA received IAEA inspections in 2007, the continuation of QMS structuring activity was recommended. The structuring and implementation of the QMS by the nuclear regulatory agency is an absolute requirement for shoring up Japan's nuclear energy safety regulations to an international level. Naturally, the actual QMS operations must not remain confined to documentation work, but have substance. Here again, the pedigree of the leader is in question, as to whether implementation with actual effectiveness is possible. Otherwise, no nation—Japan included—has the qualifications to handle nuclear energy.

Table 3. Comparison of Government Proposal vs. LDP-New Komeito Proposal

	<b>Govt. Proposal</b>	<b>LDP-New Komeito Proposal</b>
Authority under accident	Nuclear Energy Disaster Response HQ (Headed by PM)	Nuclear Regulatory Commission (55 commissioners)
Positioning of regulatory agency	External bureau of Ministry of the Environment (scale of 500 people). Parallel installment of Nuclear Safety Commission (5 commissioners)	Secretariat of NRC (scale of 500 people)
Dependence	Regulatory Agency entrusted by MOE in establishing regulatory legislation. Minister of the Environment appoints Agency Head.	NRC established as Article 3 Committee under MOE jurisdiction. Regulatory legislation drafted independently by NRC, and submitted by Minister of the Environment. Commission members to be approved by the Diet.

Reference: Tetsuo Sawada, *The Truth about Fukushima Nuclear Power Plant that Nobody Wrote About*, Chapter 5: Four Keys to Recovery of Nuclear Power Plants [title trans.], (2012, WAC).

### III. Co-operative Researches

#### III.1 Co-operative Researches within Tokyo Institute of Technology

Under the generic proposition: "The Release and Utilization of Energies existing in Atoms, Molecules and Nuclei" which has been hoisted since the reorganization of RLNR, we advertise for collaborations with any department and laboratory within Tokyo Institute of Technology in order to develop researches for the improvement of energy utilization with safety, mass transmutation by nuclear reactions with high efficiency, and construction of energy system concept with high societal acceptability. The RLNR will promote these collaborations by offering the organizations, facilities, equipments and space as the research base for research project teams and research groups crossing over within Tokyo Tech. We are going to adopt unique and innovative themes which make maximum use of the activities of this research laboratory.

- Heavy-Ion Inertial Fusion and High Energy-Density Physics Driven by Heavy-Ion Beams  
Interdisciplinary Graduate School of Science and Engineering
- Building study of active carbon recycling energy system  
Tokyo Tech AES Center

#### III.2 Co-operative Researches with Outside of Tokyo Institute of Technology

- Fundamental Study of Thermo-Hydraulic Instability on Reduced-Moderation Natural Circulation BWR Concept (Clarification of Condensation Phenomena under Non-Condensable Gas)  
Japan Atomic Power Co.
- Study on Technical Standards for Safety Transportation of Decommissioned Wastes of Nuclear Power Plant  
Nuclear Fuel Transport Co., Ltd.
- Development of Measurement Instrument of Void Fraction in Steam Generator  
IHI Corporation
- Study on Innovative Nuclear Reactor Systems  
Hitachi Research Laboratory,  
Hitachi, Ltd.
- Fundamental Study on Transport and Storage Dual Purpose Metal Cask Safety  
OCL CORPORATION
- Fundamental Study on Advanced Turbid Water Treatment  
NPO. Saiseisya
- Two-Phase Flow Dynamics for Future Light Water Reactor Development  
Korea Atomic Energy Research Institute, Korea
- Experimental and Analytical Studies on Multi-Dimensional Two-Phase Flow  
PSF Zittau, Germany
- Advanced Fluid Dynamics and Developed of Measurement Technique  
Chulalongkorn University, Thailand
- Thermal Hydraulics for Advanced Water Cooling Reactors  
Bhabha Atomic Research Center, India
- Future Light Water Reactor Development  
Chulalongkorn University, Thailand
- Research and Development of High Performance Ceramics  
Chiba Institute of Technology,  
Tokai University
- Study on Novel Process of SiC/SiC Composite by Electrophoretic Deposition Method  
Japan Aerospace Exploration Agency (JAXA)

- Study on the Improvement of Irradiation Resistance of Ceramics by Their Orientation Control  
National Institute for Materials Science (NIMS)
- Evaluation of Sinterability and Properties of SiC Ceramics using Al<sub>4</sub>SiC<sub>4</sub> as Sintering Additives  
National Institute for Materials Science (NIMS)
- Studies on Separation of Uranium Species Using Polyvinylpyrrolidone  
Japan Atomic Energy Agency and Tokai University
- A Study of Extraction Behavior of ReO<sub>4</sub><sup>-</sup> by Using Monoamide Compounds  
Japan Atomic Energy Agency
- A Study on Partitioning of Lanthanoid and Actinoid Species  
Japan Atomic Energy Agency
- A Study on Separation of Uranyl Species Using Alginic Acid  
Prof. R.M. Hassan, Assiut University, Egypt
- A Study on Structures of Lanthanoid(III) Complexes with Monoamide Compounds in Solutions Using NMR  
Professor Z. Szabo, Royal Institute of Technology, Sweden
- Studies on Structures of Uranyl Complexes in Ionic Liquids  
Dr. C. Hennig, Forschungszentrum Rossendorf, Germany
- Neutron Capture Cross Section Measurement n\_TOF Collaboration
- Development of a new gamma-ray detector for keV-neutron capture experiment  
Osaka University,  
Japan Atomic Energy Agency
- Study on keV-Neutron Capture Cross Sections of Fe isotopes  
Dong-A University,  
Kyungpook National University
- Study on Glass Vitrification Process  
Japan Nuclear Fuel Limited
- Study on Extraction Chromatographic Process using Multidentate Encapsulating Ligands for Recovery of Minor Actinides  
Japan Science and Technology Agency
- Research of Separation/Removal Techniques of Radioactive Cesium from Agricultural Soil using Hydrothermal and Blasting Reaction  
Tokyo Institute of Technology
- Development of Functional Sheet for the Removal of Platinum Group Metals from High-level Radioactive Waste  
Nitto Denko Corporation
- Basic Study on Advanced ORIENT Cycle  
Japan Atomic Energy Agency
- Surface Modification of Silicon Wafer by Low-Pressure High-Frequency Plasma Chemical Vapor Deposition Method  
University of Miyazaki,  
Minami-Kyushu Junior College,  
King Mongkut's University of Technology Thonburi,  
Kagawa University,  
Hiroshima National College of Maritime Technology,  
ADTEC Plasma Technology Co. Ltd.,  
Miyazaki Technical High School
- Cleaning Process for Semiconductor Equipment Process on Atmospheric-Pressure Non-Equilibrium DC Pulse Plasma Jet  
University of Miyazaki,  
King Mongkut's University of Technology Thonburi,  
Kagawa University,  
Miyakonojo National College of Technology
- Diagnostics of Vibration and Rotational Temperatures in Atmospheric-Pressure Non-Equilibrium Discharge Electrodeless-Type Microwave Plasma Jet  
University of Miyazaki,  
King Mongkut's University of Technology Thonburi,  
Osaka University,  
Kagawa University
- Radical Simulation in Atmospheric-pressure Non-equilibrium DC Pulse Plasma of Euler's Method  
University of Miyazaki,  
Kagawa University,  
Hiroshima National College of Maritime Technology,  
Osaka University
- Observation of OH Radicals on Imaging Spectroscopy Measurement in Atmospheric-Pressure DC Pulse Discharge Plasma Jet  
University of Miyazaki,  
Osaka University,  
Tokyo Metropolitan University
- Basic Characteristics for PEN Film Surface Modification Using Atmospheric-Pressure Nonequilibrium Microwave Plasma Jet  
University of Miyazaki,  
ADTEC Plasma Technology Co. Ltd.,  
JEOL Ltd. Japan,  
Kagawa University

- Optical Emission Spectroscopy Measurement of High-Frequency Low-Pressure at Plasma-Enhanced Chemical Vapor Deposition  
University of Miyazaki,  
Osaka University
- Chemical heat pump for waste heat recovery from iron making process  
Environmentally Friendly Steel Process Technology,  
NEDO commissioned project
- Study on low-carbon and carbon recycling iron-making system using ACRES  
Sumitomo Metal Ind
- Study on Chemical Heat Storage System  
Tokyo Gas
- *In situ* high-resolution photoemission spectroscopic study of 1D peanut-shaped C<sub>60</sub> polymers  
UVSOR Facility,  
Institute for Molecular Science Department of Materials Science, Nagoya University
- DFT study of low-dimensional peanut-shaped C<sub>60</sub> polymers  
Yokohama National University
- Photodynamic properties of nanomaterials  
Department of Applied Physics, Hokkaido University
- Riemannian geometrical effects on physical properties of 1D uneven peanut-shaped C<sub>60</sub> polymer  
Department of Environmental Sciences and Interdisciplinary Graduate School of Medicine and Engineering, University of Yamanashi Department of Physics,  
Nara Women's University
- Fabrication of AZO transparent electrodes for Organic Photovoltaic cells  
Department of Electronic Engineering and Applied Physics, Osaka City University
- Application of 1D uneven peanut-shaped C<sub>60</sub> polymer to a detector for THz wave spectroscopy  
Department of Electronic Engineering and Applied Physics, Osaka City University
- High-resolution TEM observation of 1D uneven peanut-shaped C<sub>60</sub> polymer  
UHP-TEM center, Osaka University  
Rensselaer Nanotechnology Center, Rensselaer Polytechnic Institute (USA)
- A Study of Surface and Interfaces of Organic Photovoltaic Cells  
J-Power Co. Ltd
- Elucidation of DNA Damage Recognition/Repair Mechanism and Its Application to Cancer Therapy  
Invitation Grant for Asian Researchers  
Tokyo Biochemical Research Foundation
- Study on Electron density fluctuations by Microwave Imaging Reflectometry  
National Institute for Fusion Science
- Development of ECE imaging system by the use of 1-D horn antenna array  
National Institute for Fusion Science
- Experimental investigation of positional stabilization of torus plasma with helical coils  
National Institute for Fusion Science
- Development of Fiber-Optic Diagnostic on Vacuum Vessel Current of QUEST  
Research Institute for Applied Mechanics, Kyushu University
- Characterization of structure and physico-chemical properties of molten rare-earth metal halides  
Japan Atomic Energy Agency
- Innovative characterization of materials under severe condition (Conditions Extrêmes et Matériaux)  
Haute Température et Irradiation, Centre National de la Recherche Scientifique
- Structure and physico-chemical properties of thorium fluoride mixtures  
Institute of Multidisciplinary Research for Advanced Materials,  
Tohoku University (Network Joint Research Center for Materials and Devices)
- Pyro-reprocessing of rare earth elements from Ni-MH battery  
The Shinsei Foundation
- XAFS analysis of actinide chlorides and chlorides of fission products  
Kyoto University Research Reactor Institute
- Characteristics of MHD equilibrium, stability and transport in high-beta plasmas  
National Institute for Fusion Science
- Gyrokinetic simulation study on turbulence in finite beta plasmas  
National Institute for Fusion Science
- Study of Decision Mechanism of Plasma Current Decay Time in Disruption  
Japan Atomic Energy Agency

### **III.3 Themes Supported by Grants-in-Aid for Scientific Research of the Ministry of Education, Culture, Sports, Science and Technology**

- Recovery of Neutron-Induced Defects and Release of Helium Gas using Nano-Dilatometry Equipped with Mass Spectroscopy
- Systematic Study on Neutron Capture Reaction Cross Sections for the Technological Development of Nuclear Transmutation of Long-Lived Nuclear Waste.
- Development of Liquid-liquid Counter-current Centrifugal Extractor for Nuclide Separation
- Grant-in-Aid No.21246146
- Angiocinematography Using Particle-Induced Dual-Wavelength Pulsed-X-rays for Minimization of Dosages of Contrast-Medium and Radiation
- Development of a Variable-Energy, Variable-Intensity, On/Off-switchable Gamma-Ray Needle-Source for Brachytherapy
- High-Efficient High-Temperature Process by Hybrid Method using Chemical Heat Storage
- Design of future energy system by using practical energy technologies
- Development of new quantum electronic science in Riemannian geometric space
- Strategic Creation of New Radiosensitizer based on the Molecular Mechanisms of DNA Double-Strand Breaks Repair
- Development of A Novel Nanofluidic-based Separation System for Rare-Earth Elements.

#### IV. List of Publications

Yasushi Muto, Shintaro Ishiyama, Yasuyoshi Kato, Takao Ishiduka and Masanori Aritomi: Application of Supercritical CO<sub>2</sub> Gas Turbine for the Fossil Fired Thermal Plant; *Journal of Energy and Power Engineering*, **4**, No. 1, pp. 6-10 (2010).

Noriyuki Watanabe, Se-Young Chun, Masanori Aritomi and Hiroshige Kikura: Experimental Study on Heat Transfer Characteristics of Vertical 5\*5 Heated Rod Bundles around Critical Pressure with R-134a; *Journal of Nuclear Science and Technology*, **48**, No. 1, pp. 135-144 (2011).

Masanori Aritomi, Takao Ishiduka, Yasushi Muto. and Nobuyoshi Tsuzuki: Performance Test Results of a Supercritical CO<sub>2</sub> Compressor Used in a New Gas Turbine Generating System; *Journal of Power and Energy Systems*, **5**, No. 1, pp.45-59 (2011).

Atushi Ui, Shigeo Ebata, Fumio Kasahara, Tsunakiyo Iribe, Hiroshige Kikura and Masanori Aritomi: Study on Solid-Liquid Two-Phase Flow on PWR Sump Clogging Issue; *Journal of Nuclear Science and Technology*, **47**, No. 9, pp. 820-828 (2010).

Masanori Aritomi, Takao Ishiduka, Yasushi Muto and Nobuyuki Tsuzuki: Performance Test Results of the Supercritical CO<sub>2</sub> Compressor for a New Gas Turbine Generating System; *The 18th International Conference on Nuclear Engineering (ICONE18)*, ICONE18-29371, Xi'an, China (2010).

Masanori Aritomi: Asbestos harmless mobile Treatment Systems on Pulling Down Sites; *Proceedings of 24<sup>th</sup> National Congress for Environmental Studies*, Tokyo, Japan, pp.129-134, (2010-4-15~16), in Japanese.

Motoaki Utamura, Masanori Aritomi, Kei Yamamoto and Hiroshi Hasuike: Preliminary Test result of a Closed Cycle Gas Turbine with Supercritical CO<sub>2</sub> as Working Fluid; *The 15<sup>th</sup> National Symposium on Power and Energy System, (SPES 2010)*, Tokyo, Japan, CD-ROM, pp. 197-198, (2010-6-21~22), in Japanese.

Masanori Aritomi, Toshinori Takata, and Takayuki Morii: Effective technology of Preventive Measures Against Piping Damage on Stream Lines in Nuclear Power Plants; *The 15<sup>th</sup> National Symposium Power and Energy Systems (SPES 2010)*, Tokyo, Japan, pp.83-86, (2010-6-21~22), in Japanese.

Masanori Aritomi, Junko Takanashi, Shigeki Hosobuchi, Noriko Hasegawa: Development of Water System for Cutting Asphalt Road (III); *Mechanical Engineering Congress, 2010 Japan (MECJ-10)*, pp. 149-150, Nagoya Institute of Technology, Japan, (2010-9-5~8).

Masanori Aritomi, Junko Takanashi, Shigeki Hosobuchi and Noriko Hasegawa: Development of Simplified Treatment of System of Turbid Water in Disaster Area; *Mechanical Engineering Congress, 2010 Japan (MECJ-10)*, pp. 147-148, Nagoya Institute of Technology, Japan, (2010-9-5~8).

T. Yano, J. Yamane, K. Yoshida, S. Miwa and M. Ohsaka: Low Temperature Liquid-Phase-Assisted Sintering of Si<sub>3</sub>N<sub>4</sub> Ceramics as an Inert Matrix for Confinement of Minor Actinides; *ACTINIDES 2009, IOP Conf. Series: Mater. Sci. Engineer*, **9**, 012024 (2010). Doi: 10.1088/1757-899x/9/1/012024.

H. Yokota, M. Yoshida, H. Ishibashi, T. Yano, H. Yamamoto and S. Kikkawa: Concentration Effect of Cerium in (Y<sub>0.9-x</sub>Gd<sub>0.1</sub>Ce<sub>x</sub>)<sub>2</sub>SiO<sub>5</sub> Blue Phosphor; *J. Alloys and Compounds*, **495**, 162-166 (2010). Doi: 10.1016/j.alocom2010.01.112.

S. Miwa, M. Osaka, T. Ukai and T. Yano: Densification of Inert Matrix Fuels Using Naturally-Occurring Material as a Sintering Additive; *Proc. MRS* (printed).

S. Miwa, M. Osaka, Y. Akutsu, T. Yano, K. Kurosaki, S. Yamanaka, S. Takano and Y. Yamane: Inert Matrix Fuel Concept for the Rapid Incineration of Minor Actinides Harmonious with a Fast Reactor Cycle System; *Proc. International Conference on Fast Reactors and Related Fuel Cycles*, (printed).

W. Khongwong, K. Yoshida and T. Yano: Simple Approach to Fabricate SiC-SiO<sub>2</sub> Composite Nanowires and Their Oxidation Resistance; *Mater. Sci. Engineering B*, **173**, 117-121 (2010).

W. Khongwong, K. Yoshida and T. Yano: Fabrication and Properties of Core/Shell Type SiC-SiO<sub>2</sub> Nanowires through Low-Cost Production; *Nanostructured Materials and Nanotechnology IV*, American Ceramic Society, 51-62 (2010).

T. Yano: Application of Ceramics for Components of Fission and Fusion Nuclear Reactors; Present Status and Challenge ; *Text of the 42<sup>nd</sup> Seminar on Engineering Ceramics*, pp.37-46 (2010).

K. Yoshida: Development of Silicon Carbide Fiber-Reinforced Silicon Carbide Matrix Composites with High Performance Based on Interfacial and Microstructure Control; *J. Ceram. Soc. Japan*, **118** [2], 82-90 (2010).

K. Yoshida: Improvement of Sinterability and Mechanical Properties of β-Tricalcium Phosphate; *J. Soc. Inorg. Mater., Japan (Muki-Materiaru)*, **17** [346], 188-195 (2010).

K. Yoshida, H. Hyuga, N. Kondo and H. Kita: Synthesis of Precursor for Fibrous Mullite Powder by Alkoxide

- Hydrolysis Method; *Mater. Sci. Eng. B*, **173**, 66-71 (2010).
- N. Matsumoto, K. Yoshida, K. Hashimoto and Y. Toda: Dissolution Mechanisms of  $\beta$ -Tricalcium Phosphate Doped with Monovalent Metal Ions; *J. Ceram. Soc. Japan*, **118** [6], 451-457 (2010).
- N. Matsumoto, A. Yokokawa, K. Ohashi, K. Yoshida, K. Hashimoto and Y. Toda: Mechanical Properties of  $\square$ -Tricalcium Phosphate Ceramics Doped with Vanadate Ions; *Phosphorous Research Bulletin*, **24**, 73-78 (2010).
- N. Matsumoto, K. Yoshida, K. Hashimoto and Y. Toda: Preparation of Beta-Tricalcium Phosphate Powder Substituted with Na/Mg Ions by Polymerized Complex Method; *J. Am. Ceram. Soc.*, **93** [11], 3663-3670 (2010).
- K. Yoshida, A. Kawasumi, K. Hashimoto, Y. Toda, M. Imai and T. Yano: Fabrication of Three-Dimensional  $\text{Al}_2\text{O}_3/\text{YAG}$  Composites Using Porous  $\text{Al}_2\text{O}_3$  Ceramics Prepared by  $\alpha$ - $\text{Al}_2\text{O}_3$  Powder and Their Mechanical Properties; *High Temperature Ceramic Materials and Composites (Proc. 7<sup>th</sup> International Conference on High Temperature Ceramic Matrix Composites (HT-CMC7))*, pp. 492-497 (2010).
- K. Yoshida, A. Kawasumi, K. Hashimoto, Y. Toda, M. Imai and T. Yano: Fabrication and Mechanical Properties of Three-Dimensional  $\text{Al}_2\text{O}_3/\text{YAG}$  Composite Using Hollow Spherical  $\text{Al}_2\text{O}_3$  Powder Prepared by Spray Pyrolysis Method; *High Temperature Ceramic Materials and Composites (Proc. 7<sup>th</sup> International Conference on High Temperature Ceramic Matrix Composites (HT-CMC7))*, pp. 485-491 (2010).
- W. Khongwong, K. Yoshida and T. Yano: Fabrication of Core-Shell Type SiC/SiO<sub>2</sub> Nanowires through Low-Cost Production Technique; *Abst. The 34<sup>th</sup> International Conference and Exposition on Advanced Ceramics and Composites*, Daytona Beach, Florida, USA, S7-P135 (2010) p.100.
- K. Yoshida, C. C. See and T. Yano: Fabrication of Porous Silicon Carbide using in-situ Crystal Growth; *Abst. The 34<sup>th</sup> International Conference and Exposition on Advanced Ceramics and Composites*, Daytona Beach, Florida, USA, S9-P058 (2010) p.58.
- S. C. Chet, K. Yoshida, M. Imai and T. Yano: Fabrication and Properties of Porous Silicon Carbide Ceramics based on Control of Grain Growth; *Abst. Ann. Meeting of Ceram. Soc. Jpn.*, 2010, 3C04, pp.273. (2010).
- S. Miwa, M. Osaka, T. Usuki and T. Yano: Densification of Nuclear Fuel Pellets Using Asbestos Waste as a Sintering Additives; *Abst. Ann. Meeting of Ceram. Soc. Jpn.*, 2010, 3I24, pp.313. (2010).
- M. Osaka, S. Miwa, K. Kurosaki, S. Yamanaka, M. Uno, Y. Yamane, H. Mimura and T. Yano: Fundamental Study of Inert Matrix Fuels Adaptable to a Fast Reactor Cycle System, (1) Concept"; *Abst. 2010 Ann. Meetings of the Atom. Energy Soc. Jpn.*, L28, pp.560 (2010).
- T. Yano, K. Yoshida, M. Imai, S. Miwa and M. Osaka: Fundamental Study of Inert Matrix Fuels Adaptable to a Fast Reactor Cycle System, (2) Si<sub>3</sub>N<sub>4</sub> Based Fuels; *Abst. 2010 Ann. Meeting of the Atom. Energy Soc. Jpn.*, L29, pp.561 (2010).
- T. Usuki, K. Yoshida, M. Imai, T. Yano, S. Miwa and M. Osaka: Sintering and Characterization of Silicon Nitride Ceramics as Inert Matrix with Magnesium Silicates; *Abst. 2010 Ann. Meeting of the Atom. Energy Soc. Jpn.*, L31, pp.562 (2010).
- K. Yoshida, Y. Sekimoto, K. Katayama, W. Thanakorn, M. Imai and T. Yano: Change in Thermal Conductivity of Silicon Nitride Ceramics by Thermal Treatment; *Abst. 124 Committee of JSPS 134 Meeting*, pp.83-84. (2010).
- T. Yano, K. Yoshida, W. Khongwong: SiC/SiO<sub>2</sub> Core-Shell Nanowires Synthesized by Thermal Evaporation Method Using Raw Powders; *Abst. 3<sup>rd</sup> International Symposium on SiAlONs and Non-Oxides (ISSNOX3)*, pp.29. (2010).
- K. Yoshida, H. Katsumata, M. Imai and T. Yano: The Effect of BN Particle Size on Mechanical Properties and Machinability of SiC/BN Composites; *Fourth International Conference on Science and Technology of Advanced Ceramics (STAC-4)*, PP-69. (2010).
- K. Yoshida and T. Yano: Contribution of Ceramic Materials for Electric Power Generation System; *Fourth International Conference on Science and Technology of Advanced Ceramics (STAC-4)*, 2a-B01. (2010).
- K. Yoshida, A. Kawasumi, K. Hashimoto, Y. Toda, M. Imai and T. Yano: Fabrication of Three-Dimensional  $\text{Al}_2\text{O}_3/\text{YAG}$  Composites Using Porous  $\text{Al}_2\text{O}_3$  Ceramics Prepared by  $\alpha$ - $\text{Al}_2\text{O}_3$  Powder and Their Mechanical Properties; *7<sup>th</sup> International Conference on High Temperature Ceramic Matrix Composites (HT-CMC7)*, HT-CMC7-PS-264, pp.114-115(2010).
- K. Yoshida, A. Kawasumi, K. Hashimoto, Y. Toda, M. Imai and T. Yano: Fabrication and Mechanical Properties of Three-Dimensional  $\text{Al}_2\text{O}_3/\text{YAG}$  Composite Using Hollow Spherical  $\text{Al}_2\text{O}_3$  Powder prepared by Spray Pyrolysis Method; *7<sup>th</sup> International Conference on High Temperature Ceramic Matrix Composites (HT-CMC7)*, HT-CMC7-40b-263, p.114 (2010).
- M. Osaka, S. Miwa, K. Tanaka, K. Ikeda, H. Mimura, T. Usuki and T. Yano: Reformation of Hazardous Wastes into Useful Supporting Materials for Fast Reactor Fuels; *The Third International Symposium on Innovative Nuclear Energy Systems-Innovative Nuclear Technologies for Low-Carbon Society-(INES-3)*, 1B-23, pp.58. (2010).

- S. Miwa, M. Osaka, T. Usuki and T. Yano: Densification of Inert Fuels Using the Waste of Asbestos as a Sintering Additive; *The Third International Symposium on Innovative Nuclear Energy Systems–Innovative Nuclear Technologies for Low-Carbon Society– (INES-3)*, 1B-22, pp.57. (2010).
- Y. Futamura, M. Imai, K. Yoshida and T. Yano: Recovery Behavior of Neutron-Irradiation-Induced Damage of AlN by Thermal Annealing; *The Third International Symposium on Innovative Nuclear Energy Systems–Innovative Nuclear Technologies for Low-Carbon Society– (INES-3)*, P-130, pp.154. (2010).
- T. Usuki, K. Yoshida, M. Imai, T. Yano, S. Miwa, M. Osaka: Fabrication and Characterization of Silicon Nitride Based Inert Matrix Fuels; *The Third International Symposium on Innovative Nuclear Energy Systems–Innovative Nuclear Technologies for Low-Carbon Society – (INES-3)*, P-134, pp.158. (2010).
- M. Akiyoshi, H. Tsuchida, T. Yoshiie, X. Qiu, K. Sato and T. Yano: Irradiation Damage in Ceramics Induced by 30MeV Electron Linac; *The Third International Symposium on Innovative Nuclear Energy Systems–Innovative Nuclear Technologies for Low-Carbon Society – (INES-3)*, 1B-25, pp.60. (2010).
- T. Yano and K. Yoshida: Fabrication of SiC Continuous Fiber-Reinforced SiC Composite Using Electrophoretic Deposition and Hot-Pressing; *3<sup>rd</sup> International Congress on Ceramics (ICC3)*, S10-018. (2010).
- K. Yoshida, C.-C. See, M. Imai and T. Yano: Fabrication of Porous Silicon Carbide Ceramics Based on In-Situ Grain Growth; *3<sup>rd</sup> International Congress on Ceramics (ICC3)*, S12-028. (2010).
- T. Yano, Y. Horie, M. Imai and K. Yoshida: Sintering of Silicon Carbide Ceramics with Co-addition of Gadolinium Oxide and Silica and Their Mechanical Properties; *3<sup>rd</sup> International Congress on Ceramics (ICC3)*, S14-P001. (2010).
- K. Yoshida, Y. Sekimoto, K. Katayama, T. Wasanapiarnpong, M. Imai and T. Yano: The Effect of Heat-Treatment on Thermal Conductivity of Silicon Nitride Ceramics; *3<sup>rd</sup> International Congress on Ceramics (ICC3)*, S14-P016. (2010).
- K. Yoshida: Development of Silicon Carbide-Based Materials for Environmental and Energy Application; *The 33<sup>rd</sup> Nano Ceramics Center Seminar (NIMS)*, (2010).
- K. Yoshida: Development of SiC Fiber-reinforced SiC Composites with High Performance Based on Interfacial and Microstructure Control; *Ann. Meeting of The Ceram. Soc. Jpn, 2010*, 2C31A, p.107 (2010).
- K. Ohashi, S. Mitsumori, R. Miyamoto, K. Yoshida, K. Hashimoto and Y. Toda: Cellular Reactivity of Osteoclast-Like Cells on Na<sup>+</sup> Ions Doped  $\beta$ -Tricalcium Phosphate Ceramics; *Ann. Meeting of The Ceram. Soc. Jpn, 2010*, 1E28, p.38 (2010).
- N. Matsumoto, K. Sato, K. Yoshida, K. Hashimoto and Y. Toda: Substitution Model of Silicate Ions in  $\beta$ -Tricalcium Phosphate Structure ; *Ann. Meeting of The Ceram. Soc. Jpn, 2010*, 2E02, p.114 (2010).
- E. Takahashi, N. Matsumoto, K. Yoshida, K. Hashimoto, Y. Toda, S. Udagawa and T. Kanazawa: Fabrication of Sintered Body Consisted of  $\beta$ -Tricalcium Phosphates Doped with Divalent and Trivalent Metal Ions; *120<sup>th</sup> Meeting of the Soc. Inorg. Mater., Japan*, (11), pp.22-23 (2010).
- A. Yokoya, N. Matsumoto, K. Yoshida, K. Hashimoto and Y. Toda, S. Udagawa and T. Kanazawa: Substituted Mechanism of Anion into Crystal Structure of  $\beta$ -Type Tricalcium Phosphate; *120<sup>th</sup> Meeting of the Soc. Inorg. Mater., Japan*, (33), pp.66-67(2010).
- K. Ohashi, R. Miyamoto, H. Shibata, K. Yoshida, K. Hashimoto and T. Kanazawa: Cellular Evaluation of MC3T3-E1 Cells on VO<sub>4</sub><sup>3-</sup> Ions Doped  $\beta$ -Tricalcium Phosphate; *20<sup>th</sup> Meeting of Japanese Assoc. Inorg. Phosphorous Chem.*, P15-Y, pp.78-79(2010).
- A. Ozawa, R. Miyamoto, H. Shibata, K. Yoshida, K. Hashimoto and T. Kanazawa: Inhibitor Test of Osteoclast Cells on Manganese(II) Ion-Doped  $\beta$ -Tricalcium Phosphate Ceramics; *20<sup>th</sup> Meeting of Japanese Assoc. Inorg. Phosphorous Chem.*, P17-Y, pp.82-83 (2010).
- R. Miyamoto, H. Shibata, K. Yoshida and K. Hashimoto: Acceleration of Cell Behavior onto Sodium Ions Doped  $\beta$ -Tricalcium Phosphate; *20<sup>th</sup> Meeting of Japanese Assoc. Inorg. Phosphorous Chem.*, P32-Y, pp.112-113 (2010).
- K. Yoshida, C.-C. See, M. Imai and T. Yano: Fabrication and Evaluation of Porous SiC Ceramics Based on In-Situ Grain Growth; *The 1<sup>st</sup> Ceram. Eng. Workshop*, p.9 (2010).
- R. Miyamoto, K. Ohashi, H. Shibata, K. Yoshida and K. Hashimoto: ST2/C7 Cells Differentiation Ability on  $\beta$ -Tricalcium Phosphate Doped with Various Amount of Sodium Ions; *The 14<sup>th</sup> Symp. Ceram. in Medicine, Biology and Bioceramics*, 12, p.12 (2010).
- S. Hanazawa, A. Ozawa, R. Miyamoto, H. Shibata, K. Yoshida and K. Hashimoto: Evaluation of Osteoclast-Like Cells on Potassium Ion-Doped  $\beta$ -Tricalcium Phosphate Ceramics; *The 14<sup>th</sup> Symp. Ceram. in Medicine, Biology and Bioceramics*, 13, p.13 (2010).

- R. Miyamoto, H. Shibata, K. Yoshida and K. Hashimoto: Relationship between Bone Absorption and Protein Adsorption on  $\beta$ -Tricalcium Phosphate Doped with Sodium Ions; *3<sup>rd</sup> International Congress on Ceramics (ICC3)*, S13-P052 (2010).
- A. Ozawa, R. Miyamoto, H. Shibata, K. Yoshida and K. Hashimoto: Cell Test on  $\beta$ -Tricalcium Phosphate Doped with Manganese (II) Ions; *3<sup>rd</sup> International Congress on Ceramics (ICC3)*, S13-P053 (2010).
- H. Sagara, T. Yamamoto, S. Maeda, S. Koyama and M. Saito: Numerical Analysis of Am Sample Irradiation in Experimental Fast Reactor Joyo; *IOP Conf. Ser.: Mater. Sci. Eng.*, vol. **9**, no.1, 012006, p. 1-8 (2010).
- Go Chiba, Keisuke Okumura, Akito Oizumi and Masaki SAITO: Sensitivity Analysis of Fission Product Concentrations for Light Water Reactor Burned Fuel; *J. Nucl. Sci. Technol.*, Vol. **47**, No. 7, p. 652-660 (2010).
- S. Koyama, M. Osaka, M. Itoh, H. Sagara, M. Saito: Protected Plutonium Production by Transmutation of Minor Actinides for Peace and Sustainable Prosperity - Irradiation Tests of Np and Np-U Samples in the Experimental Fast Reactor JOYO (JAEA) and the Advanced Test Reactor at INL; *J. Nucl. Sci. Technol.*, **47** [8], 1-10 (2010).
- Y. Meiliza, M. Saito and H. Sagara: Denaturing Generated Pu in Fast Breeder Reactor Blanket; *J. Nucl. Sci. Technol.*, **47** [10], 1-14 (2010).
- Y. Kimura, M. Saito and H. Sagara: Development of Methodology for Plutonium Categorization (III) - Effect of Radiation -; *Trans. Am. Nucl. Soc.*, **103** (2010).
- E. Hamase, M. Saito and H. Sagara: Long-life FBR with Inner Blanket by Doping MA; *Trans. Am. Nucl. Soc.*, vol. **103** (2010).
- H. Sagara, S. Koyama, and M. Saito: Irradiation Analysis of U, Am Samples Irradiated in Experimental Fast Reactor "Joyo" for Protected Plutonium Production in Fast Breeder Reactor Blanket; *INES-3*, Oct 31 – Nov. 3 (2010).
- K. Ismailov, M. Saito, H. Sagara and Kenji Nishihara: Transmutation of Minor Actinides in Accelerator Driven System with Uranium Spallation TARGET; *INES-3*, Oct 31- Nov. 3 (2010).
- M. Nogami, Y. Sugiyama, and Y. Ikeda: Adsorptivity of Silica-supported Monoamide Resins to U(IV) in Nitric Acid Media; *J. Radioanal. Nucl. Chem.*, **283**, 177-180 (2010).
- M. Nogami, Y. Sugiyama, T. Kawasaki, M. Harada, Y. Morita, T. Kikuchi, and Y. Ikeda: Adsorptivity of Polyvinylpyrrolidone for Selective Separation of U(VI) from Nitric Acid Media; *J. Radioanal. Nucl. Chem.*, **283**, 541-546 (2010).
- A. Canlier, T. Kawasaki, S. Chowdhury, and Y. Ikeda: Structural Characterization, Electrochemistry, and Spectroelectrochemistry of *trans*-Dioxorhenium(V) Complex with 4-Methoxypyridine,  $[\text{ReO}_2(4\text{-MeOpy})_4]\text{PF}_6$ , and Characterization of  $[\text{ReO}_2(4\text{-MeOpy})_4]^{2+}$  Generated Electrochemically; *Inorg. Chim. Acta*, **364**, 1-7 (2010).
- R.M. Hassan, S.M. Ahmed, A.Fawzy, A.A. Abdel-Kader, Y. Ikeda, and H.D. Takagi: Acid-catalyzed Oxidation of Carboxymethyl Cellulose Polysaccharide by Chromic Acid in Aqueous Perchlorate Solutions. A Kinetics Study; *Cat. Commun.*, **11**, 611-615 (2010).
- K. Takao, M. Kato, S. Takao, A. Nagasawa, G. Bernahard, C. Hennig, and Y. Ikeda: Molecular Structure and Electrochemical Behavior of Uranyl(VI) Complex with Pentadentate Schiff Base Ligand: Prevention of Uranyl(V) Cation-Cation Interaction by Fully Chelating Coordination Sites; *Inorg. Chem.*, **49**, 2349-2359 (2010).
- K. Takao and Y Ikeda:  $\mu\text{-}\eta^2\text{:}\eta^2\text{-Peroxo-bis[nitratodioxidobis(pyrrolidine-2-one) uranium(VI)]$ ; *Acta Cryst.* **E66**, m539-m540 (2010).
- S.-Y. Kim, K. Takao, Y. Haga, E. Yamamoto, Y. Kaswata, Y. Morita, K. Nishimura, and Y. Ikeda: Molecular and Crystal Structures of Plutonyl(VI) Nitrate Complexes with *N*-Alkylated 2-Pyrrolidone Derivatives: Cocrystallization Potentiality of U(VI) and Pu(VI) for Uniform MOX Fuel Precursor; *Crystal Growth & Design*, **10**, 2033-2036 (2010).
- T. Kawasaki, A. Canlier, S. Chowdhury, and Y. Ikeda: *trans*-Tetrakis- (4-methylpyridine- $\kappa\text{N}$ )dioxidorhenium(V) Hexafluoridophosphate; *Acta Cryst.*, **E66**, m857-m858 (2010).
- R.M. Hassan, A. Alaraifi, A. Fawzy, I.A. Zaafarany, K.S. Khairou, Y. Ikeda, and H.D. Takagi: Acid-catalyzed Oxidation of Some Sulfated Polysaccharides, Kinetics and Mechanism of Oxidation of Kappa-carrageenan by Cerium(IV) in Aqueous Perchlorate Solutions; *J. Mole. Catal. A: Chemical*, **332**, 138-144 (2010).
- P.C. Burns, Y. Ikeda, and K. Czerwinski: Advances in Actinide Solid-state and Coordination Chemistry; *MRS Bull.*, **35**, 868-876 (2010).
- S.-Y. Kim, T. Ogura, Y. Morita, N. Asanuma, and Y. Ikeda: Electrochemical Studies of Uranyl Chloro and Nitrate complexes in 1-Ethyl-3-methylimidazolium Based Ionic Liquids; *2nd International Conference on Asian Nuclear Prospects 2010 (ANUP 2010)*, Mamallapuram, India, October 10-13, 2010.

- M. C. Ali, M. Nogami, T. Kawasaki, Y. Sasaki, and Y. Ikeda: Highly Selective Extraction of  $\text{ReO}_4^-$  in  $\text{HNO}_3$  Solution Using New Extractant, 2,2'-(Methylimino)bis(*N,N*-diethylacetamide); *The Third International Symposium on Innovative Nuclear Energy Systems (INES-3)*, Tokyo Institute of Technology, Japan, October 31-November 3, 2010.
- T. Tsukahara and Y. Ikeda: A Study on Behavior of Metal Ions in Nanospace for Separation of Radionuclides Based on Nanofluidics; *The Third International Symposium on Innovative Nuclear Energy Systems (INES-3)*, Tokyo Institute of Technology, Japan, October 31-November 3, 2010.
- M. Nogami, M. Harada, Y. Sugiyama, T. Kawasaki, Y. Kawata, Y. Morita, T. Kikuchi, and Y. Ikeda: Selectivity and Stability of 1,3-Dimethyl-2-imidazolidone for Precipitation of U(VI) in Nitric Acid Media; *The Third International Symposium on Innovative Nuclear Energy Systems (INES-3)*, Tokyo Institute of Technology, Japan, October 31-November 3, 2010.
- N. Asanuma, Y. Takahashi, and Y. Ikeda: Extraction Mechanisms of Uranyl Ions by 1-Butyl-3-methylimidazolium nonafluorobutanesulfonate Containing *N*-Dodecyl-2-pyrrolidone; *The Third International Symposium on Innovative Nuclear Energy Systems (INES-3)*, Tokyo Institute of Technology, Japan, October 31-November 3, 2010.
- T. Suzuki, M. Nogami, and Y. Ikeda: A Study on Coordination Ability of Urea Derivatives with Highly Selective Precipitation Ability to Uranyl Ions in  $\text{HNO}_3$ ; *The 60<sup>th</sup> Symposium of Coordination Chemistry of Japan* (2010).
- T. Ogura, N. Ohta, Y. Ikeda, Y. S.-Y. Kim, Y. Morita, and K. Takao: A Study on Uranyl(VI) Complexes for Producing Stable Uranyl(V) Complexes in Various Media; *The 60<sup>th</sup> Symposium of Coordination Chemistry of Japan* (2010).
- Y. Tachibana, M. Nogami, Y. Sugiyama, and Y. Ikeda: Kinetic Studies on Decomposition Reactions of Pyrrolidone Derivatives Using Ozone; *The 19<sup>th</sup> Annual Meeting of Japan Ozone Association* (2010).
- Y. Tachibana, M. Nogami, Y. Sugiyama, and Y. Ikeda: Kinetic Studies on Ozone Oxidation of Pyrrolidone Derivatives Using Pd(II) as a Catalyst; *41<sup>st</sup> Annual Meeting of Union of Chemistry-Related Societies in Chubu Area, Japan* (2010).
- Y. Takahashi, N. Asanuma, and Y. Ikeda: A Study on Mechanism of Extraction Reaction of Uranyl Ions Using BMINfO Containing Pyrrolidone Derivatives; *The Annual Meeting of the Atomic Energy Society of Japan* (2010).
- T. Tsukahara and Y. Ikeda, and T. Kitamori: Development of Partitioning Method Using Nano-fluidics; *The Annual Meeting of the Atomic Energy Society of Japan* (2010).
- M. Tokeshi, H. Hotokezaka, M. Harada, Y. Ikeda, T. Tsukahara, Y. Kikutani, T. Kitamori, Y. Morita, and Y. Ban: A Study of Partitioning Method Using Thermal Response Compounds and Microchannel; *The Annual Meeting of the Atomic Energy Society of Japan* (2010).
- M. Harada, M. Nogami, Y. Sugiyama, T. Kawasaki, Y. Ikeda, Y. Morita, and T. Kikuchi: Development of Advanced Reprocessing System Using Precipitants with High Selectivity and Control Ability (18) Examination of Masking Effect; *The Fall Meeting of the Atomic Energy Society of Japan* (2010).
- T. Kawasaki, M. Nogami, Y. Sugiyama, M. Harada, Y. Ikeda, Y. Morita, and T. Kikuchi: Development of Advanced Reprocessing System Using Precipitants with High Selectivity and Control Ability (19) Examination of Recycling Pyrrolidone Derivatives as Precipitant Using Vaporization Method; *The Fall Meeting of the Atomic Energy Society of Japan* (2010).
- M. Nogami, Y. Sugiyama, T. Kawasaki, M. Harada, Y. Ikeda, Y. Kawata, Y. Morita, and T. Kikuchi: Development of Advanced Reprocessing System Using Precipitants with High Selectivity and Control Ability (20) Examination of Decomposition of Residual Pyrrolidone Derivatives with  $\gamma$ -irradiation; *The Fall Meeting of the Atomic Energy Society of Japan* (2010).
- S.-Y. Kim, Y. Morita, Y. Kawata, Y. Ikeda, and T. Kikuchi: Development of Advanced Reprocessing System Using Precipitants with High Selectivity and Control Ability (21) Precipitation Behavior of Pu in U-Pu Co-precipitation Process; *The Fall Meeting of the Atomic Energy Society of Japan* (2010).
- T. Kikuchi, T. Chikazawa, H. Someya, Y. Morita, and Y. Ikeda: Development of Advanced Reprocessing System Using Precipitants with High Selectivity and Control Ability (22) Examination of Precipitation and Fuel Preparation in the Engineering Scale; *The Fall Meeting of the Atomic Energy Society of Japan* (2010).
- Y. Ikeda, M. Nogami, Y. Sugiyama, T. Kawasaki, M. Harada, Y. Morita, and T. Kikuchi: Development of Advanced Reprocessing System Using Precipitants with High Selectivity and Control Ability (23) Overall Evaluation; *The Fall Meeting of the Atomic Energy Society of Japan* (2010).
- S. Goko, A. Kimura, H. Harada, M. Oshima, M. Ohta, K. Furutaka, T. Kin, F. Kitatani, M. Koizumi, S. Nakamura, Y. Toh, M. Igashira, T. Katabuchi, M. Mizumoto, Y. Kiyonagi, K. Kino, M. Furusaka, F. Hiraga, T. Kamiyama, J. Hori, T. Fujii, S. Fukutani, K. Takamiya: Measurement of Neutron

- Capture Cross Section Ratios of  $^{244}\text{Cm}$  Resonances Using NNRI; *Journal of Nuclear Science and Technology*, Vol. **47**, No. 12, pp. 1097–1100 (2010).
- K. Kino, M. Furusaka, F. Hiraga, T. Kamiyama, Y. Kiyanagi, K. Furutaka, S. Goko, H. Harada, M. Harada, T. Kai, A. Kimura, T. Kin, F. Kitatani, M. Koizumi, F. Maekawa, S. Meigo, S. Nakamura, M. Ooi, M. Ohta, M. Oshima, Y. Toh, M. Igashira, T. Katabuchi, M. Mizumoto: Measurement of Energy Spectra and Spatial Distributions of Neutron Beams Provided by the ANNRI Beam Line for Capture Cross-Section Measurements at the J-PARC/MLF; *Nuclear Instruments and Methods in Physics Research A*, Vol. **626-627**, pp. 58-66 (2010).
- T. V. Daniels, W. Arnold, J. M. Cesaratto, T. B. Clegg, A. H. Couture, H. J. Karwowski, T. Katabuchi: Spin-Correlation Coefficients and Phase-Shift Analysis for  $p + ^3\text{He}$  Elastic Scattering; *Physical Review C*, **82**, 034002 (2010).
- S. Kamada, M. Igashira, T. Katabuchi, M. Mizumoto: Measurements of keV-Neutron Capture Cross Sections and Capture Gamma-Ray Spectra of  $^{77}\text{Se}$ ; *Journal of Nuclear Science and Technology*, **47**, No. 7, pp. 634 - 641 (2010).
- J. Hori, M. Ohta, M. Oshima, F. Kitatani, A. Kimura, T. Kin, M. Koizumi, S. Goko, Y. Toh, S. Nakamura, H. Harada, K. Furutaka, M. Igashira, T. Katabuchi, M. Mizumoto, T. Kamiyama, K. Kino, Y. Kiyanagi, F. Hiraga, M. Furusaka: Measurement of Neutron Capture Cross Section of  $^{93}\text{Zr}$  Using a  $4\pi$  Ge Spectrometer at the J-PARC/NNRI; *2010 Fall Meeting of the Atomic Energy Society of Japan*, pp. 481, (2010).
- T. Katabuchi, N. Canh Hai, M. Igashira, S. Kamada, M. Tajika, M. Mizumoto: Measurement of Neutron Capture Cross Section and Capture  $\gamma$ -Ray Spectrum of Sr-88 at 510 keV; *2010 Fall Meeting of the Atomic Energy Society of Japan*, pp. 479 (2010).
- M. Mizumoto, T. Katabuchi, M. Igashira, Y. Kiyanagi: The Characteristic Experiments of Neutron Flux and Neutron and Gamma-Ray Fields with Gamma-Ray Detectors at the BL04 of J-PARC MLF (2); *2010 Fall Meeting of the Atomic Energy Society of Japan*, pp. 480 (2010).
- N. Hayashizaki, T. Hattori, Y. Matsumoto, T. Katabuchi, T. Tsukahara, T. Kobayashi: Development of BNCT Irradiation System using Compact Linac; *2010 Fall Meeting of the Atomic Energy Society of Japan*, pp. 502 (2010).
- A. Kimura, M. Ohta, M. Oshima, F. Kitatani, T. Kin, M. Koizumi, S. Goko, Y. Toh, S. Nakamura, H. Harada, K. Furutaka, M. Igashira, T. Katabuchi, M. Mizumoto, K. Kino, Y. Kiyanagi, J. Hori: Measurements of Neutron-Capture Cross Sections of  $^{244}\text{Cm}$  and  $^{246}\text{Cm}$  using a  $4\pi$  Ge spectrometer at the J-PARC/NNRI; *2010 Fall Meeting of the Atomic Energy Society of Japan*, pp. 482 (2010).
- K. Terada, M. Igashira, T. Katabuchi, T. Matsuhashi: Measurements of keV-Neutron Capture Cross Sections and Capture Gamma-Ray Spectra of  $^{105}\text{Pd}$ ; *2011 Annual Meeting of the Atomic Energy Society of Japan*, pp. 611 (2011).
- T. Katabuchi, M. Mizumoto, M. Igashira, A. Kimura, Y. Toh, S. Nakamura, S. Goko, K. Hara, T. Kin, M. Ohta, F. Kitatani, K. Furutaka, M. Koizumi, K. Hirose, H. Harada, M. Oshima, J. Hori, K. Kino, T. Kamiyama, F. Hiraga, M. Furusaka, Y. Kiyanagi: Measurements of the Neutron Capture Cross Section of Tc-99 Using an Nai(Tl) Detector at J-PARC/ANNRI; *2011 Annual Meeting of the Atomic Energy Society of Japan*, pp. 613 (2011).
- T. Kobayashi, M. Takahashi, M. Aritomi, M. Nakagawa, N. Hayashizaki, T. Katabuchi, G. Bengua, K. Tanaka, T. Hattori, M. Igashira, T. Yamamoto, H. Nakamura: Development of Liquid Lithium Target for Neutron Capture Therapy Using Accelerator —(1) An Outline of the Neutron Producing Target for NCT; *2011 Annual Meeting of the Atomic Energy Society of Japan*, pp. 688 (2011).
- S. Nakamura, M. Ohta, M. Oshima, F. Kitatani, A. Kimura, T. Kin, M. Koizumi, S. Goko, Y. Toh, K. Hara, H. Harada, K. Furutaka, M. Igashira, T. Katabuchi, M. Mizumoto, K. Kino, Y. Kiyanagi, J. Hori, K. Takamiya, S. Fukutani, T. Fujii: Measurement of Neutron-Capture Cross Section of Pd-107 Using ANNRI; *2011 Annual Meeting of the Atomic Energy Society of Japan*, pp. 614 (2011).
- H. Harada, M. Ohta, M. Oshima, F. Kitatani, A. Kimura, T. Kin, M. Koizumi, S. Goko, Y. Toh, S. Nakamura, K. Furutaka, M. Igashira, T. Katabuchi, M. Mizumoto, K. Kino, Y. Kiyanagi, K. Takamiya, S. Fukutani, T. Fujii, J. Hori: Measurement of Neutron-Capture Cross Section of Am-241 Using ANNRI; *2011 Annual Meeting of the Atomic Energy Society of Japan*, pp. 615 (2011).
- T. Kida, Y. Inaba, W. Watanabe, Y. Nakajima, S. Fukuoka, K. Takeshita and A. Mori: Extraction of Cd $^{2+}$  and Am $^{3+}$  Ions into Organic and Fluorous Solvents with a TPEN Chelating Agent bearing a Fluoroalkyl Substituent; *Chem. Lett.* **39**, 774-776 (2010).
- T. Maekawa, T. Kida, Y. Miyazaki, W. Watanabe, Y. Inaba, K. Takeshita and A. Mori: Temperature-Dependent Change of Extraction Performance of Soft Cadmium(II) Ion with TPENNIPA Gel. Studies on the Effect of the Ethylenediamine Skeleton; *Bull. Chem. Soc. Jpn.* **84**, 122–124 (2011).
- K. Takeshita: Development of Liquid-liquid Countercurrent Centrifugal Extractor with Taylor-Couette Flow; *Japanese J. Multiphase Flow*, **24**, 267-274 (2010).

- H. Takahashi, H. Kikura, K. Takeshita and M. Aritomi: UVP Measurement of Taylor-Couette Vortex Flow with Trough-flow; *Transactions of the Japan Society of Mechanical Engineers, Series B*, **77**, 97-101 (2011).
- H. Takahashi, H. Kikura, K. Takeshita and M. Aritomi: Characteristics of Taylor-Couette Vortex Flow with Counter Flow; *Journal of the Japanese Society for Experimental Mechanics*, **11**, Special Issue, SS168-173 (2011).
- Y. Inaba, T. Tsumagari, T. Kida, W. Watanabe, Y. Nakajima, S. Fukuoka, A. Mori, T. Matsumura, Y. Nakano and K. Takeshita: Thermoresponsive Extraction of Cadmium(II) Ions by Poly(TPEN-NIPA) Gels. Effect of Chain Length and Branched Spacer Structure on Gel Formation and Extraction Behavior; *Polym. J.* **43**, 630-634 (2011).
- H. Takahashi, H. Kikura, K. Takeshita and M. Aritomi: Flow Field Measurement of Taylor-Couette Vortex Flow with Axial Flow using UVP; *The 14th International Symposium on Flow Visualization (ISFV14)*, ISFV14-8A-4 (2010).
- H. Takahashi, H. Kikura, K. Takeshita and M. Aritomi: H. Takahashi, H. Kikura, K. Takeshita and M. Aritomi : UVP Measurement of Taylor-Couette Vortex Flow with Axial Flow, *The 15th National Symposium on Power and Energy Systems (SPES 2010) of the Japan Society of Mechanical Engineers*, 127-128 (2010).
- T. Maekawa, T. Kida, Y. Miyazaki, Y. Inaba, K. Takeshita, A. Mori: *The 57th Kobe Polymer Research Symposium*, Pa-22 (2010).
- H. Takahashi, H. Kikura, K. Takeshita and M. Aritomi: Ultrasonic Velocity Profile Measurement of Taylor-Couette Vortex Flow in Centrifuge Extractor; *Annual Meeting 2010 of the Japanese Society for Multiphase Flow*, 302-303 (2010).
- H. Takahashi, H. Kikura, K. Takeshita and M. Aritomi: Visualization and Ultrasonic Measurement of Taylor-Couette Vortex Flow in Centrifugal Extractor; *2010 Annual Conference on Experimental Mechanics*, 17-18 (2010).
- K. Takehista, H. Kinuhata, and R. Makabe: *The 42<sup>nd</sup> Autumn Meeting of the Society of Chemical Engineers*, Japan, S32 (2010).
- K. Takeshita and H. Inazuka: *The 42<sup>nd</sup> Autumn Meeting of the Society of Chemical Engineers*, Japan, D118 (2010).
- K. Takeshita and D. Kuwae: *The 42<sup>nd</sup> Autumn Meeting of the Society of Chemical Engineers*, Japan, S122 (2010).
- T. Ogata, K. Takeshita, Y. Inaba, H. Oaki, and A. Mori: *The 42<sup>nd</sup> Autumn Meeting of the Society of Chemical Engineers*, Japan, D117 (2010).
- K. Takeshita and H. Kinuhata: *Fall Meeting of the Atomic Energy Society of Japan*, A12 (2010).
- S. Suzuki, Y. Okamoto, A. Ikeda, T. Kobayashi, H. Shiwaku, K. Akutsu, T. Yaita, T. Ogata, K. Takeshita, Y. Inaba, H. Oaki, and A. Mori: *Fall Meeting of the Atomic Energy Society of Japan*, A23 (2010).
- T. Ogata, Y. Inaba, H. Oaki, K. Takeshita, A. Mori, T. Yaita, and S. Suzuki: Separation of MA from Ln using Polymer Gels Cross-Linked with TPEN Analogs; *Fall Meeting of the Atomic Energy Society of Japan*, A24 (2010).
- H. Takahashi, H. Kikura, K. Takeshita and M. Aritomi: Flow Characteristics of Taylor Vortices in a New Type Liquid-Liquid Countercurrent Centrifugal Extractor; *The 8th International Topical Meeting on Nuclear Thermal-Hydraulics, Operation and Safety (NUTHOS-8)*, CD-ROM Paper No. N8P0304, Book of Abstract p.44 (2010).
- Y. Inaba, T. Kida, W. Watanabe, A. Mori, T. Matsumura, D. Kuwae, T. Ogata, K. Takeshita: Synthesis and Properties of Hydrophobic TPEN Derivatives for MA/Ln Separation; *The Third International Symposium on Innovative Nuclear Energy Systems (INES-3)*, Paper ID: 124 (2010).
- T. Ogata, K. Takeshita, H. Oaki, Y. Inaba, A. Mori: Separation of Am(III) from Eu(III) using Polymer Gels Cross-Linked with TPEN Analogs; *The Third International Symposium on Innovative Nuclear Energy Systems (INES-3)*, Paper ID: 127 (2010).
- K. Takeshita, H. Rokkaku and H. Kinuhata: Development of Counter-current Centrifugal Extractor with Taylor-Couette Flow for Nuclide Separation; *The Third International Symposium on Innovative Nuclear Energy Systems (INES-3)*, Paper ID: 129 (2010).
- H. Takahashi, H. Kikura, K. Takeshita and M. Aritomi: Characteristics of Taylor Vortex on Counter Flow; *5th International Symposium on Advanced Science and Technology in Experimental Mechanics (5th ISEM'10-Kyoto)*, CD-ROM Paper No. 149, Book of Abstract p.94 (2010).
- T. Maekawa, W. Watanabe, T. Kida, Y. Miyazaki, Y. Inaba, A. Mori, K. Takeshita: Temperature-Dependent Change of Extraction Performance of Soft Cadmium(II) Ion with TPEN-NIPA Gel; *The 2010 International Chemical Congress of Pacific Basin Societies (Pacifichem)*, 1790 (2010).
- H. Takahashi, H. Kikura, K. Takeshita and M. Aritomi: Visualization of Dispersed Phase Flow in Centrifugal Extractor Using Taylor-Couette Vortex Flow; *The 8th ASME-JSME Thermal Engineering Joint Conference*

- (AJTEC2011), CD-ROM Paper No. AJTEC2011-44403 (2011).
- R. Hasu, Y. Inaba, D. Kuwae, A. Mori and K. Takeshita: Separation of Heavy Metals by Hydrophobic TPEN Derivatives; *91st Annual Meeting of The Chemical Society of Japan*, 4D6-03 (2011).
- T. Ogata, K. Takeshita, H. Oaki, Y. Inaba and A. Mori: *The 76<sup>th</sup> Annual Meeting of the Society of Chemical Engineers*, Japan, O204 (2011).
- T. Ogata, K. Takeshita, H. Oaki, Y. Inaba and A. Mori, T. Yaita, and S. Suzuki: Adsorption Property of Am(III) using Polymer Gels Cross-Linked with TPEN Analogs; *Annual Meeting of the Atomic Energy Society of Japan*, D11 (2011).
- Masaki Ozawa, Akira Ohtaki and Toshihide Asakura: Rare Metals in Nuclear Spent Fuels, Their Separation and Utilization. Strategy; *INCS (International Nuclear Chemistry Society) News*, 27th issue, Volume VII, 3, pp.17-26, July (2010).
- Masaki Ozawa: Reprocessing of Radioactive Waste, Toward Recycling of Nuclear Rare Metals; (Invited, Round Table), *International Nuclear Forum "Bulgarian Nuclear Energy-National, Regional and World Energy Safety"* by Bulgarian. Nuclear Forum (bulATOM), Riviera Holiday Club, June 9<sup>th</sup> -11<sup>th</sup> 2010.
- Masaki Ozawa: Advanced ORIENT Cycle for Turning Radioactive Waste into Resource (Invited Lecture), *CIMTEC2010 5<sup>th</sup> Forum on New Materials*, Abstracts, pp.67, Montecatini Terme, Tuscany, Italy, June 13-18, 2010.
- M.Ozawa, S.Koyama, and T.Suzuki: Nuclear Rare Metals and Their Separation in Adv.-ORIENT Cycle Strategy, 2<sup>nd</sup> *International conference on Asian Nuclear Prospects 2010 (ANUP2010)*, Proceedings (CD), FR 4, Mamallapuram, India, October 10-13, 2010.
- Masaki Ozawa: Separation and Utilization of Nuclear Rare Metals and Actinides in Advanced Reprocessing System (Invited Lecture); The 389<sup>th</sup> Xiangshan Science Conference Workshop of Nuclear Fuel Reprocessing, *Proc. Radiochemical Challenges in Nuclear Fuel reprocessing*, pp.27-29, Xiangshan Hotel, Beijing, China, Dec. 22-24, 2010.
- Masaki Ozawa: Chapter 19. Rare Metals in Nuclear Industries; *Rare Metal Binran*, pp.262-273 ISBN 978-4-621-08276-8 MARUZEN, Jan. 30<sup>th</sup> 2011.(in Japanese)
- Masaki Ozawa, Shinichi Suzuki, Kenji Takeshita: Advanced Hydrometallurgical Separation of Actinides and Rare Metals in Nuclear Fuel Cycle; *Solvent Extraction Research and Development, Japan*, Vol. 17, 19-34 (2010).
- Masaki Ozawa: Considering the Utilization of Valuable Rare Metals in Spent Nuclear Fuel; *Energy Review*, 5, pp.42-46 (2010). (in Japanese)
- Masaki Ozawa: Nuclear Fuel Cycle and Resources; *Journal of the Atomic Energy Society of Japan*, Vol.52, 9, pp.48(2010). (in Japanese)
- Masaki Ozawa: Research Strategy of Advanced ORIENT Cycle; *Nuclear Viewpoints*, Vol.56, 10, pp7-11 (2010). (in Japanese)
- Masaki Ozawa, Yuezhou Wei: The 389<sup>th</sup> Xiangshan Science Conference; Radio- chemical Challenges in Nuclear Fuel Reprocessing, *Journal of the Atomic Energy Society of Japan*, Vol.53, 6, pp451-452 (2011). (in Japanese)
- Masaki Ozawa, Tatsuya Suzuki, Yoshihiko Shinoda, Naoyuki Takaki: New Strategy on Rare Earth in Advanced Nuclear Fuel Cycle; *RARE EARTHS* 56, pp.186-187, ISSN0910-2205 Kidorui CODEN:KIDOEP, May 2010. (in Japanese)
- Masaki Ozawa: Advanced ORIENT Cycle; Spinning A Dream Come True; 4<sup>th</sup> Advanced ORIENT Cycle Seminar, Swany Hall, Rokkasho-mura, Jul. 30<sup>th</sup>, 2010. (in Japanese)
- Masaki Ozawa: Rare Metals in High Level Liquid Wastes; Special Committee on Nuclear Fuel Cycle, Rokkasho-mura Village Assembly, Sep. 8<sup>th</sup>.2010. (in Japanese)
- Masaki Ozawa: Advanced ORIENT Cycle – New Resource Strategy and Issues by Forefront Nuclear Science and Technology, *JST Luncheon Seminar*, Ichigaya- office, Tokyo, Jan.17<sup>th</sup> 2011. (in Japanese)
- Masaki Ozawa, Yasuhiko Fujii: Advanced ORIENT Cycle (Phase1) 1) Strategy and Concept; *2010 Fall Meeting of Japan Atomic Energy Society of Japan*, A36, Sep.16<sup>th</sup>, 2010. (in Japanese)
- T. Tada, H. Fukuda, J. Hasegawa and Y. Oguri: Application of a Wavelength Dispersive Particle Induced X-ray Emission System to Chemical Speciation of Phosphorus and Sulfur in Lake Sediment Samples; *Spectrochim. Acta B*, 65, 46 (2010).
- S. Wonglee, T. Tada, H. Fukuda, J. Hasegawa and Y. Oguri: Development of a Target Positioning System Based on a Laser Position Sensor for High-Efficiency Wavelength-Dispersive PIXE Analysis; *Int. J. PIXE*, 20, 1 (2010).
- Y. Oguri and J. Hasegawa: Calculation of Heavy-Ion Stopping Power in Warm Dense High-Z Targets Using Temperature-Dependent Dielectric Response Functions;

Meeting Abstract of the Physical Society of Japan, **65** [2], Part 2, 118 (2010).

J. Hasegawa, S. Jaiyen and Y. Oguri: Quality Evaluation of Ion Beams Focused by Tapered Glass Capillaries; *Meeting Abstract of the Physical Society of Japan*, **65** [2], Part 2, 168 (2010).

Y. Oguri and J. Hasegawa: Calculation of Heavy-Ion Stopping Power in Warm Dense Plutonium Targets for Equation-of-State Studies; *2011 Annual Meeting of the Atomic Energy Society of Japan*, N27, 679 (2011).

J. Hasegawa and Y. Oguri: Microbeam Analyses Using Glass Capillary Lenses; *2011 Annual Meeting of the Atomic Energy Society of Japan*, N31, 683 (2011).

S. Thomyasirigul, H. Fukuda, J. Hasegawa and Y. Oguri: Speciation and Determination of Cr(III) and Cr(VI) in Water by Energy-Dispersive PIXE Analysis; *The 12th International Conference on Particle Induced X-ray Emission and its Analytical Applications*, 27 June - 2 July 2010, Guildford, UK, O05 (2010).

J. Hasegawa, Y. Oguri and S. Jaiyen: Monte-Carlo Simulation of Ion Beam Focusing Using Glancing-Angle Scattering; *The 18th International Symposium on Heavy Ion Inertial Fusion*, 30 August - 3 September 2010, Darmstadt, Germany, MON-0404 (2010).

J. Hasegawa, S. Jaiyen and Y. Oguri: Development of a Micro-PIXE System Using Tapered Glass Capillary Optics; *The 10th European Conference on Accelerators in Applied Research and Technology*, 13-17 September 2010, Athens, Greece, PII-58 (2010).

S. Wonglee, T. Tada, H. Fukuda, Jun Hasegawa and Y. Oguri: Chemical Speciation of Chlorine in Particulate Matter by Wavelength-Dispersive PIXE Technique; *The 10th European Conference on Accelerators in Applied Research and Technology*, 13-17 September 2010, Athens, Greece, PII-60 (2010).

S. Wonglee, H. Fukuda, J. Hasegawa and Y. Oguri: Chemical Speciation of Chlorine in Size-Fractioned Particulate Matter Samples by High-Resolution Measurement of Proton-Induced K-beta X-rays; *The 27th Annual Meeting of the Japan Society for Particle Induced X-ray Emission (PIXE) Research*, 17-19 November 2010, Kyoto, Japan, 29 (2010).

T. Yuji, T. Urayama, S. Fujii, Y. Iijima, Y. Suzuki, H. Akatsuka: Basic Characteristics for PEN Film Surface Modification Using Atmospheric-Pressure Nonequilibrium Microwave Plasma Jet; *Electronics Communications Jpn.*, **93**, [5], pp. 42 - 49, (2010).

H. Akatsuka: Optical Emission Spectroscopy Measurement of Processing Plasmas; *IEEEJ Trans. FM*, **130**, [10], 892 - 898 (2010) [in Japanese].

Y. Ichikawa, T. Sakamoto, A. Nezu, H. Matsuura and H. Akatsuka: Actinometry Measurement of Dissociation Degree of Nitrogen and Oxygen in N<sub>2</sub>-O<sub>2</sub> Microwave Discharge Plasmas; *Jpn. J. Appl. Phys.*, **49**, 106101 (16 pages) (2010).

H. Akatsuka: Recent Trends of Traditional Optical Emission Spectroscopic Measurement of Non-Equilibrium Plasmas - Atmospheric-Pressure Ar Plasma and Low-Pressure N<sub>2</sub> Plasma -; *IEEEJ Trans. FM*, **131**, [1], 6 - 10 (2011) [in Japanese].

H. Kataoka, N. Mungkung, T. Yuji, M. Kawano, Y. Kiyota, D. Uesugi, K. Nakabayashi, Y. Suzuki, H. Shibata, N. Kashihara, K. Sakai, T. Bouno, H. Akatsuka: Surface Modification of Silicon Wafer by Low-Pressure High-Frequency Plasma Chemical Vapor Deposition Method; *24th International Symposium on Discharges and Electrical Insulation in Vacuum (ISDEIV)*, IEEE, pp. 505 - 508 (2010).

H. Akatsuka, K. Kuwano, A. Nezu, H. Matsuura: Measurement of Nitrogen Dissociation Degree of Nitrogen Discharge Plasma by Actinometry Method with Subtraction of First Positive Band Spectrum; 63rd Gaseous Electronics Conference (GEC), *Bull. Am. Phys. Soc.*, **55**, [7], pp. 26 - 27 (2010).

H. Akatsuka, K. Kuwano, A. Nezu, H. Matsuura: Measurement of Nitrogen Dissociation Degree of Nitrogen Discharge Plasma by Actinometry Method with Subtraction of First Positive Band Spectrum; *Proc. 7th International Conference on Reactive Plasmas (ICRP)*, pp. 59-60 (2010).

H. Akatsuka, Y. Ichikawa, K. Kuwano, T. Sakamoto, A. Nezu and H. Matsuura: Measurement of Nitrogen Dissociation Degree of Nitrogen Discharge Plasma by Actinometry Method with Subtraction of First Positive Band Spectrum; *The Papers of Technical Meeting on Plasma Science and Technology*, IEEEJ, PST-10-14, pp. 23 - 28 (2010).

Y. Nagahara, H. Ichii, K. Yoshida, A. Nezu and H. Akatsuka: Effect of Collisions with Neutral Particles on Stall Phenomena of Supersonic Plasma Flow; *The Papers of Technical Meeting on Plasma Science and Technology*, IEEEJ, PST-10-45, pp. 23 - 27 (2010).

K. Kuwano, A. Nezu, H. Matsuura and H. Akatsuka: Actinometry Measurement of Nitrogen Atom Density with Subtraction of 1PS Band and Effect of Rare-Gas Admixture on the Dissociation Degree of Nitrogen; Extended Abstracts (The 71st Autumn Meeting, 2010); *The Japan Society of Applied Physics*, 08-043 (2010).

- Y. Nagahara, K. Yoshida, A. Nezu and H. Akatsuka: Effect of Collisions of Supersonic Plasma Flow with Neutral Particles on Deceleration into Subsonic Region; *Meeting Abstracts of the Physical Society of Japan*, **65** [2] p.175 (2010).
- K. Kuwano, A. Nezu, H. Matsuura and H. Akatsuka: Actinometry Measurement of Density of Nitrogen Atoms in Nitrogen Plasma and the Effect of Rare-Gas Admixture; *Proc. 27th Annual Meeting, The Japan Society of Plasma Science and Nuclear Fusion Research*, 01p15 (2010).
- H. Akatsuka: Discussion on the Collisional Radiative Model Based on Fundamentals of Linear Ordinary Differential Equations; *The Papers of Joint Technical Meeting on Plasma Science and Technology and Pulsed Power Technology*, IEEJ, PST-10-80/PPT-10-100, pp. 67 - 72 (2010).
- K. Tajima, A. Nezu, H. Matsuura and H. Akatsuka: Experimental Study of Plasma Parameters of Flowing Arc Jet Plasma along Mirror and Cusp Magnetic Fields; *The Papers of Joint Technical Meeting on Plasma Science and Technology and Pulsed Power Technology*, IEEJ, PST-10-104/PPT-10-124, pp. 59 - 64 (2010).
- T. Yuji, Y. Kiyota, M. Kawano, K. Nakabayashi, S. Tashiro, M. Tanaka and H. Akatsuka: Optical Emission Spectroscopy Measurement of High-Frequency Low-Pressure at Plasma-Enhanced Chemical Vapor Deposition; *The 2011 Annual Meeting Record*, IEEJ, p. 241 (2011).
- K. Tajima, A. Nezu, H. Matsuura and H. Akatsuka: Experimental Study of Velocity and Space Potential of Stationary Arc-Jet Flowing in Mirror-Type and Cusp-Type Magnetic Field; *The 2011 Annual Meeting Record*, IEEJ, p. 260 (2011).
- H. Akatsuka: Discussion on Ordinary Differential Equations Required for Analysis of Pulse-like Optical Emission Spectroscopy by Collisional Radiative Model; *Extended Abstracts (The 58th Spring Meeting)*; The Japan Society of Applied Physics and Related Societies, 08-036 (2011).
- Abu Khalid Rivai, Minoru Takahashi: Investigations of a Zirconia Solid Electrolyte Oxygen Sensor in Liquid Lead; *Journal of Nuclear Materials*, Vol.**398** (2010) pp.160 - 164.
- Abu Khalid Rivai, Minoru Takahashi: Corrosion Investigations of Al-Fe-coated Steels, High Cr Steels, Refractory Metals and Ceramics in Lead Alloys at 700°C; *Journal of Nuclear Materials*, Vol.**398** (2010) pp.146 - 152.
- Abu Khalid Rivai, Minoru Takahashi: Corrosion Characteristics of Materials in Pb-Bi under Transient Temperature Conditions; *Journal of Nuclear Materials*, Vol. **398** (2010) pp.139 - 145.
- Minoru Takahashi, Tooru Kobayashi, Masashi Nakatsuka, Teddy Ardiansyah, Martin Kulhanek, Ales Vojacek, Vaclav Dostal, Shoji Uchida and Mingguang Zhang: Study on Liquid Lithium Target System for Boron Neutron Capture Therapy (BNCT); *18th International Conference on Nuclear Engineering (ICONE18)*, May 17-21, 2010, Xi'an, China, ICONE18-29516.
- Minoru Takahashi, Takanori Yumura, Isao Yoda, Rongyuan Sa: Visualization of Bubbles Behavior in Lead-bismuth Eutectic by Gamma-ray; *18th International Conference on Nuclear Engineering (ICONE18)*, May 17-21, 2010, Xi'an, China, ICONE18-29522.
- Teddy Ardiansyah, Minoru Takahashi, Yoshio Yoshizawa, Masamichi Nakagawa, Makoto Asaba, Kuniaki Miura: Numerical Simulation of Cavitation for Comparison of Sodium and Water Flows; *18th International Conference on Nuclear Engineering (ICONE18)*, May 17-21, 2010, Xi'an, China, ICONE18-29659.
- Teddy Ardiansyah, Makoto Asaba, Kuniaki Miura, Minoru Takahashi: Characteristics of Cavitation Erosion Phenomena in Sodium Flow; *18th International Conference on Nuclear Engineering (ICONE18)*, May 17-21, 2010, Xi'an, China, ICONE18-29545.
- Asril Pramutadi Andy Mustari, Minoru Takahashi: Corrosion Properties of Welded Ferritic-Martensitic Steels In Liquid Lead-Bismuth At 600C; *18th International Conference on Nuclear Engineering (ICONE18)*, May 17-21, 2010, Xi'an, China, ICONE18-29927.
- Rongyuan Sa, Minoru Takahashi: Thermal Interaction of Lead-alloy Droplet with Subcooled Water in Pool Water Tank; *Proc. of 18th Int. Conf. on Nucl. Eng. (ICONE18)*, May 17-21, 2010, Xi'an, China, ICONE18-29621.
- Asril Pramutadi Andi Mustaria, Minoru Takahashi: Study on Corrosion of Welded Steel for LBE-Cooled Fast Reactors; *3rd International Symposium on Innovative Nuclear Energy Systems (INES-3)*, October 31 - November 3, 2010, Tokyo Institute of Technology, Japan (2010), P-133.
- Rongyuan Sa, Minoru Takahashi, Kiyofumi Moriyama: Study on Thermal Interactions of Lead Alloy and Water; *3rd International Symposium on Innovative Nuclear Energy Systems (INES-3)*, October 31 - November 3, 2010, Tokyo Institute of Technology, Japan (2010), P-104.
- Minoru Takahashi, Masatoshi Kondo: Corrosion Resistance of Ceramics SiC and Si<sub>3</sub>N<sub>4</sub> in Flowing Lead-bismuth Eutectic; *3rd International Symposium on Innovative Nuclear Energy Systems (INES-3)*, October 31 - November 3, 2010, Tokyo Institute of Technology, Japan (2010), 1B-35.

- Teddy Ardiansyah, Minoru Takahashi: Investigation of Cavitation Phenomena for Innovative Sodium- and Lead-bismuth-cooled Fast Reactors; *3rd International Symposium on Innovative Nuclear Energy Systems (INES-3)*, October 31 - November 3, 2010, Tokyo, Japan (2010), P-132.
- Eriko Yamaki-Irisawa, Shunichi Numata, Minoru Takahashi: Corrosion Behavior of Heat-treated Fe-Al Coated Steel in Lead-bismuth Eutectic under Loading; *3rd International Symposium on Innovative Nuclear Energy Systems (INES-3)*, October 31 - November 3, 2010, Tokyo Institute of Technology, Japan (2010), P-131.
- Teddy Ardiansyah, Makoto Asaba, Kuniaki Miura, Minoru Takahashi: Experimental Study on Cavitation Erosion and Onset Condition in Sodium Flow; *Proceedings of 2nd Multidisciplinary International Student Workshop 2010 (MISW 2010)*, August 5-6, 2010, Tokyo, Japan.
- Rongyuan Sa, Minoru Takahashi: Thermal Interaction of lead and lead-bismuth Droplets with Subcooled Water; *2010 Annual Meeting of Atomic Energy Society of Japan*, Ibaraki March 25-28, 2010, E31.
- Teddy Ardiansyah, Minoru Takahashi, Makoto Asaba, Kuniaki Miura: Study on Sodium Cavitation for Fast Reactors (III) Analysis of Cavitation with FLUENT and Erosion Experiment; *2010 Annual Meeting of Atomic Energy Society of Japan*, Ibaraki, March 25-28, 2010, E28.
- Masamichi Nakagawa, Toru Kobayashi, Minoru Takahashi, Masanori Aritomi: Momentum Defects of Sheet Jets / Film Flows of Liquid Lithium for the Target and Coolant of BNCT using Accelerators; *Meeting of JSME Fluids Engineering Division*, Yonezawa, Oct. 30-31, 2010, O117.
- Yuki Tagawa, Shinsuke Mori, Masaaki Suzuki, Ichiro Yamanaka, Toru Obara, Ryu Junichi, Yukitaka Kato: Synergistic Decomposition of CO<sub>2</sub> by Hybridization of a Dielectric Barrier Discharge Reactor and a Solid Oxide Electrolyser Cell; *KAGAKU KOGAKU RONBUNSHU*, **37** (2), pp. 114-119 (2011).
- Hirokazu Ishitobi, Yoshitomo Sato, Keirei Uruma, Junichi Ryu, and Yukitaka Kato: Dehydration and Hydration Behavior of LiCl-Modified Mg(OH)<sub>2</sub> as a Material for Chemical Heat Pumps; *Proc. of Int'l Symposium on Innovative Materials for Processes in Energy Systems 2010 (IMPRES2010)*, Furama Riverfront Hotel, Singapore, 30 November, 2010.
- Junichi Ryu, Rui Takahashi, Hirokazu Ishitobi, Yoshitomo Sato, Keirei Uruma, Yukitaka Kato: Dehydration and Hydration Behavior of Magnesium-Aluminum Mixed Hydroxide for Chemical Heat Pump; *Proc. of Int'l Symposium on Innovative Materials for Processes in Energy Systems 2010 (IMPRES2010)*, Furama Riverfront Hotel, Singapore, 30 November, 2010.
- Yukitaka Kato, Kanta Inoue, Michito Urasaki, Satoshi Tanaka, Hiroaki Ninomiya, Tomoya Minagawa, Azusa Sakurai and Junichi Ryu: Development of Composite Hydrogen Permeation Membrane Using a Reverse Build-Up Method; *Proc. of Int'l Symposium on Innovative Materials for Processes in Energy Systems 2010 (IMPRES2010)*, Furama Riverfront Hotel, Singapore, 30 November, 2010.
- Yukitaka Kao, Yutaka Ujisawa: Iron Making Process; PCT patent, PCT/JP2011/050400, 13 January, 2011.
- Y. Kato., Y. Yasunaga, T. Kashiwaya edited: Energy beyond '20, Honebuto-no-Energy Road Map 2; Kagaku Kogyo Sha, 2010.
- Y. Kato: Energy beyond '20 Outline; *Kagaku Kogaku*, **75** (3), pp. 110-114 (2011).
- Y. Kato, M. Matsukata: Energy beyond '20 (3) Manufacturing and Energy; *75* (3), pp. 110-114 (2011).
- Andreas Hauer, Stefan Gschwander, Yukitaka Kato, Viktoria Martin, Peter Schossig, Fredrik Setterwall: FINAL REPORT for IEA/ECES Annex 18 on "Transportation of Energy by Utilization of Thermal Energy Storage Technology", IEA, 2010.
- Zamengo Massimiliano, Seon-Tae Kim, Ryu Junichi, Kato Yukitaka: Performances of a MgO-expanded Graphite Packed Bed Reactor of Chemical Heat Pump; *SCEJ 76<sup>nd</sup> Annual Meeting*, J206, Tokyo Univ. A&T, Tokyo, 22-24 March, 2011.
- Kim Seon Tae, Uruma Keirei, Ryu Junichi, Kato Yukitaka: Expanded Graphite Mixture for Packed Bed Reactor of Chemical Heat Pump; *SCEJ 76<sup>nd</sup> Annual Meeting*, J207, Tokyo Univ. A&T, Tokyo, 22-24 March, 2011.
- Dipu Arnoldus, Uruma Keireim, Ryu Junichi, Kato Yukitaka: Reactivity Measurement of High Temperature Electrolysis of Carbon Dioxide; *SCEJ 76<sup>nd</sup> Annual Meeting*, I209, Tokyo Univ. A&T, Tokyo, 22-24 March, 2011.
- Kim Seon Tae, J. Ryu, Y. Kato: Reactivity Enhancement of Chemical Materials for Packed Bed Reactor of Chemical Heat Pump; *SCEJ 42<sup>nd</sup> Autumn Meeting*, C121, Doshisha Univ., 6<sup>th</sup> September, 2010.
- Y. Sato, H. Ishitobi, K. Uruma, J. Ryu, Y. Kato: Application of Magnesium - Transition Metal Hydroxide Composites on Chemical Heat Storage; *SCEJ 42<sup>nd</sup> Autumn Meeting*, C120, Doshisha Univ., 5<sup>th</sup> September, 2010.
- A. Sakurai, K. Inoue, J. Ryu, Y. Kato: An Experimental Study of Making Method of a Composite of Hydrogen Permeable Membrane using Reverse Build-up Method; *SCEJ 42<sup>nd</sup> Autumn Meeting*, C205, Doshisha Univ., 6<sup>th</sup>

September, 2010.

H. Ishitobi, Y. Sato, K. Uruma, J. Ryu, Y. Kato: Repetitive Reaction Durability of Lithium Chloride Modified Magnesium Hydroxide; *SCEJ 42<sup>nd</sup> Autumn Meeting*, C119, Doshisha Univ., 6<sup>th</sup> September, 2010.

Y. Kato: Concept of the Energy Beyond '20; *SCEJ 42<sup>nd</sup> Autumn Meeting*, C207, Doshisha Univ., 6<sup>th</sup> September, 2010.

Y. Kato, Y. Ujisawa: Thermal Feasibility Study on Carbon Recycling Iron Making System; *160th ISIJ Autumn Meeting*, No. 156, 25 September, 2010, Hokkaido Univ.

Y. Kato: Effective Use of Surplus Heat by Chemical Heat Pump using Magnesium; *160th ISIJ Autumn Meeting*, 26 September, 2010, Hokkaido Univ.

J. Ryu, Y. Kato, K. Aika: Ammine Complex of  $\text{CaCl}_2\text{-CaBr}_2$  Mixed Halide as a Material for Hydrogen Storage; *Pacificchem 2010*, 16 December, 2010, Honolulu.

H. Shima, H. Yoshioka and J. Onoe: Curvature Effects on Collective Excitations in Dumbbell-Shaped Hollow Nanotubes; *Physica E*, **42**, 1151-1154 (2010).

A. Takashima, J. Onoe and T. Nishii: In situ Infrared Spectroscopic and Density-Functional Studies on the Cross-Linked Structure of One-Dimensional  $\text{C}_{60}$  Polymer; *J. Appl. Phys.* **108**, 033514 (2010).

J. Onoe, A. Takashima and Y. Toda: Infrared Phonon Anomaly of One-Dimensional Metallic Peanut-Shaped  $\text{C}_{60}$  Polymer; *Appl. Phys. Lett.* **97**, 241911 (2010).

J. Onoe: Exotic-Nanocarbons: Toward the Development of New Riemannian Space Quantum Systems; *Proc. Optical-electronic device committee of the electronic society of Japan*, OQD-10-001 (2010).

J. Onoe: Exotic-Nanocarbons: The Development of New Quantum Electronic Systems in a Curved Space; *SCAT Tech. J.* **66**, 16-32 (2010).

J. Onoe: Riemannian Geometric Effects on the Tomonaga-Luttinger Liquids of One-Dimensional Metallic Exotic Nanocarbons with Positive and Negative Gaussian Curvatures; (invited lecture), Institute "Jozef-Stefan", Department of Complex Matter, Ljubljana (Slovenia), Sept. 17 (2010).

J. Onoe: In situ Infrared Spectroscopic and Density-Functional Studies of the Cross-Linked Structure of One-Dimensional Metallic  $\text{C}_{60}$  Polymer; (invited talk), *6<sup>th</sup> International Conference on DV-X $\alpha$  Method*, Daejeon (Korea), Aug. 4-6 (2010).

J. Onoe: The Crystallization Effects on the External Quantum Efficiency of Organic Photovoltaic Cells with a  $\text{Zn(OEP)/C}_{60}$  Layered Structure; (invited talk), *KRICT workshop on "Recovery of rare metals from useless module of Solar cells and Battery"*, Daejeon (Korea), Dec. 3 (2010).

S. Ryuzaki, T. Kai, and J. Onoe: The Dependence of Open Circuit Voltage on Incident Light Wavelength for Organic Photovoltaic Cells Consisting of Zinc-Porphyrin and Fullerene Films; *4th Asian Consortium on Computational Materials Science-Virtual Organization*, Sendai, Jan. 12-14 (2010).

A. Takashima, T. Nishii, and J. Onoe: Structural Properties of an Electron-Beam Irradiated  $\text{C}_{60}$  Film Studied by Vibrational Spectroscopy and Density-Functional Calculations; *4th Asian Consortium on Computational Materials Science-Virtual Organization*, Sendai, Jan. 12-14 (2010).

T. Kai, S. Ryuzaki, and J. Onoe: An Impedance Spectroscopic Study on the Carrier Dynamics in Zinc-Porphyrin / Fullerene Photovoltaic Cells; *4th Asian Consortium on Computational Materials Science-Virtual Organization*, Sendai, Jan. 12-14 (2010).

J. Onoe, A. Takashima and Y. Toda: In situ Low-Temperature Infrared Spectroscopic Study on Kohn Anomaly of One-Dimensional Metallic Exotic-Nanocarbon; (selected paper), *9th Conference on Solid State Chemistry*, Prague (Czech Republic), Sept. 10-15 (2010).

J. Onoe, M. Hirata and M. Kurihara: Relativistic Density-Functional Study of Nuclear Materials; (selected paper), *3rd International Symposium on Innovative Nuclear Energy Systems (INES-3)*, Tokyo, Oct. 31-Nov.3 (2010).

J. Onoe, S. Ryuzaki and Y. Toda: The Roles of Intra- and Inter-Molecular Excitons on the External Quantum Efficiency of Organic Photovoltaic cells with  $\text{Zn(OEP)/C}_{60}$  Layered Structures; (selected paper), *5th International Conference on Surface, Coatings and Nanostructured Materials*, Reims (France), Oct. 19-21 (2010).

A. Takashima, S. Ono, H. Shima and J. Onoe: Anomalous Increase in the Infrared Peak Intensity of One-Dimensional Metallic Peanut-shaped  $\text{C}_{60}$  Polymer; *5th International Conference on Surface, Coatings and Nanostructured Materials*, Reims (France), Oct. 19-21 (2010).

J. Onoe, A. Takashima and T. Nishii: Riemannian Geometrical Effects on the Electronic Properties of One-Dimensional Metallic  $\text{C}_{60}$  Polymers with a Periodic Peanut-Shaped Unevenness Structure; (Selected paper), *The Fifth General Meeting of ACCMS-VO(Asian Consortium on Computational Materials Science - Virtual*

Organization), Sendai, Dec. 10-12 (2010).

T. Orikoshi, T. Nishii and J. Onoe: Photocurrent Properties of Organic Photovoltaic Cells Laterally Contacted with Metal Electrodes; (Selected paper), *The Fifth General Meeting of ACCMS-VO (Asian Consortium on Computational Materials Science - Virtual Organization)*, Sendai, Dec. 10-12 (2010).

A. Takashima, M. Nishiyama and J. Onoe: Infrared Spectroscopic Study of the Reaction Mechanism of One-Dimensional Metallic Peanut-Shaped C<sub>60</sub> Polymer; *The Fifth General Meeting of ACCMS-VO (Asian Consortium on Computational Materials Science - Virtual Organization)*, Sendai, Dec. 10-12 (2010).

J. Onoe and S. Ryuzaki: An Impedance Spectroscopic Study of the Open-Circuit Voltage of Zn(OEP)/C<sub>60</sub> Layered Photovoltaic Cells; *Hybrid Materials 2011*, Strasbourg (France), March 6-10 (2010).

T. Orikoshi, T. Nishii and J. Onoe: The Photo-Current Characteristics of Multilayered Organic Photovoltaic Cells with Lateral Electrodes; *Hybrid Materials 2011*, Strasbourg (France), March 6-10 (2010).

J. Onoe: Low-Dimensional Exotic-Nanocarbon Fabricated using Photo- and Electron-Beam-Induced Excitation of C<sub>60</sub>; *A workshop on advanced quantum beams and their application to nanomaterials*, Tokyo, Feb. 15 (2010).

S. Ryuzaki, T. Kai and J. Onoe: The Capacitance-Voltage Characteristics and Open-Circuit Voltage of Zn(OEP)/C<sub>60</sub> Layered Photovoltaic Cells; (Selected paper), *57<sup>th</sup> spring meeting of the Applied Physics Society of Japan*, Kanagawa, March 17-20 (2010).

T. Kai, S. Ryuzaki and J. Onoe: Impedance Characteristics of Zn(OEP)/C<sub>60</sub> Layered Photovoltaic Cells; (Selected paper), *57<sup>th</sup> spring meeting of the Applied Physics Society of Japan*, Kanagawa, March 17-20 (2010).

A. Takashima, Y. Toda and J. Onoe: In situ Low-Temperature Infrared Spectra of One-Dimensional Metallic Peanut-Shaped C<sub>60</sub> Polymers; (selected as a B-type oral paper), *90<sup>th</sup> spring meeting of the Chemical Society of Japan*, Osaka, March 26-29 (2010).

J. Onoe, A. Takashima, and Y. Toda: In situ Infrared Spectroscopy of One-Dimensional Metallic Exotic-Nanocarbon at a Low Temperature; (selected paper), *8<sup>th</sup> annual meeting of the Nano-Society*, Okazaki, May 13-15 (2010).

S. Ryuzaki, T. Kai, and J. Onoe: The Origins of the Open-Circuit Voltage for Zinc-Porphyrin/C<sub>60</sub> Hetero-Junction Solar Cells; *8<sup>th</sup> annual meeting of the Nano-Society*, Okazaki, May 13-15 (2010).

S. Ryuzaki, T. Kai, and J. Onoe: The Carrier Mobility of Zn(OEP)/C<sub>60</sub> Hetero-Junction Solar Cells under Photo-Irradiation Studied using in Situ Impedance Spectroscopy; *8<sup>th</sup> annual meeting of the Nano-Society*, Okazaki, May 13-15 (2010).

J. Onoe: External Quantum Efficiency and Open-Circuit Voltage of Zn(OEP)/C<sub>60</sub> Hetero-Junction Solar Cells; (Invited talk), *A workshop on "Current status and perspective of Opto-electronic materials"*, Kagawa Univ., Takamatsu, May 28 (2010).

A. Takashima and J. Onoe: Synthesis and Physical Properties of New Form of Nanocarbon Materials Utilizing Electron-Beam Induced Coalescence between C<sub>60</sub> Molecules; *A workshop on "Current status and perspective of Opto-electronic materials"*, Kagawa Univ., Takamatsu, May 28 (2010).

T. Orikoshi, T. Nishii, and J. Onoe: The Effects of the Number of Layers on the Photo-Current for Organic Solar Cells with Lateral-Type Electrodes; *71<sup>st</sup> fall meeting of the Applied Physics Society of Japan*, Nagasaki, Sept. 14-17 (2010).

T. Orikoshi, T. Nishii, and J. Onoe: The Effects of the Number of Layers on the Photo-Current for Organic Solar Cells with Lateral-Type Electrodes; *39<sup>th</sup> symposium of the Fullerene and Nanotube Society of Japan*, Kyoto, Sept. 5-7 (2010).

J. Onoe:  $\pi$ -Electron Conjugated Nanocarbons – from Low Dimensionality to Topology-; (Invited lecture), *Science of Tokyo Univ.*, Tokyo, June 2 (2010).

J. Onoe: Carbon-Based Nanoscience – Structure, Properties, and Functions –; (Invited talk), *16<sup>th</sup> seminar on photo-science project at Miyazaki Univ.*, Miyazaki, Nov. 19 (2010).

T. Tsuchimoto, K. Sakata, M. Someya, H. Yamamoto, R. Hirayama, Y. Matsumoto, Y. Furusawa and M. Hareyama: Gene Expression Associated with DNA-Dependent Protein Kinase Activity under Normoxia, Hypoxia and Reoxygenation; *J.Radiat.Res.*, **52**, 464-471 (2011).

M. Someya, K. Sakata, Y. Matsumoto, Kamdar, R. P., M. Kai, M. Toyota and M. Hareyama: The Association of DNA-Dependent Protein Kinase Activity of Peripheral Blood Lymphocytes with Prognosis of Cancer; *Brit.J.Cancer*, **104**, 1724-1729 (2011).

M. Takagi, K. Sakata, M. Someya, H. Tauchi, K. Iijima, Y. Matsumoto, T. Torigoe, A. Takahashi, M. Hareyama and M. Fukushima: Gimeracil Sensitizes Cells to Radiation via Inhibition of Homologous Recombination; *Radiother. Oncol.*, **96**, 259-266 (2010).

- Kumar, A., and Y. Matsumoto: Radiation Protection by Herbs and Plants; *Emerging Trends in Zoology*,. Edit. Srivastva, U.C. and Kumar, S., Narendra Publishing House (2011).
- Sharma, M.K., and Y. Matsumoto: DNA-PK Phosphorylation Targets in XRCC4 and XLF Proteins in DNA Double-Strand Break Repair; *Ataxia-Telangiectasia Workshop 2010*, Redondo Beach (Crowne Plaza Hotel), CA, USA, 11-14 April 2010, Poster #168.
- Kamdar, R.P. and Y. Matsumoto: Assembly of Non-Homologous End-Joining Machinery on Radiation-Induced DNA Double-Strand Breaks; *Ataxia-Telangiectasia Workshop 2010*, Redondo Beach (Crowne Plaza Hotel), CA, USA, 11-14 April 2010, Poster #122.
- Y. Matsumoto: XRCC4: a Bona Fide Substrate of DNA-PK in DNA Double-Strand Break Repair; *56th Annual Meeting Radiation Research Society*, Maui (Grand Wailea Resort Hotel and Spa), Hawaii, USA, 25-29 September 2010, Symposium Talk (Invited) S1201.
- Sharma, M.K. and Y. Matsumoto: Identification of DNA-PK Phosphorylation Targets in XRCC4 & XLF Proteins and Their Physiological Significance in the Process of DNA Double-Strand Break Repair; *56th Annual Meeting Radiation Research Society*, Maui (Grand Wailea Resort Hotel and Spa), Hawaii, USA, 25-29 September 2010, Poster Session PS2.36.
- M. Someya, M. Takagi, K. Sakata, H. Tauchi, Y. Matsumoto, M. Hareyama and M. Fukushima: Radiosensitizing Effects of Gimeracil; *56th Annual Meeting Radiation Research Society*, Maui (Grand Wailea Resort Hotel and Spa), Hawaii, USA, 25-29 September 2010, Poster Session PS2.15.
- Y. Matsumoto, Sharma M. K., Kamdar R. P. and Sharma, A: Missing Links in the DNA Double-Strand Break Repair Mechanism and Its Possible Application to Cancer Therapy. International Conference on Radiation Biology: Nanotechnology, Imaging and Stem Cell Research in Radiation Oncology, Chennai (Sri Ramachandra University), India, 15-17 November 2010, Symposium Talk (Invited) S14-IL-86.
- D. Kuwahara, S. Tsuji-Iio, Y. Nagayama, T. Yoshinaga, M. Sugito, Z. Shi, S. Yamaguchi, Y. Kogi, A. Mase: Upgrade of 2-D Antenna Array for Microwave Imaging Reflectometry and ECE Imaging; *J. Plasma Fusion Res. SERIES*, **9**, 125-130 (2010).
- T. Habuchi, H. Tsutsui, S. Tsuji-Iio, R. Shimada: 3-Dimensional Stress Analysis of Virial-Limit Coils; *IEEE Transactions on Applied Supercond.*, **20** [3], 1924-1927 (2010).
- S. Maeyama, A. Ishizawa, T.-H. Watanabe, M. M. Skoric N. Nakajima, S. Tsuji-Iio, and H. Tsutsui: Effects of Time-Varying  $E \times B$  flow on Slab Ion-Temperature-Gradient Turbulence; *Phys. Plasmas*, Vol. **17**, 062305-1-9 (2010).
- T. Akiyama, K. Kawahata, K. Tanaka, T. Tokuzawa, Y. Ito, S. Okajima, K. Nakayama, C.A. Michael, L.N. Vyacheslavov, A. Sanin, S. Tsuji-Iio: Interferometer Systems on LHD; *Fusion Sci. Technol.* **58** [1] 352-363 (2010).
- T. Yoshinaga, Y. Nagayama, D. Kuwahara, H. Tsuchiya, S. Yamaguchi, Y. Kogi, S. Tsuji-Iio, and A. Mase: Simultaneous Projection and Detection System of Four Different Frequencies for Microwave Imaging Reflectometry in Large Helical Device; *Rev. Sci. Instrum.* **81**, 10D915-1-4 (2010).
- D. Kuwahara, S. Tsuji-Iio, Y. Nagayama, T. Yoshinaga, H. Tsuchiya, S. Sugito, S. Yamaguchi, Y. Kogi, K. Akaki, and A. Mase: Development of Electron Cyclotron Emission Imaging System on Large Helical Device; *Rev. Sci. Instrum.* **81**, 10D919-1-3 (2010).
- T. Yoshinaga, Y. Nagayama, D. Kuwahara, H. Tsuchiya, S. Yamaguchi, Y. Kogi, S. Tsuji-Iio, H. Hojo, A. Mase: Optics Design for Microwave Imaging Reflectometry in LHD; *Plasma Fusion Res.* **5**, 030-1-3 (2010).
- D. Kuwahara, S. Tsuji-Iio, Y. Nagayama, T. Yoshinaga, H. Tsuchiya S. Yamaguchi, Y. Kogi, A. Mase: ECE Imaging Diagnostics on LHD; *27th Annual Meeting of the Japan Soc. of Plasma Sci. and Nucl. Fusion Res.*, 01P3, Sapporo, Nov. 30 - Dec. 3, 2010.
- T. Yoshinaga, Y. Nagayama, D. Kuwahara. H. Tsuchiya, S. Yamaguchi, Y. Kogi, S. Tsuji-Iio, A. Mase: Microwave Imaging Reflectometry Diagnostics in LHD; *27th Annual Meeting of the Japan Soc. of Plasma Sci. and Nucl. Fusion Res.*, 01P37, Sapporo, Nov. 30 - Dec. 3, 2010.
- G. Fujii, S. Tsuji-Iio, H. Tsutsui, O. Mitarai, K. Nakamura, M. Hasegawa, H. Zushi, T. Akiyama: Development of Fiber-Optic Diagnostics on Vacuum Vessel Current of QUEST; *27th Annual Meeting of the Japan Soc. of Plasma Sci. and Nucl. Fusion Res.*, 01P51, Sapporo, Nov. 30 - Dec. 3, 2010.
- D. Kuwahara, S. Tsuji-Iio, Y. Nagayama, T. Yoshinaga, H. Tsuchiya, S. Yamaguchi, Y. Kogi and A. Mase: Development of ECE Imaging Diagnostic System on LHD; *20th International Toki Conference*, Toki, Dec. 7-10, 2010.
- T. Habuchi, H. Tsutsui, S. Tsuji-Iio, R. Shimada: Force Balance and Stability of Circular Cross Section Toroidally Helical Coil; *20th International Toki Conference*, Toki, Dec. 7-10, 2010.

- S. Maeyama, A. Ishizawa, T.-H. Watanabe, N. Nakajima, S. Tsuji-Iio, H. Tsutsui: Numerical Methods for Parallel Particle Motions in Gyrokinetic Vlasov Simulation; *20th International Toki Conference*, Toki, Dec. 7-10, 2010.
- T. Habuchi, H. Tsutsui, S. Tsuji-Iio, R. Shimada: Optimization of the Stress Distribution of Helical Coils With a Cable-in-Conduit Configuration; *IEEE Transactions on Applied Superconductivity*, **21**, Issue 5, p. 3494 – 3500.
- T. Dwi Irwanto, Toru Obara, Yukitaka Kato, Ichiro Yamanaka: 2-dimensional Core Temperature Profile During Operation in the Small Simplified Pebble Bed Reactor with PeU a PeU Fuel Loading; *The Third International Symposium on Innovative Nuclear Energy Systems*, 31<sup>st</sup> October – 3<sup>rd</sup> November, 2010, Tokyo Institute of Technology, Japan, P-113, (2010).
- Munkhbat Byambajav, Toru Obara: Design Concept of Small Reactor for Larger Diameter neutron Transmutation Doping using Conventional PWR Fuel Assemblies; *The Third International Symposium on Innovative Nuclear Energy Systems*, 31<sup>st</sup> October – 3<sup>rd</sup> November, 2010, Tokyo Institute of Technology, Japan, P-108, (2010).
- Toru Obara, Yu Yamazawa: Decontamination Efficiency of Metal Mesh Plonium Filter for Lead Alloy Cooled Reactors; *The Third International Symposium on Innovative Nuclear Energy Systems*, 31<sup>st</sup> October – 3<sup>rd</sup> November, 2010, Tokyo Institute of Technology, Japan, 1B-34, (2010).
- Dwi Irwanto and Toru Obara: Burnup Analysis of a PeU a PeU Fuel-loading Scheme in a Pebble Bed Reactor Using the Monte Carlo Method; *Proc. of Joint International Conference on Supercomputing in Nuclear Applications and Monte Carlo 2010(SNA+MC2010)*, October 17-21, 2010, Tokyo, Japan, 10190, (2010).
- Toru OBARA, Hiroki TAKEZAWA: Kinetic Analysis of Weakly Coupled Systems Using Probability Density Function of Coupling Coefficient Obtained by Monte Carlo; *Proc. of Joint International Conference on Supercomputing in Nuclear Applications and Monte Carlo 2010(SNA+MC2010)*, October 17-21, 2010, Tokyo, Japan, 10258, (2010).
- Toru Obara and Hiroki Takezawa: Kinetic Analysis of Coupled Pulse Reactor for NPL Experiment; *Trans. American Nuclear Society*, **103**, 775 (2010).
- Byambajav Munkhbat and Toru Obara: Design Study on Nuclear Reactor for Large Diameter NTD Using PWR Fuel; *Trans. American Nuclear Society*, **103**, 756 (2010).
- Dwi Irwanto, Toru Obara, Yukitaka Kato, and Ichiro Yamanaka: Burnup Characteristics of PeU-a-PeU Fuel Loading Scheme in Small PBR; *Trans. American Nuclear Society*, **103**, 791 (2010).
- Dwi Irwanto, Toru Obara: Design Study of Innovative Simplified Small Pebble Bed Reactor; (3) Analysis of the 110MWt Simplified PBR Design with PeU a PeU fuel loading scheme; *2011 Atomic Energy Society Japan Annual Meeting*, I34 (2011).
- Piyatida Trinuruk, Toru Obara: Effect on Burnup Performance in HTGR by Neutron Spectrum Shift; *2011 Atomic Energy Society Japan Annual Meeting*, I34 (2011).
- Topan Setiadipra, Toru Obara: Development of Equilibrium Burnup Analysis Code for OTTO Cycle in Pebble Bed Reactor; *2011 Atomic Energy Society Japan Annual Meeting*, I34 (2011).
- Byambajav Munkhbat, Toru Obara: Design Study on Small Reactor for Silicon Semiconductor Production using LWR Fuel; (2) Reactor Optimization; *2011 Atomic Energy Society Japan Annual Meeting*, I34 (2011).
- Haruka Kikuchi, Toru Obara: Fundamental Study on Criticality Safety Transient Analysis in Weakly Coupled System; *2011 Atomic Energy Society Japan Annual Meeting*, I46 (2011).
- Dwi Irwanto and Toru Obara: Design Study of Innovative Simplified Small Pebble Bed reactor; (2) Steady State Thermal Hydraulic Analysis of Reference Design; *2010 Atomic Energy Society Japan Fall Meeting*, Q22(2010).
- Yuji Fukuda, Yong-Hong Zhang, Masao Nomura, Tatsuya Suzuki, Yasuhiko Fujii and Takao Oi: Strontium Isotope Effects Observed in Liquid Chromatography with Crown Ether resins; *J. Nucl. Sci. technol.*, **47** (2010) 176-183.
- Xingcheng Ding, Masao Nomura, Tatsuya Suzuki and Yasuhiko Fujii: Chromatographic Zinc Isotope Separation by Chelating Exchange Resin; *Chromatographia*, **71** (2010) 195-199.
- Shin-ichi Koyama, Tatsuya Suzuki, Masaki Ozawa: From Waste to Resource, Nuclear Rare Metals as a Dream of Modern Alchemists; *Energy Conversion and Management*, **51** (2010) 1799-1805.
- Minori Abe, Tatsuya Suzuki, Yasuhiko Fujii, Masahiko Hada, and Kimihiko Hirao: Ligand Effect on Uranium Isotope Fractionations Caused by Nuclear Volume Effects: An ab Initio Relativistic Molecular Orbital Study; *J. Chem. Phys.*, **133**, 044309 (2010) (5 pages).
- Tatsuya Suzuki, Masao Nomura, Yasuhiko Fujii, Atsushi Ikeda-Ohno, Toru Takaoka, and Koichi Oguma: Zinc Isotope Fractionation in Anion Exchange in Hydrochloric Acid Solution; *Journal of Ion Exchange*, **21** (2010) 328-333.
- Y. Fujii, M. Nomura, T. Kaneshiki, Y. Sakuma, T. Suzuki, S. Umehara, T. Kishimoto: Mass Dependence of Calcium

- Isotope Fractionations in Crown-ether Resin Chromatography; *Isotopes in Environmental and Health Studies*, **46** (2010) 233-241.
- Masao Nomura, Toshitaka Kaneshiki, Tatsuya Suzuki, Kazuhiro Otaka, Toshihiko Okazaki, Takashi Hoshi and Yasuhiko Fujii: Separation of Carbon Isotopes by Adsorption Chromatography; *The 5th International Conference on Ion Exchange*, Melbourne, Australia, July 18-21, (2010) 5B-4.
- Tatsuya Suzuki, Masao Nomura, Yasuhiko Fujii, Atsushi Ikeda-Ohno, Toru Takaoka and Koichi Oguma: Zinc Isotope Fractionation in Anion Exchange in Hydrochloric Acid Solution; *The 5th International Conference on Ion Exchange*, Melbourne, Australia, July 18-21, (2010) 2P-36.
- Tatsuya Suzuki, Maiko Tanaka, Yasuyuki Ikeda, Shin-ichi Koyama: Adsorption Behaviors of Trivalent F-Elements on Pyridine Resin in Lithium Chloride Aqueous Solution; *The 6th International Conference on Rare Earth Development and Application*, Beijing, China, August 2-6, (2010) P16.
- T. Suzuki, S. Koyama, M. Ozawa, M. Osaka: Extraction of Valuable elements in Spent Nuclear Fuel by using Pyridine Resin; *The 2nd International Conference on Asian Nuclear Prospects 2010 (ANUP 2010)*, Chennai, India, Oct. 11-13 (2010).
- Tatsuya Suzuki, Maiko Tanaka and Shin-ichi Koyama: Recovery of Minor Actinides from Spent Molten Salt Waste and Decontamination of Molten Salt Waste; *The 3rd International Symposium on Innovative Nuclear Energy Systems*, Tokyo, Japan, Oct.31- Nov.3, (2010) 2C-21.
- Minori Abe, Tatsuya Suzuki, Yasuhiko Fujii, Masahiko Hada: Theoretical Study of Nuclear Volume Effects in Uranium Enrichment; *The 3rd International Symposium on Innovative Nuclear Energy Systems*, Tokyo, Japan, Oct.31- Nov.3, (2010) 2C-23.
- Shin-ichi Koyama, Isao Yamagishi, Tatsuya Suzuki, Hitoshi Mimura, Reiko Fujita, Masaki Ozawa: Current Status and Future Plan of Advanced ORIENT Cycle Strategy; *The 3rd International Symposium on Innovative Nuclear Energy Systems*, Tokyo, Japan, Oct.31- Nov.3, (2010) 2C-24.
- Yoshihiko Sato, Ken Okada, Miyako Akiyoshi, Takehiro Matsunaga, Shin-ichi Koyama, Tatsuya Suzuki, Masaki Ozawa: Thermochemical Safety Evaluation of Tertiary Pyridine Resin for the Application to Multi-Functional Reprocessing Process - Adv.-ORIENT Cycle Development -; *The 3rd International Symposium on Innovative Nuclear Energy Systems*, Tokyo, Japan, Oct.31- Nov.3, (2010) 2C-25.
- Masao Nomura, Toshitaka Kaneshiki, Tatsuya Suzuki, Yasuhiko Fujii, Kazuhiro Otaka, Toshihiko Okazaki and Takashi Hoshi: Carbon Isotope Effect in the Carbon Dioxide Adsorption by the Column Method which Filled up Zeolite; *2010 fall meetings of atomic energy society of Japan*, (2010) p.657.
- Tatsuya Suzuki, Yasuyuki Ikeda, Shin-ichi Koyama, Masahiko Osaka and Masaki Ozawa: Advanced ORIENT Cycle Study (Phase I) 4) Separation Process Flowsheet and Element Distribution; *2010 fall meetings of atomic energy society of Japan*, (2010) p.708.
- Ken Okada, Yoshihiko Sato, Miyako Akiyoshi, Takehiro Matsunaga, Tatsuya Suzuki, Shin-ichi Koyama and Masaki Ozawa: Advanced ORIENT Cycle Study (Phase I) 6) Study on Thermal Stability of Tertiary Pyridine Resin; *2010 fall meetings of atomic energy society of Japan*, (2010) p.710.
- Yoshihiro Okadome, Masayuki Iwata, Katsuhisa Nagayama, Tsuyoshi Arai, Tatsuya Suzuki, Kenichi Horiguchi and Atsushi Sugaya: Study for Separation and Stabilization of Sodium from Low Level Liquid Waste Using Inorganic Ion Exchanger; *2010 fall meetings of atomic energy society of Japan*, (2010) p.752.
- Masayuki Iwata, Yoshihiro Okadome, Tsuyoshi Arai, Katsuhisa Nagayama, Tatsuya Suzuki, Kenichi Horiguchi and Atsushi Sugaya: A Basic Study for Solidification of Low Level Liquid Waste with Iron Phosphate Glass; *2010 fall meetings of atomic energy society of Japan*, (2010) p.753.
- T. Suzuki, Y. Ikeda, M. Honda, N. Asanuma, M. Osaka: Recovery of Molybdenum by using Pyridine Resin from Simulant Irradiated Nuclear Fuel Solution; *2010 annual meeting of the Japan society of nuclear and radiochemical sciences*, (2010) 1P17.
- Masao Nomura, Yiqun Zhang, Tatsuya Suzuki and Yasuhiko Fujii: Lithium Isotope Effect by Ion Exchange Chromatography with Li-6 Enriched Sample Material; *2011 annual meetings of atomic energy society of Japan*, (2011) p.534.
- Fumiaki Kawakami, Moriyasu Tokiwai, Yasuhiko Fujii and Tatsuya Suzuki: Plant Designing of Chemical Uranium Enrichment and Its Characteristics; *2011 annual meetings of atomic energy society of Japan*, (2011) p.535.
- Shin-ichi Koyama, Masaki Ozawa, Yasuhiko Fujii, Kiyoko Kurosawa, Yukio Hanamoto, Katsuyoshi Tatenuma and Tatsuya Suzuki: Metal Corrosion Evaluation in Hydrochloric Acid Media on Tertiary Pyridine-Type Resin Applying to Fuel Reprocessing System (5); *2011 annual meetings of atomic energy society of Japan*, (2011) p.583.
- Tatsuya Suzuki, Toshitaka Kaneshiki, Masao Nomura, Yasuhiko Fujii, Hidekazu Kobayashi, Shigeru Kano and Teruo Yamashita: Development of water absorptive porous glass beads; *Proceedings of Annual / Fall Meetings of*

*Atomic Energy Society of Japan, 2011 annual meetings of atomic energy society of Japan, (2011) p.604.*

M. Numakura, Y. Okamoto, T. Yaita, H. Shiwaku, H. Akatsuka, A. Nezu, K. Tajima, Y. Shimohara, C. Bessada, O. Pauvert, D. Zanghi, P. Chamelot, H. Matsuura: Local Structural Analyses on Molten Terbium Fluoride in Lithium Fluoride and Lithium – Calcium Fluoride Mixtures; *J. Fluor. Chem.* **131**, 1039-1043, (2010).

O. Pauvert, D. Zanghi, M. Salanne, C. Simon, A. Rakhmatullin, H. Matsuura, Y. Okamoto, F. Vivet, C. Bessada: In situ Experimental Evidence for an Nonmonotonous Structural Evolution with Composition in the Molten LiF-ZrF<sub>4</sub> System; *J. Phys. Chem. B*, **114**, 6472-6479, (2010).

Haruaki Matsuura, Masahiko Numakura, Hiroshi Akatsuka, Nobuaki Sato: Structure and Physico-Chemical Properties of Thorium Fluoride Mixtures (1) Synthesis of Thorium - Lithium Fluoride Mixture; *2010 Annual Meeting of the Atomic Energy Society of Japan*, J39, 465, (2010).

Masahiko Numakura, Haruaki Matsuura, Atsushi Nezu, Hiroshi Akatsuka, Nobuaki Sato, Catherine Bessada, Didier Zanghi, Olivier Pauvert, Pierre Chamelot: Structure and Physico-Chemical Properties of Thorium Fluoride Mixtures (2) XAFS Analysis on Molten ThF<sub>4</sub>-LiF; *2010 Annual Meeting of the Atomic Energy Society of Japan*, J40, 466, (2010).

Masahiko Numakura, Haruaki Matsuura, Hiroshi Akatsuka, Atsushi Nezu, Tsuyoshi Yaita, Yoshihiro Okamoto, Hideaki Shiwaku, Catherine Bessada: Structural Analyses on Terbium Fluorides in Molten Alkali and Alkaline Earth Fluorides; *The 27<sup>th</sup> symposium on rare earths*, 1C-05, 86-87, 2010.

Masahiko Numakura, Catherine Bessada, Nobuaki Sato, Hiroshi Akatsuka, Atsushi Nezu, Yasuaki Shimohara, Keisuke Tajima, Hirokazu Kawano, Takeshi Nakahagi, Haruaki Matsuura: Structural Analysis of Molten Terbium Fluoride Mixtures; *The 13<sup>th</sup> XAFS symposium*, 5O-03, 57-58, 2010.

Yasuaki Shimohara, Atsushi Nezu, Masahiko Numakura, Hiroshi Akatsuka, Haruaki Matsuura: Electrochemical Behaviour of Neodymium in Molten LiCl-KCl-LiF; *The 42<sup>nd</sup> symposium on molten salt chemistry*, 1A01, 1-2, 2010.

Masahiko Numakura, Nobuaki Sato, Catherine Bessada, Hiroshi Akatsuka, Atsushi Nezu, Yasuaki Shimohara, Keisuke Tajima, Hirokazu Kawano, Takeshi Nakahagi, Haruaki Matsuura: The variation of Local Structure Around Thorium Fluoride and Terbium Fluoride Melts by Addition of Alkali and Alkaline Fluorides; *The 42<sup>nd</sup> symposium on molten salt chemistry*, 1B10, 43-44, 2010.

Masahiko Numakura, Haruaki Matsuura, Atsushi Nezu, Yasuaki Shimohara, Keisuke Tajima, Hiroshi Akatsuka, Nobuaki Sato, Olivier Pauvert, Didier Zanghi, Pierre Chamelot, Catherine Bessada: Structure and Physico-Chemical Properties of Thorium Fluoride Mixtures (3) XAFS Analyses on Molten Fluoride Mixtures Containing ThF<sub>4</sub>; *2010 Fall Meeting of the Atomic Energy Society of Japan*, B40, 103, (2010).

Masahiko Numakura, Nobuaki Sato, Catherine Bessada, Hiroshi Akatsuka, Pierre Chamelot, Haruaki Matsuura: Structural Investigation on Thorium Fluoride in Molten Alkali-Alkaline Earth Fluoride Mixtures; *NuMat 2010 the Nuclear Materials Conference*, MSNA17, 2010.

Haruaki Matsuura, Atsushi Nezu, Hiroshi Akatsuka: Pyrochemical Reprocessing Based on Co-Electrodeposition Technique – Speciation of Uranyl Ion in Various Molten Salts and In-situ Observation of Electrodeposition Reaction Investigated by X-ray from Synchrotron Source; *The 3<sup>rd</sup> International symposium on Innovative Nuclear Energy Systems*, 1C-12, 68, 2010.

Masahiko Numakura, Hiroshi Akatsuka, Atsushi Nezu, Keisuke Tajima, Yasuaki Shimohara, Haruaki Matsuura: Feasibility Study of Pyrochemical Reprocessing using Molten Lithium- Calcium Fluoride Mixtures in Salt Treatment Process for Molten Salt Reactor; *The 3<sup>rd</sup> International symposium on Innovative Nuclear Energy Systems*, P-125, 149, 2010.

S. Nomura, K. Tsuboi, K. Ito, H. Tsutsui, S. Tsuji-Iio, A. Ninomiya R. Shimada: Acoustic Emission in a Superconducting Force-Balanced Helical Coil; *IEEE Trans. Appl. Supercon.*, Vol **21**, 1636-1639 (2011).

"Simulations", S. Maeyama, A. Ishizawa, T.-H. Watanabe, N. Nakajima, S. Tsuji-Iio, H. Tsutsui: A Numerical Method for Parallel Particle Motions in Gyrokinetic Vlasov ; *Plasma and Fusion Research*, **87**, 359-370 (2011).

Yasuyuki Sakamoto, Kiichi Sato, Mitsuru Abo, Takehiko Tsukahara, Takehiko Kitamori, Keiko Abe, and Etsuro Yoshimura: Cell Culture and Motility Study on a Polymer Surface with a Nanometer-Scaled Stripe Structure; *Biosci. Biotechnol. Biochem.*, **74** (3), 569-572 (2010).

kyojiro Morikawa, Kazuma Mawatari, Masaru Kato, Takehiko Tsukahara, and Takehiko Kitamori: Streaming Potential/Current Measurement Systems for Investigating Liquid Properties Confined in Extended-Nano Space; *Lab on a Chip*, **10** (7), 871 - 875 (2010).

Masaru Kato, Masanori Inaba, Takehiko Tsukahara, Kazuma Mawatari, Akihide Hibara, and Takehiko Kitamori: Femto Liquid Chromatography with Atto-Liter Sample Separation in the Extended Nanospace Channel; *Analytical Chemistry*, **82**, 543 - 547 (2010).

Kazuma Mawatari, Takehiko Tsukahara, Yasuhiko Sugii, Takehiko Kitamori: Extended-nano Fluidic Systems for Analytical and Chemical Technologies; *Nanoscale*, **2**, 1588-1595 (2010).

Takehiko Tsukahara, Kazuma Mawatari, and Takehiko Kitamori: Integrated Extended-nano Chemical Systems on a Chip; *Chemical Society Reviews*, **39**, 1000 - 1013 (2010).